
Synthesis and Characterization of Homogeneous and Surface Attached Catalysts for Small Molecule Activation

DISSERTATION SUBMITTED TO THE

FACULTY OF MATHEMATICS AND NATURAL SCIENCES
INSTITUTE OF INORGANIC CHEMISTRY
CHRISTIAN-ALBRECHTS-UNIVERSITY
OF KIEL

FOR THE DEGREE OF

Dr. rer. nat.

SUBMITTED BY

Sven Froitzheim

Kiel, 2024

-
1. Gutachter: Prof. Dr. F. Tuczek
 2. Gutachter: Prof. Dr. C. Näther

Tag der mündlichen Prüfung: 08.11.2024

Zum Druck genehmigt: 08.11.2024

Der Dekan; Prof. Dr. Frank Kempken

This Thesis was written at the Institute of Inorganic Chemistry
of the Christian-Albrechts-University of Kiel
under the supervision of Prof. Dr. Felix Tuczek
between March 2018 and October 2023.

Acknowledgement

Als erstes möchte ich mich bei meinem Doktorvater Prof. Dr. Felix Tuczek für die Möglichkeit meine Doktorarbeit in seinem Arbeitskreis anzufertigen bedanken. Neben den spannenden und vielseitigen Themen in der Forschung, gelang es uns ein paar sehr hochwertige und lehrreiche Vorlesungen in den drei Coronasemestern zu gestalten.

Herrn Prof. Dr. Christian Näther danke ich für die Übernahme des Zweitgutachtens, dem Lösen der Einkristallstrukturen und die Mitarbeit an den Publikationen.

Ein besonderer Dank geht auch an Dr. Tobias Engesser. Danke für die vielen Stunden der Diskussion über Spektren, Rechnungen und unverstandene Ergebnisse, die Unterstützung bei der zweiten Publikation, das Korrekturlesen der Arbeit und wenn es nötig war - das Stubsen in die richtige Richtung.

Dr. Jan Krahmer danke ich für die vielen und teilweise sehr langen NMR-Messungen. Auch danke ich dir für die Starthilfe bei der Elektrochemie. Das Entenzeichnen hat Spaß gemacht. Nicolas Le Poul danke ich für die tolle Kooperation, den Wissensaustausch und die intensive Betreuung während unseres Aufenthalts in Brest. Danke auch für die Aufnahme jenen Fotos, welches die Basis für das Frontcover unserer Publikation bildet.

Mein Dank geht auch an Stephanie Pehlke und Jaqueline Pick für die Aufnahme der Elementar- und Halogenidanalysen.

Dem Arbeitskreis Tuczek danke ich für die tolle Zusammenarbeit und Stimmung während meiner Zeit. Die Aufenthalte in Sehendorf gehören dabei definitiv zu meinen Highlights. Ein besonderer Dank geht auch an die Stickstofffixierung und vor allem an Jannik Junge. Danke für 5 Jahre mit viel Spaß, wertvollem wissenschaftlichen Austausch und einer tollen Zusammenarbeit - ohne dich hätte es nur halb so viel Spaß gemacht.

Ein großer Dank geht auch an meine Kommilitonen und Freunde, die mich über die vielen Jahre begleitet haben. Christoph Bohl, Daniel Hugenbusch, Marc Lehr, Jonas van Dinter, Jannik Junge, Jannik Benecke, Tobias Haase, Felix Hartmann, Kai Uwe Clausen und Timo Rabe - ihr seid die besten und habt meine Zeit in Kiel zu etwas ganz besonderem gemacht.

Zu guter letzt möchte ich mich noch bei meiner Familie bedanken. Besonders bei meiner Mutter und Rolf. Ohne eure riesige und bedingungslose Unterstützung wäre ich nie soweit gekommen. Abschließend möchte ich mich noch bei meiner Verlobten Sina bedanken. Danke für den Rückhalt und den gemeinsamen Alltag. Ich freue mich auf unsere gemeinsame Zukunft!

List of Publications

This thesis consists of three parts. Two of them are based on the following publications, which are published in different journals:

1. J. Junge, S. Froitzheim, T. A. Engesser, J. Krahmer, C. Näther, N. Le Poul and F. Tuczek

"Tungsten and Molybdenum Dinitrogen Complex Supported by a Pentadentate Tetrapodal Phosphine Ligand: Comparative Spectroscopic, Electrochemical and Reactivity Studies"

Dalton Trans., 2022, 51, 6166-6176. DOI: 10.1039/D1DT04212B

2. S. Froitzheim, J. Junge, C. Barnehl, T. A. Engesser, J. Krahmer, C. Näther and F. Tuczek

"Molybdenum tricarbonyl complexes supported by linear PNP ligands: Influence of P- and N-substituents on relative stability, stereoisomerism and on the activation of small molecules"

Eur. J. Inorg. Chem. 2023, 26, e202300280. DOI: 10.1002/ejic.202300280

Kurzzusammenfassung

Die synthetische Stickstofffixierung befasst sich mit der Bindung und Derivatisierung des sonst inerten Distickstoffmoleküls mithilfe von Übergangsmetallkomplexen. Im Fokus der Betrachtungen stehen hierbei vor allem Molybdän und Wolfram, die häufig multidentate Liganden binden. Diese Arbeit ist drei in Abschnitte unterteilt. Im ersten Abschnitt ist die Synthese und Charakterisierung des $[\text{W}(\text{N}_2)(\text{P}^{\text{Me}}_2\text{PP}^{\text{Ph}}_2)]$ Komplexes beschrieben, welcher auf dem von der Arbeitsgruppe TUCZEK entwickelten pentaPod-Ligandsystem basiert. Auch wenn dieser Komplex eine geringere katalytische Aktivität (mit $\text{SmI}_2/\text{H}_2\text{O}$) als sein molybdänbasiertes Analogon hinsichtlich der Erzeugung von Ammoniak zeigte, ist dieser Komplex das erste Beispiel für einen wolframbasierten Distickstoffkomplex, der überstöchiometrische Mengen NH_3 generieren konnte. Ein Vergleich der Einkristallstrukturen der Mo- & W(N_2) Komplexe zeigt nur geringe strukturelle Unterschiede. Um Hinweise auf die Ursache für die unterschiedliche katalytische Aktivität zu finden, wurden elektrochemische und spektroelektrochemische Untersuchungen durchgeführt. Es wurde gefunden, dass die Komplexe große Unterschiede hinsichtlich ihrer Stabilität im oxidierten Zustand aufweisen.

Im zweiten Teil dieser Arbeit wird, statt N_2 , CO als Ligand verwendet. Kohlenstoffmonoxid ist isoelektronisch zu Distickstoff, bildet jedoch stabilere Komplexe, was die Untersuchung des Koordinationsverhaltens von Ligandensystemen ermöglicht. Es wurde das Koordinationsverhalten von tridentaten $\text{PN}^{\text{Ph}}\text{P}^{\text{R}}$ Liganden ($\text{R} = \text{Ph}_2, \text{Et}_2, \text{Cyp}_2, {}^i\text{Pr}_2, \text{Cy}_2$) an das $\text{Mo}(\text{CO})_3$ Strukturfragment untersucht. Es wurde gefunden, dass alle Liganden in einer facialen Geometrie koordinierten, obwohl DFT-Rechnungen zeigen, dass eine meridionale Geometrie für sterisch anspruchsvolle Reste bevorzugt wäre. Diese Ergebnisse stehen im Gegensatz zu den in der Literatur bekannten $[\text{Mo}(\text{CO})_3\text{PN}^{\text{H}}\text{P}]$ Komplexen, die für Phosphindonoren mit sterisch anspruchsvollen Substituenten auch eine meridionale Geometrie zeigen. DFT-Studien mit $[\text{Mo}(\text{CO})_2\text{PN}^{\text{R}}\text{P}^{\text{Me}}]$ ($\text{R} = \text{N}, \text{Ph}$) zeigten unter anderem, dass der Übergangszustand des $\text{PN}^{\text{Ph}}\text{P}^{\text{Me}}$ haltigen Komplexes energetisch höher liegt, was auf die Bildung agostischer Wasserstoffbrückenbindungen zurückzuführen ist.

Im dritten Teil dieser Arbeit wurden tridentate Ligandsysteme für eine mögliche Fixierung auf einer Goldoberfläche untersucht. Hierzu wurden verschiedene Ansätze gewählt, wobei der Hauptfokus auf der Synthese eines $[\text{Mo}(\text{CO})_3\text{PN}^{\text{Ph}}\text{P}^{\text{Ph}}]$ Komplexes lag, der in *para*-Position zum N-Donor mit einer Thio-Gruppe versehen war, die als Ankergruppe auf der Oberfläche dienen sollte. Als größte Herausforderung stellte sich hierbei die Einführung der gewählten SCN-Gruppe heraus, da im Zuge dieser Reaktion Br_2 freigesetzt wird, welches die Phosphine oxidierte. Die Schützung der Phosphine mit Borangruppen erlaubte schlussendlich die Einführung der SCN-Gruppe. Leider konnte der gewünschte Ligand dennoch nicht erhalten werden, da Sauerstoffverunreinigungen im Morpholin bei der Entfernung der Borangruppen die Phosphine oxidierten. Nichtsdestotrotz stellt die vorgestellte Route eine vielversprechende Methode zur Darstellung des $\text{PN}^{\text{Ph}}\text{-SCN-P}^{\text{Ph}}$ Liganden dar, welcher im Anschluss für die Koordination an $[\text{Mo}(\text{CO})_3(\text{cht})]$ verwendet werden könnte.

Abstract

Synthetic nitrogen fixation deals with the binding and derivatization of the otherwise inert dinitrogen molecule with transition metal complexes. These complexes primarily contain molybdenum and tungsten centers, which mostly bind multidentate ligands. This work is divided into three sections. The first section describes the synthesis and characterization of the $[\text{W}(\text{N}_2)(\text{P}^{\text{Me}}_2\text{PP}^{\text{Ph}}_2)]$ complex, which is based on the pentaPod ligand system developed by the TUCZEK group. Although this complex showed lower catalytic activity (with $\text{SmI}_2/\text{H}_2\text{O}$) than its molybdenum-based analogue in terms of ammonia generation, it is the first example of a tungsten-based dinitrogen complex that is able to generate overstoichiometric amounts of NH_3 . A comparison of the single crystal structures of the Mo- & W(N_2) complexes shows only minor structural differences. Electrochemical and spectroelectrochemical investigations were carried out to determine the cause of the different catalytic activities. It was found that the complexes exhibit large differences in terms of their stability in the oxidized state.

In the second part of this work, CO is used as a ligand instead of N_2 . Carbon monoxide is isoelectronic to dinitrogen, but tends to form more stable complexes, which allows for the investigation of the coordination behavior of ligand systems. The coordination behavior of tridentate $\text{PN}^{\text{Ph}}\text{P}^{\text{R}}$ ligands ($\text{R} = \text{Ph}_2, \text{Et}_2, \text{Cyp}_2, {}^i\text{Pr}_2, \text{Cy}_2$) to the $\text{Mo}(\text{CO})_3$ fragment was investigated. It was found that all ligands coordinated in a facial geometry, although DFT calculations show that a meridional geometry would be preferred for sterically demanding residues. These results are in contrast to $[\text{Mo}(\text{CO})_3\text{PN}^{\text{H}}\text{P}]$ complexes reported in literature, which do show a meridional geometry for phosphine donors with sterically demanding substituents. DFT studies using $[\text{Mo}(\text{CO})_2\text{PN}^{\text{R}}\text{P}^{\text{Me}}]$ ($\text{R} = \text{N}, \text{Ph}$) complexes showed, that among other things, the transition state of the $\text{PN}^{\text{Ph}}\text{P}^{\text{Me}}$ containing complex is energetically higher, due to the formation of agostic hydrogen bonds.

In the third part of this work, tridentate ligand systems were investigated for possible deposition on a gold surface. Various approaches were chosen for this purpose, with the main focus on the synthesis of a $[\text{Mo}(\text{CO})_3\text{PN}^{\text{Ph}}\text{P}^{\text{Ph}}]$ complex, which was modified with a thio group in the *para*-position to the N-donor, intended to serve as an anchor group to the surface. The introduction of the selected SCN group proved to be the greatest challenge, as Br_2 is released in the course of this reaction, which oxidized the phosphines. Protecting the phosphines with borane groups ultimately allowed the introduction of the SCN group. Unfortunately, the desired ligand could not be obtained because oxygen impurities in the morpholine oxidized the phosphines when attempting to remove the borane groups. Nevertheless, the presented route appears to be a promising method for the preparation of the $\text{PN}^{\text{Ph-SCN}}\text{P}^{\text{Ph}}$ ligand, which could subsequently be used for coordination to $[\text{Mo}(\text{CO})_3(\text{cht})]$.

Contents

Acknowledgement	IV
List of Publications	V
Kurzzusammenfassung	VI
Abstract	VII
1 Introduction	1
2 Scientific Background	3
2.1 The Haber-Bosch Process	3
2.2 Biological Nitrogen Fixation	5
2.2.1 The Nitrogen Cycle	5
2.2.2 Biological Nitrogen Fixation	7
2.2.3 Nitrogenase	7
2.2.4 Mechanism of Nitrogenase	10
2.3 Synthetic Nitrogen Fixation	13
2.3.1 Chatt system	15
2.3.2 Systems of the Schrock group	17
2.3.3 Systems of Peters' group	20
2.3.4 Systems of the Nishibayashi group	22
2.3.5 Systems of the Tuzcek group	25
3 Project 1	29
3.1 Tungsten and molybdenum dinitrogen complexes supported by a pentadentate tetrapodal phosphine ligand: comparative spectroscopic, electrochemical and reactivity studies	30
3.2 Electrochemical and Electrocatalytic Studies	43
4 Project 2	47
4.1 Molybdenum tricarbonyl complexes supported by linear PNP ligands: Influence of P- and N-substituents on structure, stability and on the activation of small molecules	48
5 Project 3 - Surface functionalization of tridentate PNP and PPP Ligands	65
5.1 Acetylene functionalization of the $\text{PN}^{\text{Ph}}\text{P}^{\text{Ph}}$ ligand	70

5.2	Thiofunctionalization of the $\text{PN}^{\text{Ph}}\text{P}^{\text{Ph}}$ ligand	76
5.3	Functionalization of the prPPHP-ligand	87
6	Conclusion & Outlook	91
6.1	Project 1	91
6.2	Project 2	92
6.3	Project 3	94
7	Experimental Section	97
7.1	Materials and Methods	97
7.2	4-Bromo- <i>N,N</i> -bis(2-chloroethyl)aniline	98
7.3	<i>N,N</i> -Bis(2-chloroethyl)-4-((trimethylsilyl)ethynyl)aniline	99
7.4	<i>N,N</i> -Bis(2-(diphenylphosphanyl)ethyl)-4-((trimethylsilyl)ethynyl)aniline . . .	100
7.5	<i>N,N</i> -Bis(2-chloroethyl)-4-thiocyanatoaniline	102
7.6	<i>N,N</i> -Bis(2-(diphenylphosphino)ethyl)aniline-borane-complex	103
7.7	<i>N,N</i> -Bis(2-(diphenylphosphaneyl)ethyl)-4-thiocyanatoaniline-borane-complex	104
8	References	107
9	Appendix	121
	Supplementary Material to section 3.1: Tungsten and Molybdenum Dinitrogen Com- plex Supported by a Pentadentate Tetrapodal Phosphine Ligand: Comparative Spectroscopic, Electrochemical and Reactivity Studies	121
	Supplementary Material to section 4.1: Molybdenum tricarbonyl complexes sup- ported by linear PNP ligands: Influence of P- and N-substituents on relative stability, stereoisomerism and on the activation of small molecules	150
	Declaration	199
	List of Figures	204
	List of Tables	205

Introduction

The current world population is about to reach 8 billion.^[1,2] In order to sustain the world's population, high yields in agriculture are necessary. This is achieved, among other things, by large amounts of nitrogen based fertilization.^[3–5] Nitrogenous fertilizers are based on ammonia which is produced on an industrial scale by the so-called Haber-Bosch process (see section 2.1).^[6,7] The conventional Haber-Bosch process utilizes an iron catalyst, developed for the synthesis of ammonia from its elements nitrogen and hydrogen.^[8,9] The process was developed by Fritz Haber on laboratory scale and industrialized by Carl Bosch.^[6] Due to the inert character of the very stable $\text{N}\equiv\text{N}$ -triple bond and the associated energy for bond dissociation high temperatures are required.^[10] Furthermore, the actual catalyst (α -iron) only forms at high temperatures. In order to increase the yield of this exothermic reaction, the pressure is increased to around 200 bar, favoring the product side of the equilibrium.^[11] Although the process requires a large energy input, a major portion of energy is expended for the provision of hydrogen by steam reforming and water-gas shift reaction.^[12] Also coal, oil and natural gases are used as energy source increasing the CO_2 emission even further.^[11]

Although the fertilizers made from the Haber-Bosch process contribute a lot to the availability of nitrogenous compounds in the soil, plants who live in symbiosis with diazotrophic microorganisms can also access nitrogenous compounds.^[13] These microorganisms are able to bind and convert the inert dinitrogen molecule into bioavailable compounds. This is known as biological nitrogen fixation (see section 2.2.2) and represents the first step of the nitrogen cycle. Nitrogen fixing microorganisms (e.g. *Azotobacter vinelandii*) utilize an enzyme called *Nitrogenase*.^[14] There are multiple types of nitrogenases with the main variant being the molybdenum iron nitrogenase.^[15–17] Other than in the Haber-Bosch process, nitrogenase is able to convert dinitrogen under ambient conditions, yet the biological energy expenditure is considerably large with 16 MgATP.^[18] Besides some geochemical ways to convert dinitrogen into ammonia the last major field is the synthetic nitrogen fixation (see section 2.3). This is an area in coordination chemistry where attempts are made to understand the processes of the nitrogenase through simpler model systems, to obtain insight knowledge into the mechanism and maybe find a process which has a lower energy consumption and CO_2 emission.^[19,20] One of the main challenges is the bonding and activation of the N_2 molecule, making it accessible for derivatization. This is achieved by coordination of the dinitrogen molecule to transition metal complexes and tuned by the surrounding ligand sphere.^[21] Due to the sensitivity of these dinitrogen complexes, isoelectronic carbonyl ligands are often used as well. Carbonyl ligands form more stable compounds and have excellent spectroscopic properties making them a good alternative for the investigation of ligand and complex properties.

Scientific Background

2.1 The Haber-Bosch Process

The Haber-Bosch process is one of the most important industrial processes today. It is used to synthesize ammonia from its elements.^[6,7,11] The process was developed by FRITZ HABER in 1908 who studied the thermal reaction equilibrium of dinitrogen and dihydrogen to ammonia, which was discovered in the 20th century.^[22] He found that the reaction is increasingly in favour of ammonia when high pressures are applied in the presence of osmium and uranium catalysts.^[23,24] In the following years CARL BOSCH engineered the reaction to an industrial scale with the first plant being operational in 1913.^[7,25,26] In order to accomplish the industrialization of the reaction, several obstacles had to be overcome. The first being the provision of the raw materials as well as the catalysts. HABER used the electrolysis of hydrogen chloride as dihydrogen source which was not sufficient for the industrial process.^[24] For the first plant, coal was used as hydrogen source obtained by a catalytic process developed for the ammonia synthesis.^[24,26,27]

Nitrogen was obtained from air distillation via the Linde process like it is today.^[24,28] Another obstacle was the catalyst. FRITZ HABER found osmium and uranium catalysts to be effective. However, due to the low natural abundance of osmium and the tendency to form oxides it was not suitable for an industrial process. A similar problem was found for the uranium catalyst, which tends to be too sensitive towards water and air in view of an application in the industrial process.^[24,27] ALVIN MITTASCH was tasked with finding a suitable catalyst that was robust, active and accessible.^[8,27] After an extensive empirical study he found a fused iron catalysts made from different oxides like hematite, magnetite or wüstite with added promoters to be the most efficient and enduring for the process.^[7,27]

Most modern industrial catalysts use magnetite as iron oxide with Al_2O_3 and CaO as structural and K_2O as electronic promotor.^[9,27] By melting the iron and promoters under reductive conditions with hydrogen, crystallites (α -iron) are formed which are stabilized and activated by the electronic promotor. The catalyst operates at high temperatures, because an equilibrium between the promoters and the crystallites is formed, stabilizing the active sites.^[9,29] The requirement for high temperatures is problematic for the conversion to ammonia due to the exothermic nature of the reaction (see eqn. 2.1).^[30]



The amount of energy release even increases with rising temperatures leading to a value of $\Delta_R H$ of -109 kJ/mol at 500 °C.^[31] Following Le Chateliers principle the equilibrium changes in favor of ammonia by increasing the pressure. In the industrial process usually around 200-300 bar of pressure are applied.^[12,30,31] The reduction in volume shifts the reactions equilibrium towards the product side, increasing the yield from 0.13 vol.-% to 17.6 vol.-%. Depending on the contact time between the catalyst and the synthesis gas this yield can vary and yield lower amounts, yet be more economical for a company due to fast reaction times.^[30] Both HABER (1919) and BOSCH (1931) were awarded the Nobel prize for their accomplishments. In 2007 another Nobel prize was awarded in relation to the Haber-Bosch process. This time it was given to Gerhard Ertl for elucidation of the mechanism on the catalysts surface.^[32] The reaction is usually divided into several steps. The first step is the physisorption of dihydrogen and dinitrogen on the iron surface, followed by the dissociative formation of iron nitride species.^[30,32,33] The dissociative chemisorption was identified as rate limiting step of the industrial ammonia synthesis as suggested by EMMETT.^[34] As a consequence of the electronic promoters in the catalyst this reaction is not only exothermic but lowers the very high activation energy that would be associated with a reaction in the gaseous phase.^[30,33-36] Interestingly, the dissociation of the dihydrogen molecule seems barrier less and is therefore often neglected in discussions.^[37]

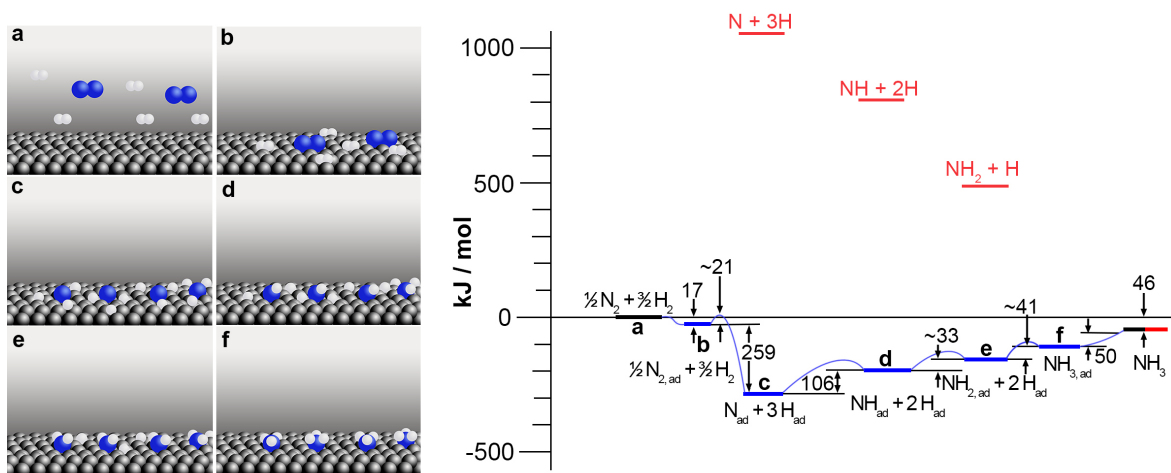


Fig. 2.1: Energy diagram of the conversion from N_2 and H_2 to NH_3 . The blue reaction pathway describes the reaction on the catalysts surface, the red path the direct reaction in the gaseous phase. Adapted from.^[36,37]

The dissociative mechanism of the dinitrogen molecule can be separated into three steps. In the first step the dinitrogen molecule is bound in an *end-on* fashion to the α -iron. Upon transition to a *side-on* coordination mode the bonds between the nitrogen atoms are weakened.^[38,39] Ultimately, this leads to homolytic dissociation of the $N \equiv N$ bonds and the formation of surface nitrides. Although endergonic, chemisorbed hydrogen gets added sequentially. These

reaction steps aren't limiting as the hydrogen has a high mobility on the surface and the energetic requirements are easily overcome by the reaction temperature.^[30,36,37] After around a century of industrial ammonia synthesis, the Haber-Bosch process evolved to one of the most important chemical processes with ammonia being one of the mostly produced chemicals worldwide.^[40] Nonetheless, the process and especially the generation of hydrogen gas are not only very energy-intensive, but also high in expenditure of resources.^[22,41] Furthermore, the emission of carbon dioxide is high, especially in view of the challenges posed by climate change. For these reasons, a lot of resources are invested in improving the process with new catalysts^[7,42] or finding ways to electrochemically generate ammonia for which the energy needed can be obtained from renewable sources.^[22,43,44] The ammonia containing fertilizers are an important factor concerning crop yields and therefore for humanity. Yet nature has found a different way to access and convert atmospheric nitrogen to ammonia. This process is called biological nitrogen fixation.

2.2 Biological Nitrogen Fixation

2.2.1 The Nitrogen Cycle

Nitrogenous compounds are essential for plant growth, yet they are unable to produce the needed compounds themselves. Certain microorganism on the other hand are able to convert atmospheric dinitrogen into ammonia. The conversion of dinitrogen to ammonia is the first step in the nitrogen cycle (Figure 2.2), which describes the fixation, conversion and the re-release of nitrogen in nature.^[14,45,46] The nitrogen cycle can be separated into three main stages. The first stage is the biological nitrogen fixation (BNF) in which atmospheric dinitrogen is converted into bioavailable compounds by microorganisms.^[13,14,46] The fixation and the mechanisms will be discussed in more detail in section 2.2.2. The second stage of the nitrogen cycle is called nitrification. The ammonia generated by nitrogen-fixing bacteria is either assimilated by plants or further oxidized by communities of bacteria generating nitrate.^[46,47] Ammonia-oxidizing bacteria and nitrite-oxidizing bacteria convert the ammonia to nitrate via hydroxylamine and nitrite.^[48–50] These reactions are an energy source as well as growth factor for the bacteria.^[48,49,51] This leads to ammonia and nitrate being the two predominant nitrogen species in the soil.^[52]

Denitrification, i.e. the degradation of nitrogen species, is the third and final step in the nitrogen cycle. During this step nitrate is reduced to molecular nitrogen and released back into the atmosphere. This is done by sequential reduction of the nitrogen atom.^[53,54] The nitrate is reduced to nitrite which in turn is reduced to nitric oxide. The nitric oxide is then converted to nitrous oxide and after a final reduction step dinitrogen is formed.^[53,54] Each of these steps is part of an anaerobic respiratory chain and requires its own enzyme as a catalyst.^[53–55] A

final process to mention is the dissimilatory nitrate ammonification in which the nitrate is not reduced to N_2 but to NH_4^+ instead. This respiration reaction is not as efficient as the denitrification because the energy gain is less compared to the release of a dinitrogen molecule. Due to this reason the ammonification is mostly used as energy conservation method.^[54,56] Not only plants and bacteria are part of the nitrogen cycle. Every living organism takes part in it, yet there is an increasing anthropogenic influence due to extensive fertilization, combustion of fossil fuels, burning of biomass or domestication of animals.^[13,45] Due to the success of the Haber-Bosch process and the availability of fertilizers, about half of all nitrogen species in organic matter can be traced back to this process while the other half results from biological nitrogen fixation.^[13]

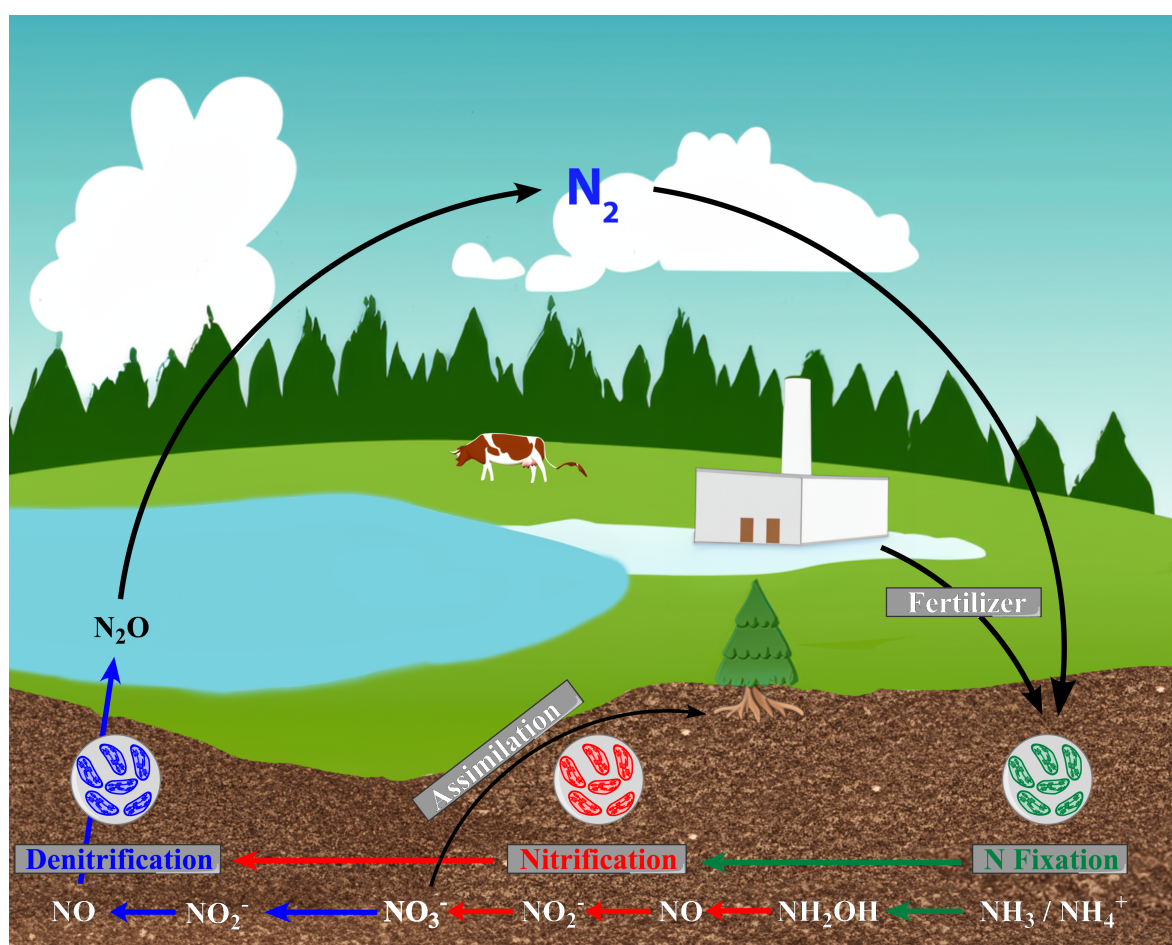
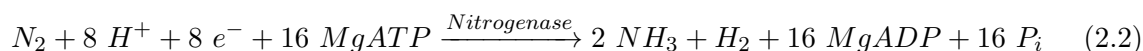


Fig. 2.2: Simple illustration of the nitrogen cycle. The three main stages of the nitrogen cycle are the Fixation, Nitrification, and Denitrification. Adapted from^[13]

2.2.2 Biological Nitrogen Fixation

In general the microbial binding and conversion of dinitrogen to ammonia from the air is called biological nitrogen fixation. Similar to the nitrogen cycle itself, the biological nitrogen fixation can be divided into the respective ecosystems in which the associated microbes occur: marine, terrestrial and freshwater systems.^[57–59] Depending on the ecosystem different microbes are the main protagonists. Marine nitrogen fixation is mainly associated with cyanobacteria (e.g. *Trichodesmium* and *Richelia*).^[57,60–62] Terrestrial nitrogen fixation is the second important field of study concerning nitrogen fixation. The most prominent organism being *Azotobacter vinelandii*. This microorganism was discovered in 1903 and has since been the focus of research related to biological nitrogen fixation.^[63] Furthermore, it was used to isolate and investigate the structure of the enzyme enabling its nitrogen fixating capabilities - the nitrogenase (see section 2.3).^[64,65] Unlike the marine and terrestrial ecosystems, there have not yet been extensive studies on nitrogen fixation in freshwater and was long considered irrelevant.^[59] Due to that reason not much is known, yet some nitrogen fixating species like the freshwater cyanobacterium *Anabaena variabilis* have been studied.^[15,59,66,67] All aforementioned species are diazotrophs meaning they use N_2 as nitrogen source in order to grow. In contrast to the Haber-Bosch process, the biological nitrogen fixation is performed under physiological conditions and although a considerable amount of biochemical energy in form of ATP is required (e.g. from photosynthesis in cyanobacteria), the reaction is more efficient in the nitrogenase compared to the industrial heterogeneous catalysis.^[66] Besides the ATP as energy source, eight protons and electrons are required for the conversion of dinitrogen to ammonia. The enzymatically catalyzed reaction is as follows:^[18]



2.2.3 Nitrogenase

Nitrogenase was isolated for the first time in 1966 by BULEN and LECOMTE, but it took another 45 years before the structure could be fully elucidated with the identification of the C^4 -carbide in the center of the active site.^[64,68–70] There are multiple isoforms of the nitrogenase. The most common and best studied is the molybdenum nitrogenase. Due to that reason, this section will focus on the Mo-Nitrogenase only. Alternative forms include a vanadium and an iron nitrogenase.^[15–17] These forms are expressed under molybdenum limiting conditions and are much more inefficient compared to the molybdenum containing nitrogenase.^[16,17] The nitrogenase complex consists of three protein units: the $\alpha_2\beta_2$ -hetero tetramer called the dinitrogenase (MoFe-protein) and two units of the dinitrogenase reductase (Fe-protein) - one on each end. Two clusters can be found in each $\alpha\beta$ -subunit of the nitrogenase. The first one is a Fe_8S_7 -cluster (P-cluster), which is involved in the electron transfer from the

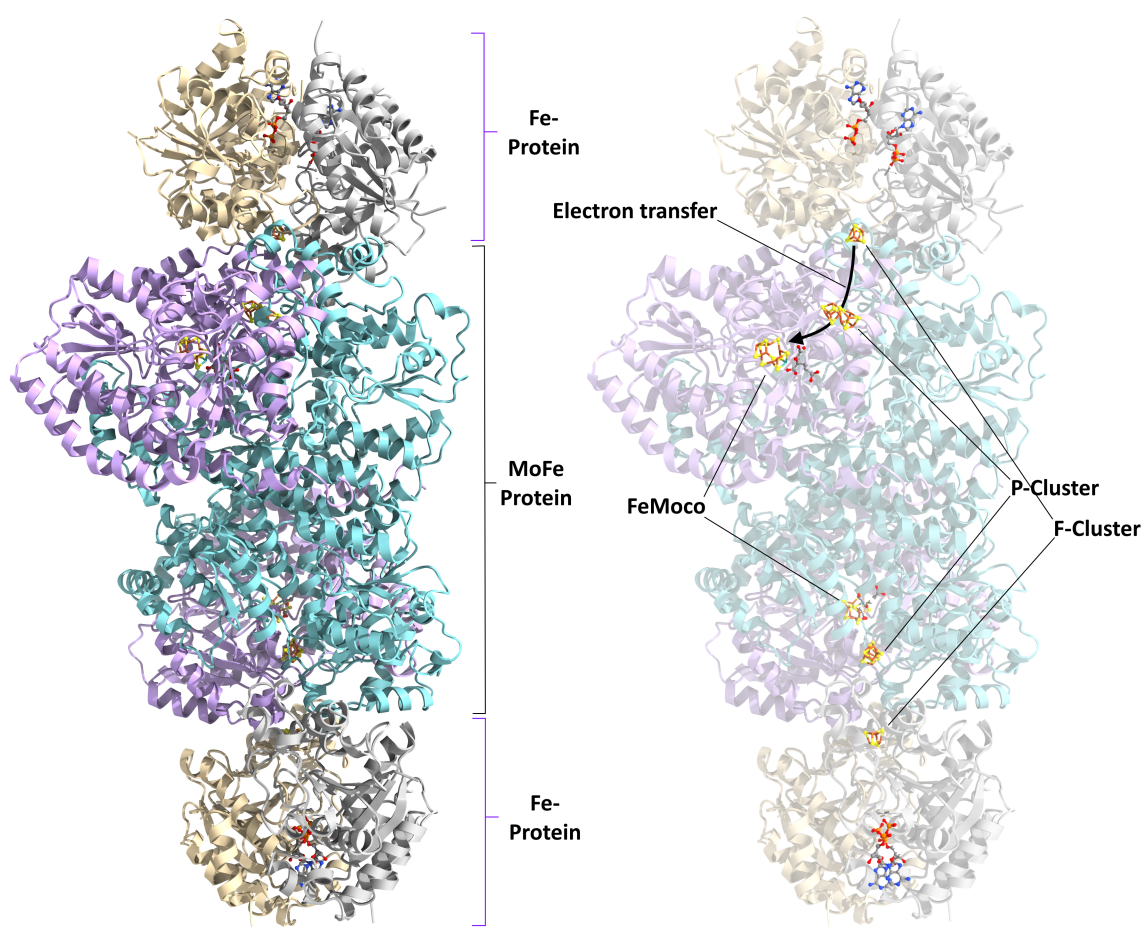


Fig. 2.3: Ribbon diagram of the Nitrogenase enzyme complex. Located within the MoFe-protein (light blue & purple) are two units of the FeMoco and the P-cluster. On both ends of the MoFe protein binds the dinitrogenase reductase also called Fe-protein (gold & silver). The active components within the Fe-protein are the F-cluster as well as 2 MgATP. This image was created using PDB entry 1N2C and ChimeraX.^[71–73]

dinitrogenase reductase to the active site of the enzyme. The P-cluster is composed of two Fe_4S_4 units, but the fourth sulfur atom of each subunit is split, so there are only seven sulfur atoms in the complete cluster (see Figure 2.4B). The reaction shown in eqn. 2.2 takes place at the active center of the dinitrogenase. The active center is an iron-sulfur cluster with an additional molybdenum, hence the name: Iron-Molybdenum-cofactor (FeMoco, see Figure 2.4A). The FeMoco is composed of a molybdenum, seven iron, nine sulfur and a very rare carbidic carbon atom as well as a coordinating homocitrate molecule. Each of the iron atoms is coordinated by three sulfur atoms. Six of the seven iron atoms also bind to the carbidic carbon atom in the center of the cluster, while the seventh iron atom saturates the remaining coordination site with the sulfur of a cysteine. The molybdenum is found in an octahedral geometry, binding three sulfur atoms a homocitrate and completed by a histidine. The cluster was first isolated in 1977, followed by the first structural models in 1978 and the first crystal

structure 1992.^[74–77] The structure revealed by the crystallography showed an unexpected structure of the FeMoco as it appears to feature a hole in the center.^[77] Technical progress made it possible to record X-ray spectra with higher resolution, which showed a light atom in this very hole.^[78] It took 19 years from the publication of the crystal data to the elucidation of the complete structure with the identification of the carbidic carbon in the center of the cluster. This missing puzzle piece was found by LANCASTER *et al.* and SPATZAL *et al.* and resulted the structure displayed in Figure 2.4A.^[74,79,80]

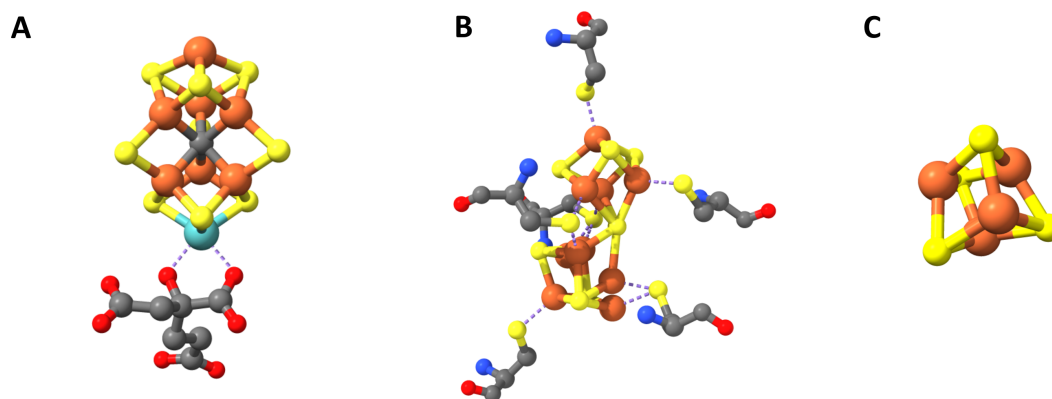


Fig. 2.4: Structure of the active site of the Nitrogenase - the iron-molybdenum cofactor (A), the P-cluster with surrounding aminoacids (B) and the F-Cluster (C) of the dinitrogenase reductase. Iron is shown in orange, sulfur in yellow, carbon in gray, nitrogen in blue, oxygen in red and the molybdenum in light blue. This image was created using PDB entries 1N2C, 3U7Q and ChimeraX.^[71–73,80]

Located between the FeMoco and the Fe-protein is the P-cluster, which is necessary for the electron transfer and the reductive function of the enzyme.^[81,82] The electron is transferred to the P-cluster from the $[\text{Fe}_4\text{S}_4]$ -cluster (F-cluster, Figure 2.4C) which is located at the interface between the dinitrogenase and dinitrogenase reductase.^[82] Within the dinitrogenase reductase the $[\text{Fe}_4\text{S}_4]$ -cluster is embedded into the structure via four cysteinyl residues two of which are provided by each γ -chain.^[83,84] Within the dinitrogenase reductase two binding sites for MgATP can be found. The MgATP plays a vital role in the mechanism in the substrate reduction activity of the nitrogenase.^[85,86] Not only is it a source of energy for the reaction, but the binding results in structural changes within the protein unit that allow the reaction to occur.^[81,83]

2.2.4 Mechanism of Nitrogenase

The elucidation of the structure of nitrogenase took several decades, but the structure is not the only aspect that concerns researchers. The mechanism of enzymatic N_2 -to- NH_3 conversion has been the focus of investigation for almost as long and is still not fully understood. The first description of the mechanism was postulated by THORNELEY and LOWE after performing a series of kinetic measurements.^[87–90] The model unifies assumptions derived from model systems prepared in the context of synthetic nitrogen fixation with kinetic experiments.^[87,89,91] CHATT stated that dihydrogen coordinated to a metal center can be displaced by dinitrogen under reductive conditions and that conversion to ammonia occurs through successive protonation and single-electron reduction steps.^[89,91] As seen from eqn. 2.2 one equivalent of hydrogen is produced with each turnover of the catalytic cycle. The catalytic cycle described in the THORNELEY-LOWE-model is divided into eight distinct one-electron steps (Figure 2.5B). The electrons needed for the catalytic cycle stem from another cycle which is intertwined with the cycle of the FeMoco. The two mechanisms are the cycle of the Fe-protein (Figure 2.5A) which transfers the electrons to the FeMoco and the catalytic cycle itself in which ammonia is generated (Figure 2.5B). During the Fe-protein cycle the cluster is found in two oxidation states. The oxidized and the reduced form in which the cluster is found in the oxidation states 1+ and 2+ respectively.^[92] Before association and electron transfer to the MoFe-protein two ATP molecules bind to the protein, changing its structural arrangement.^[93] This change in the conformation has multiple effects the first being the ability for association of Fe- and MoFe-Protein.^[93–95] In the course of the structural changes, the F-cluster is also rotated closer to the interface between the proteins, bringing it within Van der Waals reach of the P-cluster.^[93] As the iron protein is the only known electron source for the reduction and only one electron can be transferred from a protein unit, the dinitrogenase reductase cycle involves association and dissociation after every single-electron transfer.^[92,93] Comparing experimental results trying to determine the order of reaction steps in the associated state of the proteins several discrepancies arise.^[94] Depending on the method different rate constants were determined. Furthermore, the extremely sensitive protein complex and its environment-dependent properties cause deviations and differences in the experiments, respectively.^[94,96–102] Independent of the order of events concerning ATP hydrolysis and electron transfer, phosphate is released after the electron transfer and the protein complex dissociates. The hydrolysis to MgADP reverses the previous conformational change and thus prevents the precondition for the assembly of the Fe- and MoFe-proteins.^[96]

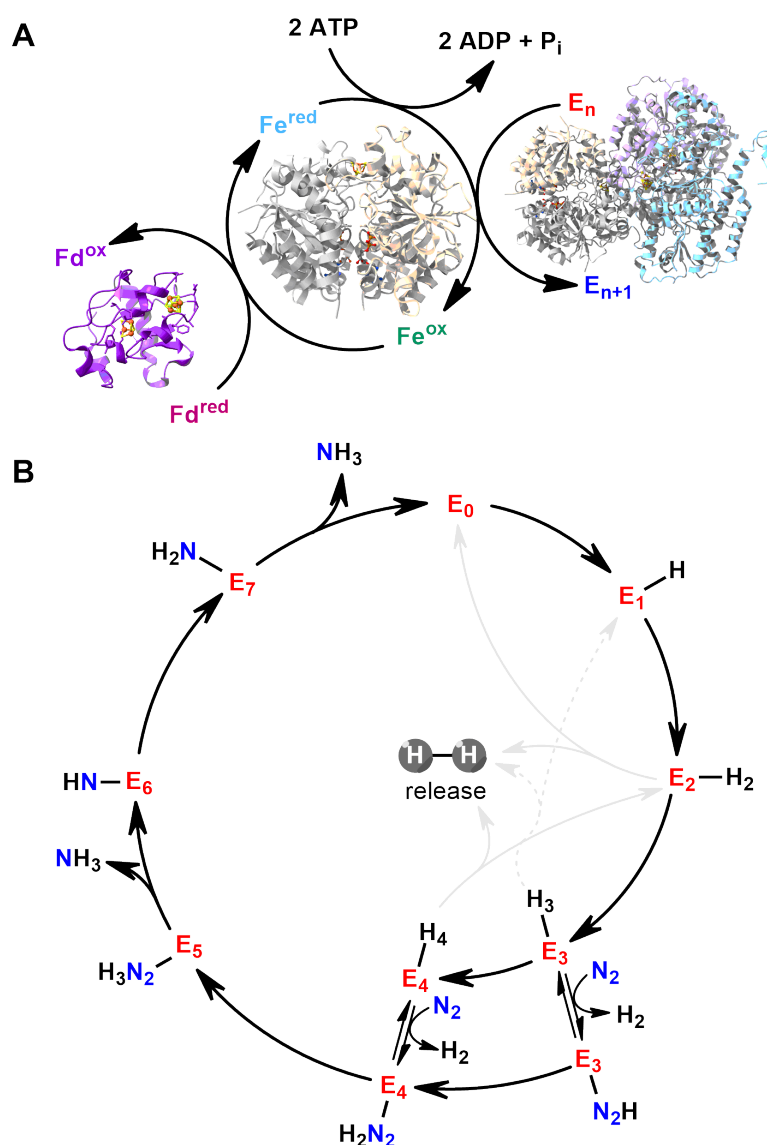


Fig. 2.5: Illustration of the THORNELEY-LOWE-model describing the catalytic cycle of the biological nitrogen fixation. Each step of the cycle is represented by an E with an index reflecting the number of electrons transferred. PDB entries 1N2C^[71] and 3U7Q^[80] were used for creating the MoFe-, Fe-protein and ferredoxine (PDB 1FRI) images in the iron cycle. Adapted from EINSLE and REES.^[89]

In the oxidized form the Fe-protein detaches from the MoFe-protein and can be regenerated by reduction. Upon reduction the MgADP is also exchanged with two MgATP molecules, allowing the cycle to start again. For each step, denoted E in Figure 2.5B, the nitrogenase and dinitrogenase reductase must associate and dissociate.^[103] Besides the ongoing investigations concerning the order of events as well as the kinetics, determination of the rate limiting step is still part of current discussions in literature.^[89,94]

The second part of the mechanism is the nitrogen reduction itself. Herein, two parts must

be considered during the cycle in the MoFe protein: The electron transfer via the P-cluster and the reactions at the active site of the enzyme. As described above, the catalytic cycle of the MoFe-protein is divided into eight steps (E_0 - E_7) following the THORNELEY-LOWE-model.^[88–90,104,105] In the first three steps (E_0 - E_3) four reduction equivalents are accumulated as bridging hydrides between the iron atoms in the FeMoco.^[104–107] The additional two protons are bound to sulfur atoms.^[104] The exact structure of the reduced state of the active site is to date not known for certain as the calculated energetics of the cluster show massive variations depending on the DFT method chosen.^[104,108,109] The key intermediate of the cycle is found in the E_4 stage which is also called the *Janus-Intermediate*. In this step, the N_2 substrate is bound to the FeMoco. The exact nature of this step is not yet fully understood and different approaches including an active role of the homocitrate ligand as a transitional proton store as well as displacement of the belt sulfurs has been discussed.^[110,111] What is known is the fact that the E_4 stage can react in two different directions: back towards the resting state E_0 or continue to protonate and reduce the N_2 .^[89,105] Continuing the path towards generation of ammonia, two general mechanisms are proposed: a distal and an alternating pathway.^[107,112,113]

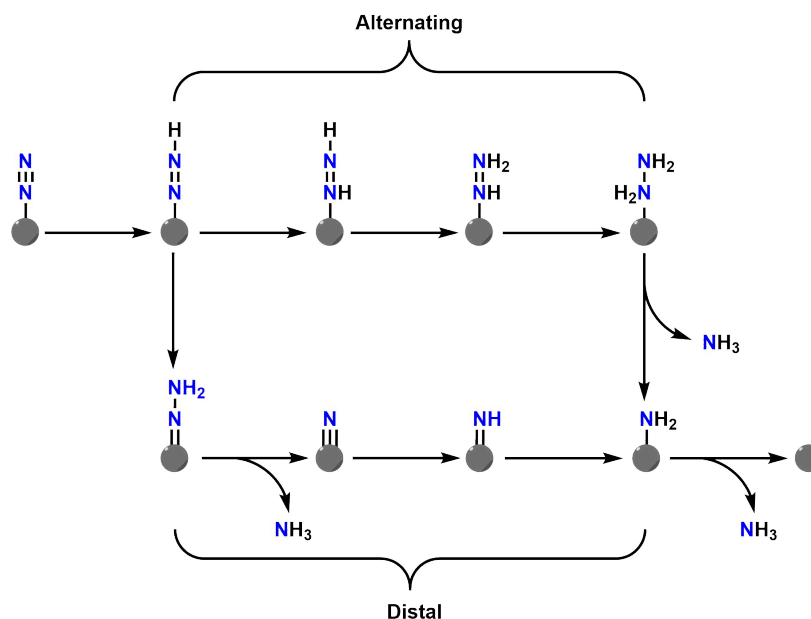


Fig. 2.6: Schematic representation of the alternating and distal mechanism of nitrogenase.^[107,113]

In the distal path, the terminal nitrogen is first protonated/reduced and then, after the formation of a nitrido species, the second equivalent ammonia is generated.^[107,113] This model is also discussed as mechanism in Chatt-type catalysts in synthetic nitrogen fixation (cf. section 2.3.1). The second pathway is the alternating mechanism. Unlike the distal mechanism, in the alternating mechanism, the nitrogen atoms are alternately protonated/reduced and the two equivalents of ammonia are released in the last two steps of the cycle.^[107,113] Although

not yet fully proven, the alternate path seems to be more likely. In addition to experimental detection of hydrazine and diazene under catalytic conditions, these compounds can also be used as substrates for the generation of ammonia by nitrogenase.^[107,114–116]

2.3 Synthetic Nitrogen Fixation

Inspired by nature, synthetic nitrogen fixation deals with the conversion of dinitrogen to ammonia using transition metal complexes. Investigations of the properties of these simpler model systems and their catalytic ability will provide important clues to the mechanism of nitrogenase. Over the decades, however, synthetic nitrogen fixation has developed into a broad branch of research in coordination chemistry, which, in addition to studying different systems and their reactivity as well as developing new catalytic pathways, is also concerned with fundamental questions of coordination chemistry.^[19,20,89,117,118] The foundation to synthetic nitrogen fixation was laid by ALLEN and SENOFF (1965) with the synthesis of the first complex bearing a dinitrogen ligand and a ruthenium center ($[\text{Ru}(\text{N}_2)(\text{NH}_3)_5]\text{X}_2$; $\text{X} = \text{Br}, \text{I}, \text{BF}_4, \text{PF}_6$).^[119] Addition of NaBH_4 to the complex with iodine counterions also generated the first amounts of ammonia.^[119] The first complex coordinating a dinitrogen from nitrogen atmosphere was reported two years later.^[120] The coordination of a dinitrogen ligand is observed by infrared spectroscopy as the coordination of the dinitrogen causes a shift to lower wavenumbers compared to free N_2 molecule.^[117] This shift is commonly referred to as activation. The further the N_2 stretch is shifted to smaller wavenumbers, the stronger the dinitrogen ligand is activated with regard to derivatization.^[21,121] The cause of the shift is found in the change of the $\text{N}\equiv\text{N}$ bonds due to the coordination to the metal center. The formation of a bond between the metal center and the nitrogen leads to an electron density transfer, which is described by the Dewar–Chatt–Duncanson model.^[122] At first electron density is transferred from the nitrogen to the metal center, known as σ -donation, followed by a π -backdonation, in which electron density is transferred from the metal center back to the ligand (Figure 2.7).^[123–125]

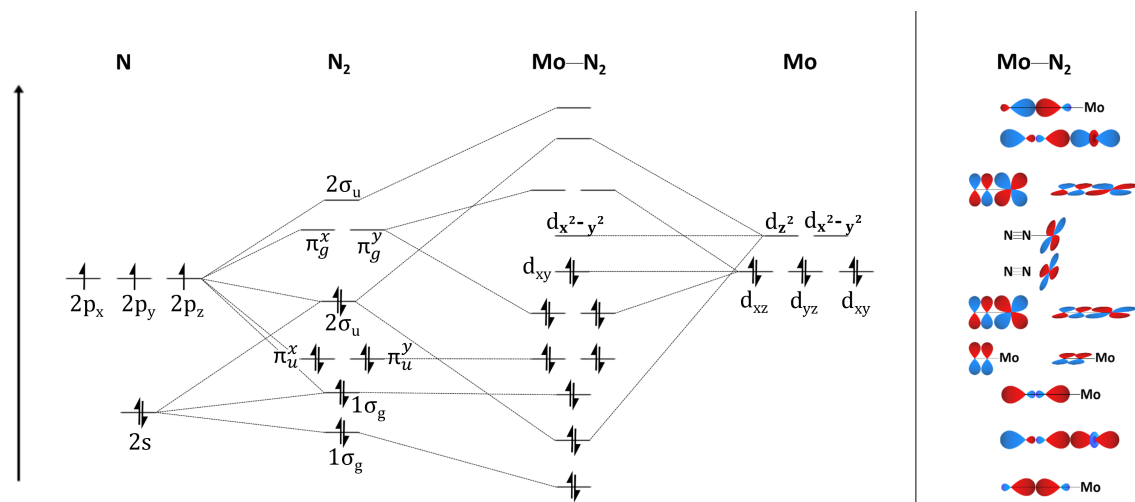


Fig. 2.7: Left: Illustration of molecular orbital scheme starting from a single nitrogen atom, to the dinitrogen molecule and finally to the bonding situation in a terminal molybdenum complex. Right: Illustration of the interacting orbitals in their respective orientation of the Mo-N₂ fragment.^[126–130]

From figure 2.7 (right) it can be seen that the σ -donation originates from the interaction of the 2σ -MO of the N₂ molecule and the d_{z^2} -orbital of the molybdenum center, while the π -backdonation results from the interaction of the $\pi^{x/y}$ -orbitals of the N₂ with the d_{xz} - and d_{yz} -orbitals. The degree of activation can be separated into different categories starting with no activation in the free N₂ molecule to high activation or even NN cleavage.^[20,131,132] Multiple factors influence the activation like the metal center, its oxidation state and the coligands completing the surrounding sphere as well as the *trans*-influence.^[21,133–137] Low oxidation states are associated with higher electron density at the metal center, which improves the ability for backdonation and enhances activation.^[131,133,138] Furthermore, early transition metals are more commonly encountered and have better activating properties compared to late transition metals as the relative energetic position between the metal and ligand orbitals is generally favored.^[137] Heavier homologues (cf. molybdenum and tungsten), although similar in structure, have a higher activation as well because of more diffuse d-orbitals.^[21,139,140] Ligand sphere and *trans*-influence are the last two main factors except the coordination mode itself. Ligands with σ -donation properties and weak to no π -acceptor properties increase the electron density on the metal center making more electron density available for the π -backdonation to the N₂-ligand, hence increasing the activation.^[21] An example for this is the comparison between aryl- and alkylphosphines as the π -acceptor properties decreases for alkylphosphines as systematized by TOLMAN and others.^[21,141–143] The strongest influence of the ligand sphere is exerted by the donor in *trans*-position of the nitrogen ligand.^[21,144,145]

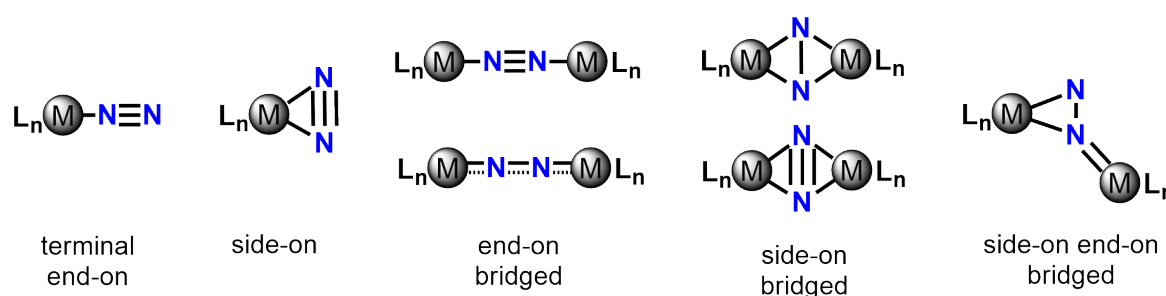


Fig. 2.8: Coordination modes of dinitrogen molecule to transition metal centers.^[123]

Dinitrogen can coordinate in 5 different ways to transition metal centers (Figure 2.8).^[21,133,136] The coordination mode is besides the ligand sphere a very important factor with regards to the activation of the ligand. In mononuclear complexes the end-on coordination mode is clearly preferred over side-on.^[135] In dinuclear systems the dinitrogen ligand can act as bridging ligand. It can act as end-on bridge, side-on bridge or in rare cases as side-on end-on bridge.^[20,123,146,147] Activation of the N_2 ligand is stronger in the end-on bridged variant compared to the end-on terminal coordination of the mononuclear complexes as can be seen from several examples in which the dinitrogen is split into nitrides between two metal centers.^[20,148–150] Nonetheless, within the context of this work the end-on terminal coordination mode is the most important as the systems investigated bare this structural feature.

In the decades following the first report by ALLEN and SENOFF, many groups have made important contributions to synthetic nitrogen fixation advancing the field even further. In the context of this thesis, the work of CHATT, SCHROCK, PETERS, and NISHIBAYASHI are particularly noteworthy and will be discussed in detail in the next sections.

2.3.1 Chatt system

10 years after the first dinitrogen complex, in 1975, substoichiometric quantities of ammonia were generated. CHATT *et al.* added sulfuric acid to different molybdenum and tungsten bis-dinitrogen complexes bearing four monodentate phosphine coligands (PMe_2Ph & $PMPh_2$).^[151] Addition of acid in methanol or tetrahydrofuran (thf) to the *cis*- $[W(N_2)_2(PMe_2Ph)_4]$ complex yielded 90% ammonia generation proving a derivatization of dinitrogen via transition metal complexes. Utilizing the similar hydrazido(2-) complex $[W(NNH_2)(OTs)(dppe)_2]^+$ ($dppe = 1,2$ -bis(diphenylphosphino)ethane), which is generated from the bisdinitrogen complex and tosylic acid, PICKETT and TALAMARIN presented the first cyclic ammonia generation under reductive conditions. They used a mercury pool cathode to generate 0.73 mol of NH_3 .^[152,153] Based on the findings of CHATT, PICKETT and TALAMARIN a catalytic cycle was postulated (Figure 2.9).^[118,154,155]

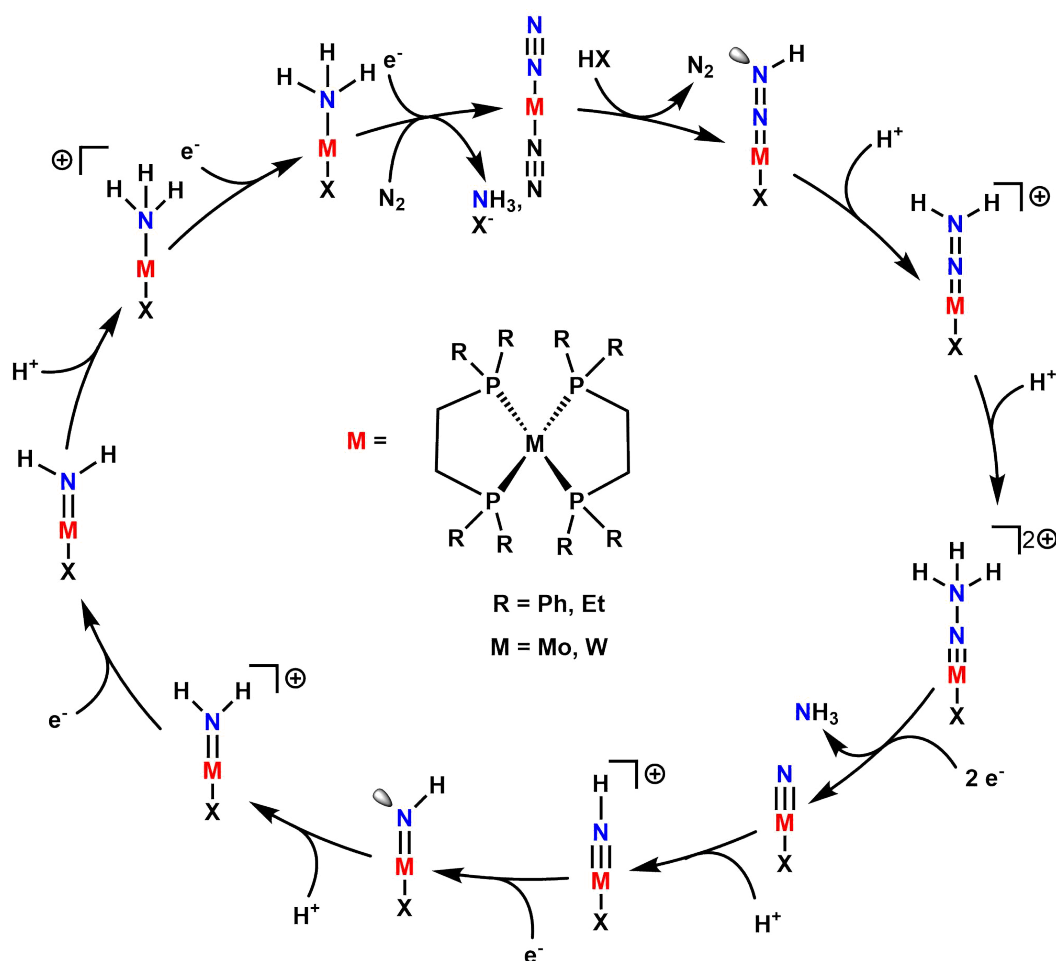


Fig. 2.9: Illustration of the CHATT cycle, in which dinitrogen is converted to ammonia by a sequence of protonating and reducing steps.^[21,154,155]

In the first step of the CHATT cycle, one of the two nitrogen ligands is exchanged by the added conjugated base while the other nitrogen ligand gets protonated at the β -nitrogen. A second protonation leads to the formation of an isodiazene complex, which is able to shift the bond arrangement into a hydrazido(2-) complex. The following reactions differ for the isodiazene- and hydrazido(2-) complex as the isodiazene complex is protonated again forming the hydrazidium complex, while the hydrazido(2-) complex is reduced in a two electron reduction upon release of the basic anion (X^-). Addition of two reduction equivalents to the hydrazidium complex results in the release of the first equivalent of ammonia from the pentacoordinated complex upon reaction with a third equivalent of acid. In both pathways the nitrido complex is formed after release of the first molecule of NH_3 .^[21,118,154–157] The cycle continues with alternating protonation and reduction steps until the second equivalent of ammonia is released from the ammine complex in a final two electron reduction step. In the course of the two-electron reduction to $Mo(0)$, two N_2 molecules are also bound and the initial complex is regenerated.^[21,118,154–157] Unfortunately, the complexes described in the

CHAT cycle were not catalytic. This can be attributed to two main reasons, the elimination of which is one of the main topics of our working group. Throughout the cycle, the metal centers occur in very high oxidation states (e.g. the nitrido stage), which can lead to a bond break between the hard metal center and the soft phosphine donors. The second problem arises from a disproportionation reaction in the last step of the cycle leading to the loss of 50% of the catalyst used.^[21]

2.3.2 Systems of the Schrock group

Due to the problems mentioned afore, the CHAT cycle is not a truly realized catalytic cycle. This milestone was achieved by SCHROCK *et al.* in 2003.^[158] They presented a molybdenum complex bearing a tetradentate ligand (Figure 2.10) which generated 7.6 equivalents of ammonia in four cycles. As a proton source [LutH][BAr^F] ([2,6-lutidinium][tetrakis-{3,5-bis(trifluoromethyl)phenyl}borate]) was employed and decamethylchromocene was added as electron source.^[158] Due to the sterically demanding ligand, the authors assume that the conversion of the nitrogen ligand to ammonia occurs only at the complex and that no binuclear species are formed during the reaction. This is also supported by experimental studies.^[158,159] Besides the catalytic reduction of dinitrogen to ammonia, the group also isolated and characterized several intermediates of a proposed catalytic cycle.^[158,159] Additional quantum chemical calculations filled the gaps of the non-isolable intermediate and thus completed the proposed cycle. Reasons for the inaccessibility can be associated with instabilities and high reactivities.^[160–162] Attempts to improve the system by altering the ligand were unsuccessful rendering the complex inactive towards dinitrogen reduction.^[163] The cycle starts with the dinitrogen complex in which the molybdenum is found in the oxidation state +III. After a sequence of three alternating protonation and one electron reduction steps, the first equivalent of ammonia is released leaving the nitrido complex.^[160,161] This sequence is repeated, generating the second ammonia molecule which is released upon exchange by a nitrogen molecule.^[160,161]

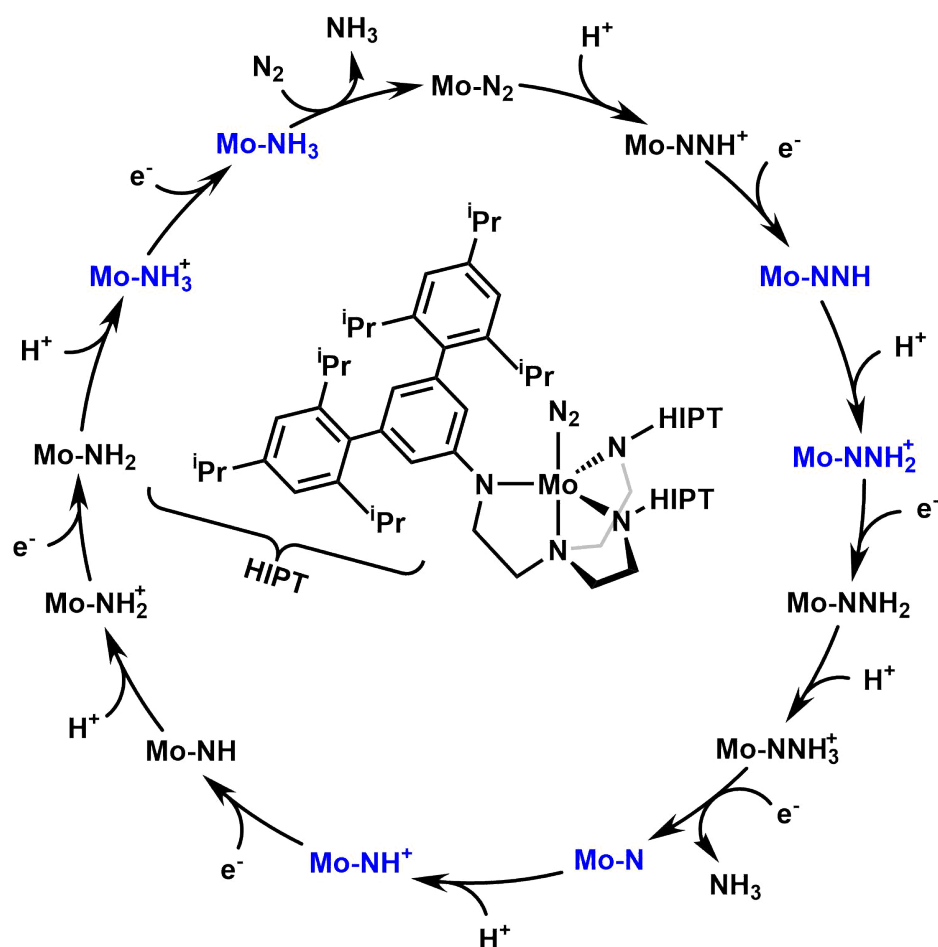


Fig. 2.10: Illustration of the SCHROCK cycle, in which dinitrogen is converted to ammonia by a strictly alternating sequence of protonating and reducing steps. The blue intermediates have been isolated.^[158–162]

The SCHROCK cycle is very similar to the CHATT cycle as both of them follow a distal mechanism: first the β -nitrogen atom is converted to ammonia followed by the α -nitrogen. The main differences are: 1) the protonation and reduction steps are strictly alternating in the SCHROCK cycle while two protonation steps are followed by the reduction by two electrons in the CHATT cycle (cf. Figure 2.9; hydrazido(2-) path) and 2) the oxidation states of the metal center are different throughout the cycle. Besides the unsuccessful variation of the ligand, SCHROCK *et al.* also exchanged the molybdenum center with tungsten. Unfortunately, this exchange rendered the system catalytically inactive as well. Although they were able to isolate several intermediates associated with the cycle, only 1.51 equivalents of ammonia were generated leading to the conclusion that the initial catalyst is not recovered.^[164] It was found that the W(NH₃) complex does not convert to the W–N₂ complex even when the system is exposed to pressure under nitrogen atmosphere (55 bar). Furthermore, the equilibrium found between the molybdenum variants of the complexes is very different compared to the one of the W(NH₃)- and W(N₂)-complexes.^[164]

In 2017 SCHROCK *et al.* presented a pincer based system with a higher catalytic activity than the original SCHROCK system. This amine based pincer (Figure 2.11) was able to generate 10.3 equiv. of ammonia using diphenylammonium triflate and decamethylcobaltocene. The complex presented is not a dinitrogen complex but a molybdenum(IV) nitride complex with a *tert*-butyl alcohol coligand.^[165]

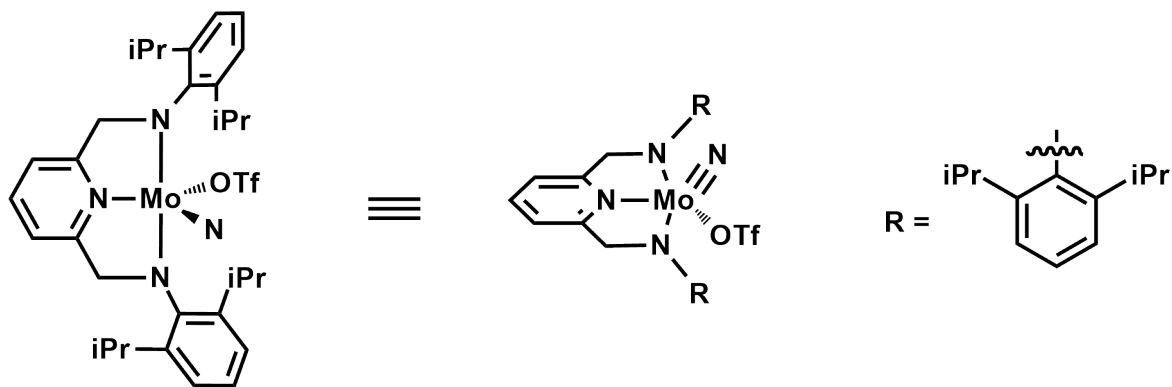


Fig. 2.11: The pincer based system by SCHROCK *et al.*^[165]

A special feature of the Schrock systems compared to most other complexes in synthetic nitrogen fixation is the use of amine donors. Usually, phosphine donors are used in nitrogen fixation because they have very good donor properties and form stable complexes.^[21,155]

2.3.3 Systems of Peters' group

Although iron is mainly discussed to be the active site of the nitrogenase, synthetic nitrogen fixation mostly evolves around molybdenum and tungsten complexes. The PETERS group set another important milestone as they presented the first iron based catalyst capable of N_2 -to- NH_3 reduction, using an iron dinitrogen complex bearing the tris[*o*-(diisopropylphosphino)phenyl]borane ligand (P_3^{B} , Figure 2.12 left).^[166]

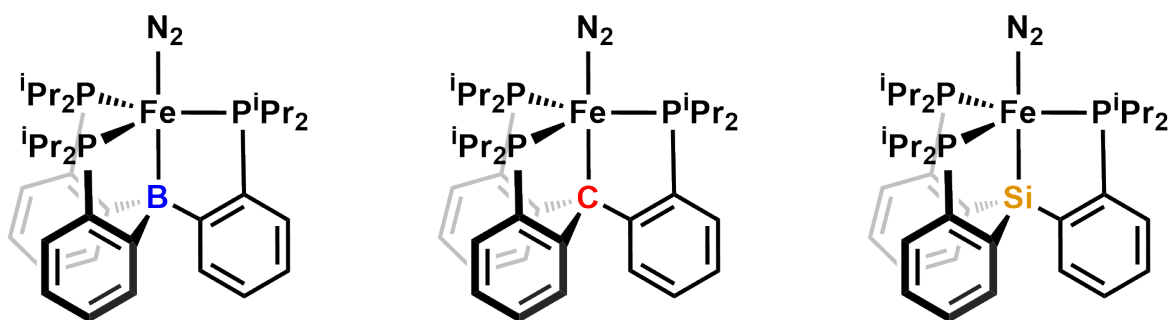


Fig. 2.12: Iron dinitrogen complexes bearing the variations of the ligand for synthetic nitrogen fixation developed by PETERS *et al.*^[166,167]

Addition of HBAr^{F} and KC_8 yielded 7 equivalents of ammonia.^[166] The amount of ammonia was increased drastically (to 64 equiv.) by increasing the amount proton- and electron sources.^[167] Further optimization and additional irradiation of the solution increased the ammonia yield again to 94 equivalents.^[168] Unlike the reactions presented by CHATT and SCHROCK, this catalysis is not carried out under ambient conditions, but at a temperature of $-78\text{ }^\circ\text{C}$. Exchanging the reducing agent as well as the acid with less potent compounds ($[\text{Ph}_2\text{NH}_2]\text{OTf}$ and Cp_2^*Co) a yield of 89 equivalents of ammonia were generated - still using the presented iron system.^[169] The peculiarity of this combination lies in the transfer mode of the protons and reduction equivalents as the combination of the Cp_2^*Co with the acid acts as PCET reagent (PCET = **P**roton **C**oupled **E**lectron **T**ransfer).^[169] This insight was used as a starting point towards electrocatalytic nitrogen fixation, which the group demonstrated in 2018 using $[\text{Cp}_2^*\text{Co}]^+$, $[\text{Fe}(\text{N}_2)(\text{P}_3^{\text{B}})]^-$ and anilinium acids in controlled potential electrolysis experiments. In this way, 6.7 equivalents of ammonia could be generated.^[170] The main issue of electrocatalytic ammonia generation is the competing hydrogen evolution reaction which is often dominating.^[169,170] Early, yet unsuccessful attempts used a mercury pool electrode as the overpotential of mercury allows more negative potentials.^[152,171,172] In 2022 the group found an alternative approach towards electrocatalysis by employing a mediator complex that accepts the electrons from the cathode and transfers them as a PCET agent to the actual catalyst (Figure 2.13).^[173]

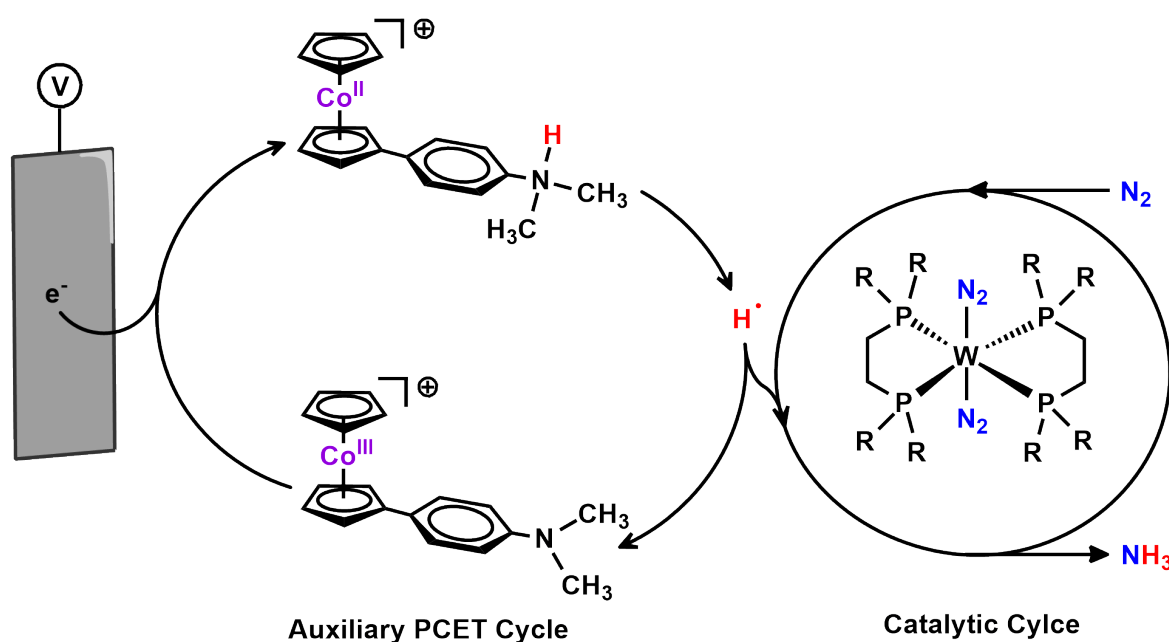


Fig. 2.13: Illustration of the PCET mediated electrochemical N_2 -to- NH_3 reduction by PETERS *et al.*, exemplified with a tungsten bisdinitrogen complex. Edited after.^[173]

A number of catalysts were investigated using this approach, with the best producing 40 equiv. of ammonia.^[173] Interestingly, the best catalyst was found to be the very complex employed in the original experiments by PICKETT and TALAMIN in 1985. In the same year the group could also demonstrate direct electrocatalysis on a pyridine based pincer system. Starting from the well known $[\text{MoBr}_3(\text{PNP}^{\text{tBu}})]$ complex 11.7 equiv. NH_3 were generated.^[174] These impressive results were achieved by very conscious selection of the components involved.

Parallel to the efforts invested into the $[\text{Fe}(\text{N}_2)(\text{P}_3^{\text{B}})]^-$ complex the PETERS group also investigated the influence of the donor *trans* to the dinitrogen ligand by synthesizing two variants of the P_3^{B} ligand. The boron was exchanged by carbon (P_3^{C}) (Figure 2.12 middle) as well as silicon (P_3^{Si}) (Figure 2.12 right).^[167] However, the catalytic activity of the corresponding iron complexes was lower than that of the $[\text{Fe}(\text{N}_2)(\text{P}_3^{\text{B}})]^-$ complex. 47 equiv. of ammonia were found for the $[\text{Fe}(\text{N}_2)(\text{P}_3^{\text{C}})]^-$ complex, while $[\text{Fe}(\text{N}_2)(\text{P}_3^{\text{Si}})]^-$ generated only 4.4 equiv.^[167] Not only variations of the ligands were investigated but also different metal centers. Using the least active P_3^{Si} ligand low valent dinitrogen complexes with osmium and ruthenium centers were synthesized.^[175,176] Using large amounts of $[\text{Ph}_2\text{NH}_2][\text{OTf}]$ (1500 equiv.) and Cp_2^*Co (1800 equiv.) the osmium complex was able to generate 120 equivalents of NH_3 .^[176]

2.3.4 Systems of the Nishibayashi group

The NISHIBAYASHI group focuses on pincer based systems. Per definition pincer ligands are rigid ligands that enforce a meridional coordination geometry.^[177] Not only their variability, but also their often high catalytic activity has increased interest in pincer-based systems in recent decades.^[178–180] The catalytic activity is often related to the rigidity and high thermal stability of the complexes allowing well defined catalytic reactions.^[179–183] Although the term pincer is now used in a broadened sense from its original definition, it usually refers to a tridentate system with 3 donor atoms. Often, amines in the form of pyridines or carbenes are found at the central position. Typical groups for linkage are amines or CH₂-groups but also silicone groups are well known modifications.^[182–185] The NISHIBAYASHI group utilizes pincer ligands to develop very active catalysts for synthetic nitrogen fixation. The first system presented by the group capable of catalytic N₂ reduction was an end-on bridged binuclear molybdenum complex bearing a PNP pincer with P^tBu₂ donors on each center (Figure 2.14B). The ligand sphere was completed by two more N₂ ligands on each molybdenum (Figure 2.14A).^[186] The best results were achieved by addition of [LutH][OTf] and Cp₂Co with 23.2 equiv. of ammonia were generated per dinuclear complex.^[186] Based on these initial results, the PNP pincer ligand was modified by variation of the substituents on the phosphine donors and in the *para*-position of the pyridine.^[187,188] Variation of one of the phosphines, and thereby creating asymmetric catalysts, did not increase the amount of ammonia generated,^[187] but introduction of different groups on the pyridine ring increased the nitrogen conversion up to 34 equiv. with a methoxy group.^[188] This could be improved again (52 equiv. NH₃) by increasing the added protons and reduction sources. A comparable result with 31 equiv. was found for the 4-methyl-pyridine.^[188] In 2015 the system was modified again by exchanging the methoxy group by a ferrocene moiety, which could generate two equivalents more under the same conditions as the methoxy system.^[189] Besides the PNP pincer and its modified variants, the group also presented results evolving around a PCP pincer with a *N*-heterocyclic carbene (NHC) as central donor.^[190] Using the [Mo(N₂)₂(PCP)₂(μ-N₂)] complex and large amounts of [LutH][OTf] and [Cp₂^{*}Co] (1920 and 1440 equiv.) the complex generated 230 equiv. of ammonia.^[190]

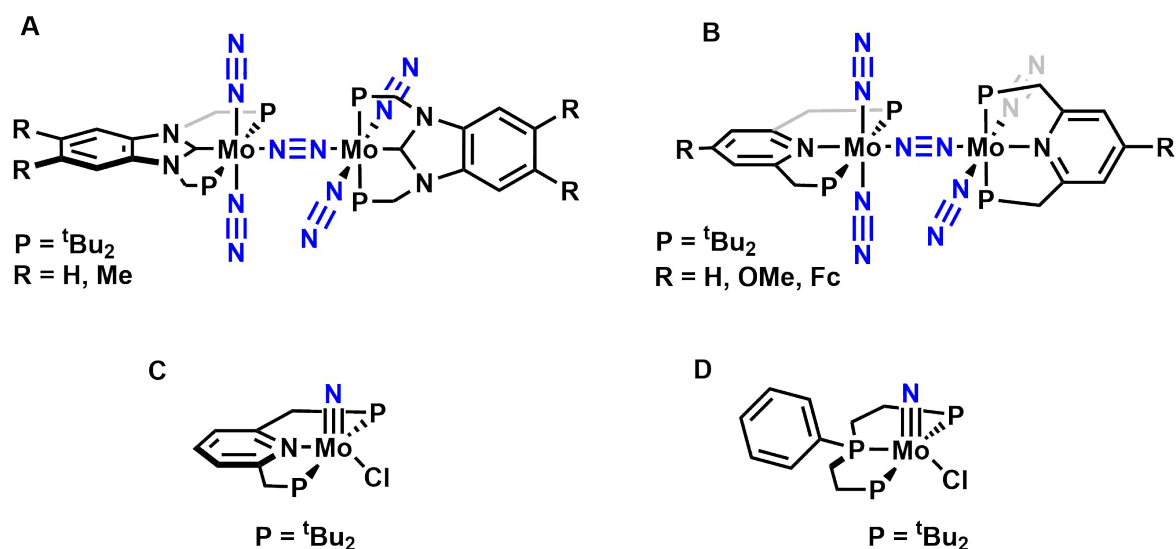


Fig. 2.14: Selection of complexes used for synthetic nitrogen fixation by NISHIBAYASHI *et al.*^[186,190–192]

The dinuclear systems were not the only ones in the scope of the NISHIBAYASHI group. Using the PNP^{tBu} pincer ligand and starting from $[MoCl_3(thf)_3]$ they generated the nitrido complex $[MoNCl(PNP)]$ (Figure 2.14C), which was also catalytically active towards N_2 reduction. Using this complex, $[LutH][OTf]$ and Cp_2Co a total of 6.6 equiv. of ammonia were generated.^[191] This type of nitrido complex was also obtained by use of a tridentate triphosphine ligand, whose catalytic activity was significantly higher in comparison.^[192] The ligand is composed of a central phenyl phosphine which is connected to two terminal di-*tert*-butyl phosphine groups via ethyl bridges (Figure 2.14D). Addition of Cp_2^*Co (540 equiv.) and 2,4,6-trimethylpyridinium triflate ($[ColH][OTf]$, 720 equiv.) yielded a total of 63 equiv. of ammonia.^[192] Use of these two reagents as proton and electron source, while starting from the molybdenum(III) precursor $[MoI_3(thf)_3]$, in combination with their well established PNP pincer, they managed to obtain a staggering amount of 415 equiv. of ammonia.^[193]

A major breakthrough was presented that shows parallels to the work of PETERS *et al.* As found for the iron systems, using a PCET agent greatly improved the catalytic activity of the aforementioned pincer systems. The PCET agent used is a combination of samarium diiodide and water or simple alcohols such as methanol, ethylene glycol or ethanol.^[194] Using 180 equiv. of SmI_2 and ethylene glycol the $[MoI_3(PNP)]$ complex bearing two P^{tBu_2} groups generated 42.8 equiv. of ammonia while the corresponding nitrido complex generated 50.0 equiv. For the end-on bridged dinitrogen complex bearing the NHC pincer ligand this combination generated 53.3 equiv. of ammonia.^[194] The mononuclear trichlorido molybdenum complex bearing this NHC pincer yielded 4350 equiv. of ammonia upon reaction with SmI_2/H_2O (14400 equivalents each). This effective catalyst is the first system to use water as proton source to generate ammonia.^[194] The use of water proofed to yield larger amounts of ammonia compared to the small alcohols. In 2023 the group presented a trichlorido molybdenum complex bearing a

modified PCP (similar to Figure 2.14 A, with R = CF₃ & H), which is even more active and generated 60.000 ± 4300 equiv. of ammonia per Mo.^[195] The difference in reactivity is very well expressed by the use of classical Chatt type complexes which under protic and reductive conditions were not catalytically as they face some problems during the catalytic cycle (cf. section 2.3.1). Application of the SmI₂/H₂O allowed for catalytic ammonia generation using these simple molybdenum complexes.^[196] Notably, the reaction pathway is expected to differ from the CHATT cycle described above. The *trans*-[Mo(N₂)₂(PMe₂Ph)₄] complex resulted 40 equiv. of ammonia while the *in situ* generated complex with two equivalents of dpppe (1,5-bis-(diphenylphosphino)-pentane) from MoI₃(thf)₃ resulted 46 equiv. NH₃. Increasing the amount of PCET agent, this could be scaled to 83 equiv. of ammonia.^[196] The approach with samarium diiodide and water/alcohols are the first conditions in which a CHATT-type system is capable of catalytic ammonia generation. The second example for this is presented by our group (section 2.3.5).^[197] Interestingly, the tungsten analogues were not catalytic under these conditions.^[197] Investigations concerning the mechanism are a major focus of the NISHIBAYASHI group. Several approaches based on experimental findings and DFT calculations a likely mechanism involves a bridged intermediate with a dinuclear molybdenum complex that splits the bridging dinitrogen ligand into nitrides.^[197,198] In order to gain further insights into the mechanism, they presented a detailed study on the structure of the SmI₂/H₂O structures formed in solution.^[199] Other than predicted previously, the experimental results point towards the formation of samarium water and samarium thf complexes, depending on the amount of water, without direct Sm-I bonds.^[200]

Besides the molybdenum based systems, the group also presented several studies investigating the activity of pincer complexes with other transition metal centers including iron,^[201] cobalt,^[202] chromium,^[203] vanadium,^[204,205] rhenium^[206,207] and manganese.^[208] Although the ligands used all belong to the pincer category and the terminal phosphines chosen bare ^tBu₂ substituents, they were very different as were the conditions used in order to obtain catalytic activity. To elaborate on these system a few examples will be explained more detailed. The iron system was based on an anionic PCP pincer with the anionic center being on the central benzene. Upon addition of 8000 equiv. of KC₈ and 7360 equiv. of HBar^F 252 equiv. of ammonia and 68 equiv. of hydrazine were generated.^[201] Rhenium complexes bearing the pyridine based PNP pincer or a variant with a slight modification in the 4-position generated between 3 and 9 equiv. of ammonia with 800 equiv. of KC₈ and 800 equiv. of [HPCy₃][Bar^F].^[206] The cobalt system was very different as the ammonia was generated by hydrolysis of a previously formed silylamine. A cobalt dinitrogen complex bearing the PNP pincer was reacted with 600 equiv. KC₈ and Me₃SiCl. Addition of acid yielded a total of 44 equiv. of ammonia. Scaling this reaction to 6000 equiv. of substrate, 351 equiv. of ammonia were found.^[202]

The latest approach of the group involves light driven ammonia generation.^[200] Using a molybdenum catalysts (e.g. [MoI₃(PCP)]) and photoactive cocatalysts, they were able to

catalytically generate ammonia upon irradiation.^[200] The $[\text{MoI}_3(\text{PCP})]$ complex generated 29.5 equiv. of ammonia. This was increased by slight modification of the ligand. Introduction of a CF_3 -group on one side of the benzimidazole backbone increased the yield to 41.3 ± 6.2 equiv. of ammonia.^[200]

2.3.5 Systems of the Tuczek group

The TUCZEK group focuses on CHATT type systems. As described above the classical CHATT systems are facing two major problems (cf. section 2.3.1). The first problem occurs in the nitrido stage, where the oxidation state of the molybdenum center is high, making it a hard Lewis acid that can lead to decoordination of the phosphine donors. The second problem occurs in the regeneration of the catalysts in the last step. In addition to the desired regeneration of the catalyst, a disproportionation reaction occurs that produces inactive dihalide complexes.^[21,154] This side reaction leads to a catalyst loss of about 50% with each run of the cycle.^[21,154] The TUCZEK group is addressing precisely these two points and developing CHATT type systems that attempt to circumvent these problems. This is done in two ways: suppression of the disproportionation reaction by occupation of the *trans*-position to the dinitrogen, which could also enhance the activation of the ligand, and the decoordination in the high oxidation states is counteracted by increasing the stability by exploiting the chelating effect of multidentate ligands. At first two main strategies were pursued in order to fulfill the set goals. The ligands which meet both criteria for bypassing the problems of the CHATT cycle were characterized by tripodal or tridentate structural motifs. The tripodal ligands are usually based on either an *iso*-butyl or *neo*-pentyl backbone.^[209–211] The backbone and tripodal geometry of the ligand enforces a facial coordination of the ligand. With addition of a bidentate coligand and reductive conditions mono-dinitrogen complexes were synthesized.^[209–211] Besides the *iso*-butyl and *neo*-pentyl backbones, our group also succeeded in synthesizing dinitrogen complexes bearing a cyclohexane based tripod and a tripodal system similar to the *neo*-pentyl system but the quaternary carbon was substituted by silicon.^[212–215] Unlike the other tripodal systems, coordination of the cyclohexyl-based ligand requires higher temperatures and reaction times because the donors must be oriented in the axial direction for coordination, which is the less favorable conformation.^[212] The silicon substituted ligand was used to investigate the different influence of alkyl- and aryl-phosphines as donors. It was found that by subsequent exchange of diarylphosphine by dimethylphosphine led to an increase in activation of the N_2 ligand.^[212] Comparison of the tripod/diphos combination bearing all PMe_2 -donors to a mono-dinitrogen complex bearing five PMe_3 -donors showed a lower activation for the tripodal complex, illustrating the effect of steric influence on activation.^[213,215] To gain further insight into the sterical aspect similar study was performed by SÖNCKSEN *et al.* who chose the *iso*-butyl (when more than one iPr_2 groups were involved) based tripod ligand and sequentially substituted diphenylphosphine by the sterically demanding diisopropylphosphine. Interestingly,

the increase in steric demand lead to the formation of the bis-dinitrogen complexes whereas the complex bearing only arylphosphines formed the mono-dinitrogen complex.^[210] A similar study was performed by PFEIL *et al.* who prepared ligands containing between 1 and 3 phospholano groups. Phospholano groups are characterized by different behavior as found from regular alkylphosphines.^[216–218] For the phospholano tripod - even with three phospholano groups - the mono-dinitrogen complex was found as long as dpmm (diphenylphosphinomethane) was used as coligand.^[216,218] The activation found for the N₂ ligand in the complex with three phospholano groups is lower compared to its PMe₂ analogue but higher than the complex with all diphenylphosphine.^[216] An important way to tune the activation and thereby the reactivity towards derivatization is careful selection of the *trans* ligand.^[145] The activation should also be increased by substitution of the donor in *trans*-position to the dinitrogen ligand. Coordination of an amine donor *trans* to the N₂ should increase the activation due to elimination of π -acceptor properties, hence increasing the electron density on the molybdenum and further weaken the N \equiv N-triple bond.^[219] Unfortunately, the mono-dinitrogen complex bearing the tripodal ligand with two phosphines and a diethylamine residue could not be obtained, due to the weak coordination behavior of the amine. The product obtained instead was the bisdinitrogen variant.^[219]

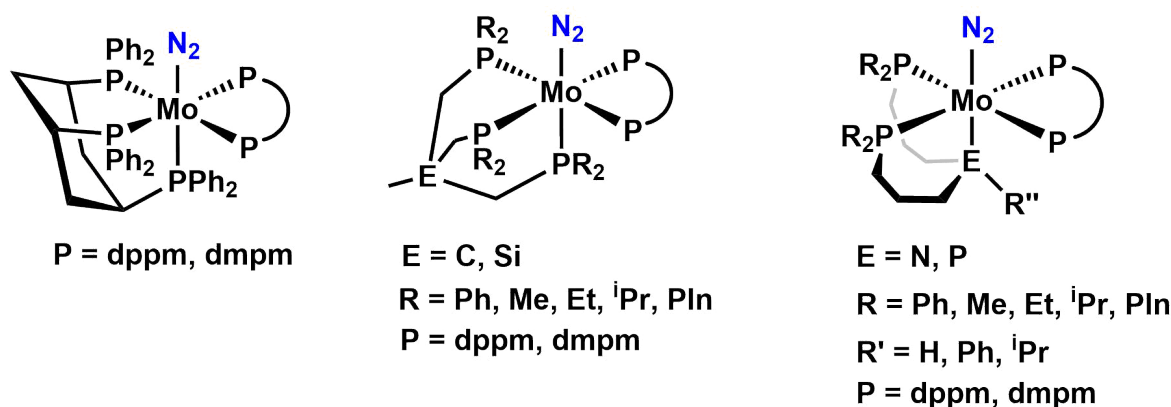


Fig. 2.15: Examples of different nitrogen complexes synthesized by the TUCZEK group for synthetic nitrogen fixation.^[214,215,218–223]

In addition to the tripodal systems, the TUCZEK group also investigated nitrogen complexes bearing tridentate and pincer ligands.^[145,220,221,224] Following on from the work of GEORGE *et al.*, who prepared nitrogen complexes with different tridentate ligands, the group also investigated the influence of different substituents on the donor atoms, as well as the influence of phosphine and amine donors in *trans* position to the dinitrogen ligand.^[145,225,226] The findings of this group regarding the tridentate systems will be discussed in detail in the introduction to chapter 4 as it focuses around tridentate PNP ligands.

Marrying the two concepts of tridentate and tripodal ligands, a new singular ligand with pentaphosphine environment emerged, resulting in a pentadentate tetrapodal ligand (pentaPod).

This concept not only eliminates the need for an additional coligand, but also increases the chelate effect even more, stabilizing the corresponding complexes. Furthermore it creates a single site CHATT-type catalyst which would go hand in hand with improved elucidation opportunities regarding the mechanism.

The first generation of the pentaPod ($P_2^{Ph}PP_2^{Ph}$) featured only PPh_2 donors besides the phosphine donor linking the tripodal and tridentate part. Coordination of the ligand to $[MoCl_3(thf)_3]$ turned out to be quite difficult due to the topology of the precursor and the two possible coordination modes.^[222] As the Mo(III) complex is in meridional arrangement, the tridentate part is favored, which was experimentally proven by EPR spectroscopy. Due to this preference the complex has to undergo severe structural changes in order to form the desired mono-dinitrogen complex. It was found that upon reduction several species were formed some of which appear to be coordination polymers with the ligand interconnecting molybdenum centers.^[222,227] Adapted from the silicon based tripod ligand, a modified version of the pentaPod with a silicon in the tripodal backbone was synthesized. Using this approach a mono-dinitrogen complex was obtained. Like the tripod systems the resulting complex was labile against acids and due to the difficult synthesis could not be obtained in its pure form.^[222]

The problems of the first generation system, which were, among other things, due to the insufficient reactivity differences of the terminal phosphines, were resolved in the second generation of the pentaPod ligand ($P_2^{Me}PP_2^{Ph}$, Figure 2.16).^[222] Substitution of the diphenylphosphine groups on the tripod site by dimethylphosphine introduced nucleophilic gradient into the system with the PMe_2 groups, favoring the *facial* geometry in the Mo(III) stage and enabling the isolation of a mono-dinitrogen complex upon reduction bearing the entire pentaPod ligand.^[222,227] The $[Mo(N_2)(P_2^{Me}PP_2^{Ph})]$ complex not only showed the expected AA'XX'M pattern in the ^{31}P NMR spectrum but also a very strong activation of the N_2 ligand as can be seen from the stretching vibration ($\nu_{NN} = 1929\text{ cm}^{-1}$) in the IR spectrum.^[222,227]

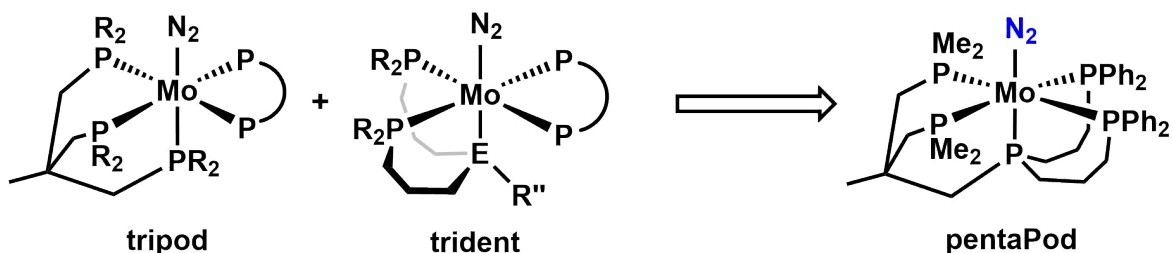


Fig. 2.16: The pentaPod concept arose from combination of the tridentate PPP and tripodal PPP ligands.^[222,227]

Although the activation of the N_2 ligand is high and the corresponding hydrazido(2-) complex was obtained, the complex did not show any catalytic behavior under conditions reported by PETERS *et al.* or NISHIBAYASHI *et al.*^[222,223,227,228] The only system found to be active under

these type of conditions found in our group is the PN^3P pincer system reported by STUCKE *et al.*, which generated 3.12 equiv. of NH_3 using Cp_2^*Cr and $[\text{ColH}][\text{OTf}]$ (Figure 2.17).^[229]

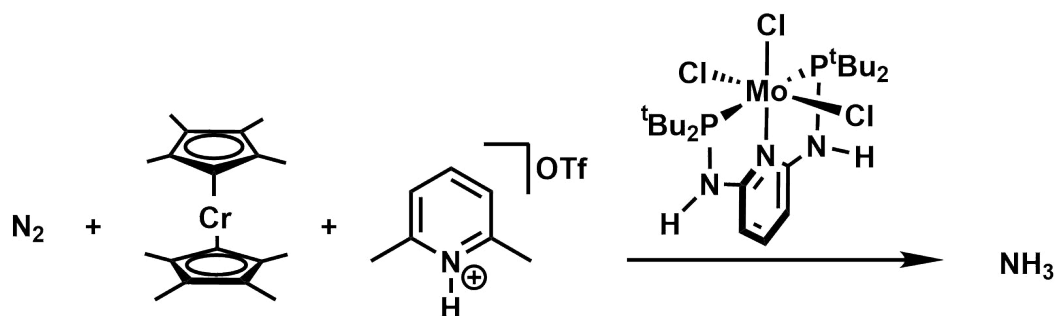


Fig. 2.17: $[\text{MoCl}_3(\text{PN}^3\text{P})]$ complex synthesized by STUCKE capable of ammonia generation (3.12 equiv.) upon addition of $[\text{Cp}_2^*\text{Cr}]$ and $[\text{ColH}][\text{OTf}]$. This is the first system of the TUCZEK group which exhibited catalytic activity.^[229]

Although the first attempts towards the catalytic activity of the pentaPod systems were not successful the development continued. JUNGE *et al.* succeed in coordinating to the $\text{P}_2^{\text{Me}}\text{PP}_2^{\text{Ph}}$ ligand to Rh and Ru. The resulting complexes were used towards activation of small molecules such as CN^- or N_3^- .^[230]

Project 1

Even though a variety of different combinations of acids and reducing agents were tested, no successful catalytic generation of ammonia was achieved until the proton coupled electron transfer (PCET) approach presented by NISHIBAYASHI was applied. Using samarium diiodide and water in thf the pentaPod dinitrogen complex exhibited catalytic behavior. Using this method 25.7 equiv. of ammonia were generated.^[231] To investigate the role of the ligand as an aspect of the newly discovered catalytic activity, similar mono-dinitrogen complexes with pentaphosphine environment were synthesized and tested towards their catalytic activity. The complexes prepared were a *neo*-pentyl based tripodal PPP ligand bearing all terminal PPh₂ groups with a dmpm (dimethylphosphinomethane) coligand and the analogue tridentate variant with the prPPHP ligand, which is also used as tridentate building block for the pentaPod ligand. Both complexes were tested toward their catalytic activity under identical conditions as the pentaPod complex, however, only substoichiometric amounts of ammonia were found, proofing the effectiveness of the pentaPod concept.^[231] The system is a single coordination site CHATT-type catalyst and one of the main intermediates of the CHATT cycle is the hydrazido(2-) complex, ENGESSER *et al.* were also able to isolate and thoroughly characterize the corresponding NNH₂ complex after protonation with HBar^F.^[231] In order to prove the role of the [Mo(NNH₂)(P₂^{Me}PP₂^{Ph})]Bar^F complex in the catalytic cycle, this complex was also used as catalyst with SmI₂/H₂O. Due to stability issues in the required solvent, the complex was generated *in situ* and added to the PCET-agent containing solution. This approach yielded 26.1 equiv. of ammonia proving the hydrazido(2-) stage to be an entry point in the catalytic cycle.^[231]

Chatt systems do not only involve molybdenum but also tungsten complexes. In fact the first systems of the CHATT-type complexes that yielded the best results for ammonia generation (90 %) were the *cis*-[W(N₂)₂(PMePh₂)₄] complex by CHATT *et al.* and the [W(NNH₂)(OTs)(dppe)₂]⁺ complex employed for electrocatalysis by PICKETT and TALAMARIN.^[151–153] Besides molybdenum, tungsten is another transition metal often found in synthetic nitrogen fixation. Due to its important role and the effectiveness of the pentaPod concept, combination of tungsten and the pentaPod complex is an interesting approach, which will be the first project presented in this thesis.

3.1 Tungsten and molybdenum dinitrogen complexes supported by a pentadentate tetrapodal phosphine ligand: comparative spectroscopic, electrochemical and reactivity studies

In this study we present the tungsten analogue of the previously reported molybdenum(N_2)-pentaPod complex.^[140,227] The synthetic access to the tungsten complex is a bit different as the precursor ($[\text{WCl}_3(\kappa^3\text{-P}_2^{\text{Me}}\text{PP}_2^{\text{Ph}})]$) to the $[\text{W}(\text{N}_2)(\text{P}_2^{\text{Me}}\text{PP}_2^{\text{Ph}})]$ complex is obtained from a tungsten(IV) complex ($[\text{WCl}_4(\text{PMePh}_2)_2]$), which is reduced to the tungsten(III) complex bearing the pentaPod via oxidation of a PMePh_2 ligand. After sodium amalgam reduction, the desired tungsten mono-dinitrogen complex was obtained. Besides the characterization by IR and NMR spectroscopy, single crystals suitable for single crystal structure determination were obtained. Comparison of the crystal structure data of the $[\text{W}(\text{N}_2)(\text{P}_2^{\text{Me}}\text{PP}_2^{\text{Ph}})]$ complex to its molybdenum analogue showed almost identical bond length and angles. The $\text{N}\equiv\text{N}$ stretch, which is commonly used as an indicator for the activation of the dinitrogen, was observed at 1901 cm^{-1} . The N_2 ligand is therefore more activated in the tungsten complex. The higher activation, despite identical structure, can be attributed to more diffused d-orbitals in the tungsten.^[21] Although the activation was higher the catalytic activity with $\text{SmI}_2/\text{H}_2\text{O}$ towards ammonia generation was lower than found for the molybdenum analogue.^[231] Nonetheless, 2.8 equiv. of ammonia were found, thus being the first catalytically active tungsten system reported, proving again the peculiarity of the pentaPod ligand. A theory as to why the molybdenum complex was much more active was that the complexes may have different redox potentials and the reduction potential of SmI_2 maybe being insufficient to reduce the tungsten complex back to the $\text{W}(0)$ stage. In order to investigate this theory and gain further insight into the characteristics of both complexes, electrochemical and spectroelectrochemical investigations were performed. From cyclic voltammetry very similar redox potentials were found excluding our theory. Furthermore, a fully reversible system was found for the first oxidation of the tungsten complex while the first redox event was not fully reversible for the molybdenum complex. Combination of IR spectroscopy and electrochemistry revealed some interesting differences between the molybdenum and tungsten complexes on the +I oxidation state. While the $\text{N}\equiv\text{N}$ stretch vanished upon oxidation for the molybdenum complex while the $\text{N}\equiv\text{N}$ -stretch of the $[\text{W-N}_2]$ complex shifted from 1915 cm^{-1} ($\text{N}\equiv\text{N}$ -stretch in solution) to 1951 cm^{-1} . From this observation it can be deduced that the oxidized tungsten complex is more stable than the molybdenum complex. This also explains the observations at the second redox system which is irreversible at low scan rates for the tungsten complex but gets more reversible with increasing scan rates meaning the rate of the electron transfer gets faster than the dissociation of the N_2 ligand. For the molybdenum complex the second redox system was found to be irreversible and independent of the scan rate.

Reprinted with permission from J. Junge, S. Froitzheim, T. A. Engesser, J. Krahmer, C. Näther, N. Le Poul and F. Tucek, Dalton Trans., 2022, 51, 6166-6176.

<https://doi.org/10.1039/D1DT04212B>

DOI: 10.1039/D1DT04212B Copyright ©2022 The Royal Society of Chemistry

Dalton Transactions

An international journal of inorganic chemistry
rsc.li/dalton

Volume 51
Number 16
28 April 2022
Pages 6115-6488



ISSN 1477-9226



PAPER

Nicolas Le Poul, Felix Tucek *et al.*
Tungsten and molybdenum dinitrogen complexes supported by a pentadentate tetrapodal phosphine ligand: comparative spectroscopic, electrochemical and reactivity studies

PAPER

View Article Online
View Journal | View IssueCite this: *Dalton Trans.*, 2022, **51**, 6166

Tungsten and molybdenum dinitrogen complexes supported by a pentadentate tetrapodal phosphine ligand: comparative spectroscopic, electrochemical and reactivity studies†

Jannik Junge,^{‡a} Sven Froitzheim,^{‡a} Tobias A. Engesser,^{§a} Jan Krahmer,^a Christian Näther,^{§a} Nicolas Le Poul^{§*b} and Felix Tuczek^{§*a}

The tungsten dinitrogen complex $[\text{W}(\text{N}_2)(\text{P}^{\text{Me}}_2\text{PP}^{\text{Ph}}_2)]$ (**2**) ($\text{P}^{\text{Me}}_2\text{PP}^{\text{Ph}}_2 = [2-\{[\text{bis}(3\text{-}(\text{diphenylphosphino})\text{propyl}]\text{-phosphino})\text{methyl}\}-2\text{-methylpropane-1,3-diyl}]\text{bis}(\text{dimethylphosphine})]$) is synthesized and characterized by X-ray diffraction as well as IR and NMR spectroscopies, showing strong analogies to its molybdenum analogue $[\text{Mo}(\text{N}_2)(\text{P}^{\text{Me}}_2\text{PP}^{\text{Ph}}_2)]$ (**1**). Whereas cyclic voltammetry studies indicate very similar redox potentials, detailed electrochemical and IR-spectroelectrochemical investigations reveal characteristic differences between **1** and **2** upon electrochemical oxidation in THF. Protonation of **2** with HBAr^{F} ($\text{BAr}^{\text{F}} = \text{tetrakis}(3,5\text{-bis}(\text{trifluoromethyl})\text{-phenyl})\text{borate}$) leads to the hydrazido(2-) derivative **3** which is spectroscopically characterized as well. In the presence of $\text{SmI}_2/\text{H}_2\text{O}$ slightly overstoichiometric conversion of N_2 to ammonia (2.75 equiv.) is observed. Although this is far below the activity of the Mo-complex **1**, it renders **2** the first W complex to produce more than 2 equivalents of NH_3 from N_2 upon addition of protons and reductant.

Received 15th December 2021,
Accepted 8th March 2022

DOI: 10.1039/d1dt04212b

rsc.li/dalton

Introduction

The conversion of dinitrogen to ammonia under ambient conditions is one of the most challenging tasks of bioinorganic chemistry.¹ In nature, microorganisms which contain the enzyme nitrogenase perform this reaction.² In industry, ammonia is produced with the Haber–Bosch process, involving drastic conditions.³ The activation of the highly inert dinitrogen molecule and the catalytic N_2 -to- NH_3 conversion by transition metal complexes have been subjects of research for decades. While Allen and Senoff succeeded in synthesizing the first dinitrogen complex in 1965,⁴ the groups of Chatt and Hidai demonstrated the generation of ammonia from molybdenum and tungsten bis(dinitrogen) complexes with up to 90% yield.⁵ Later on, Pickett and Talarmin were able to electrochemically generate 0.73 equivalents of ammonia in a cyclic process.⁶ The first truly catalytic system was developed by

Schrock *et al.* in 2003 based on the molybdenum triamidoamine complex $[\text{Mo}(\text{N}_2)((\text{HIPT-NCCH}_2\text{CH}_2)_3\text{N})]$ (HIPT = hexaisopropylterphenyl).^{7,8} Using molybdenum complexes supported by different pincer ligands along with various protonating and reducing agents Nishibayashi *et al.* could gradually increase the amount of ammonia.⁹ The best results were obtained with SmI_2 and H_2O , employing a Mo(III) complex with a PCP-pincer ligand as precatalyst.¹⁰

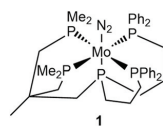
Differences in reactivity between molybdenum and tungsten complexes have been of continued interest in nitrogen fixation.¹ Whereas $[\text{W}(\text{N}_2)_2(\text{PMePh}_2)_4]$ is known to stoichiometrically generate ammonia upon addition of H_2SO_4 ¹¹ and $[\text{W}(\text{N}_2)_2(\text{dppe})_2]$ has been employed as redox mediator in an electrocatalytic formation of NH_3 from N_2 ,¹² no (chemo)catalytic activity of tungsten complexes has been observed so far,^{7,13,14} in contrast to their molybdenum congeners. Sometimes, tungsten analogues of molybdenum catalysts could not be prepared,¹³ and even if the former were synthetically accessible, they so far always turned out to be catalytically inactive.¹⁴ For the tungsten triamidoamine system, it was speculated that, due to a more negative reduction potential of the $\text{W}(\text{I})\text{-NH}_3$ intermediate as compared to its Mo(I) analogue, the starting dinitrogen complex could not be reformed with the employed reductant.¹⁴ On the other hand, oxidation potentials for the corresponding Mo(0) and W(0) N_2 -complexes turned out to be quite similar.¹⁴

^aInstitut für Anorganische Chemie, CAU Kiel, Max-Eyth-Str. 2, 24118 Kiel, Germany. E-mail: f.tuczek@ac.uni-kiel.de

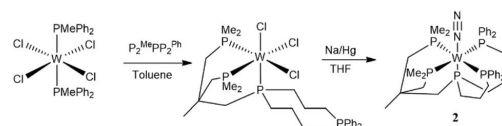
^bLaboratoire de Chimie, Électrochimie Moléculaires et Chimie Analytique (UMR CNRS 6521), Université de Bretagne Occidentale, 6 Avenue Le Gorgeu, 29238 Brest, France. E-mail: Lepoul@univ-brest.fr

† Electronic supplementary information (ESI) available. CCDC 2127859. For ESI and crystallographic data in CIF or other electronic format see DOI: 10.1039/d1dt04212b

‡ The authors contributed equally to this paper.



Scheme 1 Molybdenum dinitrogen complex $[\text{Mo}(\text{N}_2)(\text{P}^{\text{Me}_2}\text{PP}^{\text{Ph}_2})]$ (**1**) supported by a pentadentate tetrapodal phosphine ligand.¹⁵



Scheme 2 Synthesis of $[\text{W}(\text{N}_2)(\text{P}^{\text{Me}_2}\text{PP}^{\text{Ph}_2})]$ (**2**).

In 2016, our working group presented the molybdenum dinitrogen complex $[\text{Mo}(\text{N}_2)(\text{P}^{\text{Me}_2}\text{PP}^{\text{Ph}_2})]$ (**1**) supported by the pentadentate tetrapodal (pentaPod) ligand $\text{P}^{\text{Me}_2}\text{PP}^{\text{Ph}_2}$ (Scheme 1).¹⁵ This system was, with 26 equivalents of NH_3 , the first catalytic single-coordination site complex which follows the mechanism of the so-called Chatt cycle, showing that the pentaPod ligand eliminates the problems encountered with Chatt complexes; *i.e.*, the loss of 50% of the catalyst for each cycle and the dissociation of the M–P bonds which can occur at higher oxidation states when ligands with lower denticity are used.¹⁶

Despite the fact that this Mo(0) dinitrogen complex and its hydrazido(2-) derivative were found to be active catalysts, DFT calculations of the N–H bond dissociation free energy (BDFE) of the respective diazenido complex in the framework of a PCET mechanism indicated that the reaction path could also involve a cationic, mononuclear $\text{Mo}^{\text{I}}(\text{N}_2)^+$ intermediate.¹⁶

In order to gain more information about the differing behaviour of molybdenum and tungsten complexes towards catalytic N_2 -to- NH_3 conversion, we herein present the tungsten dinitrogen complex $[\text{W}(\text{N}_2)(\text{P}^{\text{Me}_2}\text{PP}^{\text{Ph}_2})]$ (**2**) supported by the above-mentioned pentaPod ligand for comparative investigations with its molybdenum analogue (**1**). Notably, with $[\text{W}(\text{N}_2)(\text{PMe}_3)_5]$, there has been only one example of a tungsten dinitrogen complex with a pentaphosphine environment so far.¹⁷ Moreover, in order to determine the role of $\text{M}^{\text{I}}(\text{N}_2)^+$ complexes during the catalytic process, the electrochemical properties of the $\text{M}^{\text{I}}(\text{N}_2)$ pentaPod complexes ($\text{M} = \text{Mo}$ (**1**) and W (**2**)) as well as the stabilities of their one-electron oxidized $\text{M}^{\text{I}}(\text{N}_2)^+$ counterparts are investigated. To this end, cyclic voltammetry investigations combined with *in situ* IR-spectroelectrochemical experiments are conducted on **1** and **2**. Finally, the reactivities of the W complex **2** towards acids and the reduction of N_2 to ammonia using $\text{SmI}_2/\text{H}_2\text{O}$ are investigated and compared with results obtained on the analogous molybdenum system **1**. The implications of the experimental findings regarding the role of the two metal centers in synthetic nitrogen fixation and the corresponding mechanistic pathways are discussed.

Results and discussion

Synthesis and characterization of the W– N_2 complex $[\text{W}(\text{N}_2)(\text{P}^{\text{Me}_2}\text{PP}^{\text{Ph}_2})]$ (**2**)

The synthesis and characterization of the Mo(N_2) complex $[\text{Mo}(\text{N}_2)(\text{P}^{\text{Me}_2}\text{PP}^{\text{Ph}_2})]$ (**1**) was described before.^{15,16} The analogous

tungsten(0) dinitrogen complex **2** was synthesized by sodium amalgam reduction of $[\text{WCl}_3(\kappa^3\text{-P}^{\text{Me}_2}\text{PP}^{\text{Ph}_2})]$ (for EPR and IR data see Fig. S1, S2 and Table S1†). This W(III) complex with a pre-coordinated pentaPod ligand was in turn obtained through reaction of $\text{P}^{\text{Me}_2}\text{PP}^{\text{Ph}_2}$ with $[\text{WCl}_4(\text{PMePh}_2)_2]$ in toluene (Scheme 2). Thereby the released methyl-diphenylphosphine partly acts to reduce W(IV) to W(III), being converted to methyl-diphenylphosphine dichloride.¹⁸

In agreement with Mo(N_2) complexes exhibiting a topologically related pentaphosphine coordination,^{15,19} the ^{31}P NMR spectrum of **2** exhibits an AA'MXX' pattern (Fig. 1b, c and Fig. S3–S11;† minor impurities (<5%) derive from oxidized complex and free ligand). In order to obtain information about the bonding situation between the coordinated N_2 ligand, the tungsten atom and the phosphine ligands, the ^{15}N -labelled complex was synthesized and the couplings were analyzed by NMR (Fig. 1a). ^{183}W satellites were detected with $^1J_{\text{W-P}}$ coupling constants between 254 Hz and 315 Hz, similar to the values found in the literature for a comparable complex.¹⁷

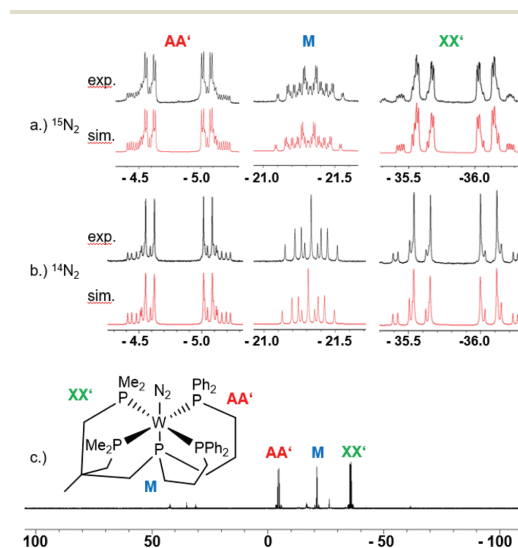


Fig. 1 Experimental and simulated $^{31}\text{P}\{^1\text{H}\}$ NMR spectra of $^{15}\text{N}_2$ -**2** (a) and **2** (b). (c) Overall spectrum of **2** in tetrahydrofuran- d_8 at 300 K. The signals were assigned based on the ^1H – ^{31}P -HMBC NMR spectrum (Fig. S10†).

Table 1 Chemical shift and coupling constants of $[\text{Mo}(\text{N}_2)(\text{P}^{\text{Me}}_2\text{PP}^{\text{Ph}}_2)]$ (1),¹⁵ $[\text{W}(\text{N}_2)(\text{P}^{\text{Me}}_2\text{PP}^{\text{Ph}}_2)]$ (2), $[\text{Mo}(\text{NNH}_2)(\text{P}^{\text{Me}}_2\text{PP}^{\text{Ph}}_2)]^{2+}$ 16 and $[\text{W}(\text{NNH}_2)(\text{P}^{\text{Me}}_2\text{PP}^{\text{Ph}}_2)]^{2+}$ (3). AA', M and XX' refer to Fig. 1

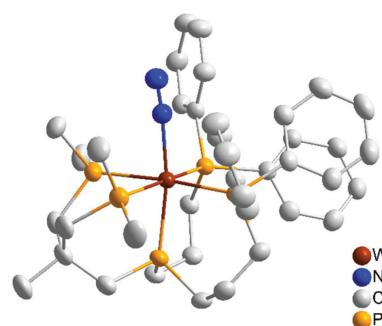
Complex	δ/ppm			J/Hz						Ref.
	M	AA'	XX'	$J_{\text{MA/MA'}}$	$J_{\text{MX/MX'}}$	$J_{\text{AA'}}$	$J_{\text{AX/A'X}}$	$J_{\text{AX/A'X'}}$	$J_{\text{XX'}}$	
$[\text{W}(\text{N}_2)]$ (2)	−21.3	−4.8	−35.8	11.2	18.5	4.5	85.7	−11.1	17.4	This study
$[\text{Mo}(\text{N}_2)]$ (1)	12.4	25.5	−3.7	20.4	28.7	14.7	83.4	−19.8	27.4	15
Δ	−33.7	−30.3	−32.1	−9.2	−10.2	−10.2	2.3	8.7	−10.0	
$[\text{W}(\text{NNH}_2)]^{2+}$ (3)	−48.5	−15.9	−45.8	28.2	31.3	6.3	53.9	−12.2	16.1	This study
$[\text{Mo}(\text{NNH}_2)]^{2+}$	−32.3	11.4	−14.7	32.7	39.1	16.5	56.5	−20.8	26.9	15
Δ	−16.2	−27.3	−31.1	−4.5	−7.8	−10.2	−2.6	8.6	−10.8	

Mo = $\text{Mo}(\text{P}^{\text{Me}}_2\text{PP}^{\text{Ph}}_2)$; W = $\text{W}(\text{P}^{\text{Me}}_2\text{PP}^{\text{Ph}}_2)$.

Comparison between the ^{31}P NMR spectrum of the tungsten complex with the molybdenum analogue showed a high-field shift of the tungsten signals between −30 and −34 ppm. In addition, the *cis* coupling constants in the tungsten complex all are about 10 Hz smaller than in the molybdenum complex whereas the *trans* coupling constants of both complexes are about equal (Table 1). Similar trends have been described in the literature.²⁰ The ^{15}N – ^{15}N and the ^{15}N – ^{31}P coupling constants differ by less than 1 Hz between 1 and 2 (see Table S2†).

IR spectroscopy of crystalline 2 shows an N–N stretching vibration at 1901 cm^{-1} which shifts to 1840 cm^{-1} for the ^{15}N isotope labelled complex (^{15}N -2; for an analysis of the IR spectra see Table S3†). Notably, this frequency is lower than $\nu(\text{NN})$ determined for the Mo analogue 1 (1929 cm^{-1}) (Fig. 2).¹⁵

By layering a benzene solution with *n*-pentane, single crystals of 2 could be obtained. X-ray analysis shows a molecular structure with a pentaphosphine environment, thus confirming the results of ^{31}P NMR spectroscopy (Fig. 3, for crystal data see ESI Fig. S12 and Table S4†). Comparison with the molyb-

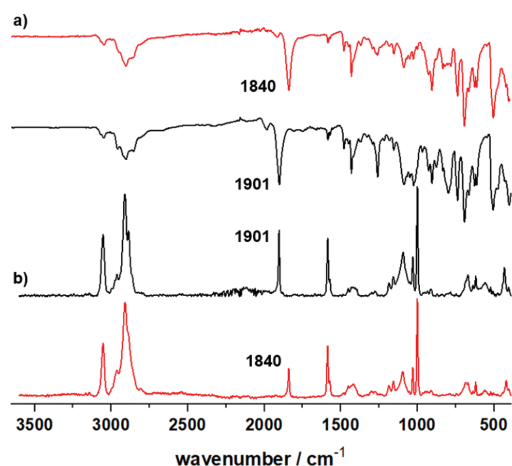
**Fig. 3** Single-crystal structure of $[\text{W}(\text{N}_2)(\text{P}^{\text{Me}}_2\text{PP}^{\text{Ph}}_2)]$ (2). Thermal ellipsoids are shown at the 50% probability level. The hydrogen atoms have been omitted for clarity.

denum analogue shows similar metal–ligand bond lengths which agrees with the literature and can be explained with almost the same ionic radius (Table S5†).^{17,21} The N_α – N_β bond distance is also practically identical to that of the Mo complex (Table S6†).

The ligand sphere of 2 corresponds to a distorted octahedron with the $\text{P}_{\text{ax}}\text{--W--N}_\alpha$ angle ($170.65(9)^\circ$) significantly deviating from linearity. Notably, the W--P_{ax} bond length ($2.3828(1)\text{ \AA}$) is shorter than the average W--P_{eq} bond length (2.4375 \AA , Fig. 3). In the other known tungsten dinitrogen complex with a pentaphosphine ligation, $[\text{W}(\text{N}_2)(\text{PMe}_3)_5]$,¹⁷ the M--P bond length of the phosphine in *trans* position to the N_2 ligand is longer than the M--P bond lengths of the equatorial phosphines. The shortening of the *trans* M--P bond length thus appears to be due the topology of the pentaPod ligand. As already noticed for the Mo-complex 1, this does not cause an elongation of the M--N_2 bond ($\text{W--N}_\alpha = 2.020(5)\text{ \AA}$, $\text{Mo--N}_\alpha = 2.033(5)\text{ \AA}$), indicating that the *trans*-phosphine, apart from being a strong σ -donor, also exhibits a significant degree of π -backbonding.

Electro- and spectroelectrochemical studies

Cyclic voltammetry and IR spectroelectrochemistry were carried out in order to determine the redox potentials and

**Fig. 2** (a) IR and (b) Raman spectra of 2 (black) and $^{15}\text{N}_2$ -2 (red).

characterize the species formed upon oxidation of the tungsten(0) and molybdenum(0) pentapod-N₂ complexes 2 and 1, respectively. The studies were performed in dry THF/NaBPh₄ (20 mM) under argon atmosphere in a glovebox. Since both complexes are extremely sensitive, their stability in THF/NaBPh₄ was first checked by IR spectroscopy. In that electrolyte, no change in the N₂ stretching signal could be observed over 6 days, ensuring that the electrochemical results can in fact be assigned to the tungsten and molybdenum N₂ species.

Cyclic voltammetry at a Pt electrode was first performed at different scan rates ($0.02 \text{ V s}^{-1} < \nu < 5 \text{ V s}^{-1}$) for the tungsten complex 2. In reduction, no cathodic peak could be observed at potentials down to the limit where electrolyte reduction occurs ($-2.9 \text{ V vs. Fc}^+/\text{Fc}$). On the anodic side, for low-to-moderate scan rates ($0.02 \text{ V s}^{-1} < \nu < 0.2 \text{ V s}^{-1}$), two main systems were detected upon oxidation, the first one being reversible at $E_{1/2}(1) = -1.16 \text{ V}$ while the other appeared as irreversible at *ca.* $E_{\text{pa}}(2) = -0.25 \text{ V vs. Fc}^+/\text{Fc}$ (Fig. 4A). When increasing ν up to 5 V s^{-1} , the second system displayed more reversibility (Fig. 4B) whereas the first remained fully reversible, hence suggesting that a moderately fast (ms) chemical process follows the second oxidation. Linear plots of the anodic peak current i_{pa} vs. $\nu^{1/2}$ (Fig. S13A†) not only pointed to a diffusion-limited process for the first oxidation, but also allowed the determination of the number of electrons from the Randles-Sevcik equation,²² applying a diffusion coefficient $D = 9.5 \times 10^{-6} \text{ cm}^2 \text{ s}^{-1}$ determined by ¹H NMR DOSY for the W(N₂) complex 2 (see

ESI Fig. S14†). This treatment indicated that the latter process is a one-electron redox event. In addition, the anodic peak current function ($i_{\text{pa}} \nu^{-1/2}$) was plotted against ν for both oxidation processes. As clearly shown in Fig. 4C, the value of $i_{\text{pa}}(1) \nu^{-1/2}$ remains relatively constant whatever ν for the first oxidation, as expected for a simple electron transfer. However, for the second oxidation process, a significant increase of $i_{\text{pa}}(2) \nu^{-1/2}$ is detected for $\nu < 0.2 \text{ V s}^{-1}$. This is consistent with a multiple electron transfer that is kinetically limited by a chemical process, as classically found for an ECE mechanism (E = electrochemical, C = chemical).²² The chemical process is likely here a N₂-solvent ligand exchange at the W(II) redox state,²³ which is followed by an electrochemical oxidation, generating a W(III) species (Scheme 3).

In order to characterize the species generated at the first and second oxidation processes, IR-spectroelectrochemical studies were performed for [W(N₂)(P^{Me}₂PP^{Ph}₂)] (2, see Experimental part for details). As shown in Fig. 4D, oxidation at $E_{\text{pa}}(1)$ caused disappearance of the N₂ band at 1915 cm^{-1} concomitant with the emergence of a new band at 1951 cm^{-1} . Switching back the potential to its initial value allowed complete recovery of the original infrared spectrum. This demonstrates the full reversibility of the process, in agreement with low-scan-rate CV studies. Upon further oxidation at $E_{\text{pa}}(2)$, the newly-formed band at 1951 cm^{-1} disappeared and could only be obtained upon back-reduction to the initial potential (Fig. S13D†).

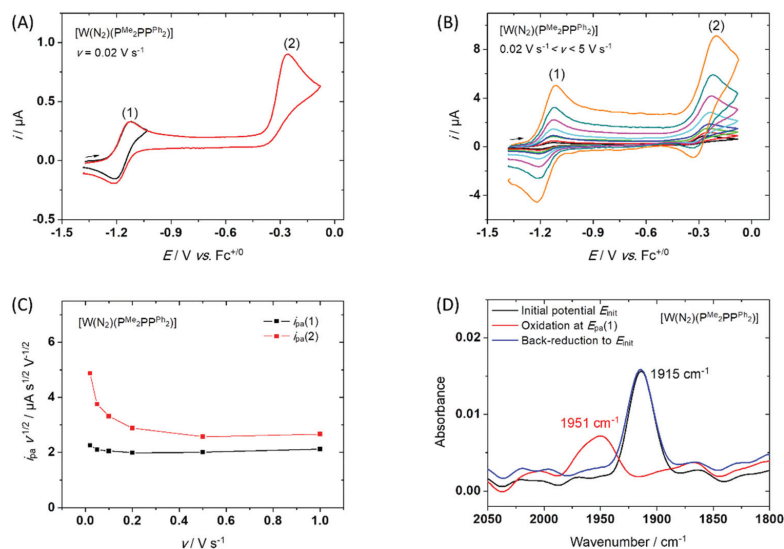
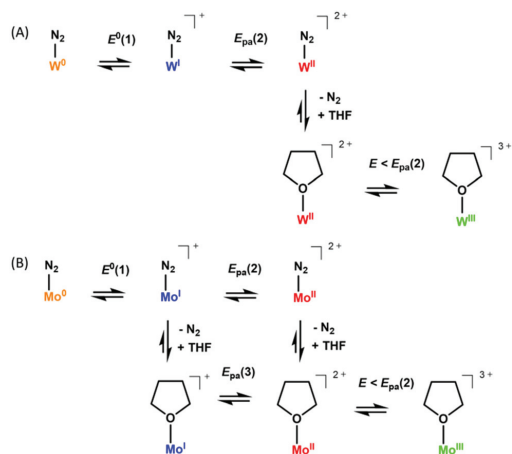


Fig. 4 CVs ($E/\text{V vs. Fc}^+/\text{Fc}$) at a Pt working electrode (diam. 1 mm) of [W(N₂)(P^{Me}₂PP^{Ph}₂)] (0.4 mM) in THF/NaBPh₄ 0.02 M (A) at $\nu = 0.02 \text{ V s}^{-1}$ and (B) for $\nu = 0.02 \text{ V s}^{-1}$ (black), 0.05 V s^{-1} (red), 0.1 V s^{-1} (green), 0.2 V s^{-1} (blue), 0.5 V s^{-1} (cyan), 1 V s^{-1} (pink), 2 V s^{-1} (olive) and 5 V s^{-1} (orange); the numbers (1) and (2) on the graphics are related to the redox systems, see details in text. (C) Plots of $i_{\text{pa}}(1) \nu^{-1/2}$ (black squares) and $i_{\text{pa}}(2) \nu^{-1/2}$ (red squares) against ν from CV data in (B); (D) infrared spectra of [W(N₂)(P^{Me}₂PP^{Ph}₂)] (15 mM) in THF/NaBPh₄ 20 mM recorded during *in situ* spectroelectrochemical measurements before (black) and after oxidation at $E_{\text{pa}}(1)$ (red), then returning back to the initial potential (blue).

Paper



Scheme 3 Proposed mechanism for the oxidation processes of the tungsten (A) and molybdenum (B) pentaPod N_2 complexes.

Aiming at determining the role of the metal in the described redox processes, we carried out the same experiments for $[Mo(N_2)(P^{Me}_2PP^{Ph}_2)]$ (1). CV studies revealed several differences compared to the W- N_2 complex. For instance, the

first oxidation process at $E_{1/2}(1)$ was found to be not fully reversible at low scan rate ($\nu < 0.1 \text{ V s}^{-1}$). Moreover, a supplementary irreversible anodic peak at $E_{pa}(3)$ (ca. $-0.7 \text{ V vs. Fc}^+/Fc$) was detected for $\nu < 0.5 \text{ V s}^{-1}$ (Fig. 5A). Further oxidation at $E_{pa}(2)$ was also accompanied by a supplementary oxidation peak at $E_{pa}(4)$ which disappeared at high scan rate (Fig. 5B). At last and conversely to complex 2, the Mo complex displayed no sign of reversibility for the second reduction process at $E_{pa}(2)$ for high values of ν (Fig. 5B and Fig. S13B†).

Spectroelectrochemical studies performed with the Mo- N_2 complex 1 also revealed some differences to its W congener 2. While oxidation at $E_{pa}(1)$ led to disappearance of the N_2 stretching band at 1942 cm^{-1} , no new IR-detectable species could be detected in the $1800\text{--}2100 \text{ cm}^{-1}$ frequency range (Fig. 5C). Moreover, upon back reduction, the initial spectrum could only be partially recovered. Interestingly, analysis at lower frequencies (1400 to 1700 cm^{-1}) displayed further spectral changes upon electrochemical oxidation (Fig. 5D). Pushing the potential until $E_{pa}(2)$ induced even larger modification of the spectra in this frequency region. Returning to the initial potential value partially restored the N_2 stretching band at 1942 cm^{-1} (Fig. 5D). Notably, the changes in the 1400 to 1700 cm^{-1} frequency range were not observed for the tungsten complex upon oxidation at $E_{pa}(2)$ (Fig. S13D†).

Altogether, these electrochemical and spectroelectrochemical investigations essentially revealed two results. First, they

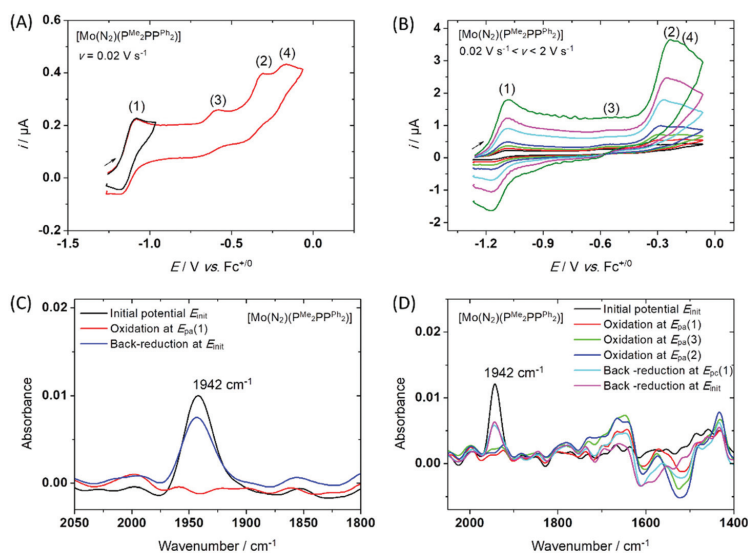


Fig. 5 CVs (E/V vs. Fc^+/Fc) at a Pt working electrode (diam. 1 mm) of $[Mo(N_2)(P^{Me}_2PP^{Ph}_2)]$ (0.4 mM) in THF/NaBPh₄ 0.02 M (A) at $\nu = 0.02 \text{ V s}^{-1}$ and (B) for $\nu = 0.02 \text{ V s}^{-1}$ (black), 0.05 V s^{-1} (red), 0.1 V s^{-1} (green), 0.2 V s^{-1} (blue), 0.5 V s^{-1} (cyan), 1 V s^{-1} (pink) and 2 V s^{-1} (olive); the numbers (1), (2), (3) and (4) on the graphics are related to the redox systems, see details in text. (C) Infrared spectra of $[Mo(N_2)(P^{Me}_2PP^{Ph}_2)]$ (15 mM) in THF/NaBPh₄ 20 mM recorded during *in situ* spectroelectrochemical measurements before (black) and after oxidation at $E_{pa}(1)$ (red), then returning back to the initial potential (blue); (D) the same as (C) except that oxidation at $E_{pa}(1)$ (red) is followed by oxidation at $E_{pa}(3)$ (green), $E_{pa}(2)$ (blue), then returning back to the $E_{pa}(1)$ (cyan) and finally the initial potential (magenta).

clearly show that one-electron oxidation of the neutral W and Mo dinitrogen complexes occurs at almost the same $E_{1/2}(1)$ value (−1.16 V and −1.13 V vs. Fc^+/Fc , respectively). This result is reasonable on the basis of experimental data obtained from NMR and IR spectroscopies as well as X-ray diffraction (*vide infra*), which have shown minor differences between the two neutral Mo and W complexes in solution and in the solid state. It is also in line with electrochemical investigations reported on Mo and W bis- N_2 complexes supported by $\text{P}^{\text{Ph}}\text{N}^{\text{Me}}\text{P}^{\text{Ph}}$ ligands, exhibiting a difference of only 20 mV for the first oxidation potential.²⁴ Hence, our results suggest that the structural properties of the W and Mo mono-oxidized dinitrogen species are very similar.

The second information which can be taken from electrochemistry and spectroelectrochemistry is that, although $\text{W}^{\text{I}}(\text{N}_2)^+$ and $\text{Mo}^{\text{I}}(\text{N}_2)^+$ pentaPod complexes can be reduced at similar potential values, they display very different stabilities in THF (*cf.* Scheme 3): whereas the mono-oxidized tungsten N_2 species seems to be highly stable, yielding back the neutral N_2 complex upon reduction, spectroelectrochemistry suggests that its Mo analogue evolves rapidly (*sec*) towards a new Mo^{I} species, probably a $\text{Mo}^{\text{I}}(\text{thf})^+$ complex. Likewise, the $\text{W}^{\text{II}}(\text{N}_2)^{2+}$ species appears at the second oxidation process as fairly unstable (*msec*) and may exchange its N_2 ligand by a THF ligand. Upon back reduction, N_2 re-binds to the metal center since the N_2 stretching band is detected. In the case of the molybdenum complex, oxidation beyond $E_{\text{pa}}(1)$ leads to a more complicated situation and probably induces N_2 -THF ligand exchange. The anodic peak at $E_{\text{pa}}(3)$ may be thus ascribed to the oxidation of $\text{Mo}^{\text{I}}(\text{thf})^+$ species.

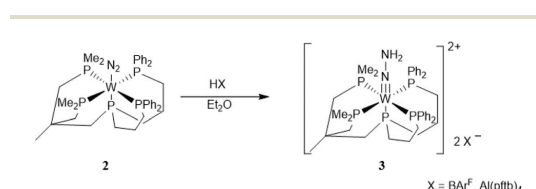
At last, comparison with redox data reported for other dinitrogen Mo and W complexes offers interesting information (see Table 2). In particular, oxidation potentials of mononuclear *trans*-bis- N_2 W and Mo complexes are clearly more positive than those of W and Mo pentaPod complexes by 150–370 mV, likely resulting from replacement of one dinitrogen ligand by a P-donor. In some cases, such as for *trans*- $[\text{Mo}(\text{N}_2)_2(\text{dppe})_2]$, the CV reversibility for the first oxidation was found to be dependent on the experimental conditions. Whereas Chatt *et al.* described a reversible system in THF/ NBu_4BF_4 for the first oxidation process,²⁶ Elson reported an irreversible anodic peak at room temperature when using a THF/MeOH (26% v/v) mixture with LiCl or LiClO_4 as supporting electrolyte.²³ In the latter case, a *trans*- $[\text{Mo}^{\text{I}}(\text{dppe})_2(\text{MeOH})_2]^+$ species was characterized

resulting from the release of N_2 according to a dissociative pathway. On the other hand, for *trans*- $[\text{Mo}(\text{N}_2)_2(\text{depe})_2]$,²⁵ longer timescale yielded $\text{N}\equiv\text{N}$ bond cleavage and Mo^{IV} nitride formation, differently to the complex 1.

Reactivity of Mo and W complexes towards acids and $\text{SmI}_2/\text{H}_2\text{O}$

In case of the molybdenum pentaPod complex $[\text{Mo}(\text{N}_2)(\text{P}^{\text{Me}}_2\text{PP}^{\text{Ph}}_2)]$ (1) the corresponding hydrazido(2-) complex could be generated by addition of Brookhart's acid (HBAr^{F} , $[\text{H}(\text{OEt})_2][\text{BAr}^{\text{F}}]$, 2.5 equiv.). Notably, this complex also exhibited catalytic activity towards ammonia generation, indicating that it is an intermediate of the catalytic cycle.¹⁶ Treatment of the tungsten dinitrogen complex 2 with 3 equiv. of HBAr^{F} was similarly found to generate the corresponding hydrazido(2-) complex 3- BAr^{F} (Scheme 4; for IR data see ESI Fig. S15 and Table S7†). Using smaller amounts of acid did not lead to a pure product.

The ^{31}P NMR spectrum of 3- BAr^{F} exhibits an AA'MXX' pattern (Fig. 6, see Fig. S16–S26† for full NMR data), demonstrating retention of the pentaphosphine environment (a signal at about 0 ppm shows a small impurity which most likely is caused by protonation of the ligand, also tiny amounts of free ligand can be observed in the enlargement in Fig. 7). However, all signals of 3- BAr^{F} have undergone a high field shift compared to 2 (Fig. 7), indicating an increased shielding of the P-donors in the former complex which is attributed to an elongation of the metal-P bonds and a loss of σ -donation to the metal centre. The particularly large high-field shift of the M-signal upon protonation of the N_2 -complex is due to the large *trans*-influence of the π -donating hydrazido(2-) ligand, weakening the W- P_{ax} bond. This analysis is supported by DFT calculations which show an increase of the W-P bond lengths upon going from 2 to 3- BAr^{F} , with a larger elongation of the



Scheme 4 Protonation of $[\text{W}(\text{N}_2)(\text{P}^{\text{Me}}_2\text{PP}^{\text{Ph}}_2)]$ (2) to $[\text{W}(\text{NNH}_2)(\text{P}^{\text{Me}}_2\text{PP}^{\text{Ph}}_2)]\text{X}_2$ ($\text{X} = \text{BAr}^{\text{F}}, \text{Al}(\text{pftb})_4$) (3).

Table 2 Electrochemical data for $[\text{LM}^{\text{I/0}}]$ dinitrogen species

Complex	$E_{1/2}/\text{V}$ vs. Fc^+/Fc	Conditions	Ref.
$[\text{W}(\text{N}_2)(\text{P}^{\text{Me}}_2\text{PP}^{\text{Ph}}_2)]$ (2)	−1.16	THF/ NaBPh_4	This work
$[\text{Mo}(\text{N}_2)(\text{P}^{\text{Me}}_2\text{PP}^{\text{Ph}}_2)]$ (1)	−1.13	THF/ NaBPh_4	This work
<i>trans</i> - $[\text{Mo}(\text{N}_2)_2(\text{depe})_2]$	−1.01	THF/ Pyr_4FAP	25
	−0.99 ^a	THF/ NBu_4BF_4	26
<i>trans</i> - $[\text{W}(\text{N}_2)_2(\text{dppe})_2]$	−0.82	THF/ $\text{NBu}_4[\text{B}(\text{C}_6\text{F}_5)_4]$	24
<i>trans</i> - $[\text{W}(\text{N}_2)_2(\text{dppe})(\text{dppp})]$	−0.79	THF/ $\text{NBu}_4[\text{B}(\text{C}_6\text{F}_5)_4]$	24

^a Experimentally measured at $E_{1/2} = -0.43$ V vs. SCE.

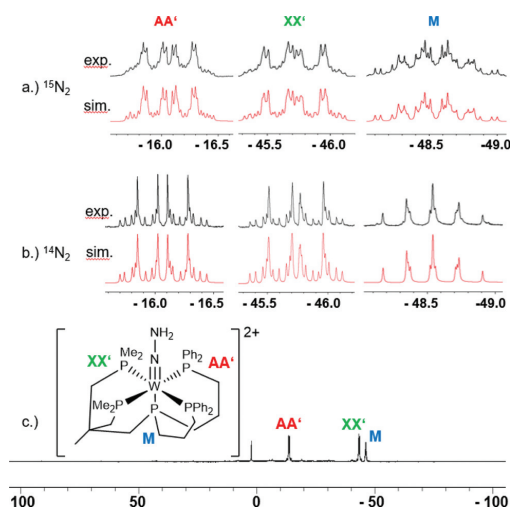


Fig. 6 Experimental and simulated $^{31}\text{P}\{^1\text{H}\}$ NMR spectra of $^{15}\text{N}_2$ -**3-BAr^F** (a) and **3-BAr^F** (b). (c) Overall spectrum of **3-BAr^F** in diethylether- d_{10} .

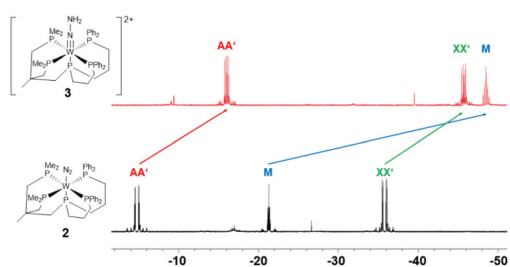


Fig. 7 Comparison of the $^{31}\text{P}\{^1\text{H}\}$ NMR spectra of **2** (black) and **3-BAr^F** (red).

W-P_{ax} bond length in comparison to W-P_{eq} (Table S6†). Notably, protonation of **2** with $[\text{H}(\text{OEt}_2)_2][\text{Al}(\text{OC}(\text{CF}_3)_3)_4]$ (HAL (pftb)₄) led to similar results (cf. Fig. S27†).

The ^{31}P - ^{31}P coupling constants of the hydrazido(2-) complex **3-BAr^F** show some differences compared to the parent dinitrogen complex **2** (Table 1). While the *cis* couplings among the equatorial phosphines are almost unchanged ($\Delta J = 1$ –2 Hz), the corresponding *trans* coupling gets smaller by about 30 Hz. On the other hand, the *cis* couplings of the equatorial phosphines with the axial P donor are increased by 17 and 13 Hz, respectively. Similar protonation-induced changes have been observed in the corresponding molybdenum system (Table 1).^{15,16}

Comparison of the hydrazido(2-) complexes of tungsten and molybdenum show similar differences as for the dinitrogen complexes, except that the changes in the *cis* coupling constants between the equatorial phosphines and the axial P-donor are smaller than for the corresponding dinitrogen complexes (Table 1). The ^1H - ^{15}N , ^{15}N - ^{15}N and ^{15}N - ^{31}P cou-

pling constants show nearly identical, the corresponding values for the tungsten complexes always being slightly smaller than for their molybdenum counterparts (see Table S8 in ESI†). Nevertheless, the ^1H - ^{15}N coupling constant of **3-BAr^F** (92.0 Hz) is still larger than for a W-hydrazido(2-) complex supported by two bidentate ligands (80 Hz).²⁷ Analogous to the dinitrogen complexes, DFT calculations indicate that the bond lengths and bond angles for the molybdenum and tungsten hydrazido(2-) complexes are very similar (Table S6†). Moreover, the calculated N-N bond lengths (~ 1.31 Å) correspond to those obtained for classic Chatt-type hydrazido(2-) complexes.²⁸

In order to investigate a potential catalytic activity of the new tungsten complex, a 0.1 M solution of samarium diiodide and water (5 ml) was treated with a THF solution of **2** (2 μmol in 1 ml THF) under nitrogen in a 50 mL Schlenk flask at room temperature. After the solution turned yellow the amount of produced ammonia was determined by the indophenol method.²⁹ In contrast to its molybdenum congener **1**, complex **2** just generated a slightly over-stoichiometric amount of ammonia (2.75 ± 0.23 eq., 5% yield related to the reducing agent). Whereas ammonia could be stoichiometrically produced by protonation of $[\text{W}(\text{N}_2)_2(\text{PMePh}_2)_4]$,¹¹ a lack of (chemo)catalytic NH_3 formation from N_2 is well known for tungsten systems (see above).^{13,14} Thus, **2** is the first W complex that is able to generate more than 2 equivalents of NH_3 in relation to the metal centre upon addition of protons and reductant. However, it appears that just a small fraction of the dinitrogen complex is regenerated, suggesting that most of the catalyst is converted to a different complex that is inactive towards nitrogen reduction. In this context we note that addition of water to the tungsten dinitrogen complex without samarium diiodide resulted in the decomposition of the complex.

Summary and conclusions

The tungsten dinitrogen complex $[\text{W}(\text{N}_2)(\text{P}^{\text{Me}}_2\text{PP}^{\text{Ph}}_2)]$ (**2**) supported by a pentadentate tetrapodal phosphine ligand ($\text{P}^{\text{Me}}_2\text{PP}^{\text{Ph}}_2$) has been synthesized and characterized regarding its electronic structure and reactivity, allowing comparison with the analogous molybdenum complex $[\text{Mo}(\text{N}_2)(\text{P}^{\text{Me}}_2\text{PP}^{\text{Ph}}_2)]$ (**1**). Reaction of $[\text{W}(\text{N}_2)(\text{P}^{\text{Me}}_2\text{PP}^{\text{Ph}}_2)]$ (**2**) with samarium iodide/water was found to mediate a slightly overstoichiometric formation (2.75 ± 0.23 eq.) of NH_3 from N_2 which makes **2** the first tungsten complex generating more than 2 equivalents of ammonia from N_2 . Notably, the analogous molybdenum complex **1** catalytically generates 25.7 eq. NH_3 from N_2 .¹⁶ This contrasting behaviour of tungsten vs. analogous molybdenum complexes regarding the catalytic conversion of N_2 to NH_3 is well known in the literature,^{8,13} but not fully understood. With a ν_{NN} value of 1901 (**2**) vs. 1929 cm^{-1} (**1**) the activation of the N_2 ligand is higher in the W complex than in its Mo analogue, which therefore cannot be the reason for the differing behaviour. Apart from that, however, differences in structural parameters are small. Correspondingly, a single-crystal structure determination

of **2** only showed minor differences of bond distances and angles with respect to **1**. Likewise, the ^{31}P - and ^{15}N -NMR-spectroscopic properties of **2** were found to be quite similar to those of **1**, apart from characteristic differences in chemical shifts and coupling constants. Based on the strong activation of N_2 , **2** could be converted to the hydrazido(2-) derivative **3** by protonation with HBAr^{F} , similar to **1**, rendering comparison to the analogous $\text{Mo}-\text{NNH}_2$ complex possible as well.

In order to obtain information about the electronic-structural properties of the tungsten and molybdenum pentaPod systems, electro- and spectroelectrochemical investigations were performed on **1** and **2**. Both dinitrogen complexes exhibit remarkably similar redox potentials. Moreover, two main systems can be detected in oxidation. For tungsten, the first system is found to be reversible and the second, being irreversible at low scan rates, gets more reversible at higher scan rates. By contrast, the first system is only partially reversible for the molybdenum complex and irreversible for the second system. The origin of these differences could be elucidated with spectroelectrochemistry: upon oxidation of **2**, a stable $\text{W}^{\text{I}}\text{N}_2^+$ complex is formed whereas for the molybdenum complex **1** loss of N_2 occurs, probably going along with a ligand exchange and formation of a THF-bound complex. For W, loss of N_2 only occurs upon further oxidation of the $\text{W}^{\text{I}}\text{N}_2^+$ complex.

In conclusion, the spectroelectrochemical studies as well as the voltammetric studies showed that both systems can regenerate the zerovalent dinitrogen complexes around the same potential. Furthermore, a stable tungsten dinitrogen complex is already formed at the level of a $\text{W}(\text{I})$ intermediate, exhibiting a fairly activated N_2 ligand with a ν_{NN} of 1951 cm^{-1} in solution. By contrast, the corresponding $\text{Mo}(\text{I})$ dinitrogen complex is thermally unstable. A theoretical mechanism evaluated for N_2 -reduction of the molybdenum pentaPod system indicated that PCET to the $\text{Mo}(\text{N}_2)$ -complex, generating a diazenido(-) intermediate, is energetically more favourable for a $\text{Mo}(\text{I})$ - than for a $\text{Mo}(\text{0})$ -species.¹⁶ Based on the results presented here, the tungsten complex **2** would fit much better to such a scenario than its molybdenum analogue **1**. Nevertheless, NH_3 formation mediated by **2** is only slightly overstoichiometric. The reason(s) for this observation must therefore lie in some other stage of the catalytic cycle. Further investigation of this question is underway.

Experimental section

All syntheses were performed under N_2 or argon atmosphere using standard Schlenk line and glovebox techniques. The solvents were dried and freshly distilled under argon prior to use. $[\text{H}(\text{OEt})_2][\text{Al}(\text{OC}(\text{CF}_3)_3)_4]$ was received from the working group of I. Krossing in Freiburg i. Br.. All other reagents were commercially available and were used as received. $[\text{WCl}_4(\text{PMePh}_2)_2]$,¹⁸ $[\text{Mo}(\text{N}_2)(\text{P}^{\text{Me}}_2\text{PP}^{\text{Ph}}_2)]$ (**1**)¹⁵ and $[\text{Mo}(\text{NNH}_2)(\text{P}^{\text{Me}}_2\text{PP}^{\text{Ph}}_2)]$ ¹⁶ were prepared according to the literature. NMR spectra were recorded with a Bruker AVANCE III HD Pulse Fourier transform spectrometer operating at frequencies of

400.13 MHz (^1H), 376.50 (^{19}F), 161.98 MHz (^{31}P), 128.38 (^{11}B), and 40.56 MHz (^{15}N). Referencing was performed either using the solvent residue signal (5.32 ppm for CD_2Cl_2 , 3.58 ppm for $\text{thf}-d_8$ and 7.16 ppm for C_6D_6) or TMS ($\delta^1\text{H} = 0$ ppm), CFCl_3 ($\delta^{19}\text{F} = 0$ ppm), 85% H_3PO_4 ($\delta^{31}\text{P} = 0$ ppm), BF_3 ($\delta^{11}\text{B} = 0$ ppm), and CH_3NO_2 ($\delta^{15}\text{N} = 0$ ppm) serving as substitutive standards. IR spectra were recorded at RT on a Bruker Vertex70 FT-IR spectrometer using a broadband spectral range extension VERTEX FM for full mid and far IR in the range of $6.000\text{--}80\text{ cm}^{-1}$.

Electrochemical studies were performed in a glovebox (Jacomex) ($\text{O}_2 < 1$ ppm, $\text{H}_2\text{O} < 1$ ppm) with a home-made 3-electrode cell (WE: Pt or glassy carbon, RE: Pt wire in a 1 mM Fc^+/Fc , 0.02 M THF/ NaBPh_4 solution, CE: Pt). Ferrocene was added at the end of the experiments to determine the exact redox potential values. The potential of the cell was controlled by an AUTOLAB PGSTAT 100 (Metrohm) potentiostat monitored by the NOVA© software (Metrohm). The working electrodes were polished over a $1\text{ }\mu\text{m}$ alumina slurry with water, sonicated in H_2O ($18.2\text{ }\Omega\text{ cm}$) and acetone, then dried with N_2 flush.

Thin layer IR spectroelectrochemistry was carried out with a previously described set-up consisting of a commercial IR Si ATR probe (Artphotronics), which can fit into a thin space created on the surface of a glassy carbon electrode.³⁰ The thin layer between the probe and the electrode allows fast (seconds) electrolysis, hence time-resolved monitoring of the electrochemical reaction. Detection of the IR signal (2 cm^{-1} resolution, one spectrum every 10 s) was obtained by using a FTIR optic-fiber-coupled spectrometer purchased from Arcoptix (FTMIR-FC-120-LN2).

Single crystal structure determination

Data collection was performed using an Imaging Plate Diffraction System (IPDS-2) from Stoe & Cie with $\text{Mo}-\text{K}\alpha$ radiation. A numerical absorption correction was performed using X-Red and X-Shape of the software package X-Area. The structures were solved with SHELXT³¹ and structure refinement was performed against F^2 using SHELXL-2018³². The C-H hydrogen atoms were positioned with idealized geometry (methyl H atoms allowed to rotate but not to tip) and were refined isotropically with $U_{\text{iso}}(\text{H}) = 1.2U_{\text{eq}}(\text{C})$ (1.5 for methyl H atoms) using a riding model.

CCDC 2127859 (**2**) contains the supplementary crystallographic data for this paper.†

Computational details

Calculations of the tungsten dinitrogen $[\text{W}(\text{N}_2)(\text{P}^{\text{Me}}_2\text{PP}^{\text{Ph}}_2)]$ (**2**) and hydrazido(2-) complexes $[\text{W}(\text{NNH}_2)(\text{P}^{\text{Me}}_2\text{PP}^{\text{Ph}}_2)]^{2+}$ (**3**) were conducted with the ORCA 4.2.1 program package.³³ Geometries were optimized on PBE0³⁴/def2-TZVP³⁵ level of theory. In addition, Grimme's dispersion correction with Becke-Johnson damping (D3BJ)³⁶ and the RI approximation using the def2-TZVP/J fitting basis set³⁷ were used.

[WCl₃(κ³-P^{Me}₂PP^{Ph}₂)]

1.11 g (1.53 mmol) of [WCl₄(PMePh₂)₂] and 1.24 g (1.83 mmol) of P^{Me}₂PP^{Ph}₂ were dissolved in 50 ml toluene and stirred for 3 h at 70 °C. The mixture was filtrated and concentrated *in vacuo* to 5 ml and 10 ml of diethyl ether was added. The green precipitate was filtered and washed with 10 ml diethyl ether and 10 ml *n*-pentane. Drying *in vacuo* gave a dark green solid. Yield: 1.26 g (1.30 mmol, 85%). Anal. calcd for C₃₉H₅₃Cl₃P₅W: C, 48.4; H, 5.52; found: C, 48.9; H, 5.65. IR (300 K): $\tilde{\nu}$ = 3067 (w), 3051 (w), 2954 (sh), 2919 (m), 2867 (sh), 2801 (w), 1589 (m), 1568 (w), 1551 (vw), 1480 (m), 1455 (vw), 1430 (m), 1412 (w), 1381 (w), 1330 (vw), 1297 (w), 1279 (w), 1260 (vw), 1241 (w), 1182 (w), 1156 (w), 1119 (w), 1096 (m), 1069 (w), 1025 (w), 1000 (w), 945 (m), 917 (m), 880 (m), 843 (w), 805 (vw), 739 (s), 693(s), 639 (vw), 617 (w), 577 (vw), 543 (w), 508 (s), 479 (m), 442 (vw), 425 (w), 404 (vw), 362 (vw), 340 (sh), 323 (sh), 294 (s), 271 (vs), 252 (sh), 221 (vw), 208 (vw), 178 (w), 158 (w), 133 (m), 120 (w) cm⁻¹. Raman (300 K): $\tilde{\nu}$ = 6054 (m), 2982 (w), 2913 (s), 1586 (s), 1455 (vw), 1414 (w), 1306 (vw), 1210 (vw), 1186 (w), 1160 (w), 1100 (w), 1073 (vw), 1028 (m), 1000 (vs), 960 (w), 786 (w), 688 (w), 619 (w), 400 (vw), 328 (w), 258 (w), 150 (vw) cm⁻¹.

[W(N₂)(P^{Me}₂PP^{Ph}₂)] (2)

290 mg (300 μmol) of [WCl₃(κ³-P^{Me}₂PP^{Ph}₂)] were dissolved in 20 ml THF and added to sodium amalgam prepared of 2 ml Hg and 200 mg (8.7 mmol) of sodium. The reaction mixture was stirred for 16 h under an atmosphere of nitrogen. The supernatant red solution was transferred into another flask and the solvent was removed *in vacuo*. The residue was resolved in 10 ml of diethyl ether and filtered over neutral alumina. The orange solution was concentrated to dryness and shed with small amounts of cold *n*-pentane or *n*-hexane. Drying *in vacuo* gave an orange solid. Crystals suitable for X-ray single crystal diffraction were obtained by slow diffusion of *n*-pentane into a benzene-*d*₆ solution of 2. Yield: 118 mg (133 μmol, 44%). Anal. calcd for C₃₉H₅₃N₂P₅W: C, 52.7; H, 6.01; N, 3.15. Found: C, 53.4; H, 6.04; N, 2.30. The nitrogen value is too low because of the thermal instability of the product. ¹H NMR (400.13 MHz, *d*₆-benzene, 300 K): δ = 0.51 (d, ²*J* = 5.2 Hz, 6H, P^{Me}₂), 0.81 (d, ²*J* = 7.7 Hz, 2H, PCH₂), 0.97 (m, 7H, Me₂PCH₂, CH₃), 1.27 (m, 4H, PCH₂), 1.93 (m, 4H, CH₂CH₂CH₂), 2.03 (m, 2H, Ph₂PCH₂), 2.43 (m, 2H, Ph₂PCH₂), 6.41 (m, 5H, PPh₂), 6.75 (m, 2H, PPh₂), 6.86 (m, 6H, PPh₂), 7.09 (m, 4H, PPh₂), 7.16 (m, 1H, PPh₂), 7.28 (m, 2H, PPh₂) ppm. ¹³C NMR (100.61 MHz, *d*₆-benzene, 300 K): δ = 16.3 (m, 2C, P^{Me}₂), 23.9 (m, 4C, CH₂CH₂CH₂), 26.2 (m, 2C, P^{Me}₂), 30.3 (s, 2C, Ph₂PCH₂), 34.6 (m, 1C, PCH₂), 38.6 (m, 2C, PCH₂), 40.6 (s, 1C, H₃C), 42.0 (m, 1C, H₃CC), 43.0 (m, 2C, Me₂PC), 126.4 (s, 8C, PPh₂), 127.3 (d, ²*J* = 7.4 Hz, 4C, PPh₂), 127.8 (s, 2C, PPh₂), 128.1 (m, 4C, PPh₂), 129.1 (m, 2C, PPh₂), 147.2 (m, 2C, PPh₂), 150.0 (m, 2C, PPh₂) ppm. ³¹P{¹H} NMR (161.98 MHz, *d*₆-benzene, 300 K): δ = -4.8 (m, ²*J*(P_{AX}, P_{AX}) = 85.7, ²*J*(P_{AM}, P_{AM}) = 11.2, ²*J*(P_{AX}, P_{AX}) = -11.1, ²*J*(P_A, P_A) = 17.4 Hz, 2P, PPh₂, P_A/P_A), -21.3 (tt, ²*J*(P_{MX}, P_{MX}) = 18.5 Hz, 1P, P_M), -35.8 (m, ²*J*(P_X, P_X) = 4.5 Hz, 2P, P^{Me}₂, P_X/P_X) ppm. IR (300 K): $\tilde{\nu}$ = 3139 (vw), 3069

(w), 3049 (w), 2994 (vw), 2959 (m), 2920 (sh), 2906 (m), 2855 (m), 2812 (sh), 1982 (w), 1901 (vs, ν (N–N)), 1805 (vw), 1750 (vw), 1585 (w), 1571 (w), 1481 (m), 1448 (w), 1431 (s), 1418 (sh), 1373 (w), 1328 (vw), 1293 (w), 1258 (s), 1218 (vw), 1184 (vw), 1153 (w), 1089 (s), 1072 (m), 1048 (m), 1025 (s), 970 (w), 925 (m), 905 (s), 875 (m), 832 (w), 798 (s), 737 (s), 693 (vs), 662 (s), 625 (s), 612 (s), 544 (vw), 506 (vs), 475 (m), 429 (w, ν (W–N)), 402 (s), 372 (vw), 345 (m), 313 (w), 290 (w), 263 (vw), 240 (m), 191 (vw) cm⁻¹. Raman (300 K): $\tilde{\nu}$ = 3053 (s), 2963 (w), 2912 (vs), 2888 (s), 2863 (sh), 1903 (s, ν (N–N)), 1587 (s), 1572 (w), 1451 (vw), 1434 (vw), 1418 (vw), 1405 (vw), 1297 (vw), 1274 (vw), 1186 (w), 1156 (w), 1093 (m), 1029 (m), 1001 (vs), 933 (vw), 910 (vw), 670 (w), 637 (vw), 618 (w), 505 (vw), 431 (w, ν (W–N)), 403 (vw), 364 (vw), 350 (vw), 315 (vw), 292 (vw), 257 (vw), 242 (w), 193 (w) cm⁻¹.

¹⁵N-[W(N₂)(P^{Me}₂PP^{Ph}₂)] (¹⁵N-2) was prepared in a similar fashion as 2 under a ¹⁵N₂ atmosphere and characterized by IR, Raman, ³¹P- and ¹⁵N NMR spectroscopy. ¹⁵N{¹H} NMR (40.56 MHz, *d*₁₀-Et₂O, 300 K): δ = -18.7 (d, ¹*J*_{NN} = 7.5 Hz, 1N, N_β), -48.4 (m, 1N, N_α) ppm. ³¹P{¹H} NMR (161.98 MHz, *d*₆-benzene, H₃PO₄, 300 K): δ = -4.8 (m, ²*J*(P_{AA}N_α) = 2.7 Hz, ³*J*(P_{AA}N_β) = 0.3 Hz, 2P, PPh₂, P_A/P_A), -21.3 (ttdd, ²*J*(P_M, N_α) = 13.9, ³*J*(P_MN_β) = 1.6 Hz, 1P, P_M), -35.8 (m, ²*J*(P_{XX}N_α) = 2.6 Hz, ³*J*(P_{AA}N_β) = 0.7 Hz, 2P, P^{Me}₂, P_X/P_X) ppm. IR (300 K): $\tilde{\nu}$ = 1840 (vs, ν (N–N)), 421 (w, ν (W–N)) cm⁻¹. Raman (300 K): $\tilde{\nu}$ = 1840 (s, ν (N–N)), 419 (w, ν (W–N)) cm⁻¹.

[W(NNH₂)(P^{Me}₂PP^{Ph}₂)] (BAR^F)₂ (3-BAR^F)

A portion of 99.0 mg (97.9 μmol) of [H(OEt)₂][BAR^F] was dissolved in 0.4 mL of diethyl ether and added to 29 mg (32.6 μmol) of 3 in 0.6 mL of diethyl ether. After stirring for 5 min at room temperature the solvent was removed *in vacuo*, affording a light brown solid of nominal composition (determined by integration of the ¹H NMR signals) [W(NNH₂)(P^{Me}₂PP^{Ph}₂)](BAR^F)₂·3HBAR^F. The high fluorine content precluded an elemental analysis. ¹H NMR (400.13 MHz, *d*₆-benzene, 300 K): δ = 0.85 (d, ²*J* = 7.8 Hz, 6H, P^{Me}₂), 1.03 (m, 3H, CH₃), 1.59 (d, ²*J* = 9.7 Hz, 2H, PCH₂), 1.73 (m, 8H, Me₂PCH₂, PCH₂), 2.24 (m, 4H, CH₂CH₂CH₂), 2.66 (m, 2H, Ph₂PCH₂), 2.98 (m, 2H, Ph₂PCH₂), 6.75 (m, 6H, PPh₂), 6.90 (m, 2H, PPh₂), 7.35 (m, 6H, PPh₂), 7.42 (s, 22H, BAR^F), 7.62 (m, 38H, BAR^F), 7.68 (m, 4H, PPh₂), 7.77 (m, 2H, PPh₂) ppm. ¹³C NMR (100.61 MHz, *d*₆-benzene, 300 K): δ = 16.7 (m, 2C, P^{Me}₂), 19.3 (s, 4C, CH₂CH₂CH₂), 20.8 (m, 2C, P^{Me}₂), 26.0 (m, 2C, PCH₂), 28.5 (s, 2C, PCH₂), 35.2 (m, 1C, PCH₂), 35.4 (s, 1C, H₃CC), 36.0 (m, 2C, Me₂PC), 116.0 (s, 4C, CH(BAR^F)), 123.4 (q, ¹*J* = 271.7 Hz, CF₃), 127.4 (s, 8C, CH(BAR^F)), 128.0 (m, 8C, CCF₃), 128.0 (m, 8C, PPh₂), 128.5 (s, 2C, PPh₂), 129.6 (d, ²*J* = 15.0 Hz, 4C, PPh₂), 130.7 (m, 2C, PPh₂), 131.4 (d, ²*J* = 11.6 Hz, 4C, PPh₂), 136.1 (d, ¹*J* = 44.1 Hz, 2C, PPh₂), 136.1 (d, ¹*J* = 44.1 H 2C, PPh₂), 137.0 136.1 (d, ¹*J* = 45.8 H 2C, PPh₂), 160.2 (m, 4C, BC) ppm. ¹¹B NMR (128.38 MHz, *d*₆-benzene, 300 K): δ = -6.97 (s, 2B, BAR^F) ppm. ¹⁹F NMR (376.50 MHz, *d*₆-benzene, 300 K): δ = -63.4 (s, 48F, BAR^F) ppm. ³¹P{¹H} NMR 161.98 MHz, *d*₁₀-Et₂O, 300 K): δ = -15.9 (m, ²*J*(P_{AX}, P_{AX}) = 53.9, ²*J*(P_{AM}, P_{AM}) = 28.2, ²*J*(P_{AX}, P_{AX}) = -12.2, ²*J*(P_A, P_A) = 16.1 Hz, 2P, PPh₂, P_A/

P_A), -45.8 (m, $^2J(P_{MX}, P_{MX}) = 31.3$, $^2J(P_X, P_X) = 6.3$ Hz, 2P, PM_{E2} , P_X/P_X), -48.6 (tt, 1P, P_M) ppm. IR (300 K): $\tilde{\nu} = 3312$ (w, $\nu(N-H)$), 3076 (vw), 2960 (w), 2924 (m), 2853 (w), 1790 (vw), 1611 (m), 1443 (w), 1352 (s), 1272 (vs), 1159 (m), 1114 (vs), 1092 (sh), 998 (w), 934 (w), 918 (vw), 886 (s), 838 (s), 809 (m), 743 (m), 711 (s), 698 (w), 680 (s), 669 (s), 617 (vw), 609 (vw), 580 (w), 568 (vw), 516 (w), 507 (w), 488 (w), 449 (m), 403 (w), 392 (w), 380 (vw), 366 (m), 353 (sh), 331 (vw), 283 (w), 259 (w), 246 (vw), 210 (vw), 189 (vw), 151 (vw) cm^{-1} . Raman (300 K): $\tilde{\nu} = 3074$ (w), 3023 (vw), 2960 (8w), 2932 (m), 2906 (m), 2882 (sh), 2852 (w), 1611 (m), 1593 (s), 1523 (vw), 1464 (w), 1364 (s), 1107 (w), 1030 (w), 1003 (vs), 952 (w), 939 (vw), 914 (vw), 840 (vw), 801 (s), 745 (w), 704 (s), 689 (w), 675 (w), 617 (vw), 287 (w), 262 (w), 244 (vw), 235 (w), 183 (w), 159 (m) cm^{-1} .

$^{15}N[W(NNH_2)(P^{Me_2Ph_2})_2](BAr^F)_2$ (**15N-3-BAr^F**) was prepared in a similar fashion starting from **15N-2** and characterized by IR, Raman, ^{31}P - and ^{15}N NMR spectroscopy. $^{15}N\{^1H\}$ NMR (40.56 MHz, d_{10} -Et₂O, 300 K): $\delta = -48.4$ (m, 1N, N_α), -237 (m, 1N, N_β) ppm. $^{31}P\{^1H\}$ NMR 161.98 MHz, d_{10} -Et₂O, 300 (K): $\delta = -15.9$ (m, $^2J(P_{AA}, N_\alpha) = 5.0$ Hz, 2P, PPH_2 , P_A/P_A), -45.8 (m, $^2J(P_{XX}, N_\alpha) = 5.5$ Hz, 2P, PM_{E2} , P_X/P_X), -48.6 (ttdd, $^2J(P_M, N_\alpha) = 20.4$ Hz, $^3J(P_M, N_\beta) = 6.6$ Hz, 1P, PM) ppm. IR (300 K): $\tilde{\nu} = 3308$ (w, $\nu(N-H)$), 554 (w, $\nu(W-N)$) cm^{-1} .

$[W(NNH_2)(P^{Me_2Ph_2})_2][Al(pftb)_4]_2$ (**3-Al(pftb)₄**) was prepared similar to **3-BAr^F** with $[H(OEt_2)_2][Al(OC(CF_3)_3)_4]$ as acid.

Conflicts of interest

The authors declare no conflict of interest.

Acknowledgements

The authors gratefully acknowledge the SEA-EU program supported by Agence Nationale de la recherche (ANR-19-GURE-0001), PHC Procope Campus France (46652ZL) and Programm des Projektbezogenen Personenaustauschs Frankreich (PROCOPE) 2021–2023 (Deutscher Akademischer Austauschdienst, Projekt-Kennziffer 57560918) for funding. The authors thank Prof. Ingo Krossing for providing us with $[H(OEt_2)_2][Al(OC(CF_3)_3)_4]$.

References

- (a) Y. Tanabe and Y. Nishibayashi, *Chem. Soc. Rev.*, 2021, **50**, 5201; (b) M. J. Chalkley, M. W. Drover and J. C. Peters, *Chem. Rev.*, 2020, **120**, 5582; (c) N. Stucke, B. M. Flöser, T. Weyrich and F. Tuczek, *Eur. J. Inorg. Chem.*, 2018, **2018**, 1337.
- (a) L. C. Seefeldt, Z.-Y. Yang, D. A. Lukoyanov, D. F. Harris, D. R. Dean, S. Raugei and B. M. Hoffman, *Chem. Rev.*, 2020, **120**, 5082; (b) C. van Stappen, L. Decamps, G. E. Cutsail, R. Björnsson, J. T. Henthorn, J. A. Birrell and S. DeBeer, *Chem. Rev.*, 2020, **120**, 5005; (c) A. J. Jasniowski, C. C. Lee, M. W. Ribbe and Y. Hu, *Chem. Rev.*, 2020, **120**, 5107.
- R. Schlögl, *Angew. Chem., Int. Ed.*, 2003, **42**, 2004.
- (a) A. D. Allen and C. V. Senoff, *Chem. Commun.*, 1965, **24**, 621; (b) M. D. Fryzuk, *Chem. Commun.*, 2013, **49**, 4866.
- (a) J. Chatt, A. J. Pearman and R. L. Richards, *Nature*, 1975, **253**, 39; (b) M. Hidai, K. Tominari, Y. Uchida and A. Misono, *J. Chem. Soc. D*, 1969, 1392; (c) M. Hidai, K. Tominari and Y. Uchida, *J. Am. Chem. Soc.*, 1972, **94**, 110.
- C. J. Pickett and J. Talarmin, *Nature*, 1985, **317**, 652.
- D. V. Yandulov and R. R. Schrock, *Science*, 2003, **301**, 76.
- R. R. Schrock, *Acc. Chem. Res.*, 2005, **38**, 955.
- (a) K. Arashiba, Y. Miyake and Y. Nishibayashi, *Nat. Chem.*, 2011, **3**, 120; (b) A. Eizawa, K. Arashiba, H. Tanaka, S. Kuriyama, Y. Matsuo, K. Nakajima, K. Yoshizawa and Y. Nishibayashi, *Nat. Commun.*, 2017, **8**, 14874.
- Y. Ashida, K. Arashiba, K. Nakajima and Y. Nishibayashi, *Nature*, 2019, **568**, 536.
- J. Chatt, A. J. Pearman and R. L. Richards, *J. Chem. Soc., Dalton Trans.*, 1977, 1852.
- P. Garrido-Barros, J. Derosa, M. J. Chalkley and J. C. Peters, *ChemRxiv*, 2021, DOI: 10.33774/chemrxiv-2021-j95jg.
- K. Arashiba, K. Sasaki, S. Kuriyama, Y. Miyake, H. Nakanishi and Y. Nishibayashi, *Organometallics*, 2012, **31**, 2035.
- D. V. Yandulov and R. R. Schrock, *Can. J. Chem.*, 2005, **83**, 341.
- S. Hinrichsen, A. Kindjajev, S. Adomeit, J. Krahmer, C. Näther and F. Tuczek, *Inorg. Chem.*, 2016, **55**, 8712.
- T. A. Engesser, A. Kindjajev, J. Junge, J. Krahmer and F. Tuczek, *Chem. – Eur. J.*, 2020, **26**, 14807.
- E. Carmona, A. Galindo, M. L. Poveda and R. D. Rogers, *Inorg. Chem.*, 1985, **24**, 4033.
- Inorganic syntheses*, ed. F. Basolo and R. J. Angelici, Wiley, New York, 1990, vol. 28.
- S. L. Apps, A. J. P. White, P. W. Miller and N. J. Long, *Dalton Trans.*, 2018, **47**, 11386.
- F. B. Ogilvie, J. M. Jenkins and J. G. Verkade, *J. Am. Chem. Soc.*, 1970, **92**, 1916.
- (a) A. Galindo, E. Gutierrez, A. Monge, M. Paneque, A. Pastor, P. J. Perez, R. D. Rogers and E. Carmona, *J. Chem. Soc., Dalton Trans.*, 1995, 3801; (b) E. Carmona, J. M. Marin, M. L. Poveda, J. L. Atwood and R. D. Rogers, *J. Am. Chem. Soc.*, 1983, **105**, 3014.
- J.-M. Savéant, *Elements of Molecular and Biomolecular Electrochemistry: An Electrochemical Approach to Electron Transfer Chemistry*, Wiley, Hoboken NJ, 2006.
- C. M. Elson, *Inorg. Chim. Acta*, 1976, **18**, 209.
- C. J. Weiss, A. N. Groves, M. T. Mock, W. G. Dougherty, W. S. Kassel, M. L. Helm, D. L. DuBois and R. M. Bullock, *Dalton Trans.*, 2012, **41**, 4517.
- A. Katayama, T. Ohta, Y. Wasada-Tsutsui, T. Inomata, T. Ozawa, T. Ogura and H. Masuda, *Angew. Chem., Int. Ed.*, 2019, **58**, 11279.

Paper

Dalton Transactions

- 26 J. Chatt, H. Wasif, G. J. Leigh, H. Neukomm, C. J. Pickett and D. A. Rankin, *J. Chem. Soc., Chem. Commun.*, 1980, 1024.
- 27 C. J. Weiss, J. D. Egbert, S. Chen, M. L. Helm, R. M. Bullock and M. T. Mock, *Organometallics*, 2014, **33**, 2189.
- 28 K. H. Horn, N. Böres, N. Lehnert, K. Mersmann, C. Näther, G. Peters and F. Tuczek, *Inorg. Chem.*, 2005, **44**, 3016.
- 29 (a) M. W. Weatherburn, *Anal. Chem.*, 1967, **39**, 971; (b) M. P. E. Berthelot, *Rep. Chim. Appl.*, 1859, **1**, 284.
- 30 C. Garcia Bellido, L. Álvarez-Miguel, D. Miguel, N. Lalaoui, N. Cabon, F. Gloaguen and N. Le Poul, *ChemElectroChem*, 2021, **8**, 1899.
- 31 G. M. Sheldrick, *Acta Crystallogr., Sect. A: Found. Adv.*, 2015, **A71**, 3.
- 32 G. M. Sheldrick, *Acta Crystallogr., Sect. C: Struct. Chem.*, 2015, **C71**, 3.
- 33 F. Neese, *Wiley Interdiscip. Rev.: Comput. Mol. Sci.*, 2018, **8**, 33.
- 34 J. P. Perdew, K. Burke and M. Ernzerhof, *Phys. Rev. Lett.*, 1996, **77**, 3865–3686.
- 35 (a) A. Schäfer, C. Huber and R. Ahlrichs, *J. Chem. Phys.*, 1994, **100**, 5829; (b) A. Schäfer, H. Horn and R. Ahlrichs, *J. Chem. Phys.*, 1992, **97**, 2571; (c) F. Weigend and R. Ahlrichs, *Phys. Chem. Chem. Phys.*, 2005, **7**, 3297.
- 36 (a) S. Grimme, J. Antony, S. Ehrlich and H. Krieg, *J. Chem. Phys.*, 2010, **132**, 154104; (b) S. Grimme, S. Ehrlich and L. Goerigk, *J. Comput. Chem.*, 2011, **32**, 1456.
- 37 (a) K. Eichkorn, O. Treutler, H. Öhm, M. Häser and R. Ahlrichs, *Chem. Phys. Lett.*, 1995, **240**, 283; (b) K. Eichkorn, F. Weigend, O. Treutler and R. Ahlrichs, *Theor. Chem. Acc.*, 1997, **97**, 119; (c) F. Neese, *J. Comput. Chem.*, 2003, **24**, 1740.

3.2 Electrochemical and Electrocatalytic Studies

In order to investigate the dinitrogen complexes, which are very sensitive to air and moisture, the electrochemical measurements need to be performed under an inert atmosphere. Besides cyclic voltammetry and coulometry, investigations regarding the electrocatalytic activity of the complexes are in the scope of the present thesis. Since at the time, utilization of the glove box was not yet an option, appropriate vessels for the desired applications had to be developed. The requirements for measurements and catalytic studies are different, yet the cells should be similar. Glass vessels for electrochemistry were already available, which leaves the requirement for an air tight lid. For this, a lid composed of two elements was designed. The lower part (Figure 3.1 black) features a groove which fits a glass lip of the vessels fits. The cell is sealed by a second element made from PTFE with a groove that holds an O-ring to assure an air tight fit. The two parts of the lid are locked and held together by four screws. It is very important that the screws are not tightened too much as the PTFE of the lid could crack upon too much stress. The PTFE lid of the cell has multiple holes, which provide the possibility for different connections. Each hole perfectly fits a small rubber septum with a tight fit. In the intended uses, the rubber septa serve as insertion points for quasi-reference, auxiliary electrodes and for the addition of preparations, e.g. by a syringe pump.



Fig. 3.1: Inert gas cell designed for electrochemical analytics and use in electrocatalytical experiments

In the center of the upper lid is a hole that is larger than the other ones. This central hole can be used in two ways. For electrochemical measurements such as cv, a working electrode can be inserted which however requires an additional fitting. By cutting off the top of a small rubber septum and fixing it to the electrode with parafilm allows for an air tight fit. Using this method cyclic voltammetry measurements under inert conditions were achieved. The gas tightness of the cell was determined by means of gas chromatography. The capability of the

system was tested by measuring the $[\text{W}(\text{N}_2)(\text{P}_2^{\text{Me}}\text{PP}_2^{\text{Ph}})]$ complex (Figure 3.3).

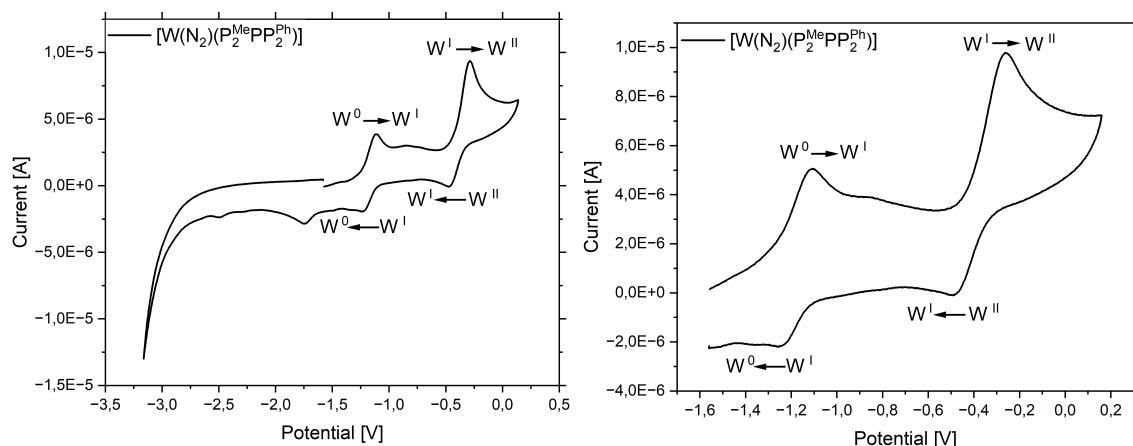


Fig. 3.2: The cyclic voltammograms of the $[\text{W}(\text{N}_2)(\text{P}_2^{\text{Me}}\text{PP}_2^{\text{Ph}})]$ complex ($c = 0.06 \text{ mmol/L}$) measured with the cells build for the electrochemical investigations (thf, $0.1 \text{ mol/L TBAPF}_6$). Display is the overview voltammogram (left) and a measurement of the redox events of the complex (right). Two redox systems are associated with the complex. The first reversible redox system can be assigned to the oxidation/reduction of $\text{W}^0 \rightleftharpoons \text{W}^{\text{I}}$ and the second, quasi-reversible system to the $\text{W}^{\text{I}} \rightleftharpoons \text{W}^{\text{II}}$.

The cyclic voltammograms obtained for this complex and its molybdenum analogue are identical to the ones obtained in cooperation with LE POUL from the Université de Bretagne Occidentale Brest. This demonstrates the functionality of the system. The cyclic voltammograms shown in Figure 3.3 are referenced to the potentials known from the measurements in Brest. The main issue at the time was that the complexes were measured against a quasi-reference electrode and no ferrocene/ferrocenium was added to compensate for the shift of the Ag-quasi-reference. Nonetheless, the cvs demonstrate the functionality of the cell design.

The second application of the cell is meant for electrocatalytic investigations. By inserting a glass tube, containing a G4 frit at the bottom, into the larger central hole, the working electrode is separated from the auxiliary electrode allowing for electrolysis experiments. The central hole is fitted with an additional o-ring inside a groove in the middle of the PTFE lid, sealing the cell. Due to the interaction of the o-rings between the two parts of the lid and in the center hole with the solvent used, the cell is sealed even better. The polymer of the o-rings takes up some of the solvent vapor, leading to an increase in their volume. As for the cyclic voltammetry configuration, the air tightness of the cell in electrocatalytic configuration was verified by GC measurements of the cell atmosphere after different time periods and after experiments. Neither water nor oxygen could not be detected in any of the performed measurements.

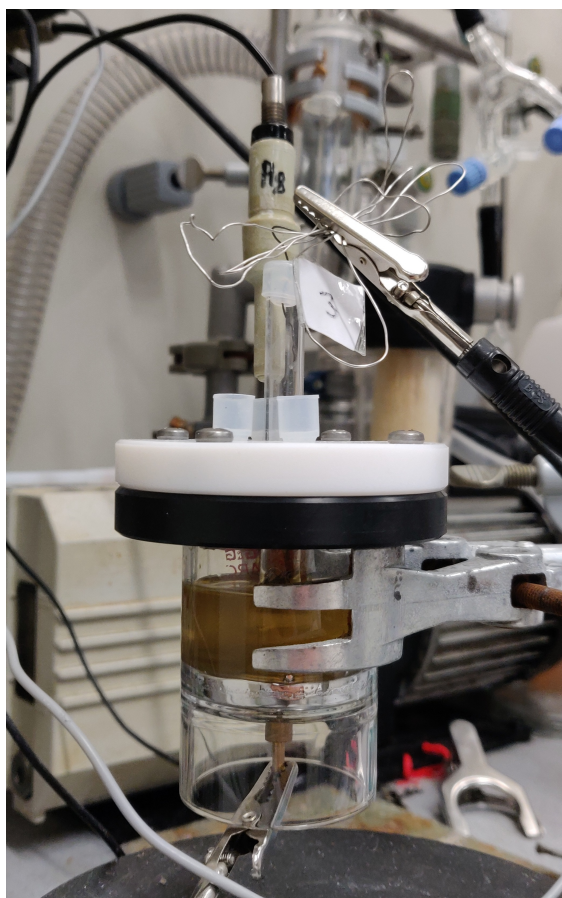


Fig. 3.3: Setup for investigations towards electrocatalytic activity of the complex using a mercury pool electrode.

In order to perform investigations regarding the electrocatalytic activity of the complexes, a mercury pool electrode was used. This type of electrodes has two main advantages. The first advantage is the big surface of the electrode, eliminating any diffusion limitations, film formation or deposition on the surface by utilization of a stirring bar. The second advantage is the overpotential of the mercury electrode. As protons are required for ammonia generation, application of low potentials would lead to the hydrogen evolution reaction (HER) at the electrodes surface as the dominant reaction, even before ammonia would be generated. Mercury has a very high overpotential, allowing relatively low potentials to be applied without hydrogen evolution. It is important to note that the vessel used for a mercury pool cathode differs from the ones used for measurements in the way that the connector for the working electrode is located on the bottom of the vessel.

The main disadvantage of the cell shown in Figure 3.1 is the volume required for measurements. Due to that reason an identical lid system for vessels with a smaller volume was build. One of the vessels was modified for electrocatalytic studies by inserting a thick platinum wire into the bottom of glass.

Many different attempts were performed in order to electrochemically generate ammonia with the molybdenum and tungsten dinitrogen complexes bearing the pentaPod ligand. The attempts included different acids like HBAr^{F} , $[\text{CoI}^{\text{H}}][\text{OTf}]$ or $[\text{Lu}^{\text{H}}][\text{OTf}]$ and different addition speeds and equivalents. Furthermore different solvents (thf and ether) as well as electrolytes were tested. Unfortunately, no significant amounts of ammonia were observed. The ammonia found can be related to the sole reaction of the complexes with the acids.

Project 2

As presented in Chapter 2 (Scientific background), there are many approaches to synthetic nitrogen fixation (cf. section 2.3). This part focuses on the coordination behavior of tridentate ligands. Like pincer and tripodal ligands, tridentate ligands have three donor atoms; however, these ligand types usually differ in their coordination behavior. Tripodal ligands prefer a facial coordination geometry, whereas pincer ligands, by definition, bind to a metal center in a meridional fashion.^[209,232] This is in contrast to the tridentate ligands, which due to their flexibility, can coordinate in facial as well as meridional geometry. As presented in section 2.3.5 our group invested a lot of efforts into the investigation of all three ligand types in the context of synthetic nitrogen fixation.^[209,210,212,216,217,224,229,233] For the tridentate systems the TUCZEK group investigated the synthesis of dinitrogen and bis(dinitrogen) complexes, the influence of the central atom (N or P) and its residues, the linkage between the terminal and central donors as well as the influence of the coligands.^[217,218,220–224,233] The complexes bear different ligand systems and were always investigated regarding their influence towards stability and N₂ activation. It was found that the replacement of the donor in *trans*-position to the N₂ ligand from a phosphine by an amine donor leads to a major increase in the activation.^[233] This can be attributed to the missing π -acceptor properties of the amine. The pure σ -donor abilities increase the electron density on the molybdenum center why more electron density is available for the backbonding to the N₂, which weakens the N \equiv N-triplebond.^[210,233,234] Although an increase in activation is desired, the missing ability for π -backdonation has some disadvantages as well. The molybdenum-N bond is weaker compared to the Mo-P bond, which led to the formation of mixtures of mono- and bis-dinitrogen complexes.^[221,233]

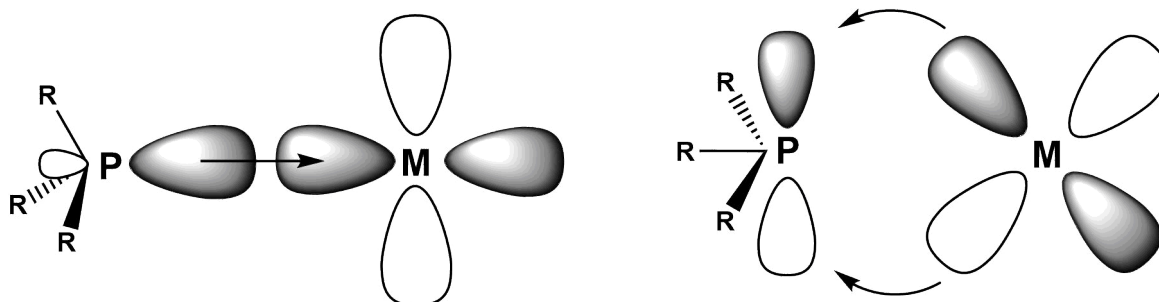


Fig. 4.1: Illustration of σ -donation from a PR₃ ligand to a metal center (left) and the π -backdonation from the d-orbital of the metal to free π^* -orbitals of the ligand (right). Edited based on ORPEN^[235] and CRABTREE.^[236]

In addition to the substitution of the central donor of the tridentate ligand, the residues bound to these donors were exchanged. Replacement of the hydrogen by a phenyl group did not show a significant influence regarding the activation.^[233] Another aspect investigated was the elongation of the linkage between the central and terminal donors, to be more specific, going from an ethyl to a propyl chain. This did not show any influence regarding the activation of the N₂ ligand. The increase in flexibility only led to the formation of multiple conformers and potential isomers.^[217,233]

Furthermore the influence of different coligands regarding the activation and stability of mono- and bis(dinitrogen) complexes was investigated as well as the difference between certain alkyl phosphines versus aryl phosphines.^[217,222,233] It is indicated that the differences in activation are depending on different steric and electronic factors.^[222]

The present study focuses on the influence of terminal phosphines, which bear various residues. In order to gain better insight into the nature of these systems and the effect of different substituents on structure and stability a series of ligands and complexes were synthesized and thoroughly characterized. Inspired by the success using pincer ligands, tridentate PN^{Ph}P ligands with bridging ethyl chains were chosen, due to the structural resemblance to the classical PNP pincer ligand. From prior studies it is known, that tridentate PNP ligands tend to form mixtures of mono- and bis(dinitrogen) complexes, are sensitive towards the choice of the coligand and have a limited stability, which increases the difficulty when investigating the behavior of the PNP ligands.^[220–222,233] To bypass these problems, tricarbonyl complexes were used instead in this project. Carbonyl complexes have excellent spectroscopic properties and are isoelectronic to the dinitrogen ligand. GRADERT *et al.* used this approach to study the behavior of NHC pincer ligands. He found that although pincer ligands, which usually coordinate in a meridional fashion, were used complexes with facial geometries were obtained. It is worth noting that the link between the central donor unit and the terminal donors was a C₂-chain, which provided the necessary flexibility needed for a facial geometry.^[232,237] In the following section the results of the study regarding tridentate PNP ligands with various phosphines will be described in detail.

4.1 Molybdenum tricarbonyl complexes supported by linear PNP ligands: Influence of P- and N-substituents on structure, stability and on the activation of small molecules

In this study a series of tridentate PN^{Ph}P^R ligands with varying moieties and corresponding Mo(CO)₃ complexes were synthesized and investigated using NMR-, IR- and Raman spectroscopy. The PNP^R ligands feature a central aniline and two ethyl bridged phosphines with different substituents (R = Ph, Me, Et, Pln, Cyp, ⁱPr, Cy and ^tBu). With [Mo(CO)₃(cht)] as

precursor, the tricarbonyl complexes bearing PPh₂, PEt₂, PCyp₂, PⁱPr₂ and PCy₂ groups were obtained. The successful coordination of the corresponding ligand is reflected in various changes in spectroscopy. For example the coordination of the phosphines leads to a low field shift of the phosphorus signal in the ³¹P NMR spectrum. The size of the shift is depending on the coordination mode. Coordination in meridional fashion leads to a bigger shift than the facial isomer. Further NMR spectroscopic investigations of the complexes revealed multiple ABX spin systems for different carbon atoms within the complex. Due to the low natural abundance of the NMR active ¹³C nucleus it can be assumed that a maximum of one carbon atom per complex is found resulting in the formation of higher order signals. The ABX spin systems show different split patterns depending on the coupling constants between the carbon atoms and the phosphines. From the NMR spectra it was also observed that all complexes adapt a facial geometry. This is confirmed by IR- and Raman spectra, which also show the expected pattern for facial complexes with C_s-symmetry. For all complexes, except the [Mo(CO)₃(PN^{Ph}P^{Cy})], Davydov splitting of the carbonyl stretches was observed which is the result of in- and out-of-phase coupling leading to a split of the CO stretches.^[238–241] Comparison of the complexes synthesized in this study to the similar complexes bearing PN^HP^R ligands revealed some interesting properties. Other than the complex with PN^{Ph}P^R ligands, the Mo(CO)₃ complexes bearing PN^HP^R ligands were not only able to adapt a meridional geometry but also the complex with PN^{Ph}P^{tBu} complex could be obtained. DFT calculations of the thermodynamics and dissociative pathways for the isomerization did not reveal the cause for the observed behavior. Only calculations the transition states of the isomerization revealed differences between the complexes. A direct rearrangement of the hexacoordinated complexes from a facial to a meridional geometry and vice versa is energetically unfavorable, leaving a dissociative pathway as possible mechanism for the isomerization. Comparison of the pathways of pentacoordinated complexes bearing PN^{Ph}P^{Me} and PN^HP^{Me} revealed that the aniline based ligand forms agostic hydrogen bridges to the free coordination site, kinetically stabilizing the intermediates, whereas the complex with NH function is unable to form such a bond leading to a lower lying transition state. This inability of the PN^{Ph}P^R systems to interchange between the isomers leads to the formation of almost purely facial complexes, predetermined by the [Mo(CO)₃(cht)] complex. Unfortunately, using the PN^{Ph}P^{Me} ligand did not lead to the formation of the desired product but in a mixture of different complexes. The PN^{Ph}P^{Ph} ligand did not yield any carbonyl complex, even with different precursors or conditions (time, solvent, temperature). Also no complex was obtained using the PN^{Ph}P^{tBu} ligand. As found from DFT calculations, this complex is energetically unfavorable in a facial as well as meridional geometry.

Article and Cover reprinted with permission from S. Froitzheim, J. Junge, C. Barnehl, T. A. Engesser, J. Krahmer, C. Näther and F. Tuczek, *Eur. J. Inorg. Chem.* 2023, 26, e202300280. <https://doi.org/10.1002/ejic.202300280>


Copyright ©2023 European Journal of Inorganic Chemistry

EurJIC

European Journal of Inorganic Chemistry

 **Chemistry
Europe**

European Chemical
Societies Publishing

Celebrating
25
Years


Front Cover:

T. A. Engesser, F. Tuczek and co-workers

Molybdenum Tricarbonyl Complexes Supported by Linear PNP Ligands:
Influence of *P*- and *N*-Substituents on Relative Stability, Stereoisomerism
and on the Activation of Small Molecules



WILEY-VCH

33/2023



Molybdenum Tricarbonyl Complexes Supported by Linear PNP Ligands: Influence of P- and N-Substituents on Relative Stability, Stereoisomerism and on the Activation of Small Molecules

Sven Froitzheim,^[a] Jannik Junge,^[a] Christopher Barnehl,^[a] Tobias A. Engesser,^{*,[a]} Jan Krahmer,^[a] Christian Näther,^[a] and Felix Tuczek^{*,[a]}

Series of linear tridentate $\text{PN}^{\text{Ph}}\text{P}^{\text{R}}$ -ligands ($\text{R} = \text{Me}, \text{Et}, \text{Ph}, \text{Cyp}, \text{Pr}, \text{Cy}, \text{tBu}$) and molybdenum tricarbonyl complexes $[\text{Mo}(\text{CO})_3\text{PN}^{\text{Ph}}\text{P}^{\text{R}}]$ ($\text{R} = \text{Ph}, \text{Et}, \text{Cyp}, \text{Pr}, \text{Cy}$) were synthesized and characterized using NMR-, IR-, and Raman spectroscopy as well as X-ray crystallography. The influence of the different phosphine donor groups of the $\text{PN}^{\text{Ph}}\text{P}^{\text{R}}$ ligands on the bonding and activation of CO ligands is investigated. Importantly, all

complexes are found to adopt a *fac* geometry, both in solution and in the solid state. This is in contrast to analogous complexes supported by $\text{PN}^{\text{H}}\text{P}$ ligands. DFT calculations reveal that the phenyl ring at the central amine function is the cause of the preferred geometry, hindering isomerization to a *mer* geometry.

Introduction

PNP ligands have been employed in coordination chemistry with a broad range of metals and coligands.^[1–10] Three main types of these ligands can be distinguished: PNP pincer, tripodal, and linear tridentate ligands. Pincer ligands enforce a meridional coordination mode through their rigid design, which confers, both, high stabilities and catalytic activities to the derived complexes.^[3,4]

They are used for many catalytic reactions such as (de)hydrogenation, ammonia synthesis, and small molecule activation.^[1,4,8] Tripodal PNP systems, on the other hand, are rarer than pincer ligands and their P_3 analogues are more commonly encountered due to the stronger coordinating third P donor.^[9,10] Herein, we focus on the third type comprising linear tridentate PNP ligands. Complexes supported by such ligands have been employed in many fields of coordination/organometallic chemistry such as bond activation,^[11,12] small molecule activation,^[13] and catalysis; e.g., for (de)hydrogenation reactions using Ru, Ir, Fe, and other metal centers.^[12,14] Linear PNP ligands may also be included in the pincer category as

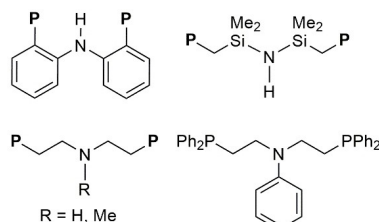
long as they coordinate in a meridional fashion.^[1,15,16] However, whereas pincer ligands only allow a meridional coordination mode, linear tridentate ligands enable both a facial and meridional coordination to the metal. Variation of the terminal donors and P–N linkages allows tailoring these ligands to specific applications (Scheme 1).^[4,16] In this regard extensive investigations have been performed to determine the influence of different terminal phosphine^[17] and central amine donors,^[18,19] as well as possible metal-ligand cooperativity on their reactivities/catalytic activities.^[12,20] Further studies involved the influence of modified linkages between the phosphorus donors and the central amine to tune the electronic properties of these systems or utilize them for asymmetric catalysis.^[1,16,21]

For a number of years our group has explored different ways of attaching molybdenum dinitrogen complexes to surfaces for applications in electrocatalytic nitrogen fixation.^[10,22] Based on the fact that carbon monoxide and dinitrogen are isoelectronic,^[23] CO can be employed as a model for N_2 binding.^[24] In this context, we succeeded to covalently attach molybdenum tricarbonyl complexes supported by a planar

[a] S. Froitzheim, Dr. J. Junge, C. Barnehl, Dr. T. A. Engesser, Dr. J. Krahmer, Prof. Dr. C. Näther, Prof. Dr. F. Tuczek
Institut für Anorganische Chemie
Christian-Albrechts-Universität zu Kiel
Max-Eyth-Straße 2, 24118 Kiel (Germany)
E-mail: tengesser@ac.uni-kiel.de
ftuczek@ac.uni-kiel.de

Supporting information for this article is available on the WWW under <https://doi.org/10.1002/ejic.202300280>

© 2023 The Authors. European Journal of Inorganic Chemistry published by Wiley-VCH GmbH. This is an open access article under the terms of the Creative Commons Attribution Non-Commercial NoDerivs License, which permits use and distribution in any medium, provided the original work is properly cited, the use is non-commercial and no modifications or adaptations are made.



Scheme 1. Examples of different tridentate PNP ligands.^[5,6,7] P = different aryl and alkyl phosphines. Bottom right: $\text{PN}^{\text{Ph}}\text{P}^{\text{Ph}}$ ligand which marks the starting point of this study.

PN^3P pincer and a tripodal triphos ligand via appended 4-ethynylphenyl units to TATA (triazatriangulenium) platforms. The resulting functionalized tricarbonyl complexes were deposited on gold and studied with a range of surface-spectroscopic methods.^[10,22] As alternative headgroups for surface studies, molybdenum dinitrogen (or carbonyl) complexes supported by linear PNP ligands may be envisioned.^[25] Notably, introducing an ethynyl group in 4-position of the central phenyl ring of the $\text{PN}^{\text{Ph}}\text{P}$ ligand (cf. Scheme 1, bottom right) would enable similar coupling strategies to platforms or organic surface layers as applied earlier for PN^3P and triphos ligands and derived complexes (see above).^[10,22]

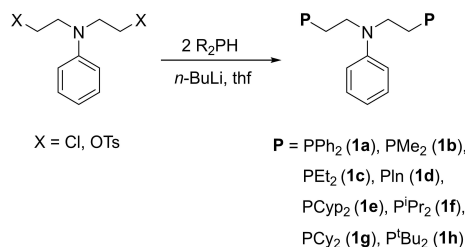
The molybdenum tricarbonyl complex $[\text{Mo}(\text{CO})_3(\text{PN}^{\text{Ph}}\text{P}^{\text{Ph}})]$ supported by the $\text{PN}^{\text{Ph}}\text{P}^{\text{Ph}}$ ligand (Scheme 1, lower right) has been prepared by KESKIN *et al.* and investigated regarding to his structural and spectroscopic properties.^[26] Various electronic factors were explored to explain the preferred formation of the *fac* isomer.^[26] In order to increase the activation of small molecules such as CO or N_2 in molybdenum complexes supported by the $\text{PN}^{\text{Ph}}\text{P}^{\text{Ph}}$ ligand,^[25] its terminal phenyl groups have to be replaced by more electron-donating alkyl residues. Correspondingly we synthesized a series of linear $\text{PN}^{\text{Ph}}\text{P}^{\text{R}}$ ligands with different alkyl residues $\text{R} = \text{Me}, \text{Et}, \text{P}^{\text{t}}, \text{Cyp}, \text{P}^{\text{t}}, \text{Cy}, \text{P}^{\text{t}}, \text{Bu}$ and studied the structural and electronic properties of derived molybdenum tricarbonyl complexes, using X-ray structure analysis and spectroscopy. As expected, all new complexes exhibit a shift of the CO-stretching frequencies to lower wavenumbers with respect to the parent complex. Surprisingly, however, *all* of these complexes are found in the *fac* geometry, regardless of the steric demand of the alkyl substituents. This is in strong contrast to analogous complexes supported by $\text{PN}^{\text{H}}\text{P}$ ligands, where both, *mer* and *fac* isomers can be identified. In an effort to understand this result (and provide arguments going beyond those advanced by KESKIN *et al.* to account for the *fac* constitution of the parent $[\text{Mo}(\text{CO})_3(\text{PN}^{\text{Ph}}\text{P}^{\text{Ph}})]$ complex; see above), hypothetical *mer-fac* isomerization processes are modeled by DFT for both $\text{PN}^{\text{Ph}}\text{P}$ and $\text{PN}^{\text{H}}\text{P}$ complexes. These calculations indicate that *mer-fac* isomerization is kinetically hindered in Mo-tricarbonyl complexes supported by $\text{PN}^{\text{Ph}}\text{P}$ ligands whereas it is thermally allowed in the analogous $\text{PN}^{\text{H}}\text{P}$ systems.

Results and Discussion

Synthesis and X-ray Structure Determination

Most of the PNP ligands (1a–1f and 1h) were prepared by reaction of *N,N*-bis(2-chloroethyl)aniline with a secondary phosphine in the presence of *n*-butyllithium (Scheme 2). For the $\text{PN}^{\text{Ph}}\text{P}^{\text{Pr}}$ ligand (terminal isopropyl groups, phenyl substituent on the central nitrogen; 1f), which was previously reported by CURLEY *et al.*,^[19,27] *N,N*-bis(2-tosylethyl)aniline instead of the chlorinated analog was employed. The latter route was also used by KOSTAS for the synthesis of $\text{PN}^{\text{Ph}}\text{P}^{\text{Ph}}$ (1a).^[6]

All ligands could be obtained in pure form and were reacted with the precursor $[\text{Mo}(\text{CO})_3(\text{cht})]$ in toluene ($\text{cht} = \text{cyclohepta-}$

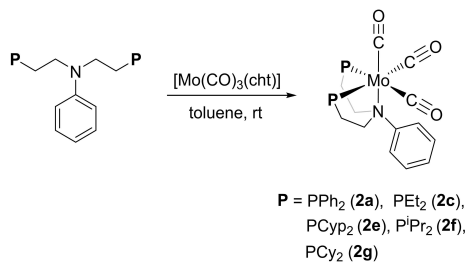


Scheme 2. Synthesis scheme of the PNP ligands used in this study (PIn = phospholano, PC_4H_9 ; Cyp = cyclopentyl).

triene), leading to $[\text{Mo}(\text{CO})_3(\text{PN}^{\text{Ph}}\text{P}^{\text{R}})]$ complexes with $\text{R} = \text{Ph}$ (2a), Et (2c), Cyp (2e), $^{\text{t}}\text{Pr}$ (2f), and Cy (2g; cf. Scheme 3 and experimental section, general procedures A and B). As expected, the solid tricarbonyl complexes showed sufficient air-stability for characterization via infrared spectroscopy. Notably, not all target compounds could be prepared in this fashion. Specifically, the Mo tricarbonyl complexes supported by the ligands $\text{PN}^{\text{Ph}}\text{P}^{\text{Me}}$ (2b), $\text{PN}^{\text{Ph}}\text{P}^{\text{In}}$ (2d) and $\text{PN}^{\text{Ph}}\text{P}^{\text{Bu}}$ (2h) could neither be isolated in pure form nor characterized in solution. For 2b and 2h, products were obtained which were insoluble. IR investigations indicate that most likely mixtures of different complexes are formed. On the other hand, DFT calculations suggest that the complex 2h containing *tert*-butyl groups may not form due to steric reasons (Table S2, Table S3, Figure S63). In particular, longer bond lengths are observed in the calculated structure of *fac*- $[\text{Mo}(\text{CO})_3(\text{PN}^{\text{Ph}}\text{P}^{\text{Bu}})]$ (2h) as compared to $[\text{Mo}(\text{CO})_3(\text{PN}^{\text{Ph}}\text{P}^{\text{Pr}})]$ (2f), which might impede a complete coordination of the ligand. Factors influencing the relative stabilities of the target complexes in solution will be analyzed later in this study, employing DFT calculations (see below).

For complex $[\text{Mo}(\text{CO})_3(\text{PN}^{\text{Ph}}\text{P}^{\text{Et}})]$ (2c), a single-crystal X-ray structure determination could be performed, showing a facial coordination mode of the PNP ligand (Figure 1, Table 1). This is analogous to the related complex *fac*- $[\text{Mo}(\text{CO})_3(\text{PN}^{\text{Ph}}\text{P}^{\text{Ph}})]$ (2a) reported by KESKIN *et al.*^[26]

The biggest structural difference between the two *fac*- $[\text{Mo}(\text{CO})_3(\text{PNP})]$ complexes 2a and 2c is exhibited by the Mo–N bond length which is 0.0703 Å shorter in 2c than in 2a. On the



Scheme 3. Synthesis of $[\text{Mo}(\text{CO})_3(\text{PN}^{\text{Ph}}\text{P}^{\text{R}})]$ complexes ($\text{R} = \text{P}$).

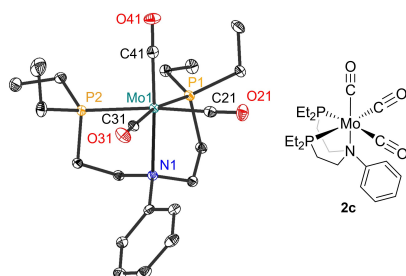


Figure 1. Molecular structure of *fac*-[Mo(CO)₃(PN^{Ph}P^{Et})] (**2c**). The hydrogen atoms have been omitted for clarity. Thermal ellipsoids are shown at 50% probability.

Mo–X bond ^[a]	[Mo(CO) ₃ (PN ^{Ph} P ^{Et})] ^[b] (2c)	[Mo(CO) ₃ (PN ^{Ph} P ^{Ph})] ^[c] (2a)	Δ
Mo–N1	2.442	2.512	–0.070
Mo–P1	2.514	2.496	0.018
Mo–P2	2.507	2.466	0.041
Mo–C41(ax)	1.938	1.933	–0.005
Mo–C21(eq)	1.978	1.977	–0.001
Mo–C31(eq)	1.973	1.979	–0.006

[a] Numbering according to Figure 1; [b] this study; [c] Ref. [26].

other hand, the Mo–P distances are increased in **2c** relative to **2a** by 0.018 and 0.041 Å. This is due to the fact that compared to the diphenylphosphine groups of **2a**, the diethyl phosphine groups of **2c** have a larger sigma donor strength and a smaller capacity for π -backbonding. Interestingly, the increased Mo–P bond length found in **2c** appears to entail a shorter Mo–N bond, suggesting a leveling effect of the central amine group on the overall binding properties of the PNP ligand. This is also evident from the fact that the Mo–C distances are very similar in **2a** and **2c**. Nevertheless, vibrational spectroscopy reveals that the CO ligands of **2c** are stronger activated than in **2a** (cf. next section).

Infrared and Raman Spectroscopy

Detailed information on the bonding and activation of CO ligands is provided by IR and Raman spectroscopy. Moreover, the CO-stretching vibrations also reflect the *mer/fac* isomerism of the title complexes. For an octahedral complex with facial M(CO)₃ coordination, group theory predicts two bands in the CO stretching region of the IR- and in the Raman-spectrum (A₁ and E). Due to the actual C_s-symmetry of complexes **2a**, **2c**, **2e**, **2f**, and **2g** (Figure 4 and Figure S36, S44, S48, and S52), E splits into A'' and A'(₂), in addition to A'(₁) which corresponds to the totally symmetric, in-phase stretching mode. In the Raman spectrum, the A'(₁) band is found to be very weak for the facial

isomer, while the A'' and A'(₂) bands are strong, clearly visible in case of **2c** (Figure 2). The meridional isomer, on the other hand, would exhibit an intense A'(₁) band.^[28] Therefore, vibrational spectroscopy shows that our [Mo(CO)₃(PN^{Ph}P^R)] complexes always adopt the facial coordination mode in the solid state.

Notably, the infrared and Raman spectra of the parent complex **2a** recorded by us differ from those published by KESKIN *et al.*^[26] While the A'(₁) and A'' vibrations appear at comparable frequencies, the frequency of the A'(₂) mode given by these authors (1782–1796 cm^{–1}) is considerably lower than observed by us (1808/1804 cm^{–1}; cf. Table 2). Moreover, the intensity of the A'(₁) peak in the Raman spectrum is fairly high, which would in principle speak against the assignment of a *fac* geometry to **2a**, as inferred by these authors on the basis of the vibrational spectra. We do not know the reason for this discrepancy, but note that our IR- and Raman data for **2a** are consistent with those obtained for the other complexes.

Interestingly, for all investigated complexes except **2g**, four instead of two bands are observed for the A'' and A'(₂) stretching vibrations in the Raman spectra (Table 2). Complex **2c**, in which this splitting is most pronounced, shows a difference of $\Delta\nu = 12$ and 10 cm^{–1} between the A'(₂) and A'' bands, respectively. This splitting is also observed when spectra of single crystals of **2c**

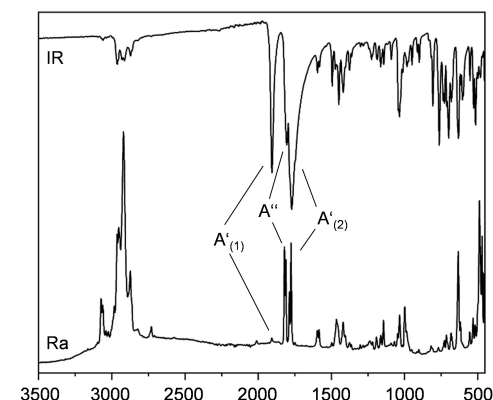


Figure 2. IR and Raman spectrum [cm^{–1}] of [Mo(CO)₃(PN^{Ph}P^{Et})] (**2c**). The CO stretching vibrations are assigned based on a C_s symmetric Mo(CO)₃ fragment.

Table 2. Experimental Raman frequencies [cm^{–1}] of the CO stretching vibrations in [Mo(CO)₃(PN^{Ph}P^R)] complexes (R = Ph (**2a**), Et (**2c**), Cyp (**2e**), ⁱPr (**2f**), Cy (**2g**)).

Complex	A'(₁)	A'' ^[a]	A'(₂) ^[a]
[Mo(CO) ₃ (PN ^{Ph} P ^{Ph})] (2a)	1921	1829/1819	1808/1804
[Mo(CO) ₃ (PN ^{Ph} P ^{Et})] (2c)	1906	1820/1810	1786/1774
[Mo(CO) ₃ (PN ^{Ph} P ^{Cyp})] (2e)	1907	1812/1795	1785
[Mo(CO) ₃ (PN ^{Ph} P ^{iPr})] (2g)	1901	1802/1794	1788/1780
[Mo(CO) ₃ (PN ^{Ph} P ^{Cy})] (2f)	1906	1810	1791

[a] In case of splitting both bands are listed.

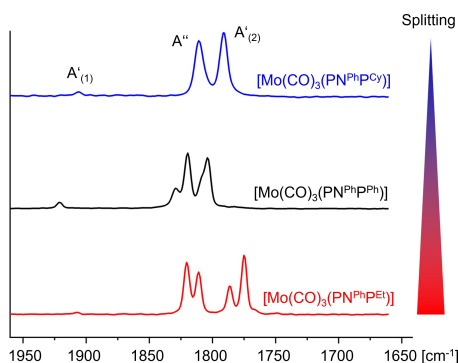


Figure 3. Splitting of the carbonyl stretches of $[\text{Mo}(\text{CO})_3(\text{PN}^{\text{R}}\text{P}^{\text{R}})]$ ($\text{R} = \text{Cy}$ (**2g**), Ph (**2a**), Et (**2c**)).

were measured, so it does not originate from impurities or a mixture of different compounds. In the crystal structures of **2c** and **2a**, more than one molecule exists within the unit cell ($Z = 8$ and 4 , respectively).^[26] In this case, the vibrations of individual molecules in the unit cell may couple (for $Z = 2$, e.g., into in-phase and out-of-phase combinations), and the corresponding bands or peaks split (Figure 3). This effect (factor group or Davydov splitting) has already been observed for molybdenum carbonyl complexes.^[29]

In addition to the coordination mode, information about the activation of the carbonyl ligands can be derived from the frequencies of the stretching vibrations of the $\text{Mo}(\text{CO})_3$ fragment. This is influenced by the σ -donation and π -acceptance properties of the phosphine and amine donors. From the literature, it is known that the difference in σ -donation properties of tertiary phosphines with different residues is small.^[30] In contrast, their π -acceptor properties change significantly, which then influences the vibrational frequency of the CO in *trans* position. Correspondingly, for the complexes bearing different alkyl phosphines (**2c**, **2e**, **2f**, and **2g**) the observed $A'_{(1)}$ CO stretching frequencies are fairly similar (Table 2), the biggest difference ($\Delta(A'_{(1)}) = 6 \text{ cm}^{-1}$) being found between the systems with PCy_2 and P^iPr_2 substituents. In contrast, the $A'_{(1)}$ frequency of complex **2a** bearing phenyl phosphines (1921 cm^{-1}) is 14 cm^{-1} higher than **2e**, the alkyl phosphine complex with the highest frequency. This conforms to aryl phosphines being more π -backbonding than their alkyl counterparts. Overall, the activation of the CO ligands as a function of the substituents on the phosphines is found to increase in the following sequence:



NMR Spectroscopy

^{31}P and ^{13}C NMR spectroscopy in solution provides information on the *mer-fac* isomerism of complexes **2a**, **2c** & **2e–2g** in

solution via the ^{31}P resonances of the P-donors and the ^{13}C atoms of the carbonyl ligands coupling with the phosphines, respectively. Importantly, the low-field shifts observed for the ^{31}P -signals of the complexes (ca. 15–22 ppm) are characteristic for a facial binding geometry. In meridional complexes, larger low-field shifts of the phosphine signals are observed.^[31] Whereas the fraction of *fac* complexes exceeds 99%, traces of *mer* isomers can also be detected ($< 1\%$; cf. Figure 4 and Table S1). Other byproducts appear to be tetracarbonyl complexes which result from decomposition of their tricarbonyl analogs, as reported in the literature.^[26] Complete NMR data are given in the Supporting Information.

Complementary information can be derived from the ^{13}C -NMR spectra. Due to the low natural abundance of this carbon isotope ($< 1.1\%$), molecules containing more than one ^{13}C nucleus can be neglected.^[32] Notably, a ^{13}C nucleus next to a ^{31}P atom leads to different chemical environments for otherwise equivalent ^{31}P nuclei. Correspondingly, the coordination mode can be derived from the signal patterns emerging in the ^{13}C NMR spectrum by coupling of the ^{31}P nuclei with the ^{13}C atoms statistically found on the different carbon positions. Specifically, a meridional coordination geometry is reflected by two triplets, one for the CO *trans* to the amine group and one for the CO ligands *trans* to each other. In contrast, a facial geometry gives rise to a triplet for the axial carbonyl carbon (resulting from the equal *cis* couplings to the equatorial phosphines) and, for the equatorial carbon atoms, to the X part of an ABX spin system with A and B represented by two equatorial ^{31}P atoms ($\text{A} = \text{P}^{\text{A}}$, $\text{B} = \text{P}^{\text{B}}$ and $\text{X} = ^{13}\text{C}$; see Figure 3 for complex **2c** as an example).^[22,28]

In agreement with the results from ^{31}P -NMR spectroscopy (see above), the facial isomers are found with ratios of more than 99% for all complexes (**2a**, **2c** & **2e–2g**). For these species, the X part of the ABX spectrum (see above) corresponds to a six-line signal (see Figure 5, top, “b” and bottom scheme). The distance between lines 2 and 5 is equal to $|J_{\text{AX}} + J_{\text{BX}}|$, while the separation between lines 1 and 6 (lines 3 and 4) equals $2|D_{+} + D_{-}|$ ($2|D_{+} - D_{-}|$, respectively). D_{+} and D_{-} are defined by Equation (1). Furthermore, the relative intensities of the inner

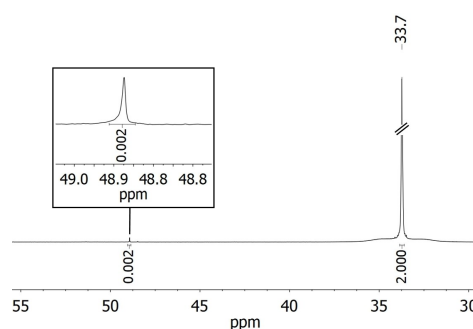


Figure 4. ^{31}P NMR spectrum of the *fac*- $[\text{Mo}(\text{CO})_3(\text{PN}^{\text{R}}\text{P}^{\text{R}})]$ complex (**2c**) including traces of the meridional isomer at 48.9 ppm.

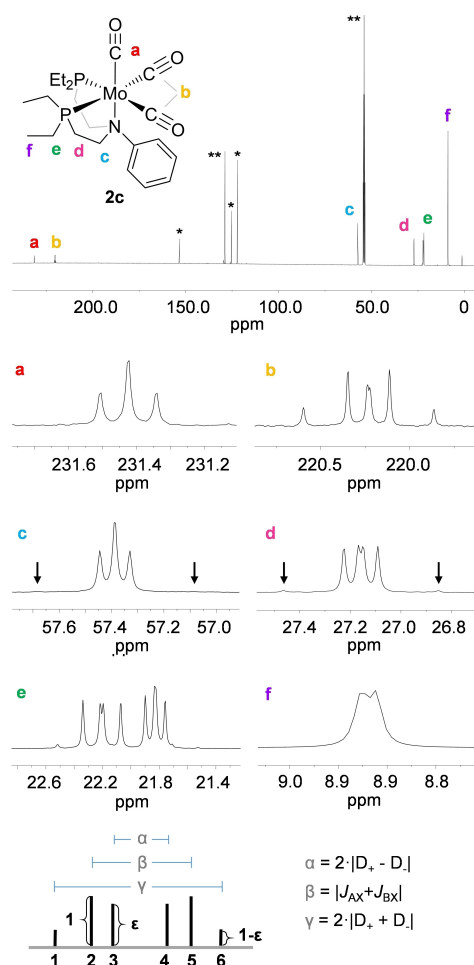


Figure 5. Top: ^{13}C NMR spectrum of $[\text{Mo}(\text{CO})_3(\text{PN}^{\text{Ph}}\text{P}^{\text{Ph}})]$ (**2c**) with the multiple ABX patterns of the different ^{13}C atoms (a-f) found due to the coupling to the phosphorus nuclei. The signals of NPh group are marked with an asterisk (*) and signals of solvents with two asterisks (**). Arrows indicate outer lines of little intensity. Bottom: Six-line pattern emerging from ABX-spectrum.

and outer lines with respect to lines 2 and 5 correspond to ϵ and $1 - \epsilon$, respectively (cf. Figure 5, bottom), with the latter given by Equation (2).^[28,33]

$$D \pm = \frac{1}{2} \sqrt{[(v_A - v_B) \pm 0.5 (J_{AX} - J_{BX})]^2 + J_{AB}^2} \quad (1)$$

$$1 - \epsilon = \frac{\frac{1}{4} (J_{AX} - J_{BX})^2}{\frac{1}{4} (J_{AX} - J_{BX})^2 + J_{AB}^2} \quad (2)$$

Based on these equations, approximate values for the coupling constants J_{AX} , J_{BX} and J_{AB} as well as the chemical shift difference $v_A - v_B$ were determined and subsequently refined by fitting to the experimental spectra (see Figures S62–S65). The shifts and coupling parameters found for the carbonyl and phosphine groups of complexes **2a**, **2c**, **2e**, and **2f** are collected in Table 3. In addition to similar chemical shifts of the CO ligands, the coupling constants to the P-nuclei are also very similar, indicating not only similar geometries but also comparable electronic structures. Unfortunately, complex **2g** showed such a weak solubility in most NMR solvents that it was impossible to obtain spectra of sufficient quality to derive these parameters.

Besides the ABX patterns of the equatorial CO ligands, the ^{13}C NMR signals of the ethylene bridges (Figure 5c and 5d) and terminal ethyl groups (Figure 5e and 5f) also reflect coupling to the phosphorus atoms. With decreasing spin-spin coupling of the ^{13}C and ^{31}P nuclei, the difference between D₊ and D₋ decreases, leading to a smaller distance between the inner lines (3 & 4). Moreover, the intensity of the outer lines (1 & 6) decreases, which in turn increases the intensity of the inner lines. This is, e.g., visible for the signal of the ethyl bridge proximal to the phosphorus atom (Figure 5d). Ultimately, the six-line pattern collapses into a triplet (Figure 5c; arrows indicate the positions of the very weak outer lines). Similar spectra are also observed for the other complexes (Figure S35, S43, S47, S51, and S53). The derived ^{13}C NMR parameters are collected in Table 3.

Thermodynamics of Metal to PNP-Ligand Bonding

Data obtained from NMR, IR, and Raman spectroscopy indicate a facial geometry of complexes **2a**, **2c**, **2e**, **2f**, and **2g** in solution and in the solid state. The meridional isomers are only visible as minor traces (< 1%) (Figure 4) in the ^{31}P NMR spectra. In order to understand the preference of the ligands for facial coordination, a DFT study was conducted. To this end ligand exchange reactions with the different ligands were treated theoretically, considering both *mer* and *fac* configurations for the entire series of complexes. This allows to directly compare their relative stabilities (Figure 6, Table S8 & S9), leading to the following conclusions: (i) in agreement with the results of KESKIN *et al.*, the facial isomer of $[\text{Mo}(\text{CO})_3(\text{PN}^{\text{Ph}}\text{P}^{\text{Ph}})]$ (**2a**) is more favorable than its *mer* counterpart; (ii) a thermodynamically more stable tricarbonyl complex (**2c**) is generated by the $\text{PN}^{\text{Ph}}\text{P}^{\text{Et}}$ ligand whereby the *fac* isomer is also at lower energy than its *mer* analogue; (iii) for all $\text{PN}^{\text{Ph}}\text{P}^{\text{R}}$ ligands with terminal alkyl substituents exhibiting a higher steric demand than ethyl, the stability of the derived $\text{Mo}(\text{CO})_3$ complex decreases and *mer* is at lower energy than *fac* (Figure 6).

Notably, both isomers of **2h** with di-*tert*-butylphosphine groups are very unfavorable. In the facial isomer, the bond lengths are too elongated to consider it a possible product; accordingly, the calculated energy is very high. The meridional geometry of **2h** is more favorable, but still at high energy compared to all other complexes (cf. $\theta_{\text{O}}(\text{P}^t\text{Bu}_3) = 167.1^\circ$).^[34] This

Complex	δ(¹³ CO _{eq}) [ppm]	δ(¹³ CO _{ax}) [ppm]	δ(³¹ P) [ppm]	² J _{AB} [Hz]	² J _{AX} (<i>trans</i>) [Hz]	² J _{BX} (<i>cis</i>) [Hz]	Δν _{AB} [Hz]
[Mo(CO) ₃ (PN ^{Ph} P ^{Ph})] (2a)	231.6	219.6	38.0	21.6	39.4	−14.0	1.30
[Mo(CO) ₃ (PN ^{Ph} P ^{Et})] (2c)	231.4	220.3	33.7	29.1	32.4	−10.8	1.80
[Mo(CO) ₃ (PN ^{Ph} P ^{Cy})] (2e)	232.0	220.8	41.6	22.7	36.5	−13.7	0.97
[Mo(CO) ₃ (PN ^{Ph} P ^{Pr})] (2f)	231.9	220.8	51.6	26.5	33.7	−8.8	1.69
[Mo(CO) ₃ (PN ^{Ph} P ^{iBu})] (2g)	232.1	221.0	40.8	–	–	–	–

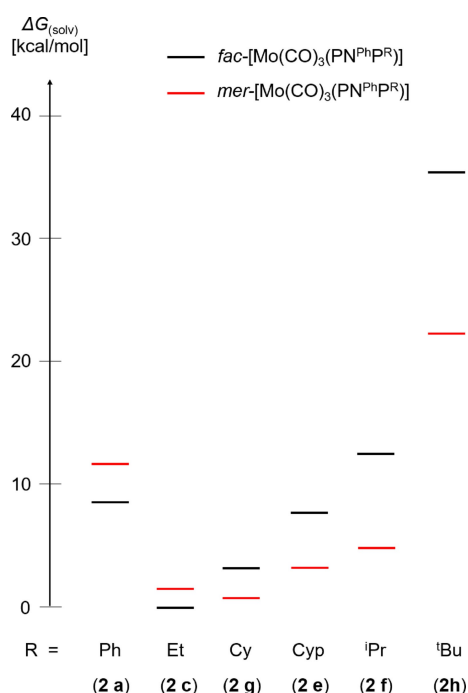


Figure 6. Theoretical relative Gibbs energies (including solvation) of the facial and meridional [Mo(CO)₃(PN^{Ph}P^R)] complexes with different phosphine groups (R = Et (2c), Ph (2a), Cyp (2e), ⁱPr (2f), Cy (2g), ⁱBu (2h)), relative to the most stable complex *mer*-2c and calculated by ligand exchange reactions (PBE0/def2-TZVPP).

may explain the experimental finding this complex could not be synthesized (see above).

Although the calculations overall suggest a preference for the meridional isomers for all Mo(CO)₃ complexes supported by PN^{Ph}P^R ligands with sterically more demanding substituents than ethyl (cf. Figure 6), only the facial isomers were obtained experimentally (see above). In order to understand this apparent contradiction to the theoretically calculated energetics, we compared our findings with results obtained on similar compounds in the literature. Notably, KESKIN *et al.* also reported that only facial [Mo(CO)₃(PN^{Ph}P^{Ph})] (2a) was obtained

initially; the meridional isomer only formed in a small amount when the facial complex was stored in solution for weeks.^[26] However, [Mo(CO)₃(PN^HP^R)] complexes with PN^HP^R ligands (R = ⁱPr, Cy, ^tBu) containing a central NH donor instead of NPh seem to behave differently.^[35,36] For [Mo(CO)₃(PN^HP^{Pr})]₂, e.g., a crystal structure with facial geometry was obtained,^[35] but the corresponding NMR and IR spectra reflect a meridional geometry (Supp. Mat. of ref. [35]). Furthermore, [Mo(CO)₃(PN^HP^{Cy})] is found to exist in, both, meridional and facial geometry in solution, with the ratio of the two isomers being solvent-dependent.^[36]

In order to identify possible differences in the stabilities of PN^{Ph}P and PN^HP complexes, analogous isodesmic calculations of ligand exchange reactions as performed for the former (Figure 6) were conducted for the latter systems as well (Figure S59 & S60). In agreement with the PN^{Ph}P complexes, the *fac* isomers tend to become more unfavorable with increasing steric demand of the phosphine residues, accounting for the experimentally observed formation of *mer* isomers (along with their *fac* counterparts). The lack of observation of *mer* isomers in case of the PN^{Ph}P complexes thus has to be of kinetic, not thermodynamic origin.

Theoretical information on possible *mer-fac* isomerisations of [Mo(CO)₃(PNP)] complexes in solution can be obtained by DFT calculations as well. In principle, these processes can occur in a non-dissociative fashion via distorted octahedral transition states (Figure 7, Figure S65 & S66). Interestingly, calculations of the corresponding energy barriers for model complexes with PMe₂ groups (PN^HP^{Me}), reveal that the transition states for the amine PN^HP^{Me} and phenylamine PN^{Ph}P^{Me} systems (Figure 7, TS_{iso}^{NR}_{CO3}) are unfavorable. The corresponding energy barriers of around 30 kcal/mol make such transformations unlikely. Additionally, no clear differences between the NH and NPh ligands were found, which contrasts with the experimental observations, showing significantly different behaviour.

Another process possibly enabling an isomeric transformation involves the preliminary dissociation of a CO ligand from the 18-electron [Mo(CO)₃(PN^{Ph}P)] complexes, leading to penta-coordinate square-pyramidal 16-electron complexes [Mo(CO)₂(PN^{Ph}P)] (Figure 8 and 9, Figure S67 & S68, Table S10).^[26,37] The resulting empty coordination site makes it energetically much more favorable for the ligand to undergo a conformational rearrangement. Notably, this dissociative substitution mechanism has been experimentally evidenced for [Mo(CO)₃(PN^{Ph}P^{Ph})] (2a) by KESKIN *et al.*^[26]

4.1 Molybdenum tricarbonyl complexes supported by linear PNP ligands: Influence of P- and N-substituents on structure, stability and on the activation of small molecules

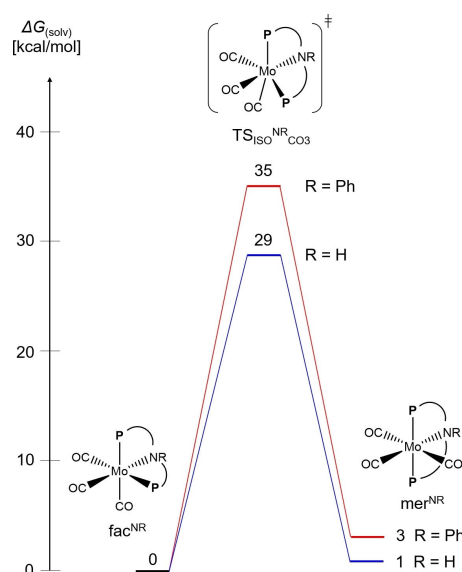


Figure 7. Theoretical relative Gibbs energies in solution of the isomeric transformation of *fac*- and *mer*-[Mo(CO)₃(PN^HP^{Me})] model complexes (R = H (red), Ph (blue)) via transition state TS_{ISO}^{NR} CO₃ (PBE0/def2-TZVPP(D3BJ)) (P = PMe₂).

The energies of the corresponding dissociative intermediates [Mo(CO)₂(PN^HP^{Me})] (R = H, Ph) indicate that only the CO ligands *trans* to P or CO coligands dissociate, leading to square-pyramidal isomers with the amine donor in equatorial position (Figure 8 and 9, *fac*1^{NH}, *mer*1^{NH}, *mer*2^{NH}, *fac*1^{NPh} and *mer*2^{NPh}). Therefore, only these are taken into account for the subsequent rebinding of CO and indeed, a significantly different behavior is observed for the NH and NPh ligands presented here:

In the case of [Mo(CO)₂(PN^HP^{Me})], two equally stable *mer* isomers are found (Figure 8, *mer*1^{NH} and *mer*2^{NH}) which are in equilibrium with each other via a very low-lying trigonal bipyramidal transition state (Figure 8, TS_{MER}^{NH} CO₂). This makes both isomers equally available for conversion into a facial isomer. The actual isomeric transformation then occurs between *mer*1^{NH} and *fac*1^{NH} via a distorted trigonal bipyramidal transition state (TS_{ISO}^{NH} CO₂). Due to the relatively low energy barrier of 11 kcal/mol from *mer*1^{NH} or 3 kcal/mol from *fac*1^{NH}, *mer* and *fac* complexes are in an equilibrium in solution, which is in accordance with the experimental observations in the literature.^[36]

In case of [Mo(CO)₂(PN^HP^{Me})], only one meridional and one facial isomer is stable due to an agostic hydrogen bond between the phenyl group and the molybdenum center, which occupies the vacant coordination site (*mer*1^{NPh} and *fac*1^{NPh}, Figure 9). This and the steric demand of the migrating N^H group lead to a much higher energy barrier of 18 kcal/mol from *mer*1^{NPh} or 9 kcal/mol from *fac*1^{NPh} complexes, making this process either impossible or at least very slow. Therefore, the initial geometry of the complex resulting from reaction of the precursor with the PNP ligand is conserved. For *fac*-[Mo-

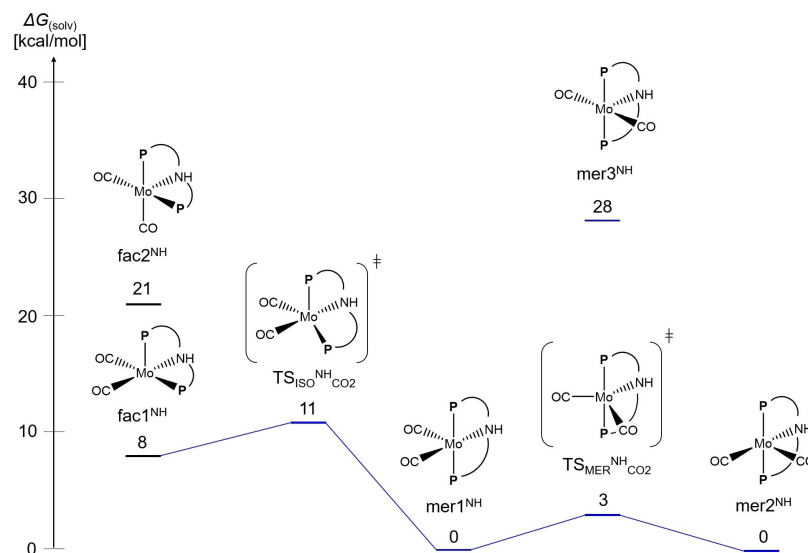


Figure 8. Theoretical relative Gibbs energies in solution of the isomers of pentacoordinated model complex [Mo(CO)₂(PN^HP^{Me})], including the isomeric transformation via transition state TS_{ISO}^{NH} and the conversion of the two possible meridional isomers via TS_{MER} (PBE0/def2-TZVPP(D3BJ)) (P = PMe₂).

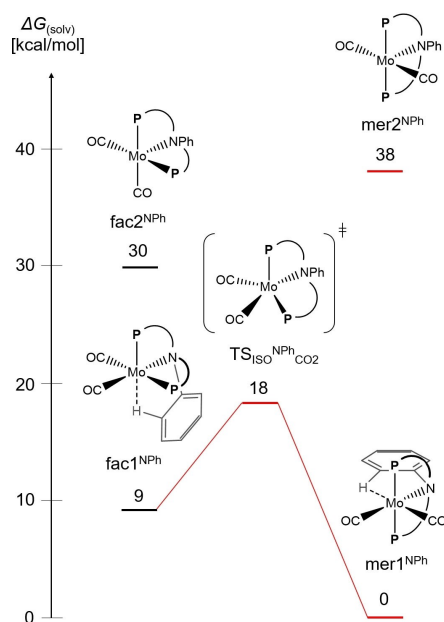


Figure 9. Theoretical relative Gibbs energies in solution of the different isomers of pentacoordinated model complex $[\text{Mo}(\text{CO})_3(\text{PN}^{\text{Ph}}\text{P}^{\text{Ph}})]$, including isomeric transformation via transition state ($\text{TS}_{\text{ISO}}^{\text{NPh CO}_2}$) (PBE0/def2-TZVPP(D3BJ)) ($\text{P} = \text{PMe}_3$).

$(\text{CO})_2(\text{cht})$], which has been used in this study for complexation of the $\text{PN}^{\text{Ph}}\text{P}^{\text{R}}$ ligands, it has been established that reaction with linear tridentate ligands exclusively leads to *fac*-complexes.^[38,39] Due to the high barriers, conversion to possibly lower-lying *mer*-isomers thus is hindered, explaining the lack of observation of *mer*-isomers.

Conclusions

In order to study the influence of the different phosphine groups on the coordination behavior of PNP ligands and examine their impact on the activation small molecules like CO, a series of tridentate $\text{PN}^{\text{Ph}}\text{P}^{\text{R}}$ ligands ($\text{R} = \text{Ph}, \text{Me}, \text{Et}, \text{P}^{\text{t}}\text{In}, \text{Cyp}, \text{Pr}, \text{Cy}, \text{tBu}$) and corresponding molybdenum tricarbonyl complexes $[\text{Mo}(\text{CO})_3(\text{PN}^{\text{Ph}}\text{P}^{\text{R}})]$ ($\text{R} = \text{Ph}, \text{Et}, \text{Cyp}, \text{Pr}, \text{Cy}$) were prepared and characterized by NMR and vibrational spectroscopy. In case of $[\text{Mo}(\text{CO})_3(\text{PN}^{\text{Ph}}\text{P}^{\text{Et}})]$ the determination of the crystal structure was possible as well.

Upon replacing the $\text{PN}^{\text{Ph}}\text{P}^{\text{Ph}}$ ligand of the parent complex $[\text{Mo}(\text{CO})_3(\text{PN}^{\text{Ph}}\text{P}^{\text{Ph}})]$ by ligands with alkylphosphine groups the activation of the bound carbonyl ligands was found to increase. Within the series of new complexes supported by $\text{PN}^{\text{Ph}}\text{P}^{\text{R}}$ ligands with alkyl substituents, however, differences in CO stretching frequencies and, thus, CO activation, were small.

Nevertheless, the relative stabilities of these complexes significantly decrease with increasing steric bulk of the terminal alkyl substituents R. This becomes evident from isodesmic calculations, replacing, e.g., the $\text{PN}^{\text{Ph}}\text{P}^{\text{Ph}}$ ligand of the parent $[\text{Mo}(\text{CO})_3(\text{PN}^{\text{Ph}}\text{P})]$ complex by corresponding ligands with PR_2 groups ($\text{R} = \text{Et}, \text{Cyp}, \text{Pr}, \text{Cy}$). This way, it becomes clear that the thermodynamically most stable member of the entire family of $\text{PN}^{\text{Ph}}\text{P}^{\text{R}}$ complexes is $[\text{Mo}(\text{CO})_3(\text{PN}^{\text{Ph}}\text{P}^{\text{Et}})]$, exhibiting strongly electron-donating PET_2 groups with little steric bulk. On the other hand, these calculations provide an explanation for the fact that the complex with the sterically most demanding *tert*-butyl substituents could not be obtained.

Experimental and theoretical information was also obtained on the preferred stereochemical configuration (*mer* vs. *fac*) of the $[\text{Mo}(\text{CO})_3(\text{PN}^{\text{Ph}}\text{P}^{\text{R}})]$ complexes. Surprisingly, all of the synthesized $[\text{Mo}(\text{CO})_3(\text{PN}^{\text{Ph}}\text{P}^{\text{R}})]$ complexes exhibit the *fac* geometry, irrespective of the electronic and steric properties of the terminal phosphine groups. This is, e.g., evident from NMR spectroscopy where the meridional isomers were only found as minor byproducts visible in small amounts (< 1 %) in the ^{31}P spectra. Moreover, the preferred formation of the *fac* isomers could also be inferred from X-ray structure determination and vibrational spectroscopy where typical CO splitting patterns were observed. Additional splittings present in the IR and Raman spectra were attributed to factor group or Davydov splittings.

For the parent $[\text{Mo}(\text{CO})_3(\text{PN}^{\text{Ph}}\text{P}^{\text{Ph}})]$ complex (2a) the preference for the *fac*-isomer had already been evidenced by KESKIN *et al.* Notably, they were able to generate the *fac* isomer from the complex $[\text{Mo}(\text{CO})_2(\kappa^2\text{-PN}^{\text{Ph}}\text{P})]$ with a yield of < 1 %. Furthermore, they found that the *mer* isomer is formed in small amounts upon letting a solution of the *fac* isomer stand for a long time. From their observations, they concluded that the *mer*-isomer is formed from its *fac* counterpart by a *fac*→*mer* isomerization process proceeding via a dissociative pathway. This scenario has also been advanced by Crabtree regarding the stereoisomerism of $[\text{Mo}(\text{CO})_3\text{L}_3]$ complexes.^[37]

Theoretical support for the hypothesis that the *fac*-isomer of the complex $[\text{Mo}(\text{CO})_3(\text{PN}^{\text{Ph}}\text{P}^{\text{Ph}})]$ is more stable than its *mer* counterpart was obtained by KESKIN *et al.* from DFT calculations.^[26] Notably, SICLOVAN *et al.* synthesized the $[\text{M}(\text{CO})_3(\text{PN}^{\text{Me}}\text{P})]$ ($\text{M} = \text{Mo}, \text{W}$) complex and also found the facial isomer to be more stable than its meridional analog.^[7] In this context it has to be noted that a general electronic-structural preference for the *fac* geometry in $\text{Mo}(\text{O})$ tricarbonyl complexes results from the fact that all three t_{2g} are able to interact in an equal fashion with the CO ligands in a π -backbonding manner whereas this is not possible for the *mer* configuration. However, this electronic effect should potentially be counteracted by a steric effect if the residues on the terminal phosphine donors become more bulky than phenyl groups. For sterically very demanding substituents, this ultimately may lead to a preference of the *mer* configuration. This is in fact observed for molybdenum tricarbonyl complexes supported by $\text{PN}^{\text{Ph}}\text{P}$ ligands,^[35,36] but apparently does not apply to our systems.

In order to address this problem, calculations of the relative stabilities of *mer*-*fac* isomers have been performed for the

entire series of complexes. While the thermal stability of these complexes overall decreases with increasing steric bulk of the substituents (see above), these calculations also reveal that a preference for the *fac* isomer is restricted to the $\text{PN}^{\text{Ph}}\text{P}^{\text{Ph}}$ complex and the $\text{PN}^{\text{Ph}}\text{P}^{\text{Et}}$ complex which exhibits the least sterically demanding alkyl substituents. For all complexes with bulkier residues the *mer* isomers are thermodynamically favored. However, this is not observed experimentally. We thus suspected that formation of the *mer* products might be kinetically hindered in all of these complexes.

In order to check this hypothesis, potential *fac-mer* isomerization processes have been treated with the help of DFT. Notably, calculations of the model systems $[\text{Mo}(\text{CO})_3(\text{PN}^{\text{R}}\text{P}^{\text{R}})]$ ($\text{R}=\text{H}$, Ph) showed that a direct isomeric transformation of these hexacoordinated complexes is unlikely. Nevertheless, it can occur after preliminary dissociation of CO, in the course of a dissociative process (see above). Our calculations indicate that such a process is thermally allowed in the $\text{PN}^{\text{H}}\text{P}$ systems, but is hindered in the $\text{PN}^{\text{Ph}}\text{P}$ systems due to the steric demand of the phenyl group and an agostic interaction present both in the facial and the meridional isomers involved in the transformation. This acts to significantly increase the energetic barrier for isomerization in $\text{PN}^{\text{Ph}}\text{P}$ systems, making it very slow or even suppressing it completely. The stereoisomeric configuration of the primary products resulting from reaction of the $\text{Mo}(\text{CO})_3$ precursor with the $\text{PN}^{\text{Ph}}\text{P}$ ligands thus is more or less retained. As it has been established that reaction of the precursor *fac*- $[\text{Mo}(\text{CO})_3(\text{cht})]$ with linear tridentate ligands exclusively leads to *fac* products,^[38,39] it becomes understandable that all of the investigated complexes **2a**, **2c**, **2e**, **2f**, and **2g** exhibit the *fac* geometry and no *mer* isomers have been observed. This stereochemical peculiarity of the $\text{PN}^{\text{Ph}}\text{P}$ ligands may entail characteristic differences in the reactivity of derived transition-metal complexes to analogues supported by $\text{PN}^{\text{H}}\text{P}$ ligands, comparable to those evidenced before in the context of CO_2 hydrogenation catalyzed by $\text{Ru}(\text{PN}^{\text{H}}\text{P})$ and $-\text{PN}^{\text{Ph}}\text{P}$ complexes.^[19]

Experimental Section

Materials and methods: All syntheses containing air- and moisture-sensitive compounds were carried out under a nitrogen atmosphere using Schlenk techniques. All solvents were dried under argon atmosphere prior to use. Commercially available substances were used as purchased without further purification. The chemicals used for synthesis were obtained from Sigma-Aldrich Co., abcr GmbH & Co. KG., and Fisher Scientific GmbH.

Spectroscopy: The NMR spectra were measured on a Bruker Avance III HD 400 pulse Fourier Transform spectrometer at 400.13 MHz (^1H), 100.61 MHz (^{13}C), and 161.98 MHz (^{31}P). The spectra were either referenced to solvent residue (5.32 ppm for CD_2Cl_2) or TMS ($\delta^{\text{H}}=0$ ppm), 85% H_3PO_4 ($\delta^{31}\text{P}=0$ ppm) as substitutive standards. The IR spectra were measured on a Bruker alpha FT-IR spectrometer and the Raman spectra on Bruker Vertex70 FT-IR with RAMII module. The elemental analyses were performed using a VarioMICRO cube element analyzer.

Single Crystal Structure Determination: Data collection was performed with an XtaLAB Synergy, Dualflex diffractometer with a microfocus tube using $\text{Cu}_{\text{K}\alpha}$ radiation ($\lambda=1.54184$). The structure

was solved with SHELXT^[40] using Intrinsic Phasing and refined with SHELXL^[41] using Least Squares minimisation. All non-hydrogen atoms were refined anisotropically. The C–H H atoms were positioned with idealized geometry (methyl H atoms allowed to rotate but not to tip) and were refined isotropically with $U_{\text{iso}}(\text{H})=1.2 U_{\text{eq}}(\text{C})$ (1.5 for methyl H atoms using a riding model). Deposition Number 2156795 contains the supplementary crystallographic data for this paper. These data are provided free of charge by the joint Cambridge Crystallographic Data Centre and Fachinformationszentrum Karlsruhe Access Structures service.

Computational details: All calculations were performed using the ORCA 4.2.1 program package^[42] with PBE0 functional^[43] and def2-TZVPP basis set.^[44] Furthermore, Grimmes dispersion correction^[45] with Becke-Johnson damping (D3BJ),^[46] density fitting approximation (RJCOSX)^[47] and solvation correction (CPCM) were applied.^[48] All minimum structures were optimized to have no imaginary frequencies. The transition states were optimized with exactly one imaginary frequency.

General procedures and synthesis: The syntheses of dimethyl phosphine,^[49] diisopropyl phosphine,^[50] phospholane,^[51] *NN*-bis(2-chloroethyl)aniline^[52] and *N,N*-bis(2-(*p*-toluenesulfonyl)ethyl)aniline^[25] were prepared according to literature.

General procedure A: Synthesis of the PNP ligands. 1 eq. of *NN*-bis(2-chloroethyl)aniline was dissolved in thf and cooled to 0 °C. In a second vessel, the phosphine (2.1 eq.) was also dissolved in THF, cooled to 0 °C and *n*-butyllithium solution (2.5 mol/L) was added dropwise over 20 min. The solution was stirred for 30 min at 0 °C. Within 15 min the *NN*-Bis(2,2-dichloroethyl)aniline solution was added to the phosphine/*n*-butyllithium solution at 0 °C. The solution was stirred for 18 h at room temperature. 0.5 mL degassed water was added and the solvent was evaporated in vacuo. The residue was resolved in *n*-pentane (30 mL) and filtered through Celite® and basic aluminum oxide.

General procedure B: Synthesis of the molybdenum tricarbonyl complexes. 1 eq. of $[\text{Mo}(\text{CO})_3(\text{cht})]$ was dissolved in 3 mL toluene giving a red solution. The PNP-Ligand was dissolved in 2 mL toluene and added to the precursor complex solution. The solution was stirred for 18 h in the glovebox. The resulting crude product was filtered and washed with *n*-pentane (5 mL). The product was dried in vacuo resulting in a yellowish solid.

NN-Bis(2-(diphenylphosphino)ethyl)aniline ($\text{PN}^{\text{Ph}}\text{P}^{\text{Ph}}$, **1a**)

Following general procedure A, the $\text{PN}^{\text{Ph}}\text{P}^{\text{Ph}}$ (**1a**) ligand was obtained as colourless solid (796 mg, 1.54 mmol, 67%).

$^{31}\text{P}\{^1\text{H}\}$ NMR: (161.98 MHz, CD_2Cl_2 , 300 K): $\delta=-20.1$ (s, 2 P, PPh_2) ppm.

^1H NMR (400.13 MHz, CD_2Cl_2 , 300 K): $\delta=7.35-7.30$ (m, 8 H, P-(CH)_{phenyl}), 7.26–7.22 (m, 12 H, P-(CH)_{phenyl}), 7.03–6.99 (m, 2 H, N-(CH)_{phenyl}), 6.56–6.52 (m, 1 H, N-(CH)_{phenyl}), 6.28–6.26 (m, 2 H, N-(CH)_{phenyl}), 3.29–3.24 (m, 4 H, N-CH₂), 2.22–2.18 (m, 4 H, P-CH₂) ppm.

$^{13}\text{C}\{^1\text{H}\}$ NMR (100.62 MHz, CD_2Cl_2 , 300 K): $\delta=145.7$ (s, 1 C, N-(C_{phenyl})), 139.9 (d, $J_{\text{PC}}=12.2$ Hz, 4 C, P-(C_{phenyl})), 131.7 (d, $J_{\text{PC}}=18.8$ Hz, 8 C, P-(C_{phenyl})), 128.2 (s, 2 C, N-(C_{phenyl})), 127.7 (s, 4 C, P-(C_{phenyl})), 127.4 (d, $J_{\text{PC}}=6.80$ Hz, 8 C, P-(C_{phenyl})), 115.4 (s, 1 C, C_{phenyl}), 111.2 (s, 2 C, C_{phenyl}), 46.6 (d, $^2J_{\text{PC}}=25.6$ Hz, 2 C, N-CH₂), 25.0 (d, $J_{\text{PC}}=14.4$ Hz, 2 C, P-CH₂) ppm.

IR (ATR): $\tilde{\nu}=3068$ (w), 3049 (w), 3025 (w), 3018 (sh), 3001 (w), 2961 (w), 2928 (w), 2902 (w), 2869 (sh), 2855 (w), 1969 (vw), 1957 (vw), 1914 (vw), 1903 (vw), 1886 (vw), 1808 (w), 1764 (vw), 1595 (s),

1571 (m), 1501 (s), 1476 (s), 1461 (w), 1429 (s), 1414 (w), 1389 (m), 1359 (w), 1352 (m), 1337 (w), 1319 (vw), 1305 (w), 1275 (sh), 1260 (s), 1218 (w), 1195 (s), 1180 (w), 1148 (m), 1094 (m), 1064 (w), 1039 (w), 1026 (w), 1011 (w), 995 (w), 984 (w), 947 (w), 913 (w), 907 (vw), 865 (m), 815 (sh), 794 (s), 734 (vs), 688 (vs), 667 (sh), 614 (vw), 554 (m), 528 (m), 504 (vs), 476 (vs), 430 (m), 411 (sh) cm^{-1} .

NN-Bis(2-(dimethylphosphino)ethyl)aniline ($\text{PN}^{\text{Ph}}\text{P}^{\text{Me}}$, **1 b**)

Following general procedure A, the $\text{PN}^{\text{Ph}}\text{P}^{\text{Me}}$ (**1 b**) ligand was synthesized, however, the phosphine solution was cooled to -78°C instead of 0°C as described in the procedure. The ligand (**1 b**) was obtained as colourless oil (236.7 mg, 0.88 mmol, 63 %).

$^{31}\text{P}\{^1\text{H}\}$ NMR: (161.98 MHz, CD_2Cl_2 , 300 K): $\delta = -54.9$ (s, 2 P, PMe_2) ppm.

^1H NMR (400.13 MHz, CD_2Cl_2 , 300 K): $\delta = 7.22\text{--}7.17$ (m, 2 H, $\text{CH}_{\text{phenyl}}$), 6.68–6.61 (m, 3 H, $\text{CH}_{\text{phenyl}}$), 3.45–3.39 (m, 4 H, CH_2), 1.70–1.65 (m, 4 H, CH_2), 1.06 (d, $^2J_{\text{PH}} = 2.29$ Hz, 12 H, $\text{CH}_{\text{methyl}}$) ppm.

$^{13}\text{C}\{^1\text{H}\}$ NMR (100.62 MHz, CD_2Cl_2 , 300 K): $\delta = 147.4$ (s, 1 C, $\text{C}_{\text{iphenyl}}$), 129.2 (s, 2 C, $\text{C}_{\text{orphenyl}}$), 115.7 (s, 1 C, $\text{C}_{\text{prphenyl}}$), 112.2 (s, 2 C, $\text{C}_{\text{mrphenyl}}$), 47.7 (d, $^2J_{\text{PC}} = 21.4$ Hz, 2 C, N-CH_2), 29.8 (d, $^1J_{\text{PC}} = 12.6$ Hz, 2 C, P-CH_2), 13.8 (d, $^1J_{\text{PC}} = 13.1$ Hz, 4 C, P-CH_3) ppm.

IR (ATR): $\tilde{\nu} = 3090$ (w), 3058 (w), 3038 (w), 3023 (w), 2951 (s), 2923 (m), 2892 (s), 2853 (sh), 2812 (w), 1598 (s), 1574 (sh), 1504 (s), 1461 (vw), 1449 (vw), 1428 (sh), 1420 (m), 1394 (w), 1354 (s), 1292 (sh), 1278 (m), 1213 (w), 1186 (m), 1159 (vw), 1142 (sh), 1128 (m), 1084 (vw), 1042 (m), 1007 (br m), 990 (w), 967 (vw), 938 (s), 885 (m), 818 (w), 747 (s), 710 (w), 694 (s), 668 (w), 531 (vw), 508 (w), 434 (vw), 416 (vw) cm^{-1} .

NN-Bis(2-(diethylphosphino)ethyl)aniline ($\text{PN}^{\text{Ph}}\text{P}^{\text{Et}}$, **1 c**)

Following general procedure A, the $\text{PN}^{\text{Ph}}\text{P}^{\text{Et}}$ (**1 c**) ligand was obtained as colourless oil (411 mg, 1.26 mmol, 25 %).

$^{31}\text{P}\{^1\text{H}\}$ NMR: (161.98 MHz, CD_2Cl_2 , 300 K): $\delta = -25.7$ (s, 2 P, PEt_2) ppm.

^1H NMR (400.13 MHz, CD_2Cl_2 , 300 K): $\delta = 7.20\text{--}7.16$ (m, 2 H, $\text{CH}_{\text{phenyl}}$), 6.67–6.60 (m, 3 H, $\text{CH}_{\text{phenyl}}$), 3.45–3.40 (m, 4 H, N-CH_2), 1.70–1.65 (m, 4 H, P-CH_2), 1.48–1.42 (m, 8 H, $\text{P-CH}_2\text{-CH}_3$), 1.11–1.03 (m, 12 H, $\text{P-CH}_2\text{-CH}_3$) ppm.

$^{13}\text{C}\{^1\text{H}\}$ NMR (100.62 MHz, CD_2Cl_2 , 300 K): $\delta = 147.4$ (s, 1 C, $\text{C}_{\text{iphenyl}}$), 129.3 (s, 2 C, $\text{C}_{\text{orphenyl}}$), 115.8 (s, 1 C, $\text{C}_{\text{prphenyl}}$), 112.3 (s, 2 C, $\text{C}_{\text{mrphenyl}}$), 48.3 (d, $^2J_{\text{PC}} = 22.6$ Hz, 2 C, N-CH_2), 24.3 (d, $^1J_{\text{PC}} = 15.9$ Hz, 2 C, P-CH_2), 19.0 (d, $^1J_{\text{PC}} = 18.9$ Hz, 4 C, $\text{P-CH}_2\text{-Me}$), 13.8 (d, $^2J_{\text{PC}} = 12.6$ Hz, 4 C, -CH_3) ppm.

IR (ATR): $\tilde{\nu} = 3085$ (w), 3043 (w, br), 2955 (w), 2923 (s), 2877 (s), 2821 (sh), 2821 (sh), 2220 (w), 2135 (w), 1600 (s), 1505 (s), 1436 (s), 1400 (m), 1368 (s), 1210 (w), 1200 (vw), 1158 (s), 1131 (s), 989 (m), 967 (vw), 842 (sh), 789 (sh), 747 (vs), 695 (s), 619 (vw), 567 (w), 513 (w), 451 (vw) cm^{-1} .

NN-Bis(2-phospholanoethyl)aniline ($\text{PN}^{\text{Ph}}\text{P}^{\text{In}}$, **1 d**)

NN-Bis(2-chloroethyl)aniline (320 mg, 147 mmol) was dissolved in THF (10 mL). In a second vessel lithium phospholanide (500 mg, 2.95 mmol) was dissolved in 8 mL THF and cooled to 0°C . 1.2 mL (3.00 mmol) of *n*-butyllithium solution was added dropwise and stirred in the cold for 40 min. The aniline solution was added slowly to the phosphine/*n*-buli solution and it was stirred for 4 d at room temperature. All volatile components were removed in vacuo and the residue was extracted with *n*-pentane and dichloromethane

before filtering through celite and basic allox. The solvents were removed yielding a yellow oil as product (233 mg, 0.72 mmol, 49 %).

$^{31}\text{P}\{^1\text{H}\}$ NMR: (161.98 MHz, CDCl_3 , 300 K): $\delta = -32.0$ (s, 2 P, PIn) ppm.

^1H NMR (400.13 MHz, CDCl_3 , 300 K): $\delta = 7.24\text{--}7.20$ (m, 2 H, $\text{CH}_{\text{phenyl}}$), 6.68–6.64 (m, 3 H, $\text{CH}_{\text{phenyl}}$), 3.41–3.36 (m, 4 H, N-CH_2), 1.85–1.65 (m, 4 H, P-CH_2), 8 H, $(\text{CH}_2)_{\text{PIn}}$, 1.63–1.59 (m, 4 H, $(\text{CH}_2)_{\text{PIn}}$), 1.53–1.46 (m, 4 H, $(\text{CH}_2)_{\text{PIn}}$) ppm.

$^{13}\text{C}\{^1\text{H}\}$ NMR (100.62 MHz, CDCl_3 , 300 K): $\delta = 146.1$ (s, 1 C, $\text{C}_{\text{iphenyl}}$), 128.3 (s, 2 C, $\text{C}_{\text{orphenyl}}$), 114.9 (s, 1 C, $\text{C}_{\text{prphenyl}}$), 111.2 (s, 2 C, $\text{C}_{\text{mrphenyl}}$), 47.7 (d, $^2J_{\text{PC}} = 21.4$ Hz, 2 C, N-CH_2), 26.8 (d, $^1J_{\text{PC}} = 3.8$ Hz, 4 C, $(\text{CH}_2)_{\text{PIn}}$), 25.8 (d, $^2J_{\text{PC}} = 18.6$ Hz, 4 C, P-CH_2), 25.0 (d, $^1J_{\text{PC}} = 11.0$ Hz, 4 C, $(\text{CH}_2)_{\text{PIn}}$) ppm.

IR (ATR): $\tilde{\nu} = 3090$ (w), 3057 (w), 3038 (w), 3023 (w), 2929 (s), 2873 (vw), 2855 (s), 2823 (sh), 2675 (vw), 1916 (w), 1905 (w), 1600 (vs), 1570 (sh), 1502 (vs), 1457 (w), 1445 (m), 1352 (s), 1322 (sh), 1298 (vw), 1275 (sh), 1256 (s), 1209 (vw), 1183 (m), 1157 (vw), 1118 (sh), 1107 (s), 1087 (sh), 1054 (vw), 1039 (w), 1013 (s), 950 (vw), To2 (vw), 859 (w), 828 (sh), 792 (s), 743 (vs), 688 (vs), 657 (vw), 620 (vw), 561 (vw), 508 (m), 466 (vw), 398 (m) cm^{-1} .

NN-Bis(2-(dicyclopentylphosphino)ethyl)aniline ($\text{PN}^{\text{Ph}}\text{P}^{\text{Cyp}}$, **1 e**)

Following general procedure A, the $\text{PN}^{\text{Ph}}\text{P}^{\text{Cyp}}$ (**1 e**) ligand was obtained with the exception that the solution was stirred for 4 d yielding the product as colourless solid (540 mg, 1.11 mmol, 76 %).

$^{31}\text{P}\{^1\text{H}\}$ NMR: (161.98 MHz, CDCl_3 , 300 K): $\delta = -7.93$ (s, 2 P, PCyp_2) ppm.

^1H NMR (400.13 MHz, CDCl_3 , 300 K): $\delta = 7.24\text{--}7.20$ (m, 2 H, $\text{CH}_{\text{phenyl}}$), 6.68–6.63 (m, 3 H, $\text{CH}_{\text{phenyl}}$), 3.49–3.44 (m, 4 H, N-CH_2), 1.97–1.85 (m, 8 H, CH_2_{Cyp}), 1.74 (m, $^2J_{\text{PH}} = 2.35$ Hz, $^3J_{\text{HH}} = 8.79$ Hz, 4 H, P-CH_2), 1.70–1.63 (m, 8 H, CH_2_{Cyp}), 1.62–1.51 (m, 8 H, CH_2_{Cyp}), 1.48–1.33 (m, 8 H, CH_2_{Cyp}) ppm.

$^{13}\text{C}\{^1\text{H}\}$ NMR (100.62 MHz, CDCl_3 , 300 K): $\delta = 147.2$ (s, 1 C, $\text{C}_{\text{iphenyl}}$), 129.5 (s, 2 C, $\text{C}_{\text{orphenyl}}$), 115.8 (s, 1 C, $\text{C}_{\text{prphenyl}}$), 112.2 (s, 2 C, $\text{C}_{\text{mrphenyl}}$), 49.2 (d, $^2J_{\text{PC}} = 40.6$ Hz, 2 C, N-CH_2), 36.2 (d, $^2J_{\text{PC}} = 10.3$ Hz, 4 C, P-C_{Cyp}), 31.3 (d, $^1J_{\text{PC}} = 16.9$ Hz, 4 C, P-C_{Cyp}), 30.5 (d, $^2J_{\text{PC}} = 12.5$ Hz, 4 C, P-C_{Cyp}), 26.6 (d, $^2J_{\text{PC}} = 7.40$ Hz, 4 C, P-C_{Cyp}), 26.3 (d, $^2J_{\text{PC}} = 6.30$ Hz, 4 C, P-C_{Cyp}), 22.8 (d, $^1J_{\text{PC}} = 17.9$ Hz, 2 C, P-C_{Cyp}) ppm.

IR (ATR): $\tilde{\nu} = 3211$ (w, br), 3089 (w), 3060 (w), 3036 (w), 3018 (w), 2942 (vs), 2902 (w), 2858 (vs), 2056 (vw), 1904 (vw), 1800 (vw), 1752 (vw), 1602 (s), 1595 (s), 1566 (m), 1506 (vs), 1466 (sh), 1455 (sh), 1444 (s), 1402 (s), 1350 (s), 1320 (vw), 1283 (s), 1260 (w), 1215 (w), 1184 (vs), 1155 (vw), 1126 (s), 1086 (sh), 1059 (vw), 1034 (m), 1002 (s), 980 (w), 942 (vw), 921 (vw), 904 (m), 853 (m), 800 (m), 755 (sh), 738 (vs), 703 (sh), 689 (vs), 545 (m), 508 (s), 490 (vw), 457 (vw), 423 (w) cm^{-1} .

NN-Bis(2-(diisopropylphosphino)ethyl)aniline ($\text{PN}^{\text{Ph}}\text{P}^{\text{IPr}}$, **1 f**)

Diisopropylphosphine (0.67 g, 5.67 mmol) was solved in 10 mL THF and cooled to 0°C . *n*-Butyllithium solution in hexane (2.4 mL, 6.00 mmol) was added dropwise and stirred for 30 min at 0°C . Afterwards, the solution was stirred for an additional 30 min at room temperature. The solution turned orange. *NN*-Bis(2-(*p*-toluenesulfonyl)ethyl)aniline (1.26 g, 2.57 mmol) was dissolved in 10 mL THF and both solutions were cooled to 0°C . The phosphine/*n*-butyllithium solution was added dropwise to the aniline giving a yellow solution. After an hour, the solution turned green and red/orange after 18 h. The reaction was quenched with degassed water (5 mL) and all volatile components were removed in vacuo. The

4.1 Molybdenum tricarbonyl complexes supported by linear PNP ligands: Influence of P- and N-substituents on structure, stability and on the activation of small molecules

residue was resolved in 40 mL diethyl ether and filtered through Celite® and basic aluminium oxide. The $\text{PN}^{\text{Ph}}\text{P}^{\text{Pr}}$ (**1f**) ligand was obtained as colourless oil (411 mg, 1.26 mmol, 25 %).

$^3\text{P}\{^1\text{H}\}$ NMR: (161.98 MHz, CD_2Cl_2 , 300 K): $\delta = 1.53$ (s, 2 P, P^{Pr}_2) ppm.

^1H NMR (400.13 MHz, CD_2Cl_2 , 300 K): $\delta = 7.24\text{--}7.20$ (m, 2 H, $\text{CH}_{\text{phenyl}}$), 6.68–6.62 (m, 3 H, $\text{CH}_{\text{phenyl}}$), 3.51–3.46 (m, 4 H, N- CH_2), 1.79 (dsept, $^2J_{\text{PH}} = 2.11$ Hz, $^3J_{\text{HH}} = 7.11$ Hz, 4 H, P-CH), 1.71–1.65 (m, 4 H, P- CH_2), 1.15–1.08 (m, 24 H, P-CH- CH_3) ppm.

$^{13}\text{C}\{^1\text{H}\}$ NMR (100.62 MHz, CD_2Cl_2 , 300 K): $\delta = 147.2$ (s, 1 C, $\text{C}_{\text{iphenyl}}$), 129.3 (s, 2 C, $\text{C}_{\text{orphenyl}}$), 115.6 (s, 1 C, $\text{C}_{\text{prphenyl}}$), 112.1 (s, 2 C, $\text{C}_{\text{mrphenyl}}$), 50.4 (d, $^2J_{\text{PC}} = 32.2$ Hz, 2 C, N- CH_2), 23.4 (d, $J_{\text{PC}} = 12.3$ Hz, 4 C, P-CH), 20.0 (d, $^2J_{\text{PC}} = 16.3$ Hz, 4 C, P-CH-Me), 19.8 (d, $J_{\text{PC}} = 12.6$ Hz, 2 C, CH_2P), 18.7 (d, $^2J_{\text{PC}} = 9.40$ Hz, 4 C, P-CH-Me) ppm.

IR (ATR): $\tilde{\nu} = 3091$ (w), 3061 (w), 3038 (w), 2958 (sh), 2945 (vs), 2923 (w), 2887 (w), 2861 (vs), 1914 (vw), 1595 (vs), 1571 (vw), 1500 (vs), 1456 (s), 1382 (m), 1361 (sh), 1350 (s), 1277 (m), 1235 (vw), 1214 (w), 1183 (m), 1158 (w), 1127 (m), 1099 (vw), 1086 (sh), 1035 (s), 1014 (w), 993 (m), 919 (m), 887 (m), 859 (w), 806 (w), 742 (vs), 716 (w), 693 (s), 649 (w), 619 (w), 572 (vw), 509 (w), 466 (w) cm^{-1} .

NN-Bis(2-(dicyclohexylphosphino)ethyl)aniline ($\text{PN}^{\text{Ph}}\text{P}^{\text{Cy}}$, **1g**)

Following general procedure A, the $\text{PN}^{\text{Ph}}\text{P}^{\text{Cy}}$ (**1g**) ligand was obtained as colourless solid (2.00 mg, 3.69 mmol, 99 %).

$^3\text{P}\{^1\text{H}\}$ NMR: (161.98 MHz, CD_2Cl_2 , 300 K): $\delta = -8.21$ (s, 2 P, PCy_2) ppm.

^1H NMR (400.13 MHz, CD_2Cl_2 , 300 K): $\delta = 7.21\text{--}7.17$ (m, 2 H, $\text{CH}_{\text{phenyl}}$), 6.63–6.59 (m, 3 H, $\text{CH}_{\text{phenyl}}$), 3.44–3.38 (m, 4 H, N- CH_2), 1.79–1.63 (m, 24 H, CH_2), 1.60–1.53 (m, 4 H, P- CH_2), 1.32–1.14 (m, 20 H, CH_2) ppm.

$^{13}\text{C}\{^1\text{H}\}$ NMR (100.62 MHz, CD_2Cl_2 , 300 K): $\delta = 147.1$ (s, 1 C, $\text{C}_{\text{iphenyl}}$), 129.2 (s, 2 C, $\text{C}_{\text{orphenyl}}$), 115.4 (s, 1 C, $\text{C}_{\text{prphenyl}}$), 112.1 (s, 2 C, $\text{C}_{\text{mrphenyl}}$), 50.4 (d, $^2J_{\text{PC}} = 33.2$ Hz, 2 C, N- CH_2), 33.3 (d, $J_{\text{PC}} = 12.7$ Hz, 4 C, CH_2), 30.4 (d, $^2J_{\text{PC}} = 14.9$ Hz, 4 C, CH_2), 29.1 (d, $J_{\text{PC}} = 7.93$ Hz, 4 C, CH_2), 27.3 (d, $J_{\text{PC}} = 19.5$ Hz, 4 C, CH_2), 27.3 (s, 4 C, CH_2), 26.6 (s, 4 C, CH_2), 19.5 (d, $J_{\text{PC}} = 20.3$ Hz, 2 C, P- CH_2) ppm.

IR (ATR): $\tilde{\nu} = 3087$ (vw), 3058 (w), 3037 (vw), 3019 (vw), 2918 (s), 2894 (sh), 2846 (s), 2788 (sh), 2654 (vw), 2262 (w br), 1603 (s), 1587 (s), 1570 (m), 1537 (vw), 1505 (s), 1461 (m), 1446 (s), 1397 (s), 1352 (s), 1268 (m), 1215 (m), 1201 (m), 1185 (s), 1178 (s), 1159 (m), 1128 (s), 1117 (sh), 1105 (m), 1089 (sh), 1072 (w), 1039 (m), 1018 (sh), 998 (s), 951 (vw), 931 (m), 921 (m), 887 (m), 851 (s), 818 (m), 807 (sh), 770 (sh), 758 (m), 739 (s), 707 (w), 687 (s), 549 (w), 507 (s), 458 (m), 439 (m), 402 (w) cm^{-1} .

NN-Bis(2-(di-tert-butylphosphino)ethyl)aniline ($\text{PN}^{\text{Ph}}\text{P}^{\text{tBu}}$, **1h**)

Following general procedure A, the $\text{PN}^{\text{Ph}}\text{P}^{\text{tBu}}$ (**1h**) ligand was obtained as white solid (1.39 g, 3.18 mmol, 79 %).

$^3\text{P}\{^1\text{H}\}$ NMR: (161.98 MHz, CDCl_3 , 300 K): $\delta = 25.0$ (s, 2 P, P^{tBu}_2) ppm.

^1H NMR (400.13 MHz, CDCl_3 , 300 K): $\delta = 7.17\text{--}7.06$ (m, 2 H, $\text{CH}_{\text{phenyl}}$), 6.62–6.52 (m, 3 H, $\text{CH}_{\text{phenyl}}$), 3.44–3.39 (m, 4 H, N- CH_2), 1.64–1.58 (m, 4 H, P-CH), 1.71–1.65 (m, 4 H, P- CH_2), 1.08 (d, $^3J_{\text{PH}} = 11.3$ Hz, 36 H, CH_3) ppm.

$^{13}\text{C}\{^1\text{H}\}$ NMR (100.62 MHz, CDCl_3 , 300 K): $\delta = 145.8$ (s, 1 C, $\text{C}_{\text{iphenyl}}$), 128.4 (s, 2 C, $\text{C}_{\text{orphenyl}}$), 114.6 (s, 1 C, $\text{C}_{\text{prphenyl}}$), 110.7 (s, 2 C, $\text{C}_{\text{mrphenyl}}$), 50.6 (d, $^2J_{\text{PC}} = 40.6$ Hz, 2 C, N- CH_2), 30.2 (d, $^1J_{\text{PC}} = 19.4$ Hz, 4 C, P-C), 28.6 (d, $^2J_{\text{PC}} = 13.6$ Hz, 12 C, CH_3), 18.2 (d, $J_{\text{PC}} = 22.7$ Hz, 2 C, CH_2P) ppm.

IR (ATR): $\tilde{\nu} = 3093$ (w), 3063 (w), 3039 (w), 3025 (w), 2982 (sh), 2950 (sh), 2937 (vs), 2892 (m), 2860 (m), 2706 (vw), 1910 (vw), 1750 (vw), 1602 (s), 1590 (w), 1569 (vw), 1541 (vw), 1503 (vs), 1462 (vs), 1452 (sh), 1408 (sh), 1393 (w), 1383 (s), 1358 (vs), 1344 (vs), 1321 (sh), 1280 (s), 1203 (sh), 1183 (vs), 1123 (vs), 1081 (vw), 1036 (s), 1014 (m), 992 (m), 933 (sh), 922 (m), 854 (m), 810 (s), 768 (sh), 750 (sh), 742 (vs), 707 (m), 688 (vs), 618 (vw), 593 (m), 578 (m), 545 (vw), 535 (vw), 506 (s), 464 (w), 434 (s) cm^{-1} .

$[\text{Mo}(\text{CO})_3(\text{PN}^{\text{Ph}}\text{P}^{\text{Ph}})]$ (**2a**)

Following general procedure B, the $[\text{Mo}(\text{CO})_3(\text{PN}^{\text{Ph}}\text{P}^{\text{Ph}})]$ (**2a**) was obtained as yellow solid (45.2 mg, 0.07 mmol, 34 %). Parts of the analytical data was already presented by Cowley *et al.*^[26]

$^3\text{P}\{^1\text{H}\}$ NMR: (161.98 MHz, CD_2Cl_2 , 300 K): $\delta = 38.0$ (s, 2 P, PPh_2) ppm.

^1H NMR (400.13 MHz, CD_2Cl_2 , 300 K): $\delta = 7.78\text{--}7.73$ (m, 4 H, $\text{CH}_{\text{phenyl}}$), 7.49–7.46 (m, 2 H, $\text{CH}_{\text{phenyl}}$), 7.42–7.35 (m, 6 H, $\text{CH}_{\text{phenyl}}$), 7.33–7.28 (m, 2 H, $\text{CH}_{\text{phenyl}}$), 7.27–7.20 (m, 2 H, $\text{CH}_{\text{phenyl}}$), 7.19–7.14 (m, 4 H, $\text{CH}_{\text{phenyl}}$), 7.13–7.07 (m, 3 H, $\text{CH}_{\text{phenyl}}$), 6.99–6.96 (m, 4 H, $\text{CH}_{\text{phenyl}}$), 3.71–3.59 (m, 2 H, N- CH_2), 3.21–3.08 (m, 2 H, N- CH_2), 2.85–2.69 (m, 4 H, P- CH_2) ppm.

$^{13}\text{C}\{^1\text{H}\}$ NMR (100.62 MHz, CD_2Cl_2 , 300 K): $\delta = 231.6$ (t, $^2J_{\text{PC}} = 8.24$ Hz, 1 C, CO_{axial}), 219.7 (ABX, 2 C, $\text{CO}_{\text{equatorial}}$), 153.8 (s, 1 C, N-($\text{C}_{\text{iphenyl}}$)), 139.1–138.5 (m, 2 C, P-($\text{C}_{\text{iphenyl}}$)), 137.0–136.7 (m, 2 C, P-($\text{C}_{\text{iphenyl}}$)), 132.4 (t, $J_{\text{PC}} = 6.13$ Hz, 4 C, P-($\text{C}_{\text{orphenyl}}$)), 131.2 (t, $J_{\text{PC}} = 6.33$ Hz, 4 C, P-($\text{C}_{\text{orphenyl}}$)), 130.0 (s, 2 C, P-($\text{C}_{\text{prphenyl}}$)), 129.4 (s, 2 C, P-($\text{C}_{\text{prphenyl}}$)), 129.1–128.9 (m, 10 C, P-($\text{C}_{\text{mrphenyl}}$), N-($\text{C}_{\text{orphenyl}}$)), 125.3 (s, 1 C, N-($\text{C}_{\text{prphenyl}}$)), 121.1 (s, 2 C, P-($\text{C}_{\text{mrphenyl}}$)), 58.0 (t, $J_{\text{PC}} = 5.86$ Hz, 2 C, N-(CH_2)), 28.8 (dd, $J_{\text{PC}} = 9.51$ Hz, $J_{\text{PC}} = 6.67$ Hz, 2 C, P- CH_2) ppm.

IR (ATR): $\tilde{\nu} = 3837$ (vw), 3717 (vw), 3616 (vw), 3599 (vw), 3548 (vw), 3078 (vw), 3055 (w), 3017 (w), 3002 (vw), 2977 (vw), 2927 (vw), 2895 (w), 2874 (w), 2849 (w), 1921 (vs, CO stretch), 1802 (sh, br, CO stretch), 1775 (sh, CO stretch), 1600 (m), 1586 (m), 1572 (m), 1494 (m), 1480 (m), 1432 (s), 1424 (sh), 1407 (w), 1377 (vw), 1331 (w), 1310 (sh), 1299 (w), 1223 (m), 1185 (m), 1095 (s), 1068 (m), 1037 (m), 1029 (m), 998 (sh), 991 (w), 971 (vw), 944 (w), 920 (vw), 905 (m), 898 (sh), 852 (sh), 843 (w), 813 (sh), 804 (s), 763 (m), 742 (vs), 695 (vs), 671 (m), 651 (s), 634 (s), 610 (m), 597 (m), 554 (m), 530 (m), 515 (vs), 499 (vs), 487 (sh), 467 (m), 459 (sh), 449 (w), 428 (vs) cm^{-1} .

Raman: $\tilde{\nu} = 3069$ (vw), 3143 (vw), 3081 (w), 3056 (vs), 3007 (br, w), 2989 (vw), 2979 (vw), 2957 (w), 2950 (w), 2926 (w), 2916 (m), 2896 (vw), 2876 (vw), 2850 (vw), 2734 (vw), 2534 (vw), 1921 (w, CO stretch), 1828 (m, CO stretch), 1819 (vs, CO stretch), 1808 (sh, CO stretch), 1804 (s, CO stretch), 1601 (w), 1586 (vs), 1573 (m), 1496 (vw), 1485 (vw), 1466 (w), 1443 (sh), 1436 (vw), 1423 (vw), 1411 (vw), 1380 (vw), 1205 (w), 1188 (w), 1163 (w), 1141 (w), 1097 (w), 1041 (sh), 1028 (m), 999 (vs), 816 (vw), 804 (vw), 786 (w), 756 (vw), 715 (sh), 703 (vw), 691 (w), 676 (w), 652 (w), 637 (vw), 617 (m), 599 (vw), 555 (s), 531 (vw), 520 (w), 489 (m), 477 (sh), 469 (m), 454 (m), 430 (w), 422 (sh), 395 (vw), 375 (vw), 344 (vw), 325 (vw), 294 (vw), 269 (w), 255 (vw), 224 (w), 201 (vw), 184 (m), 157 (m), 138 (sh) cm^{-1} .

$[\text{Mo}(\text{CO})_3(\text{PN}^{\text{Ph}}\text{P}^{\text{Et}})]$ (**2c**)

Following general procedure B, the $[\text{Mo}(\text{CO})_3(\text{PN}^{\text{Ph}}\text{P}^{\text{Et}})]$ (**2c**) was obtained as beige solid (122 mg, 0.24 mmol, 44 %). Crystals suitable for x-ray analysis were obtained by slow evaporation of the complex in dichloromethane.

Anal. Calcd $\text{C}_{21}\text{H}_{33}\text{P}_2\text{O}_3\text{NMo}$ (505.4 g/mol): C 49.9, H 6.58, N 2.77; C 50.2, H 6.59, N 3.10.

$^{31}\text{P}\{^1\text{H}\}$ NMR: (161.98 MHz, CD_2Cl_2 , 300 K): $\delta = 33.7$ (s, 2 P, PEt_2) ppm.

^1H NMR (400.13 MHz, CD_2Cl_2 , 300 K): $\delta = 7.58\text{--}7.53$ (m, 2 H, $\text{CH}_{\text{phenyl}}$), 7.35–7.29 (m, 2 H, $\text{CH}_{\text{phenyl}}$), 7.13–7.09 (m, 1 H, $\text{CH}_{\text{phenyl}}$), 3.34–3.22 (m, 2 H, N-CH_2), 2.75–2.63 (m, 2 H, N-CH_2), 2.12–2.01 (m, 2 H, $\text{P-CH}_2\text{-CH}_3$), 1.99–1.92 (m, 6 H, $\text{P-CH}_2\text{-CH}_3$, $\text{P-CH}_2\text{-CH}_2\text{-N}$), 1.85–1.73 (m, 2 H, $\text{P-CH}_2\text{-CH}_3$), 1.62–1.53 (m, 2 H, $\text{P-CH}_2\text{-CH}_3$), 1.26–1.13 (m, 12 H, $\text{P-CH}_2\text{-CH}_3$) ppm.

$^{13}\text{C}\{^1\text{H}\}$ NMR (100.62 MHz, CD_2Cl_2 , 300 K): $\delta = 231.4$ (ABX, $J_{\text{CP}} = 8.28$ Hz, 1 C, CO_{axial}), 220.2 (ABX, 2 C, $\text{CO}_{\text{equatorial}}$), 153.4 (s, 1 C, $\text{N-}(\text{C}_{\text{phenyl}})$), 128.8 (s, 2 C, $\text{N-}(\text{C}_{\text{phenyl}})$), 125.4 (s, 1 C, $\text{N-}(\text{C}_{\text{phenyl}})$), 122.2 (s, 2 C, $\text{P-}(\text{C}_{\text{phenyl}})$), 57.4 (t, $J_{\text{PC}} = 5.80$ Hz, 2 C, $\text{N-}(\text{CH}_2)$), 27.2 (ABX, 4 C, P-CH_3), 22.2 (ABX, 2 C, $\text{P-CH}_2\text{-CH}_3$), 21.8 (ABX, 2 C, $\text{P-CH}_2\text{-CH}_3$), 8.87 (d, $J_{\text{CP}} = 1.44$ Hz, 4 C, $\text{P-CH}_2\text{-CH}_3$) ppm.

IR (ATR): $\tilde{\nu} = 3095$ (vw), 3072 (sh), 3031 (w), 3038 (vw), 3022 (vw), 2995 (vw), 2961 (m), 2957 (sh), 2928 (m), 2912 (m), 2871 (m), 2861 (m), 2823 (w) 1906 (vs, CO stretch), 1805 (vs, br, CO stretch), 1785 (sh, CO stretch), 1773 (vs, CO stretch), 1744 (sh), 1595 (m), 1581 (m), 1494 (m), 1474 (m), 1451 (s), 1422 (s), 1375 (m), 1357 (w), 1299 (vw), 1243 (sh), 1226 (m), 1186 (m), 1163 (m), 1143 (m), 1088 (m), 1047 (sh), 1037 (s), 1011 (sh), 985 (m), 968 (sh), 945 (m), 911 (w), 895 (m), 831 (sh), 819 (sh), 806 (s), 760 (vs), 733 (s), 706 (sh), 697 (vs), 677 (s), 613 (m), 602 (s), 555 (s), 525 (s), 512 (vs), 478 (m), 455 (m), 442 (m), 404 (s) cm^{-1} .

Raman: $\tilde{\nu} = 3072$ (m), 3060 (m), 3038 (vw), 3022 (vw), 3003 (sh), 2982 (w), 2962 (s), 2951 (s), 2926 (sh), 2920 (vs), 2873 (m), 2862 (sh), 2728 (w), 1906 (vs, CO stretch), 1820 (vs, CO stretch), 1810 (vs, CO stretch), 1786 (s, CO stretch), 1774 (vs, CO stretch), 1749 (vw), 1596 (m), 1583 (m), 1496 (w), 1475 (sh), 1464 (m), 1457 (sh), 1419 (m), 1405 (w), 1397 (w), 1363 (w), 1303 (w), 1280 (vw), 1261 (vw), 1245 (sh), 1237 (vw), 1217 (w), 1191 (m), 1162 (m), 1142 (s), 1092 (vw), 1068 (w), 1041 (m), 1033 (s), 1000 (s), 968 (m), 950 (vw), 916 (vw), 901 (w), 817 (vw), 808 (vw), 769 (vw), 737 (sh), 728 (vw), 713 (w), 705 (vw), 673 (sh), 634 (m), 617 (w), 554 (w), 531 (w), 517 (w), 499 (sh), 489 (s), 469 (m), 454 (m), 446 (sh), 409 (w), 398 (sh), 380 (vw), 361 (vw), 341 (vw), 322 (vw), 294 (sh), 283 (w), 271 (vw), 223 (w), 190 (w), 176 (vw), 161 (vw) cm^{-1} .

[$\text{Mo}(\text{CO})_3(\text{PN}^{\text{Ph}}\text{P}^{\text{CyP}})]$ (2 e)

Following general procedure B, the [$\text{Mo}(\text{CO})_3(\text{PN}^{\text{Ph}}\text{P}^{\text{CyP}})]$ (2 e) was obtained as beige solid (145 mg, 0.22 mmol, 71 %).

Anal. Calcd $\text{C}_{33}\text{H}_{49}\text{P}_2\text{O}_3\text{NMo}$ (665.7 g/mol): C 59.5, H 7.42, N 2.10; C 59.2, H 7.39, N 1.93.

$^{31}\text{P}\{^1\text{H}\}$ NMR: (161.98 MHz, CD_2Cl_2 , 300 K): $\delta = 41.6$ (s, 2 P, PCp_2) ppm.

^1H NMR (400.13 MHz, CD_2Cl_2 , 300 K): $\delta = 7.54\text{--}7.51$ (m, 2 H, $\text{CH}_{\text{phenyl}}$), 7.35–7.30 (m, 2 H, $\text{CH}_{\text{phenyl}}$), 7.13–7.09 (m, 1 H, $\text{CH}_{\text{phenyl}}$), 3.29–3.18 (m, 2 H, N-CH_2), 2.79–2.67 (m, 2 H, N-CH_2), 2.44–2.32 (m, 2 H, P-CH_2), 2.13–1.46 (m, 38 H, P-CH_2 , P-Cp_2) ppm.

$^{13}\text{C}\{^1\text{H}\}$ NMR (100.62 MHz, CD_2Cl_2 , 300 K): $\delta = 232.0$ (t, $J_{\text{CP}} = 8.29$ Hz, 1 C, CO_{axial}), 220.8 (ABX, 2 C, $\text{CO}_{\text{equatorial}}$), 153.0 (s, 1 C, $\text{N-}(\text{C}_{\text{phenyl}})$), 128.8 (s, 2 C, $\text{N-}(\text{C}_{\text{phenyl}})$), 125.2 (s, 1 C, $\text{N-}(\text{C}_{\text{phenyl}})$), 122.0 (s, 2 C, $\text{P-}(\text{C}_{\text{phenyl}})$), 58.2 (t, $J_{\text{PC}} = 5.31$ Hz, 2 C, $\text{N-}(\text{CH}_2)$), 41.9–41.8 (m, 2 C, P-CH), 36.7–36.1 (m, 2 C, P-CH), 32.0 (t, $J_{\text{PC}} = 4.46$ Hz, 2 C, P-Cp), 30.7 (t, $J_{\text{PC}} = 3.53$ Hz, 2 C, P-Cp), 30.2 (s, 2 C, P-Cp), 28.8 (s, 2 C, P-Cp), 27.7 (dd, $J_{\text{PC}} = 6.84$ Hz, 4.90 Hz, 2 C, P-CH_2), 27.2 (t, $J_{\text{PC}} = 4.92$ Hz, 2 C, P-Cp), 26.9 (t, $J_{\text{PC}} = 4.42$ Hz, 2 C, P-Cp), 26.7 (t, $J_{\text{PC}} = 2.70$ Hz, 2 C, P-Cp), 26.0 (t, $J_{\text{PC}} = 4.67$ Hz, 2 C, P-Cp) ppm.

IR (ATR): $\tilde{\nu} = 3699$ (vw), 3680 (vw), 3582 (vw), 3549 (vw), 3062 (vw), 3028 (vw), 2949 (m), 2909 (sh), 2867 (m), 2155 (vw), 2090 (vw), 2018 (sh), 1904 (vs, CO stretch), 1798 (sh, CO stretch), 1782 (vs, br, CO

stretch), 1594 (w), 1583 (w), 1493 (m), 1472 (m), 1449 (w), 1432 (sh), 1410 (w), 1373 (w), 1359 (w), 1320 (vw), 1300 (w), 1259 (vw), 1232 (w), 1190 (w), 1160 (w), 1138 (sh), 1122 (w), 1091 (w), 1060 (w), 1034 (w), 1002 (vw), 990 (vw), 978 (vw), 949 (w), 903 (m), 850 (sh), 835 (vw), 806 (m), 760 (m), 729 (w), 700 (m), 679 (w), 666 (w), 640 (m), 609 (m), 589 (sh), 552 (m), 519 (m), 485 (m), 444 (w), 418 (sh), 411 (w), 406 (sh) cm^{-1} .

Raman: $\tilde{\nu} = 3081$ (m), 2954 (vs), 2929 (vs), 2902 (sh), 2867 (vs), 1907 (vw, CO stretch), 1812 (s, CO stretch), 1795 (s, CO stretch), 1785 (sh, CO stretch), 1605 (sh), 1597 (m), 1585 (w), 1558 (vw), 1502 (sh), 1495 (vw), 1473 (m), 1450 (s), 1321 (vw), 1307 (sh), 1298 (w, br), 1265 (vw), 1253 (vw), 1243 (vw), 1234 (vw), 1228 (sh), 1193 (w), 1165 (sh), 1160 (vw), 1143 (w), 1058 (vw), 1035 (s), 1001 (s), 894 (s), 820 (w), 712 (m), 668 (m), 642 (w), 620 (m), 556 (w), 530 (vw), 513 (vw), 488 (vs), 472 (s), 449 (m), 404 (w), 356 (m, br), 348 (m, br), 318 (w), 285 (w, br), 267 (vw), 211 (vw), 186 (w) cm^{-1} .

[$\text{Mo}(\text{CO})_3(\text{PN}^{\text{Ph}}\text{P}^{\text{Pr}})]$ (2 f)

Following general procedure B, the [$\text{Mo}(\text{CO})_3(\text{PN}^{\text{Ph}}\text{P}^{\text{Pr}})]$ (2 f) was obtained as beige solid (86 mg, 0.15 mmol, 58 %).

Anal. Calcd $\text{C}_{25}\text{H}_{41}\text{P}_2\text{O}_3\text{NMo}$ (561.5 g/mol): C 53.5, H 7.36, N 2.49; C 53.8, H 7.48, N 2.36.

$^{31}\text{P}\{^1\text{H}\}$ NMR: (161.98 MHz, CD_2Cl_2 , 300 K): $\delta = 51.6$ (s, 2 P, $\text{P}^{\text{Pr}}\text{P}^{\text{Pr}}$) ppm.

^1H NMR (400.13 MHz, CD_2Cl_2 , 300 K): $\delta = 7.57\text{--}7.54$ (m, 2 H, $\text{CH}_{\text{phenyl}}$), 7.37–7.31 (m, 2 H, $\text{CH}_{\text{phenyl}}$), 7.14–7.10 (m, 1 H, $\text{CH}_{\text{phenyl}}$), 3.30–3.19 (m, 2 H, N-CH_2), 2.77–2.66 (m, 2 H, N-CH_2), 2.41–2.32 (m, 2 H, P-CH), 2.06–1.88 (m, 4 H, $\text{P-CH}_2\text{-CH}_2\text{-N}$), 1.86–1.78 (m, 2 H, P-CH), 1.40–1.31 (m, 18 H, $\text{P-CH}_2\text{-CH}_3$), 1.27–1.23 (m, 6 H, $\text{P-CH}_2\text{-CH}_3$) ppm.

$^{13}\text{C}\{^1\text{H}\}$ NMR (100.62 MHz, CD_2Cl_2 , 300 K): $\delta = 231.9$ (t, $J_{\text{CP}} = 8.17$ Hz, 1 C, CO_{axial}), 220.8 (ABX, 2 C, $\text{CO}_{\text{equatorial}}$), 153.6 (s, 1 C, $\text{N-}(\text{C}_{\text{phenyl}})$), 128.9 (s, 2 C, $\text{N-}(\text{C}_{\text{phenyl}})$), 125.3 (s, 1 C, $\text{N-}(\text{C}_{\text{phenyl}})$), 122.1 (s, 2 C, $\text{P-}(\text{C}_{\text{phenyl}})$), 58.1 (t, $J_{\text{PC}} = 5.45$ Hz, 2 C, $\text{N-}(\text{CH}_2)$), 31.2 (dd, $J_{\text{PC}} = 5.92$ Hz, 5.09 Hz, 2 C, P-CH), 26.8–26.2 (m, 2 C, P-CH), 26.2–26.1 (m, 2 C, P-CH_2), 21.7 (t, $J_{\text{PC}} = 2.81$ Hz, 1 C, P-CH-CH_3), 21.2 (t, $J_{\text{PC}} = 3.90$ Hz, 1 C, P-CH-CH_3), 19.9 (t, $J_{\text{PC}} = 1.23$ Hz, 1 C, P-CH-CH_3), 18.1 (t, $J_{\text{PC}} = 2.51$ Hz, 1 C, P-CH-CH_3) ppm.

IR (ATR): $\tilde{\nu} = 3685$ (w), 3677 (sh), 3627 (vw), 3616 (vw), 3588 (vw), 3571 (w), 3543 (w), 3096 (vw), 3074 (w), 3058 (w), 3037 (vw), 3025 (vw), 2979 (m), 2955 (m), 2928 (m), 2899 (m), 2871 (m), 2809 (sh), 2713 (vw), 2359 (vw) 1900 (vs, CO stretch), 1793 (vs, CO stretch), 1773 (vs, br, CO stretch), 1750 (sh), 1597 (m), 1583 (m), 1494 (s), 1474 (s), 1452 (s), 1407 (m), 1385 (m), 1366 (m), 1302 (m), 1296 (m), 1277 (m), 1250 (m), 1229 (m), 1214 (m), 1188 (m), 1163 (m), 1137 (m), 1083 (m), 1058 (s), 1035 (s), 1026 (sh), 990 (m), 963 (w), 948 (m), 924 (m), 908 (m), 895 (w), 882 (w), 816 (s), 761 (s), 724 (m), 699 (s), 690 (s), 653 (s), 639 (s), 618 (s), 601 (s), 597 (sh), 570 (w), 550 (m), 521 (s), 501 (m), 481 (sh), 471 (s), 451 (m), 418 (w) cm^{-1} .

Raman: $\tilde{\nu} = 3069$ (m), 3059 (sh), 3040 (vw), 3023 (vw), 2980 (sh), 2968 (sh), 2954 (m), 2931 (vs), 2901 (sh), 2872 (m), 2811 (vw), 2760 (w), 2732 (vw), 2717 (w), 1901 (vw, CO stretch), 1802 (s, CO stretch), 1794 (vs, CO stretch), 1788 (sh, CO stretch), 1780 (s, CO stretch), 1600 (m), 1583 (m), 1498 (w), 1468 (s), 1450 (sh), 1433 (sh), 1413 (m), 1386 (w), 1368 (w), 1304 (sh), 1295 (w), 1277 (w), 1257 (w), 1227 (vw), 1217 (w), 1190 (m), 1159 (m), 1141 (m), 1109 (sh), 1092 (m), 1064 (w), 1053 (sh), 1034 (s), 1001 (s), 993 (m), 965 (w), 950 (vw), 928 (vw), 914 (vw), 897 (sh), 885 (m), 819 (w), 788 (w), 763 (vw), 703 (vw), 682 (w), 655 (w), 640 (w), 619 (s), 601 (w), 569 (m), 554 (w), 490 (vs), 474 (vs), 450 (s), 432 (vw), 402 (vw), 366 (w), 349 (w), 303 (w), 234 (w), 220 (w), 191 (w), 164 (sh), 142 (sh) cm^{-1} .

4.1 Molybdenum tricarbonyl complexes supported by linear PNP ligands: Influence of P- and N-substituents on structure, stability and on the activation of small molecules

[Mo(CO)₃(PNP^{Ph}Cy)] (2 g)

Following general procedure B, the **2g** was obtained as gray solid (46.4 mg, 64.3 μmol, 39%).

Anal. Calcd C₃₇H₃₉P₂O₃NMo (721.8 g/mol): C 61.5, H 7.96, N 1.94; C 61.2, H 7.94, N 1.81.

³¹P{¹H} NMR: (161.98 MHz, CD₂Cl₂, 300 K): δ = 40.8 (s, 2 P, PCy₂) ppm.

¹H NMR (400.13 MHz, CD₂Cl₂, 300 K): δ = 7.52–7.51 (m, 2 H, CH_{phenyl}), 7.36–7.32 (m, 2 H, CH_{phenyl}), 7.14–7.10 (m, 1 H, CH_{phenyl}), 3.27–3.17 (m, 2 H, N-CH₂), 2.75–2.63 (m, 2 H, N-CH₂), 2.12–1.19 (m, 48 H, P-CH₂, P-Cy₂) ppm.

¹³C{¹H} NMR (100.62 MHz, CD₂Cl₂, 300 K): δ = 231.7–231.6 (m, 1 C, CO_{axial}), 220.9–220.4 (m, 2 C, CO_{equatorial}), 153.5 (s, 1 C, N-(C_{phenyl})), 128.4 (s, 2 C, N-(C_{phenyl})), 126.6 (s, 1 C, N-(C_{phenyl})), 121.4 (s, 2 C, P-(C_{phenyl})), 57.3 (t, J_{PC} = 4.70 Hz, 2 C, N-(CH₂)), 40.8 (t, J_{PC} = 3.99 Hz, 2 C, P-CH), 38.6 (t, J_{PC} = 10.6 Hz, 2 C, P-CH), 31.4 (s, 3 C, P-Cy), 30.2 (s, 3 C, P-Cy), 29.4 (s, 3 C, P-Cy), 28.6 (s, 3 C, P-Cy), 28.2–27.9 (m, 2 C, P-CH₂), 27.7–27.5 (m, 3 C, P-Cy), 26.4 (d, J_{PC} = 6.87 Hz, 2 C, P-Cy), 24.2–24.1 (m, 2 C, P-Cy) ppm.

IR (ATR): $\tilde{\nu}$ = 3692 (vw), 3679 (vw), 2924 (s), 2850 (s), 2795 (sh), 2652 (w, br), 1980 (w), 1903 (vs, CO stretch), 1796 (sh, CO stretch), 1781 (vs, br, CO stretch), 1751 (sh), 1595 (w), 1583 (w), 1494 (m), 1475 (w), 1448 (s), 1412 (vw), 1375 (w), 1341 (w), 1327 (sh), 1297 (sh), 1278 (sh), 1265 (w), 1221 (w), 1194 (w), 1174 (w), 1157 (vw), 1141 (w), 1116 (w), 1090 (w), 1072 (sh), 1052 (sh), 1001 (m), 967 (vw), 952 (w), 919 (w), 900 (sh), 886 (m), 849 (m), 817 (sh), 799 (m), 758 (s), 739 (w), 272 (w), 712 (w), 700(s), 673 (m), 665 (m), 639 (s), 552 (m), 527 (s), 517 (sh), 489 (w), 477 (w), 460 (s), 449 (m), 413 (vw) cm⁻¹.

Raman: $\tilde{\nu}$ = 3077 (m), 2937 (vs), 2850 (vs), 2706 (vw), 2677 (sh), 2667 (w), 2652 (w), 1906 (vw, CO stretch), 1810 (s, CO stretch), 1791 (s, CO stretch), 1597 (w), 1586 (w), 1497 (vw), 1475 (vw), 1464 (w), 1439 (s), 1345 (w), 1298 (m), 1266 (m), 1223 (w), 1197 (m), 1172 (w), 1144 (w), 1122 (vw), 1105 (vw), 1076 (w), 1030 (s), 1001 (s), 950 (vw), 904 (sh), 889 (w), 855 (m), 819 (s), 807 (sh), 784 (w), 766 (w), 737 (m), 717 (s), 679 (w), 664 (w), 643 (w), 620 (w), 605 (w), 556 (w), 535 (vw), 524 (vw), 487 (vs), 473 (s), 450 (m), 433 (sh), 395 (vw), 379 (w), 372 (sh), 350 (w), 319 (w), 292 (sh), 280 (w), 199 (sh), 167 (w) cm⁻¹.

Acknowledgements

The authors thank the spectroscopic department of the Institute of Inorganic Chemistry for measurements, as well as CAU Kiel for the financial support of this research. Open Access funding enabled and organized by Projekt DEAL.

Conflict of Interests

The authors declare no conflict of interest.

Data Availability Statement

The data that support the findings of this study are available in the supplementary material of this article.

Keywords: Molybdenum · Carbonyl complexes · Pincer ligands · Phosphine ligands · Small molecule activation

- [1] L. Alig, M. Fritz, S. Schneider, *Chem. Rev.* **2019**, *119*, 2681.
- [2] M. B. Smith, *Molecules* **2022**, *37*, 6293.
- [3] J. I. van der Vlugt, J. N. H. Reek, *Angew. Chem.* **2009**, *48*, 8832.
- [4] C. Gunanathan, D. Milstein, *Chem. Rev.* **2014**, *114*, 12024.
- [5] a) M. D. Fryzuk, P. A. MacNeil, S. J. Rettig, A. S. Secco, J. Trotter, *Organometallics* **1982**, *1*, 918; b) D. V. Griffiths, H. J. Groombridge, P. M. Mahoney, S. P. Swetnam, G. Walton, D. C. York, *Tetrahedron* **2005**, *61*, 4595; c) L.-C. Liang, P.-S. Chien, Y.-L. Huang, *J. Am. Chem. Soc.* **2006**, *128*, 15562; d) A. M. Winter, K. Eichele, H.-G. Mack, S. Potuznik, H. A. Mayer, W. C. Kaska, *J. Organomet. Chem.* **2003**, *682*, 149; e) A. T. Radosevich, J. G. Melnick, S. A. Stoian, D. Bacciu, C.-H. Chen, B. M. Foxman, O. V. Ozerov, D. G. Nocera, *Inorg. Chem.* **2009**, *48*, 9214.
- [6] I. D. Kostas, *J. Organomet. Chem.* **2001**, 221.
- [7] O. Silcovan, R. Angelici, *Inorg. Chem.* **1998**, 432.
- [8] a) K. Arashiba, Y. Miyake, Y. Nishibayashi, *Nat. Chem.* **2011**, *3*, 120; b) G. Bauer, X. Hu, *Inorg. Chem. Front.* **2016**, *3*, 741; c) E. Peris, R. H. Crabtree, *Chem. Soc. Rev.* **2018**, *47*, 1959.
- [9] a) M. T. Whited, E. Rivard, J. C. Peters, *Chem. Commun.* **2006**, 1613; b) A. Jacobi, G. Huttner, U. Winterhalter, *Chem. Ber.* **1997**, *9*, 1279; c) A. Albinati, L. M. Venanzi, G. Wang, *Inorg. Chem.* **1993**, 3660; d) A. Muth, O. Walter, G. Huttner, A. Asam, L. Zsolnai, C. Emmerich, *J. Organomet. Chem.* **1993**, 468, 149; e) J. Schneidewind, R. Adam, W. Baumann, R. Jackstell, M. Beller, *Angew. Chem. Int. Ed.* **2017**, *56*, 1890.
- [10] F. Petersen, I. Lautenschläger, A. Schlimm, B. M. Flöser, H. Jacob, R. Amirbeigi, T. R. Rusch, T. Strunskus, O. Magnussen, F. Tuczek, *Dalton Trans.* **2021**, 50, 1042.
- [11] S. Chakraborty, U. K. Das, Y. Ben-David, D. Milstein, *J. Am. Chem. Soc.* **2017**, *139*, 11710.
- [12] J. R. Khushnutdinova, D. Milstein, *Angew. Chem. Int. Ed.* **2015**, *54*, 12236.
- [13] a) P. Zimmermann, C. Limberg, *J. Am. Chem. Soc.* **2017**, *139*, 4233; b) A. M. Tondreau, J. M. Boncella, *Polyhedron* **2016**, *116*, 96; c) C. Yoo, Y.-E. Kim, Y. Lee, *Acc. Chem. Res.* **2018**, *51*, 1144.
- [14] a) C. Prichatz, E. Alberico, W. Baumann, H. Junge, M. Beller, *ChemCatChem* **2017**, *9*, 1891; b) B. Maji, M. K. Barman, *Synth.* **2017**, 3377; c) C. Hou, Y. Li, Z. Ke, *Inorg. Chim. Acta* **2020**, *511*, 119808; d) K. V. Vasudevan, B. L. Scott, S. K. Hanson, *Eur. J. Inorg. Chem.* **2012**, 2012, 4898; e) M. Bertoli, A. Choualeb, A. J. Lough, B. Moore, D. Spasyuk, D. G. Gusev, *Organometallics* **2011**, *30*, 3479; f) L. Piccirilli, D. Lobo Justo Pinheiro, M. Nielsen, *Catalysts* **2020**, *10*, 773; g) D. Wei, T. Roisnel, C. Darcel, E. Clot, J.-B. Sortais, *ChemCatChem* **2017**, *9*, 80; h) Ekanayake, D. A., Guan, H. (Ed.) *Metal-Ligand Co-operativity. Topics in Organometallic Chemistry. Hydrogenation Reactions Catalyzed by PNP-Type Complexes Featuring a HN(CH₂CH₂PR₂)₂ Ligand*, Springer, Cham, **2020**; i) D. Pingin, J.-H. Choi, H. Allen, G. Murray, P. Ganji, P. W. N. M. van Leeuwen, M. H. G. Precht, D. Vogt, *Catal. Sci. Technol.* **2018**, *8*, 3969; j) N. Andrushko, V. Andrushko, P. Roose, K. Moonen, A. Börner, *ChemCatChem* **2010**, *2*, 640; k) T. Leischner, A. Spannenberg, K. Junge, M. Beller, *ChemCatChem* **2020**, *12*, 4543; l) J. B. Curley, N. E. Smith, W. H. Bernskoetter, N. Hazari, B. Q. Mercado, *Organometallics* **2018**, *37*, 3846; m) Z. E. Clarke, P. T. Maragh, T. P. Dasgupta, D. G. Gusev, A. J. Lough, K. Abdur-Rashid, *Organometallics* **2006**, *25*, 4113; n) J. B. Curley, W. H. Bernskoetter, N. Hazari, *ChemCatChem* **2020**, *12*, 1934.
- [15] a) G. van Koten, *Pure Appl. Chem.* **1989**, *61*, 1681; b) G. van Koten, M. Albrecht, *Angew. Chem. Int. Ed.* **2001**, *40*, 3750; c) L. S. Merz, J. Ballmann, L. H. Gade, *Eur. J. Inorg. Chem.* **2020**, 2023.
- [16] S. Schneider, J. Meiners, B. Askevold, *Eur. J. Inorg. Chem.* **2012**, 412.
- [17] a) S. Elangovan, B. Wendt, C. Topf, S. Bachmann, M. Scalone, A. Spannenberg, H. Jiao, W. Baumann, K. Junge, M. Beller, *Adv. Synth. Catal.* **2016**, *358*, 820; b) S. Kar, R. Sen, J. Kothandaraman, A. Goepfert, R. Chowdhury, S. B. Munoz, R. Haiges, G. K. S. Prakash, *J. Am. Chem. Soc.* **2019**, *141*, 3160; c) M. Nielsen, E. Alberico, W. Baumann, H.-J. Drexler, H. Junge, S. Gladiali, M. Beller, *Nature* **2013**, 495, 85.
- [18] A. Agapova, E. Alberico, A. Kammer, H. Junge, M. Beller, *ChemCatChem* **2019**, *11*, 1910.
- [19] J. B. Curley, C. Hert, W. H. Bernskoetter, N. Hazari, B. Q. Mercado, *Inorg. Chem.* **2022**, *61*, 643.
- [20] S. Weber, K. Kirchner in *Metal-Ligand Co-operativity: Catalysis and the Pincer-Metal Platform* (Eds.: G. van Koten, K. Kirchner, M.-E. Moret), Springer International Publishing, Cham, **2021**, pp. 227–261.
- [21] a) T. He, N. P. Tsvetkov, J. G. Andino, X. Gao, B. C. Fullmer, K. G. Caulton, *J. Am. Chem. Soc.* **2010**, *132*, 910; b) J. F. Sonnenberg, A. J. Lough, R. H.

- Morris, *Organometallics* **2014**, *33*, 6452; c) H. Wang, J. Wen, X. Zhang, *Chem. Rev.* **2021**, *121*, 7530; d) M. Garbe, K. Junge, S. Walker, Z. Wei, H. Jiao, A. Spannenberg, S. Bachmann, M. Scalone, M. Beller, *Angew. Chem.* **2017**, *129*, 11389; e) M. D. Fryzuk, P. A. MacNeil, *J. Am. Chem. Soc.* **1981**, *3592*; f) M. D. Fryzuk, P. A. MacNeil, *Organometallics* **1983**, *2*, 355.
- [22] A. Schlimm, N. Stucke, B. M. Flöser, T. Rusch, J. Krahmer, C. Näther, T. Strunskus, O. M. Magnussen, F. Tuczek, *Chem.* **2018**, *24*, 10732.
- [23] H. Lefebvre-Brion, B. R. Lewis, *Mol. Phys.* **2010**, *105*, 1625.
- [24] C. Flener Lovitt, G. Frenking, G. S. Girolami, *Organometallics* **2012**, *31*, 4122.
- [25] S. Hinrichsen, A.-C. Schnoor, K. Grund, B. Flöser, A. Schlimm, C. Näther, J. Krahmer, F. Tuczek, *Dalton Trans.* **2016**, *45*, 14801.
- [26] S. Goren Keskin, J. M. Stanley, A. H. Cowley, *Polyhedron* **2017**, *138*, 206.
- [27] J. B. Curley, T. M. Townsend, W. H. Bernskoetter, N. Hazari, B. Q. Mercado, *Organometallics* **2022**, *41*, 301.
- [28] C. Gradert, J. Krahmer, F. D. Sönnichsen, C. Näther, F. Tuczek, *Eur. J. Inorg. Chem.* **2013**, *2013*, 3943.
- [29] a) J. Ellermann, M. Moll, N. Will, *J. Organomet. Chem.* **1989**, *73*; b) A. S. Davydov, *Usp. Fiz. Nauk* **1964**, *393*; c) P. Dawson, *J. Phys. Chem. Solids* **1975**, *1401*; d) P. N. Ghosh, *Solid State Commun.* **1976**, *639*; e) W. Kiefer, U. Posser, V. Deckert, *Factor Group Splitting in the n(CO) Region of Polycrystalline Tetracarbonylcomplexes of Molybdenum*, Proc. XIIIth Intern. Conf. Raman Spectroscopy (Eds.: W. Kiefer et al.), Wiley, New York, **1992**, p. 354.
- [30] O. Kühl, *Coord. Chem. Rev.* **2005**, *249*, 693.
- [31] P. E. Garrou, *Chem. Rev.* **1981**, *81*, 229.
- [32] E. W. Becker, W. Vogell, *Z. Naturforsch.* **1950**, *174*.
- [33] a) H. Günther, *NMR-Spektroskopie*, Thieme Verlag, **1992**; b) W. H. Hersh, *J. Chem. Educ.* **1997**, *1485*; c) E. D. Becker, *J. Chem. Educ.* **1965**, *11*, 591; d) *Multinuclear NMR. The Parameters of NMR Spectroscopy* (Ed.: J. Mason), Springer, Boston; e) R. K. Harris, M. S. Jones, A. M. Kenwright, *Magn. Reson. Chem.* **1993**, *31*, 1085.
- [34] J. Jover, J. Cirera, *Dalton Trans.* **2019**, *48*, 15036.
- [35] T. Leischner, A. Spannenberg, K. Junge, M. Beller, *Organometallics* **2018**, *37*, 4402.
- [36] N. F. Both, A. Spannenberg, K. Junge, M. Beller, *Organometallics* **2022**, *41*, 1797.
- [37] R. H. Crabtree, *The Organometallic Chemistry of the Transition Metals*, Wiley Online Books, **2014**, p. 115–118.
- [38] E. W. Abel, M. A. Bennett, G. Wilkinson, *J. Chem. Soc.* **1959**, 2323.
- [39] F. Zingales, A. Chiesa, A. Basolo, *J. Am. Chem. Soc.* **1966**, *88*, 2707.
- [40] G. M. Sheldrick, *Acta Crystallogr. Sect. A* **2015**, *71*, 3–8.
- [41] G. M. Sheldrick, *Acta Crystallogr. Sect. C* **2015**, *71*, 3.
- [42] F. Neese, *Comput. Mol. Sci.* **2018**, *33*.
- [43] J. P. Perdew, K. Burke, M. Ernzerhof, *Phys. Rev. Lett.* **1996**, *3865–3866*.
- [44] a) F. Weigend, *Phys. Chem. Chem. Phys.* **2006**, *8*, 1057; b) A. Hellweg, C. Hättig, S. Höfener, W. Klopper, *Theor. Chem. Acc.* **2007**, *117*, 587.
- [45] S. Grimme, J. Antony, S. Ehrlich, H. Krieg, *J. Chem. Phys.* **2010**, *132*, 154104.
- [46] S. Grimme, S. Ehrlich, L. Goerigk, *J. Comput. Chem.* **2011**, *32*, 1456.
- [47] a) K. Eichkorn, O. Treutler, H. Öhm, M. Häser, R. Ahlrichs, *Chem. Phys. Lett.* **1995**, *283*; b) K. Eichkorn, O. Treutler, F. Weigend, *Theor. Chem. Acc.* **1997**, *119*; c) F. Neese, *J. Comput. Chem.* **2003**, *24*, 1740; d) F. Neese, F. Wennmohs, A. Hansen, U. Becker, *J. Chem. Phys.* **2009**, *356*, 98.
- [48] V. Barone, M. Cossi, *J. Phys. Chem. A* **1998**, *102*, 1995.
- [49] S.-A. Gentschow, S. W. Kohl, W. Bauer, F. W. Heinemann, D. Wiedemann, A. Grohmann, *Z. Naturforsch. A* **2010**, *238*.
- [50] K. Zhu, P. D. Achord, X. Zhang, K. Krogh-Jespersen, A. S. Goldman, *J. Am. Chem. Soc.* **2004**, *126*, 13044.
- [51] M. Pfeil, T. A. Engesser, A. Koch, J. Junge, J. Krahmer, C. Näther, F. Tuczek, *Eur. J. Inorg. Chem.* **2020**, 1437.
- [52] E. Hrishikesan, R. Manjunath, P. Kannan, *J. Solution Chem.* **2016**, *45*, 907.

Manuscript received: May 12, 2023
 Revised manuscript received: August 14, 2023
 Accepted manuscript online: August 15, 2023
 Version of record online: ■■, ■■

Project 3 - Surface functionalization of tridentate PNP and PPP Ligands

To date, many homogeneous catalyst are known, capable of converting dinitrogen to ammonia (section 2.3). Besides the approach presented in project 1 (cf. Chapter 3) that uses $\text{SmI}_2/\text{H}_2\text{O}$, other combinations of acids and electron sources have been investigated intensively in literature.^[21,155,165,186,190–192] Heterogeneous catalysts that utilize transition metal complexes are very rare in literature. The main focus in heterogeneous nitrogen fixation evolves around solid state materials.^[7,242,243] Neither a catalytically active system, nor a dinitrogen complex deposited as monolayer on a surface was reported yet. However, there are a few examples of surface bound dinitrogen complexes e.g. the Ru- or Rh- N_2 complexes bound to a zeolithes surface or as part of a polymer coating for electrode modifications.^[244–246] Besides homogeneous catalysis as seen in project 1, heterogeneous catalysis is an interesting, alternative approach to nitrogen fixation. Investigation of the properties of surface bound nitrogen complexes and the influence of the surface, can be achieved by modification of existing ligand designs. In order to determine the aforementioned factors as well as obtaining defined centers for catalysis, monolayers are the preferred approach. The advantage of modifying an already known system is that one can be chosen, which is catalytically active under certain conditions.

Unfortunately, N_2 complexes are quite sensitive, so replacing the dinitrogen ligand with isoelectronic carbonyl ligands, which form much more stable complexes, is a well suited way to develop ligand systems for surface-bound transition metal complexes. Another advantage of carbonyl ligands, besides the improved stability and excellent spectroscopic properties, is the elimination of an otherwise needed coligand. In order to deposit a compound like a tricarbonyl complex on a surface as a monolayer, different approaches based on physi- and chemisorption can be chosen. One possibility is "physical vapor deposition" (PVD) using evaporation and deposition on a surface under vacuum. Prerequisite for vacuum deposition is the evaporability and thermal stability of the complexes. As the complexes are in direct contact with the surface the electronic interactions can be observed. Depending on the molecule-substrate interactions, these interactions can result in a modification of the complexes properties or lead to fragmentation e.g. on a gold surface.^[247–250] A second possibility evolves around chemisorption. A well known way to modify surfaces with different types of molecules are self-assembled monolayers (SAMs). SAMs are formed by spontaneous self organization.^[251–253] The assembly results in highly oriented and ordered coating.^[251–253] Formation of an oriented monolayer is achieved by three design elements: the anchor group, the spacer and the headgroup.^[254] The anchor group is chosen depending on the desired surface, to achieves a strong connection of adsorbat

on the substrate, e.g. sulfur anchor for gold, silane anchors to oxides or carboxylate anchors to silver.^[254–256] Besides the bond strength of the anchor group the spacer chains normally consisting of alkyl chains and their Van der Waals interaction are important for the stability and order of the coated surface. The interaction not only allows spontaneous arrangement, but their length is also an important factor for stability and durability.^[251,253,254] The last part of a SAMs design is the head group. The choice of the head group allows for modification of chemical, physical, optical and electric properties.^[254] Furthermore, the head group can also act as starting point for further modification.^[257]

The third possibility is a platform approach. A platform molecule (e.g. TATA = triazatriangulene) is chosen as substitution for the anchor group.^[258–260] This approach allows for vertical orientation of a head group on the surface. Besides that, by modification of the platform itself the distance between the molecules on the surface can be adjusted.^[259]

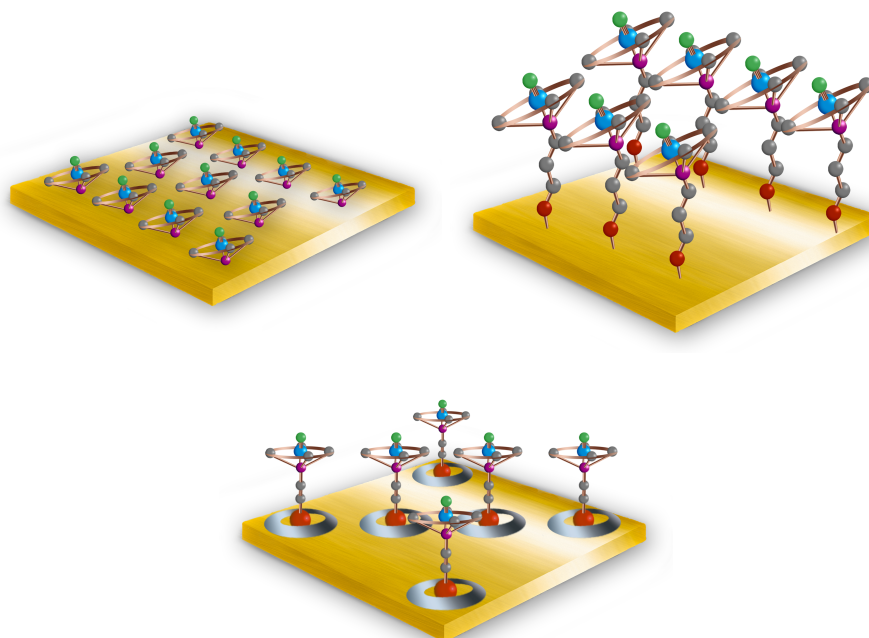


Fig. 5.1: Illustration of different methods of deposition of complexes on a surface: direct deposition (top left), self-assembled monolayers (top right) and the platform approach (bottom). It is worth noting that the uniform orientation of the complexes does not represent an experimental case.

The present approaches are based on the preliminary works of our group. In 2018 SCHLIMM and STUCKE published a pincer based system, featuring a modified PN^3P ligand (Figure 5.2).^[261] The pincer unit coordinated a molybdenum(0) tricarbonyl complex in meridional fashion while the acetylene function was attached to a TATA platform. The platform was deposited on a gold surface and the influence of the surface was investigated by infrared reflection absorption spectroscopy (IRRAS), X-ray photoelectron spectroscopy (XPS) and

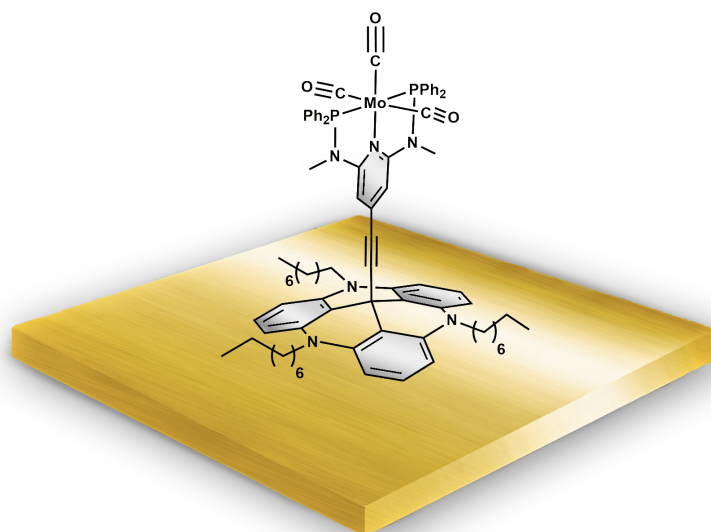


Fig. 5.2: Illustration of the molybdenum tricarbonyl complex bearing a modified PN³P pincer ligand on an Au(111) surface. The complex is attached to an octyl-TATA platform which is used to vertically deposit the headgroup on the surface.^[261]

near-edge X-ray absorption fine structure (NEXAFS).^[261] The PN³P pincer featured a pyridine as central unit, while diphenyl phosphine groups were used as terminal donors. Comparison of the data from surface active spectroscopies to the bulk and solution data, the influence of the gold surface was revealed. While the deposition of the complex and its desired oxidation state was confirmed using XPS, NEXAFS and STM imaging, the influence of the gold on the carbonyl ligands was determined by IRRA spectroscopy. Due to the electron-withdrawing properties of the gold surface, electron density shifted from the molybdenum center towards the surface. As a consequence of the partial reduction, less electron density is available for π -backbonding to the carbonyl ligands hence decreasing their activation compared to the bulk species.^[261] Interestingly, the desactivating effect of the gold did not affect all stretches equally as the symmetrical A₁(1) stretch was less desactivated than the A₁(2) and B₁ stretch. This was postulated to be originating from a dynamic charge transfer, which is exclusive to the A₁(1) stretch. The symmetric elongation of the CO bonds and the associated symmetrical shift of the dipole are partially compensated by electron density flow from the surface back to the complex utilizing the conjugated π -system of the backbone.^[261]

In 2021 PETERSEN presented another molybdenum(0) tricarbonyl system bearing a tripodal PPP ligand.^[262] The tripodal ligand features a phenyl spacer with acetylene modification and was bound to the TATA platform as well. This structural design allowed for a perpendicular orientation of the complex to the surface. Despite vertical alignment by platform and spacer, the complex is slightly tilted to the surface plane, since the quaternary carbon on the tripod leads to a tilt of the complex relative to the surface.^[262] This tilt also allows for investigation

of the equatorial carbonyl ligands in the IRRA spectrum as the dipoles are not parallel to the surface. As expected, the tricarbonyl complex bearing the tripod ligand showed global desactivation of the carbonyl ligands, due to the electron withdrawing properties of the gold surface.^[262] Just as reported by SCHLIMM and STUCKE the desactivation of the symmetrical A(1) stretch was partially compensated. This was observed even though the ligand does not have a conjugated π -system.^[261,262]

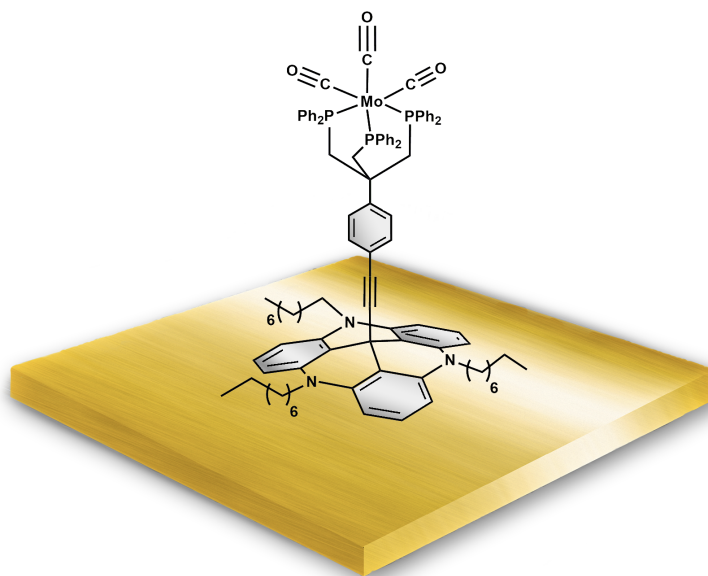


Fig. 5.3: Illustration of the molybdenum tricarbonyl complex bearing a modified tripodal P_3 ligand on a Au(111) surface. The complex is attached to a TATA-platform which is used to vertically deposit the system on the surface.^[262]

Besides pincer and tripodal systems that were reported by our group previously,^[261,262] this project focuses around the last class of ligands with three donors. Aim of this project was the functionalization of tridentate PEP ($\text{E} = \text{N}, \text{P}$) ligands for surface chemistry. As in prior projects, the ligands are to be coordinated to $\text{Mo}(0)$ tricarbonyl complexes as the stability of the complexes has been investigated in depth and no coligands are needed. A further goal is the electrochemical investigation and a possible suitability as a heterogeneous catalyst. The ligand chosen as tridentate counterpart to pincer systems was the $\text{PN}^{\text{Ph}}\text{P}^{\text{Ph}}$ ligand that was part of the second project as well (cf. Project 2, Chapter 4). Besides the PNP system a PPP system analogous to the tripodal PPP system was designed. As a starting point for the purely phosphine based system, the tridentate $\text{prPP}^{\text{H}}\text{P}$ ligand was used, which is used by our group for the synthesis of the pentaPod ligand (cf. Project 1, Chapter 3). The general composition of the systems is modified to fit the above mentioned criteria: the anchor group, the spacer and the head group. In order to attach the ligands to the gold surface, a substrate specific anchor group is needed. For this, two different approaches were chosen. One approach

includes the introduction of an acetylene group which could be either attached to a platform as presented in previous work or clicked to an azide function forming a triazole ring. The azide needed for this cycloaddition is bound to the gold surface via an alkyl SAM with a thiol group capable of forming covalent bonds to the gold surface (Figure 5.4 top right). Besides the formation of a triazole ring by HUISGEN's cycloaddition^[263] and a platform approach (Figure 5.4 top left), the ligands could be modified with a group capable of binding to a substrate. One approach to this is the utilization a thiol function as anchor group. The thiol group is part of a thiophenyl group included in the ligand backbone. The phenyl group now acts as the spacer group between the surface and the complex (Section 5.2, Figure 5.4 right). Within the scope of this thesis, this approach was only applied to a PNP type ligand, and is the main focus of this project.

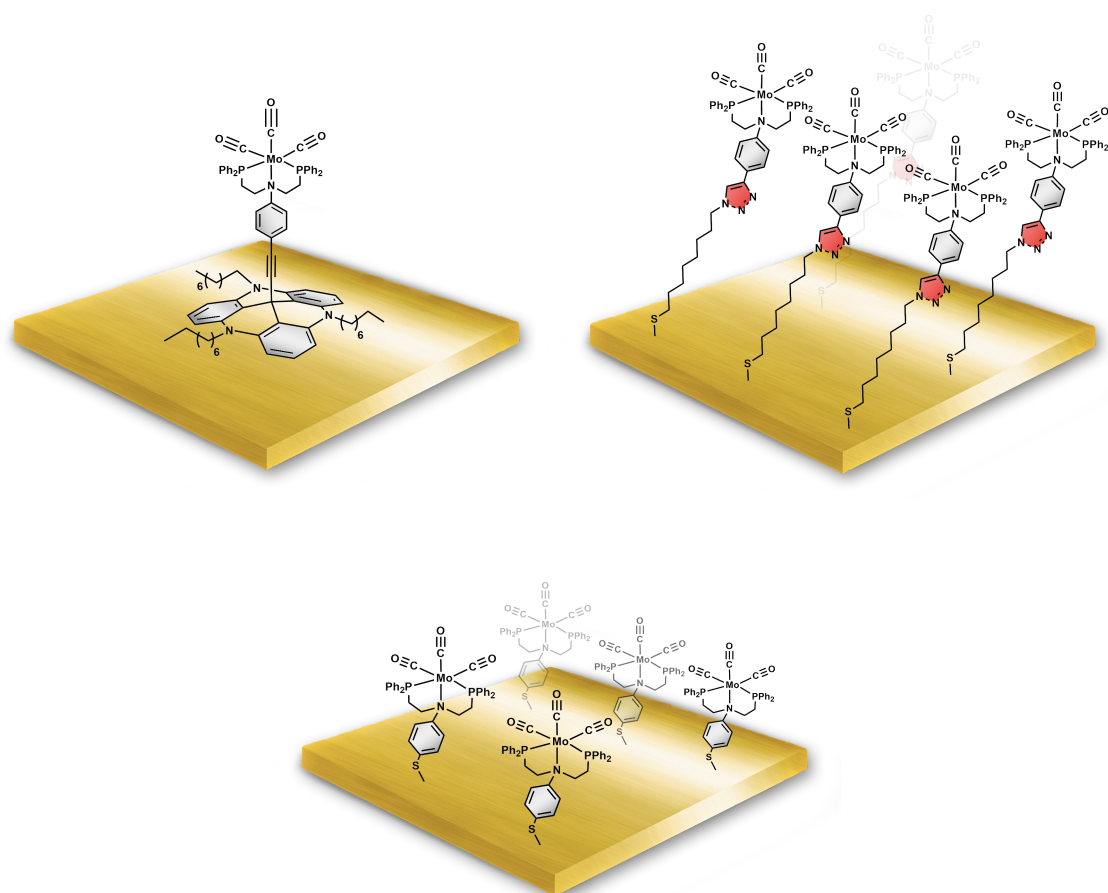
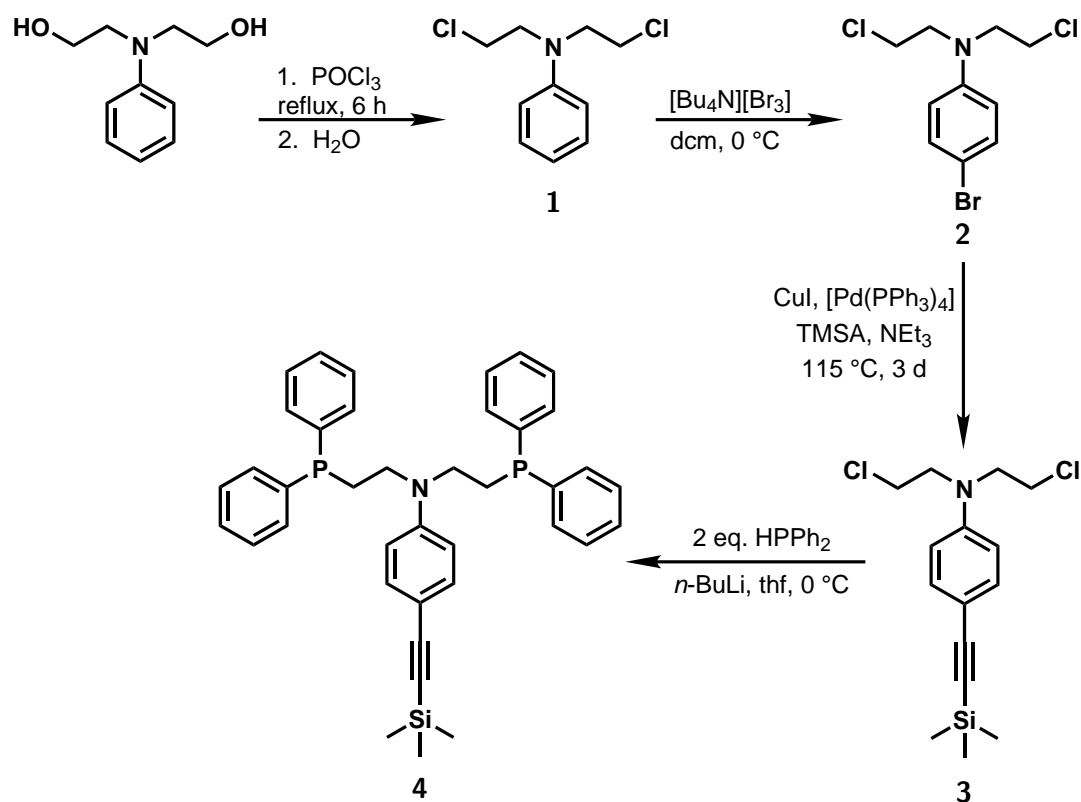


Fig. 5.4: Illustration of the approaches for depositing a Mo(0) tricarbonyl complex bearing tridentate PNP ligand on gold surface targeted in this project.

5.1 Acetylene functionalization of the $\text{PN}^{\text{Ph}}\text{P}^{\text{Ph}}$ ligand

As mentioned above, the PNP ligand chosen for the modifications towards surface attachable systems was the $\text{PN}^{\text{Ph}}\text{P}^{\text{Ph}}$ ligand. From the study in the second project (cf. Project 2, Chapter 4) the limitations of the PNP systems and their stabilities are known, which led to the decision that diphenylphosphine donors would be a well suited choice. Not only are they known to be good donors regarding molybdenum tricarbonyl complexes, but are also the least sensitive towards oxidation from the list of phosphines available. As known from previous experiences in our group, the systems will be exposed to some oxygen during preparation for the surface active spectroscopies. Either from transfer into the sample chamber or from oxygen/water adsorbed on the surface of the waiver.



Scheme 1: Synthetic access to the surface modified $\text{PN}^{\text{Ph}}\text{P}^{\text{Ph}}$ ligand **4**. TMSA = Trimethylsilylacetylene.

Starting from *N*-phenyldiethanolamine chlorination of the hydroxy groups gave *N,N*-bis(2-chloroethyl)aniline (**1**). This was done by a modified method based on the procedure by HRISHIKESAN *et al.*^[264] After the reaction was completed, excess phosphorus oxychloride was carefully neutralized with water. Cooling the reaction mixture using an ice bath suppresses

the neutralization, leading to a spontaneous and rather violent reaction upon warming to room temperature, why a water bath at room temperature was used as coolant. This synthesis was also attempted using thionyl chloride, however no product could be obtained. The completeness of the conversion from the alcohol to the chloride (**1**) was confirmed by NMR and IR spectroscopy. Especially the infrared spectrum showed the successful conversion as no characteristic OH stretches were found.

In order to introduce the acetylene function, the phenyl ring on the aniline was brominated in the 4-position, yielding 4-bromo-*N,N*-bis(2-chloroethyl)aniline (**2**). This was achieved by following the procedure described by HUFFMAN *et al.*,^[265] however the reaction was cooled to 0 °C instead of 10 °C. The crude product was dissolved in methanol and crystallized in the freezer (-32 °C). The solid was filtered and solved in methanol again to decrease the amount of $[n\text{-Bu}_4\text{N}]^+$ salts from the product. In order to fully remove the salts the crude product was recrystallized from methanol and the desired compound **2** was obtained as light pink solid. Introduction of the acetylene group was achieved by SONOGASHIRA coupling^[266] of compound **2** to obtain *N,N*-bis(2-chloroethyl)-4-((trimethylsilyl)ethynyl)aniline (**3**). Multiple attempts were made in order to obtain the desired product. The first attempts had a reaction time of 5 d, which was later reduced to 3 d. Furthermore, the catalyst was varied and changed from $[\text{PdCl}_2(\text{PPh}_3)_2]$ to $[\text{Pd}(\text{PPh}_3)_4]$.^[266,267] After column chromatography using *n*-hexane and ethyl acetate (4:1) the precursor to ligand **4** was obtained as dark orange oil. From the NMR spectra it became evident that, although purified by column chromatography, small impurities remained. Nonetheless, the introduction of the TMS-acetylene group was observed in the ^1H - and ^{13}C NMR spectra. Despite small impurities the precursor to the ligand was further reacted using the well established route for the introduction of the secondary phosphines with *n*-butyllithium and subsequent purification by filtration over Celite® and basic aluminum oxide.^[216–218,268] This yielded the desired product *N,N*-bis(2-(diphenylphosphino)ethyl)-4-((trimethylsilyl)ethynyl)aniline (**4**) as highly viscous orange oil (44%).

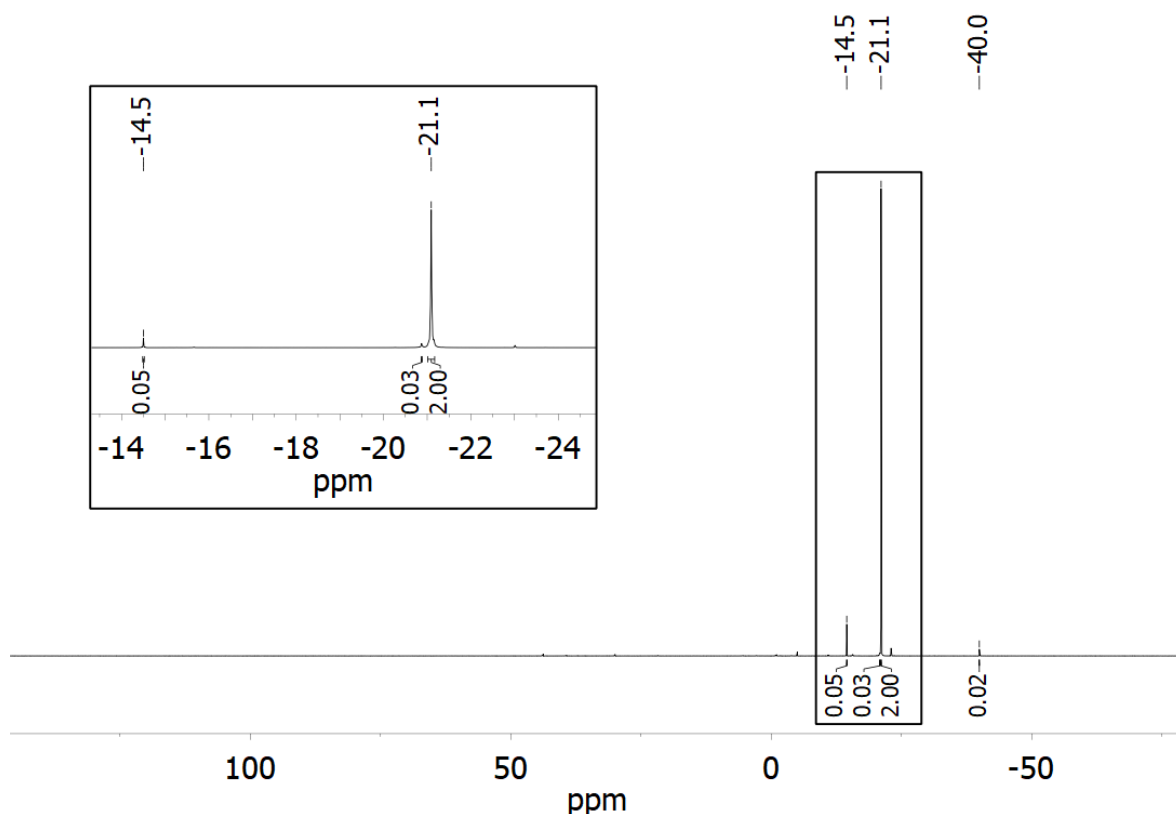


Fig. 5.5: $^{31}\text{P}\{^1\text{H}\}$ NMR spectrum of ligand **4**. The successful substitution of the terminal chlorides by diphenyl phosphine can be seen from the product signal at -21.1 ppm.

From the ^{31}P NMR spectrum (Figure 5.5) the formation of ligand **4** was confirmed. This is indicated by the signal at -21.1 ppm, which is known from the unmodified ligand. Beside the main product signal, those of some byproducts were found as well. The signal at -40.0 ppm can be assigned to excess diphenyl phosphine. Three other small impurities were found at -23.0 ppm, -20.9 ppm and -14.5 ppm which could not be identified but can possibly assigned to a singular substituted product as not all of the HPPh_2 has reacted and potentially some decomposed product. The formation of a small byproduct is also confirmed from the ^{13}C NMR spectrum as a second, smaller set of signals is found beside the product signals of the ligand. The carbon atoms of the acetylene unit on the other hand are only found once. Considering the slight high field shift of the signals, the byproduct is either the phosphinated version of the brominated compound **2** or the bromide as well as the chloride substituents were exchanged by the lithium diphenyl phosphide.

As can be seen from the integrals of the signals in the ^{31}P NMR spectrum, the impurities are rather small, which is why the ligand was still been used for the coordination to molybdenum tricarbonyl precursors. The first attempts were made using $[\text{Mo}(\text{CO})_3(\eta^6\text{-toluene})]$ as precursor complex, due to the $[\text{Mo}(\text{CO})_3(\text{cht})]$ complex not being available at that time. The $[\text{Mo}(\text{CO})_3(\eta^6\text{-toluene})]$ complex was synthesized from $[\text{Mo}(\text{CO})_6]$ after modified procedures

from RYBINSKAYA *et al.*^[269] and WHITING & NICHOLLS.^[270] The $[\text{Mo}(\text{CO})_3(\eta^6\text{-toluene})]$ was chosen as the complex is less stable compared to the cycloheptatriene analogue and more prone towards ligand exchange.^[271] Nonetheless, no reaction was observed at room temperature. Due to this, a second attempt with increased temperature was made. This led to the formation of a precipitate, which was filtered and washed. The IR spectrum (Figure 5.6, black spectrum) of the obtained complex showed a multitude of CO stretches, indicating a mixture of complexes. Although the stretches of the desired complexes are visible as shoulders, a purification of the mixture was not successful and the attempt was discarded.

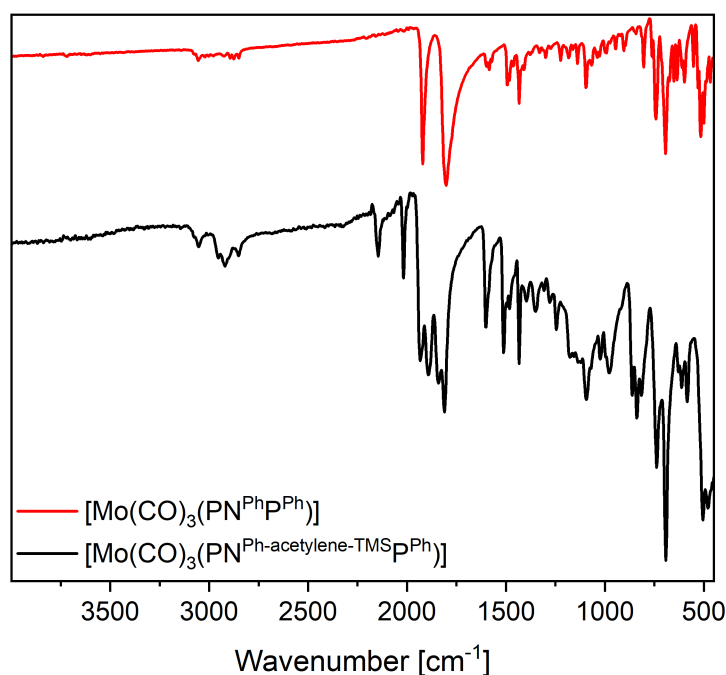


Fig. 5.6: Comparison of the infrared spectra of the $[\text{Mo}(\text{CO})_3(\text{PN}^{\text{Ph}}\text{P}^{\text{Ph}})]$ complex (top, red) to the attempted coordination of the surface modified PNP ligand **4** (bottom, black).

During the experimental work of Project 2, some experiments were conducted using $[\text{Mo}(\text{CO})_3(\eta^6\text{-toluene})]$. Nonetheless, the best results were achieved using the cycloheptatriene molybdenum tricarbonyl complex and as it was not commercially available at the time, it was synthesized from $\text{Mo}(\text{CO})_6$. The first approach to the synthesis was carried out by following a slightly modified procedure of BISNETTE *et al.*^[272] Refluxing $\text{Mo}(\text{CO})_6$ in dry *n*-octane and cycloheptatriene (cht) gave a dark red solution. Removal of the solvent and cht has to be performed with extreme caution and the temperature should not exceed 35 °C as the complex would sublime. The dried crude product was then transferred into a Soxhlet extractor and extracted using *n*-hexane. The solvent was removed carefully and the complex obtained as red solid. Due to the poor yield of the Soxhlet extraction, an alternative procedure was used for the isolation and purification of the complex during a second run. After reflux and

removal of the volatile components, the $[\text{Mo}(\text{CO})_3(\text{cht})]$ complex was extracted from the crude product upon addition of *n*-hexane. This step was repeated multiple times until the solvent did not dyed red anymore. This step removed some parts of unreacted $\text{Mo}(\text{CO})_6$, the rest was removed via sublimation. The temperature applied should not exceed 30 °C to assure the sublimated compound is the hexacarbonyl only. This process is very time consuming but yields a very pure product. Unfortunately, both procedures resulted very poor yields. The poor yield can be attributed to the $\text{Mo}(\text{CO})_6$ sublimating during the reflux in the first step of the reaction. CLAUSEN was able to improve the yield by changing the apparatus and building a custom spatula and scraping the sublimated $\text{Mo}(\text{CO})_6$ back into the solution. In addition to that the reaction time was significantly elongated.^[273]

Using the $[\text{Mo}(\text{CO})_3(\text{cht})]$ complex, another attempt to coordinate the surface modified $\text{PN}^{\text{Ph}}\text{P}^{\text{Ph}}$ ligand (**4**) was made. A successful coordination of the PNP ligands to the $\text{Mo}(\text{CO})_3$ fragment should result in the precipitation of a yellowish/beige solid. Using identical conditions for the coordination as used for the unmodified ligand, the solution remained unchanged. Due to this, the temperature was increased to 50 °C for 6 h and afterwards stirred for another 12 h. This resulted in a darkening of the solution but not to the formation of the anticipated yellowish solid, which was observed for nearly all molybdenum tricarbonyl complexes bearing PNP ligands in Project 2. Nonetheless, the solvent was removed and the crude product washed multiple times with *n*-pentane to remove ligand and precursor complex. The remaining solid was washed and dried. The synthesis resulted again in a mixture of complexes. Although the desired complex was contained in the product mixture, multiple side reactions occurred as can be seen from ^{31}P NMR spectrum (Figure 5.7)

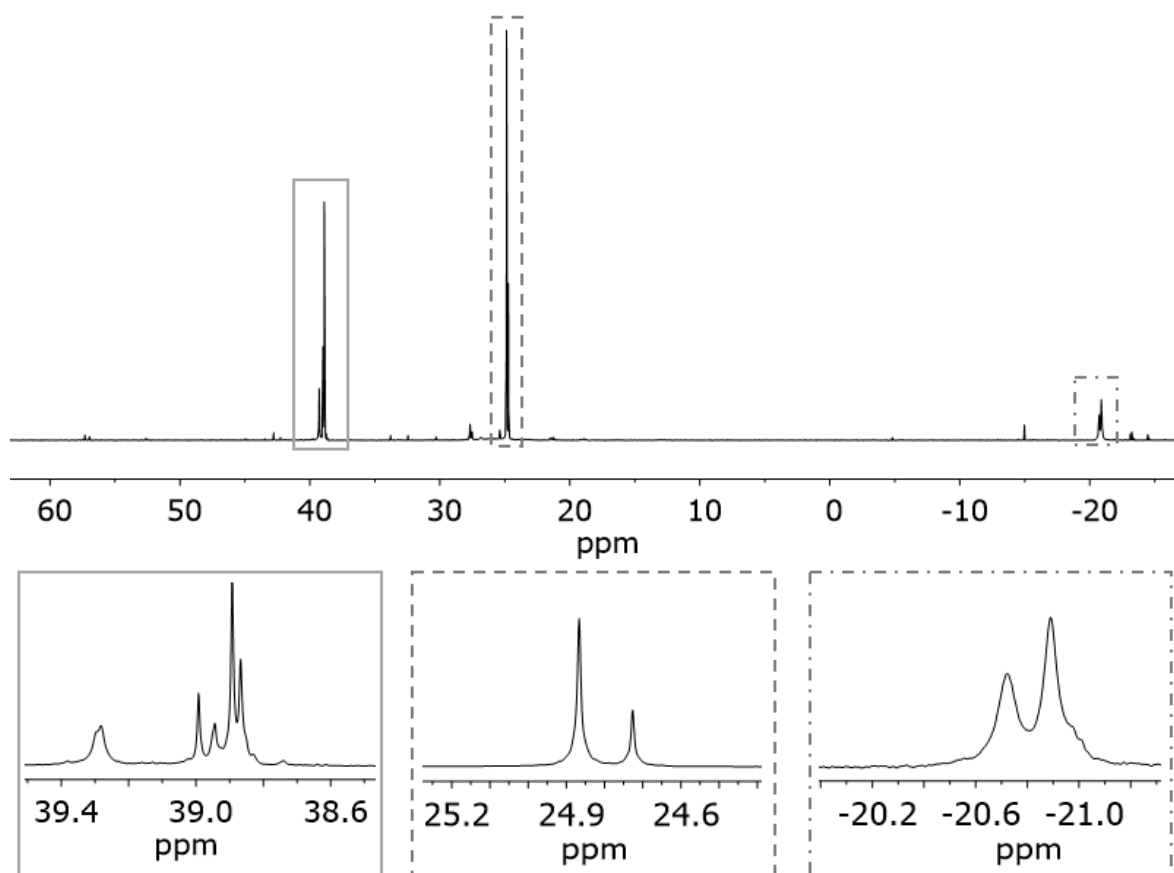
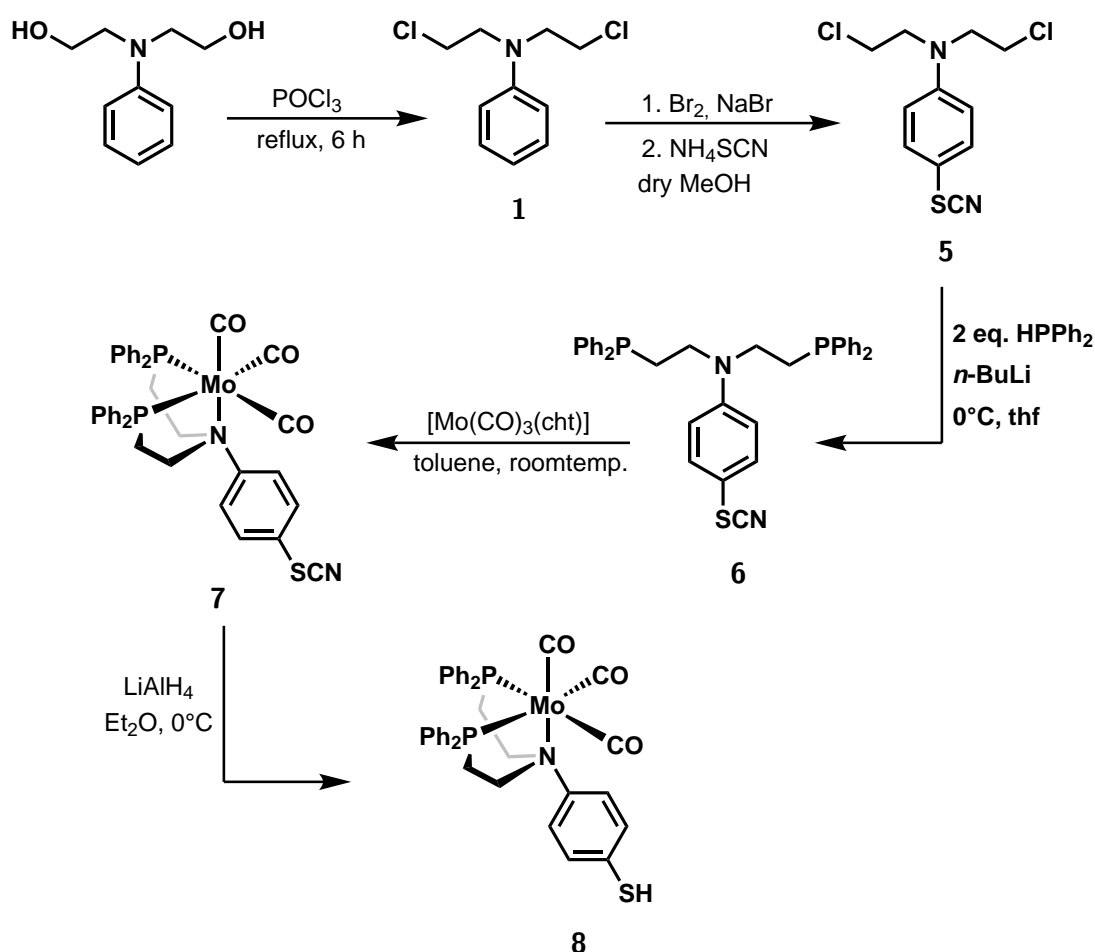


Fig. 5.7: $^{31}\text{P}\{^1\text{H}\}$ NMR spectrum of the attempted coordination of the surface modified $\text{PN}^{\text{Ph}}\text{P}^{\text{Ph}}$ ligand **4** using $[\text{Mo}(\text{CO})_3(\text{cht})]$.

From comparison to the spectrum of the unmodified $\text{PN}^{\text{Ph}}\text{P}^{\text{Ph}}$ ligand it can be seen that the desired complex was formed but many other species as well. By comparing with the literature, the signal at 25 ppm can be assigned to the tetracarbonyl complex with the phosphines coordinated.^[274] The tetracarbonyl complex is the product of a decomposition reaction of the desired complex. This can possibly be retraced to the increased temperatures applied. The desired product is expected at around 40 ppm. As can be seen from Figure 5.7, multiple species were found, indicating the formation of multiple tricarbonyl complexes with facial geometry. This leads to the conclusion that the ligand decomposed to a certain degree as well. Unfortunately, the desired carbonyl complex could not be isolated but should be obtainable under different conditions e.g. elongation of reaction times, different solvents and lower temperatures. Although the attempts made are very promising and ligand **4** was synthesized successfully, the main focus was redirected to another variant of the $\text{PN}^{\text{Ph}}\text{P}^{\text{Ph}}$ ligand that features a thio-based anchor group.

5.2 Thiofunctionalization of the $\text{PN}^{\text{Ph}}\text{P}^{\text{Ph}}$ ligand

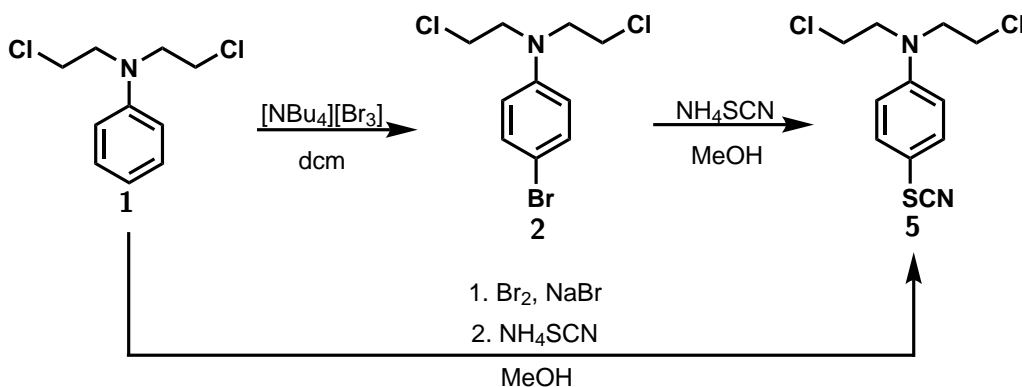
The second variant of a surface functionalized PNP ligand features a thiol anchor group. This alternative approach is another attempt continuing on from the result presented in the second project of this thesis. The sulfur anchor is chosen in order to create a direct covalent bond between the system and the gold surface. Sulfur is an excellent choice when the surface aimed for is gold as the *aurophilic* character of the sulfur helps with the formation of stable bonds.^[275] The first steps of the reaction are similar to the ones of the acetylene functionalized PNP ligand.



Scheme 2: Synthetic access to thiocyanate-functionalized $\text{PN}^{\text{Ph}}\text{P}^{\text{Ph}}$ ligand (**6**) and the corresponding tricarbonyl complex **7**. Herein the SCN group acts as protective group during the coordination and is converted to a surface active thiol via reduction.

The first step is a chlorination following the procedure described in the sections 4.1 and 5.1 resulting the PNP precursor **1**. The sulfur anchor is introduced as thiocyanate which was chosen for multiple reasons. The first reason is that the introduction of a thiocyanate group

is a well established synthesis and is selective towards the *para*-position of the amine. The second reason is that the thiocyanate group enables two methods of attachment to the gold surface. The first involves reduction to a thiol and subsequent binding to the surface (scheme 2) while the second method is a direct attachment upon a gold induced CN^- release.^[276] The introduction of the SCN group is a two step reaction (Scheme 3). In the first step of the reaction a bromine is introduced in the 4-position. This can be done in two ways: either by following the HUFFMAN procedure^[265] described in section 5.1 using $[NBu_4][Br_3]$ or following the instructions of CREIGHTON *et al.* generating the reactive Br_3^- ion *in situ* from bromine and sodium bromine in dry methanol and adding it to a solution of **1** and ammonium thiocyanate. The first variant works best when isolating the 4-bromo-*N,N*-bis(2-chloroethyl)aniline (**2**), dissolving it in methanol and adding pure NH_4SCN . The product can be recrystallized from ethanol. The advantage of the second method is that it is a one-step synthesis. The crude product of the synthesis is a brown oil, which is best purified by recrystallization from ethanol. Both methods were tried, both leading to a successful isolation of the desired product in good yields.



Scheme 3: Illustration of the two methods used to introduce the thiocyanate group into the ligand precursor.

N,N-bis(2-chloroethyl)-4-thiocyanatoaniline (**5**) is an ideal dummy molecule in order investigate and optimize the direct deposition upon CN^- release on a gold substrate. The main disadvantage is that investigations with IRRAS are problematic as no good indicator regarding the surface orientation is present in the molecule. Nonetheless, first attempts regarding a direct deposition have been made. Although the preparation method still requires optimization, it was found that a first attempt of the direct deposition worked to some extent as can be seen from the XP spectra (Figure 5.8).

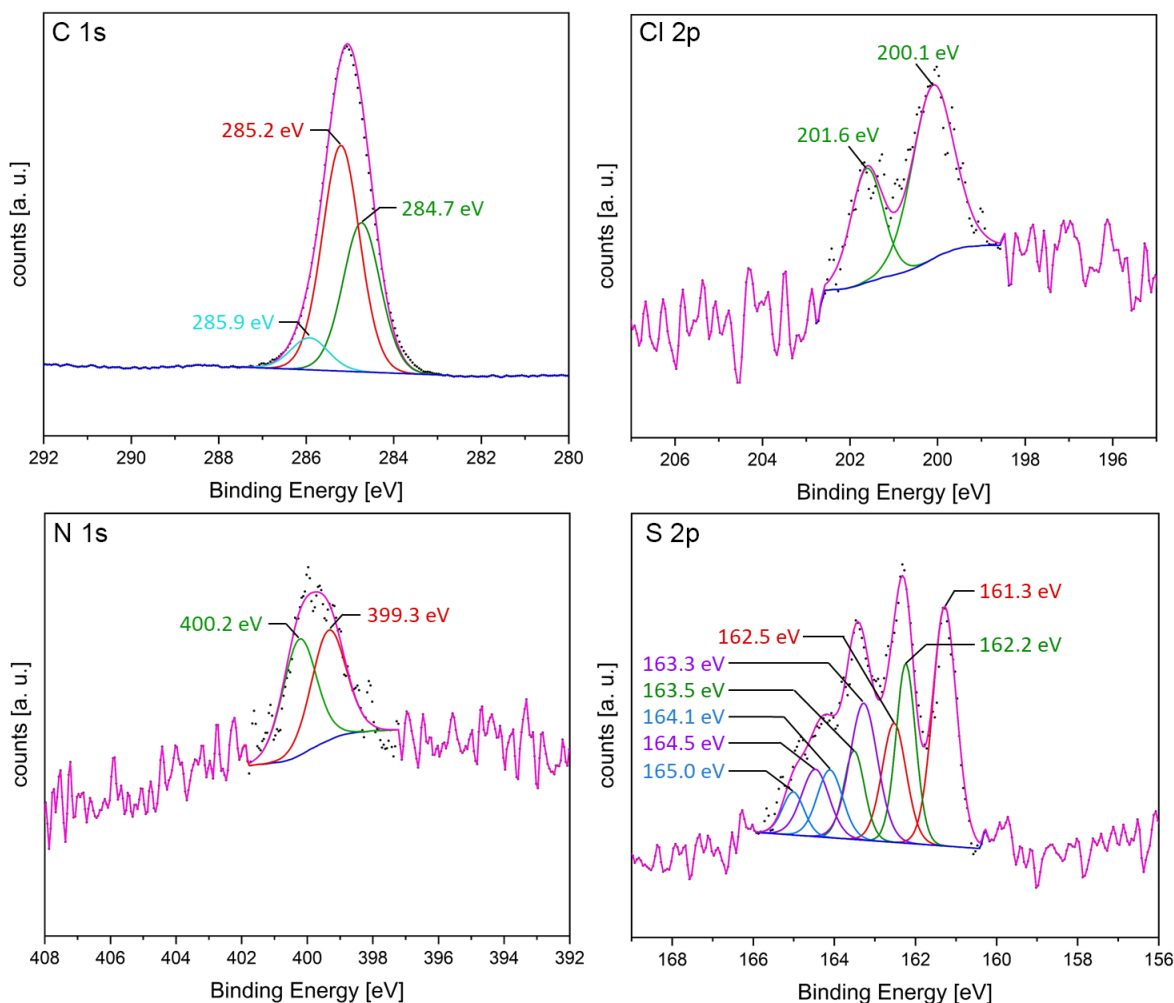


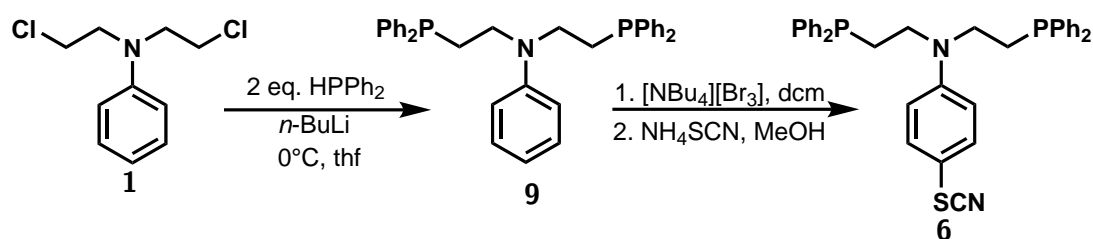
Fig. 5.8: XPS spectra of the first attempt to deposit the dummy molecule **5** in a monolayer on a gold surface without prior reductive conversion of the thiocyanate to a thiol. The deposition was attempted directly starting from the thiocyanate upon cyanide release. The spectra show the presence of multiple species on the surface especially in the sulfur 2p-spectrum (bottom right). The other element spectra (carbon 1s, top left; chlorine 2p, top right; nitrogen 1s, bottom left) show that the substance used was pure.

The carbon 1s spectrum (Figure 5.8, top left) shows one signal, which can be fitted by three species. The binding energy of 284.7 eV can be assigned to carbon atoms that are neighboring other carbon atoms. This is followed at 285.2 eV by carbons bound to a hetero atom like nitrogen, chlorine or sulfur. The final species within this fit, at 285.9 eV, can be assigned to the carbon atom in the thiocyanate group which should show the biggest shift due to the triple bond and two neighboring heteroatoms. The chlorine 2p spectrum (Figure 5.8, top right) shows only one species with two signals representing the $2p_{3/2}$ and $2p_{1/2}$ state. The signal in the nitrogen spectrum (Figure 5.8, bottom left) can be fitted with two signals, one for the aniline nitrogen (400.2 eV) and the other for the nitrogen in the thiocyanate group (399.3 eV).^[275,277]

The most interesting of the spectra displayed in Figure 5.8 is the sulfur 2p spectrum (bottom right). The formation of a gold-thiol bond can be determined from the signal at 162.2 eV and 163.5 eV, which is similar to the values found in literature.^[275,277] The species at 161.3 eV and 162.5 eV can be assigned to elemental sulfur formed by decomposition of thiol on the surface. 163.3 eV and 164.5 eV could be assigned to a disulfide species formed from two thiols. The final fitted signal at 164.1 eV and 165.0 eV can be assigned to physisorbed thiocyanate.^[277] It should be possible to reduce the amount of by-products (atomic sulfur, disulfide and physisorbed molecule) on the surface by optimizing the deposition conditions. However, this was only a first trial but shows the potential of this approach.

The next step in the synthesis of the ligand is the phosphination of the dummy molecule **5**. The first attempts were made using the well established conditions with *n*-BuLi in thf. This unfortunately did not lead to the formation of the desired PNP ligand. The problem was found to be the pseudo-halogen character of the SCN group. Not only the substitution, but also different side reactions formed a multitude of species. Different approaches were taken in order to try and solve this problem. Besides the variation of temperature, concentrations and reaction times, a different approach to phosphination was tested. Instead of the well established procedure with *n*-BuLi, potassium hydride was used as deprotonating agent. Furthermore, the addition of the diphenyl phosphine was stretched over the course of two hours. Unfortunately, the desired product could not be obtained. A last attempt to follow the synthetic route in scheme 2 was to increase the selectivity of the substitution reaction by exchanging the terminal chloride groups by iodine. This was successfully performed by means of a FINKELSTEIN reaction. However, this attempt did not lead to the formation of the desired product as well.

Due to the problems during the introduction of the phosphines the route for the synthetic access was altered. The second attempt took an inverse approach (Scheme 4).



Scheme 4: Illustration of the inverse approach to synthesize the $\text{PN}^{\text{Ph}}\text{-SCN}^{\text{Ph}}$ ligand (**6**).

The well known $\text{PN}^{\text{Ph}}\text{P}^{\text{Ph}}$ ligand (**9**) was synthesized before the introduction of the thiocyanate function. Although the phosphines feature phenyl rings as well, the activation is insufficient, allowing for a selective introduction in the 4-position of the aryl ring of the central aniline. Starting from the $\text{PN}^{\text{Ph}}\text{P}^{\text{Ph}}$ ligand (**9**), the bromide was introduced by addition of $[\text{NBu}_4][\text{Br}_3]$ and subsequent addition of NH_4SCN . The solution changed to a light pink due to the release of

molecular bromine. The bromine was deactivated by addition of thiosulfate solution. Although the resulting colorless solid looked promising, the ^{31}P NMR spectrum revealed the formation of mainly three products (Figure 5.9, middle). The desired product **6** can be assigned to the signal at -21.3 ppm, which is in accordance with the unsubstituted ligand. From comparison of the integrals it can be seen that the modified PNP ligand **6** was obtained as the product with the lowest percentage (7.3%). The main product of the reaction appears to be the ligand in which both phosphorus atoms oxidized to a phosphorus(V) species as a result of the reaction between the PPh_2 and the Br_2 resulting terminal PPh_2Br_2 groups on both sides of the tridentate ligand. The signals at 38.9 ppm and -21.4 ppm show an identical percentage of the product mixture. As the shift compared to the other two signals is small and the ratio is 1:1, it can be assumed that the signals belong to two different phosphorus groups in the same ligand. The two signals can be assigned to the version of the ligand in which only one of the phosphines was oxidized by the bromine released from the Br_3^- during the introduction of the Br substituent on the aniline.

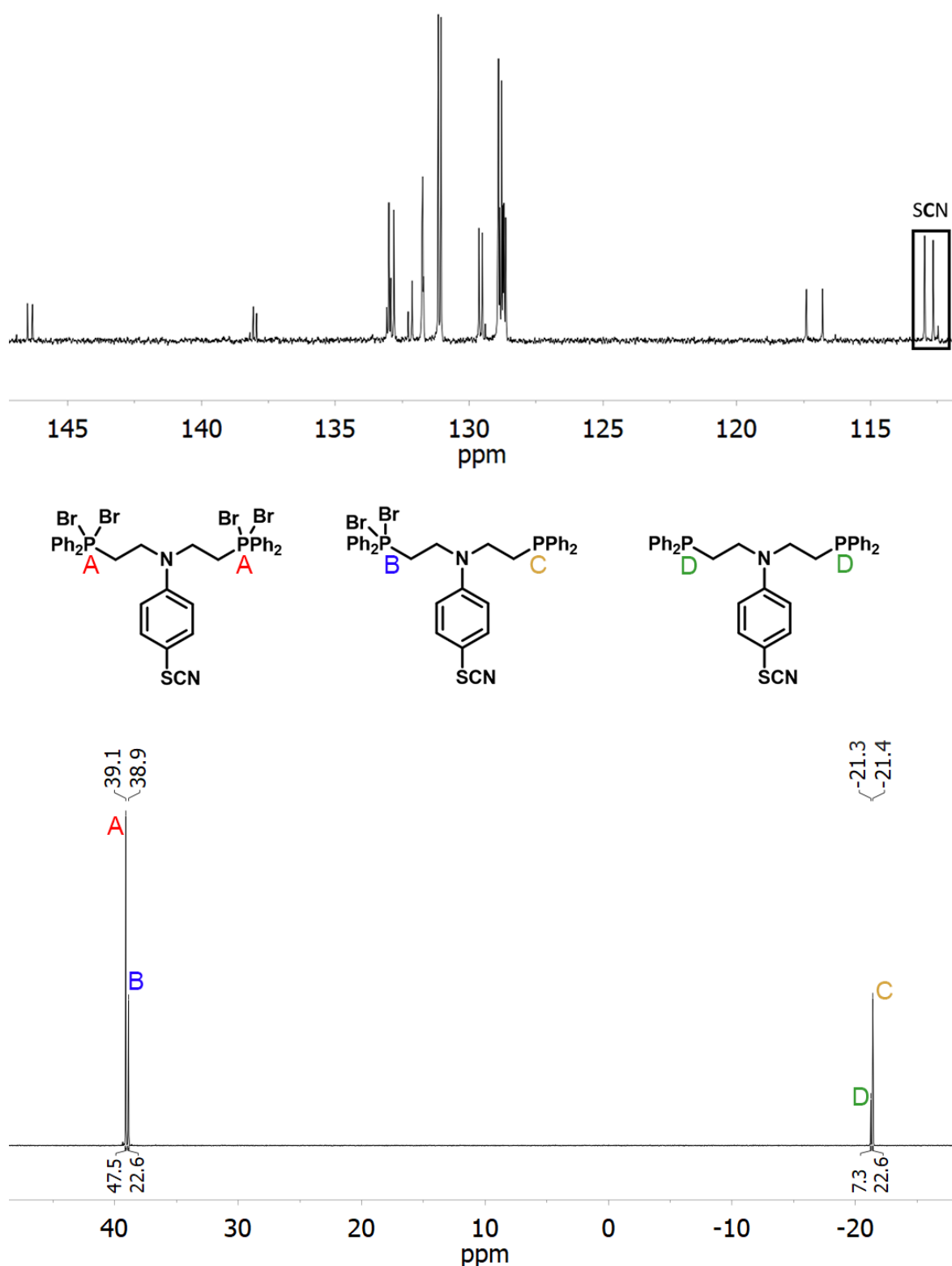
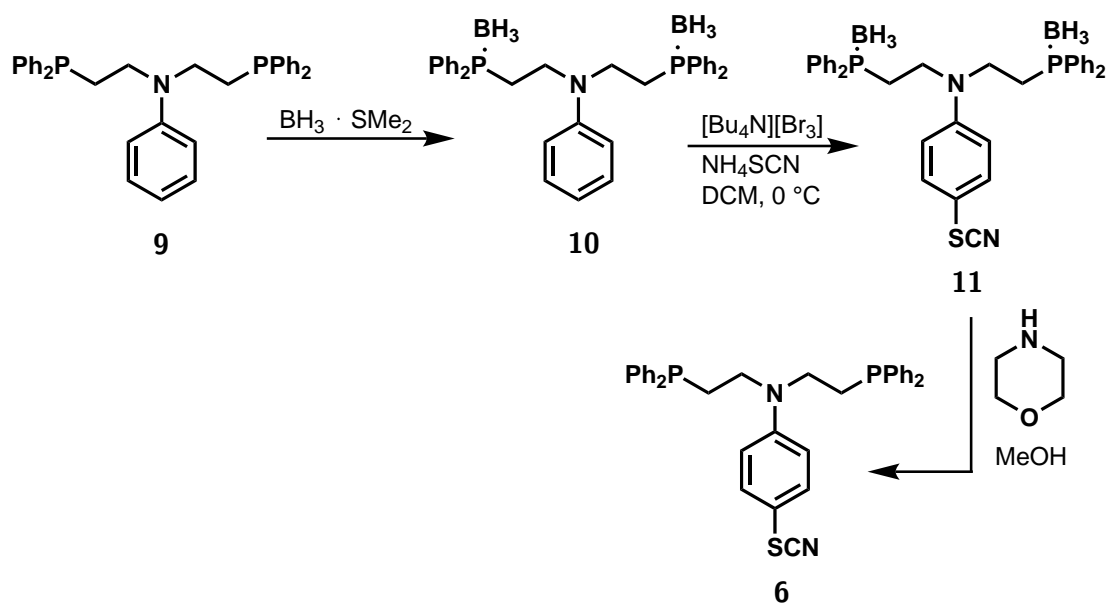


Fig. 5.9: Top: Aromatic region of the $^{13}\text{C}\{^1\text{H}\}$ NMR spectrum of the inverse attempt shows the successful introduction of the SCN group in the 4-position of the aniline group in every variant of the ligand. Middle: structures of the three ligands obtained in the reaction. Bottom: $^{31}\text{P}\{^1\text{H}\}$ NMR spectrum of the inverse attempt revealed the formation of three main products. The integrals show the percentage quantities of the products.

Although the phosphines were oxidized, from the ^{13}C NMR spectrum it became evident that the introduction of the SCN group was successful as the carbon atom in the thiocyanate group can be found for all three species. In the spectra two main sets of signals are observed, accompanied by a small signal. The small signal can be assigned to the desired product while the other two can be assigned to the halogenated ligands. As a result of these spectra, it can be concluded that the desired product should be obtained if the phosphines are reduced back to oxidation state +III under elimination of the halogens. Halogenated phosphines are often used as starting compounds for the synthesis of alkylphosphines, which are used as donors in the ligands. The halogen atoms are substituted by hydrogen atoms via reduction with lithium aluminum hydride.^[278,279] Even though the reduction to thiol was planned only in the last step after coordination to the molybdenum, a reduction of the product should lead to the formation of the desired ligand modified with SH instead of SCN and eliminate the by-products formed by the reaction with the bromine. Reaction with LiAlH_4 and acidic treatment resulted in a yellow solid which was insoluble in all NMR solvents available and could therefore not be investigated regarding the structure. As the ligand is expected to be soluble in organic solvents this approach was assumed to be unsuccessful and the route was modified again. As the main problem seems to be originating from the reaction of the bromine and the phosphines, the reaction has to be suppressed.

Two different approaches were chosen: the first was based on the fact that the intended molybdenum tricarbonyl complex is a known protective group that has been used for functionalization of phosphine ligands.^[280] Utilization of the molybdenum tricarbonyl fragment as protective group starts from the $[\text{Mo}(\text{CO})_3(\text{PN}^{\text{Ph}}\text{P}^{\text{Ph}})]$ complex, which was a key molecule in the second project of this thesis. The complex was synthesized as described in the publication in project 2 (Froitzheim 2023; Eur. J. Inorg. Chem.) and dissolved in dichloromethane with NH_4SCN . To this solution $[\text{NBu}_4][\text{Br}_3]$ was added dropwise. The isolated red solid was analyzed by NMR spectroscopy. Although the ^{31}P NMR spectrum showed that the desired complex was formed, a multitude of byproducts were found. Besides the probably unreacted complex and the desired product, the two species that may be assigned to known complexes are the meridional isomer as well as the tetracarbonyl complex, which is usually a decomposition product of the tricarbonyl complex. In addition multiple broad signals can be found indicating paramagnetic species. These species may be the result of redox reactions or CO exchange by bromine. Based on these findings, it can be stated that the molybdenum tricarbonyl fragment is not a suitable protecting group for the introduction of SCN functionalization, leading to the second method.

A known way to protect phosphines against oxidation e.g. with oxygen, is the use of boranes as protective groups. Boranes were routinely used in the Tuzek group.^[219,221,223,228] This new amendment leads to the last attempt of synthetically accessing the thiocyanate-functionalized $\text{PN}^{\text{Ph}}\text{P}^{\text{Ph}}$ ligand (**6**, Scheme 5).



Scheme 5: Modified synthetic pathway for the synthesis of the thio-functionalized PNP ligand **6**.

Starting again from the $\text{PN}^{\text{Ph}}\text{P}^{\text{Ph}}$ ligand (**9**), the first step is the introduction of borane as protective group as described by BÖRNER *et al.*^[281] The introduction is performed by addition of borane dimethylsulfide in dichloromethane. The borane attaches to the phosphines, rendering them inert towards oxidation. The phosphine-borane complex creates a broad split signal in the ^{31}P NMR spectrum due to the coupling of the quadruple nuclei of the borane (^{10}B & ^{11}B) to the phosphine (Figure 5.11, middle).^[282] The use as well as the introduction of borane as protective group for phosphines is a well established method^[219,221] and was carried out successfully in nearly quantitative yields. The protected ligand **10** was then further converted under the already tested conditions for the introduction of the thiocyanate group. Not only the selective introduction of the SCN group was successful, but also no oxidation of the phosphines was observed as can be seen from the NMR spectra (Figure 5.10 & 5.11).

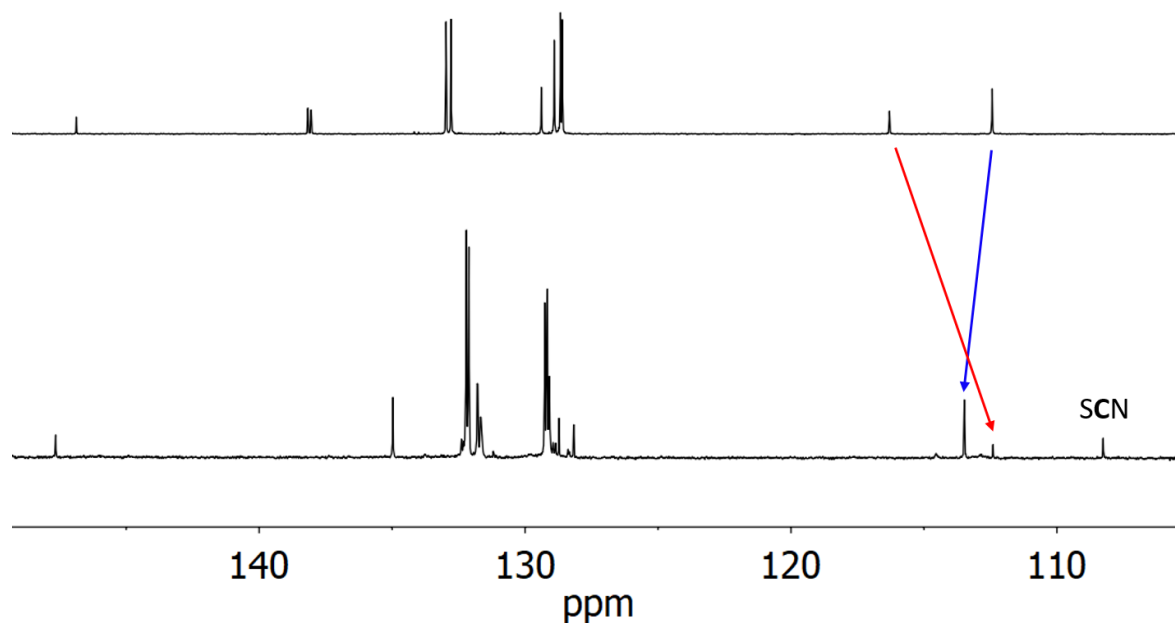


Fig. 5.10: Comparison of the aromatic region of the $^{13}\text{C}\{^1\text{H}\}$ NMR spectra of the $\text{PN}^{\text{Ph}}\text{P}^{\text{Ph}}$ ligand (top) and the borane protected $\text{PN}^{\text{Ph}}\text{P}^{\text{Ph}}$ after the introduction of the thiocyanate group (bottom). The introduction of the SCN group leads to a shift of the two meta carbons (blue arrow) and the *para*-carbon (red arrow) of the aniline ring.

The ^{13}C NMR spectrum shows the successful introduction of the SCN group into the $\text{PN}^{\text{Ph}}\text{P}^{\text{Ph}}$ giving the ligand precursor **11**. Furthermore, the ^{31}P NMR spectrum shows that the halogenation of the phosphines is only observed as minor side reaction and the borane protection has withstood the reaction conditions, especially the release of Br_2 (Figure 5.11, bottom).

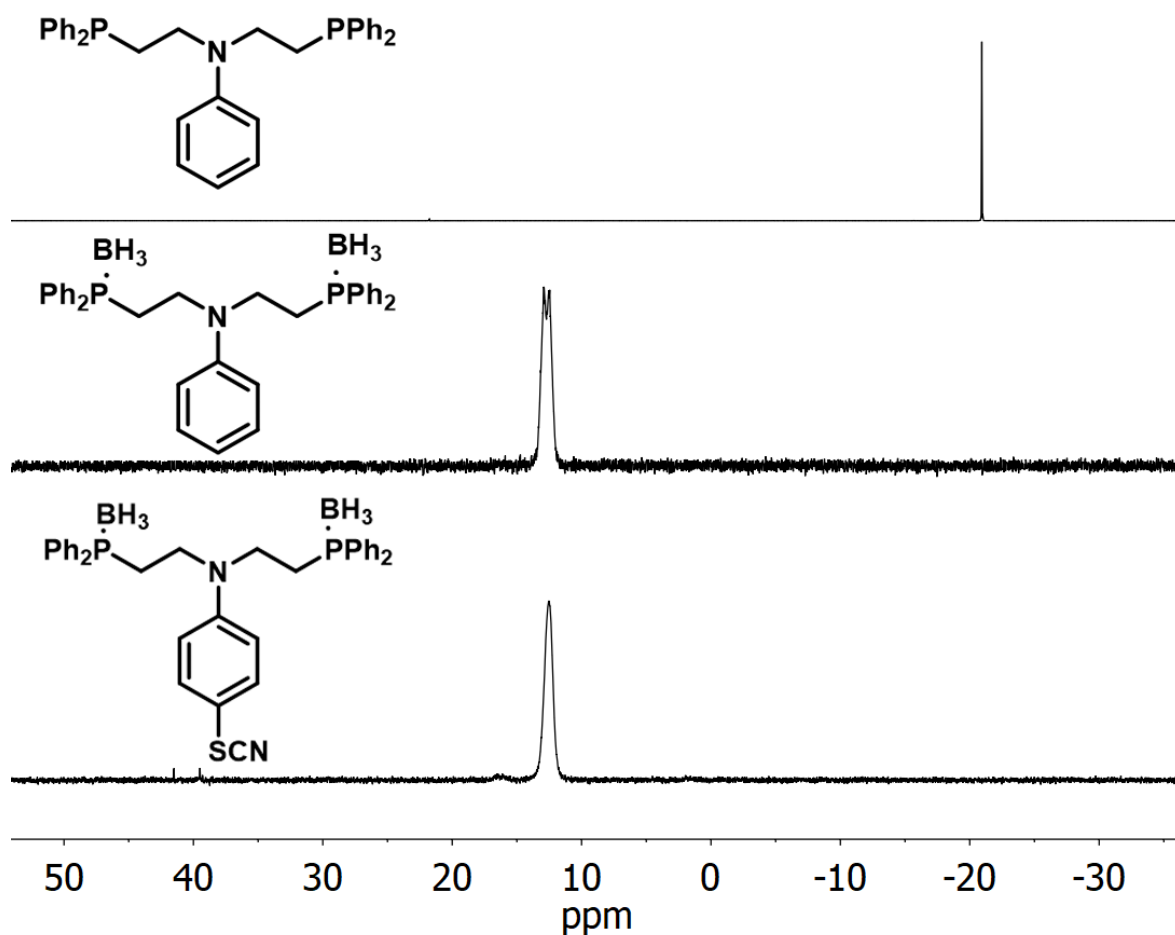


Fig. 5.11: Comparison of the $^{31}\text{P}\{^1\text{H}\}$ NMR spectra of the $\text{PN}^{\text{Ph}}\text{P}^{\text{Ph}}$ ligand (**9**, top), the borane protected $\text{PN}^{\text{Ph}}\text{P}^{\text{Ph}}$ ligand (**10**, middle) and the borane protected $\text{PN}^{\text{Ph}}\text{P}^{\text{Ph}}$ after the introduction of the thiocyanate group (**11**, bottom). The borane groups successfully withstood the reaction conditions during the introduction of the SCN group.

Besides the main product one small, broad signal is visible as well as two small, low field shifted signals. The final step in the ligand synthesis is the removal of the borane groups. The common way to remove them is by use of morpholine and temperature. The ligand precursor **11** was refluxed in morpholine and subsequently stirred at 90 °C for 3 d. The conditions applied unfortunately lead to the formation of a mixture of products as can be seen from the ^{31}P NMR spectrum (Figure 5.12). The products formed can be assigned to different species. The desired product **6**, a small fraction of the ligand with one brominated phosphine group and one non-halogenated phosphine. Furthermore, four additional signals appeared between 30.6 and 30.3 ppm. These signals may be associated with phosphine oxide variants formed during the attempted removal of the protective group. The signals found could be assigned to different combinations of fully oxidized phosphines, with only one phosphine oxide and a minor combination of an oxidized and a halogenated phosphine. This

assumption is based on the ^{31}P NMR shifts reported for different molecules based around functionalized ethyldiphenylphosphine oxides.^[283] The formation of the oxides indicates that, although Schlenk conditions were applied, the phosphines must have been exposed to oxygen. This is probably due to insufficient degassing of the morpholine prior to use.

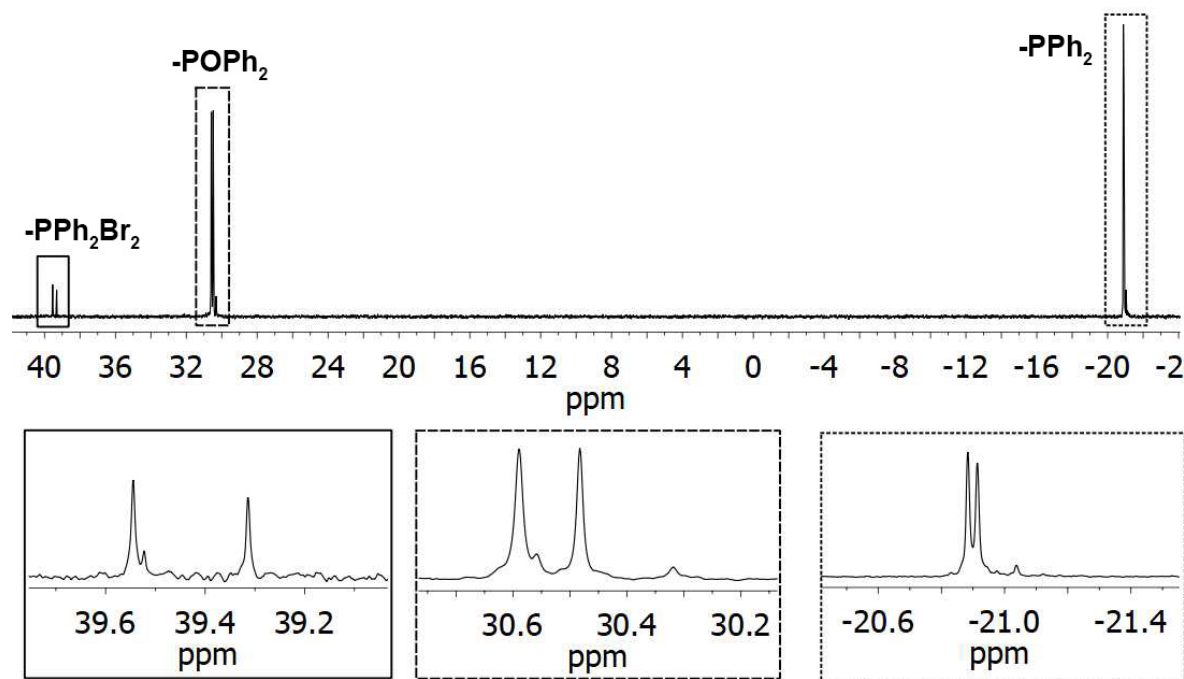
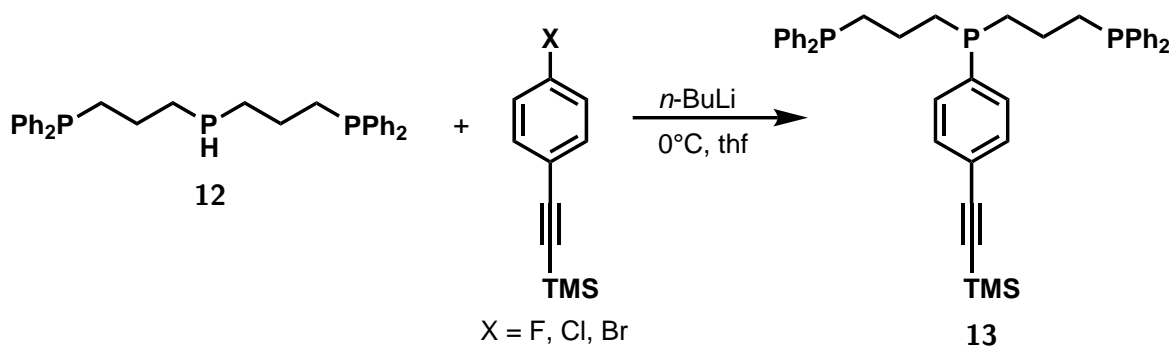


Fig. 5.12: $^{31}\text{P}\{^1\text{H}\}$ NMR spectrum of the attempted removal of the borane groups on SCN modified $\text{PN}^{\text{Ph}}\text{P}^{\text{Ph}}$ ligand (**11**). Besides the formation of the product and the halogenated phosphines from the prior step mainly phosphine oxides were formed.

Although the ligand variant with phosphine oxides would not coordinate, no coordination attempt was performed, as only a very small part of the product obtained can be assigned to the desired $\text{PN}^{\text{Ph}}\text{-SCN-P}^{\text{Ph}}$ ligand (**6**). Nonetheless, this route is very promising and should be repeated with some variations of the reaction conditions and thoroughly degassed morpholine. Besides the use of morpholine as removal agent for the protective groups, a different amine like triethylamine could be tried.

5.3 Functionalization of the prPPHP-ligand

Besides the efforts surrounding the surface modifications of the PNP ligand, attempts were made to modify a well known building block from the pentaPod synthesis - the prPPHP. The ligand was supposed to represent the tridentate PPP counterpart to the already successful deposited tripodal P₃ system by PETERSEN *et al.*^[262] The underlying synthetic route is based on a modular system (Scheme 6). The synthesis of the prPPHP ligand^[145,231] is well established in our group and halogen-containing building blocks that not only have the appropriate anchor group, but also the desired spacer are commercially available. In line with the projects already presented, the tridentate PPP system was also to be equipped with an acetylene unit to bind to a platform or an alkyl-SAM for surface fixation.



Scheme 6: Reaction scheme for the modular assembly of the surface-modified prPPHP ligand (**13**) based on the prPPHP ligand (**12**) and the ((4-halogenophenyl)ethynyl)trimethylsilane.

The idea behind this route was to apply known substitution of halogens by phosphines. Following the well established route the prPPHP ligand was synthesized. In a first attempt the prPPHP ligand was dissolved in thf and $n\text{-BuLi}$ was added. Parallel to that, the ((4-chlorophenyl)ethynyl)trimethylsilane was dissolved in thf and subsequently added dropwise to the prPPHP solution. The result of this reaction was a mixture of multiple species. As the terminal phenyl phosphines are quite resistant to air an attempt was made to purify the desired product using column chromatography. From the ^{31}P NMR spectrum of the isolated product it can be seen that the two building blocks were connected successfully (Figure 5.13, bottom).

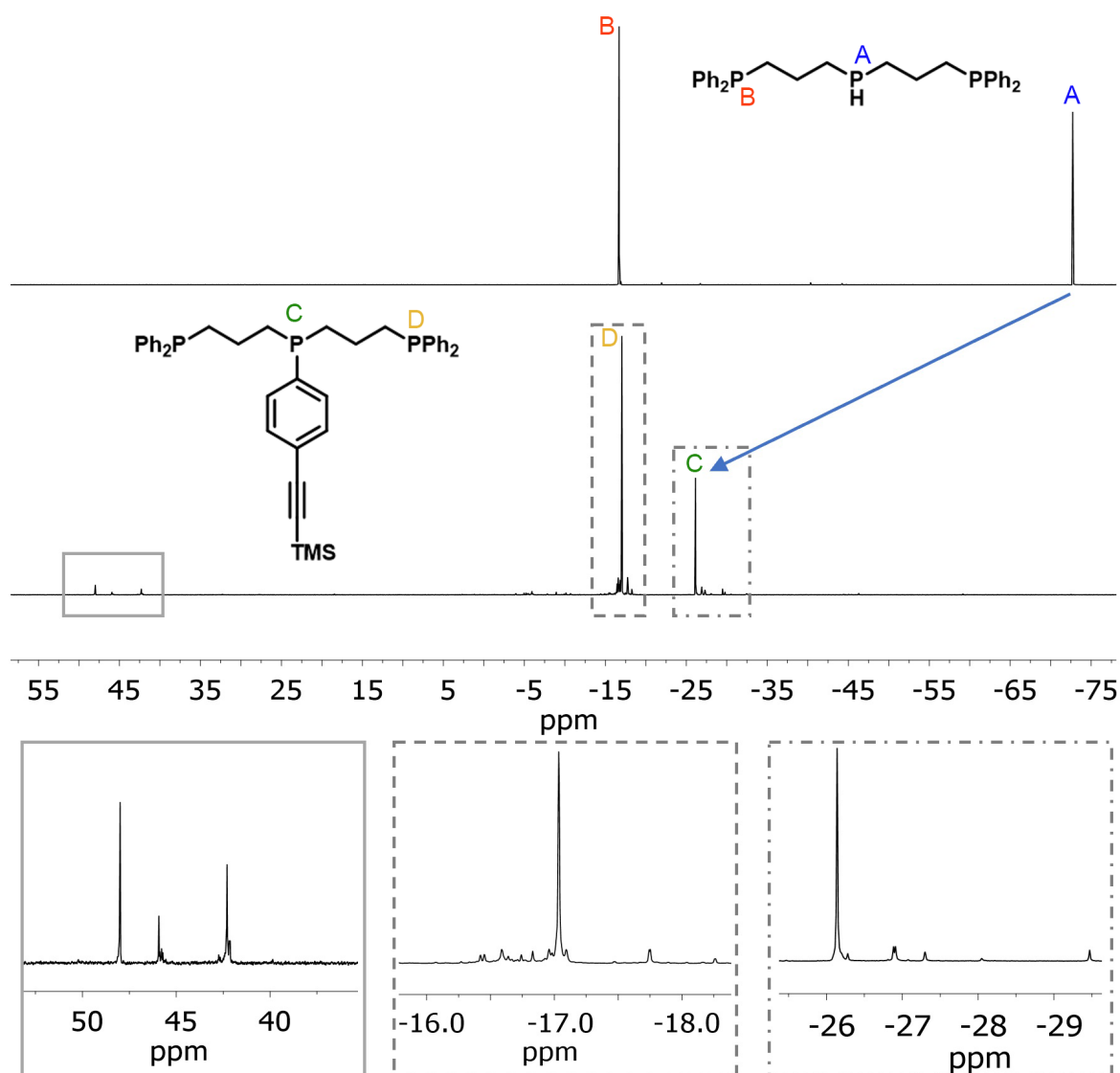


Fig. 5.13: Comparison of the $^{31}\text{P}\{^1\text{H}\}$ NMR spectrum of the prPPHP ligand (top) and the modified ligand **13** (bottom). The enlarged regions show several byproducts and oxidized species. The large signal at -17.0 ppm can be assigned to the PPh_2 groups and the signal at -26.1 ppm to the central phosphine after the substitution of the proton by the aromatic residue.

As can be seen from the top spectrum, the central PH of the prPPHP ligand can be found at -72.7 ppm. After the reaction the signal of the central phosphorus shifted to -26.1 ppm due the substitution of the hydrogen by the aromatic residue. Nonetheless, multiple by-products were still found in the product mixture. Since a second attempt at column chromatographic purification was deemed unlikely to be successful, due to repeated exposure to oxygen, a coordination attempt was started despite the lack of purity in the hope that this would yield a pure product. The impure ligand was added to the $[\text{Mo}(\text{CO})_3(\text{cht})]$ precursor complex. As it was already observed for the tricarbonyl complexes with PNP ligands, the coordination was

indicated by a color change from deep red to yellow/beige. Although the yield was poor, a solid was isolated. For analysis via NMR spectroscopy, the solid was dissolved in DCM, which led to the formation of an insoluble black solid and thus to the presumed decomposition of the product. Furthermore, an IR spectrum of the isolated product was measured. Although the color of the solid looked promising, the spectrum showed that the desired tricarbonyl complex was not obtained, because no vibrations were found in the CO stretching frequency region. By modifying the synthesis parameters and substituting the chlorine-based building block with a brominated and fluorinated analogue, the objective was to synthesize the pure ligand. The synthesis was carried out under the same reaction conditions as in the previous experiment. Unfortunately, the desired ligand was not obtained. In subsequent attempts the temperatures were varied and the *n*-BuLi was substituted by lithium diisopropylamide which also did not provide the desired results. In parallel with efforts to synthesize the prPP^{Ph-acetylene-TMS}P ligand (**13**), the successful synthesis of the ethyl-bridged analog was demonstrated by our group.^[284] It was found that in order to obtain a pure product, a halogen atom is required as substituent on the central phosphine. Nonetheless, it was also demonstrated that the linking of the prPPHP ligand and the ((4-chlorophenyl)ethynyl)trimethylsilane is possible in principle.

Conclusion & Outlook

This thesis is split into three main projects. The first focuses around the different behavior of the $[\text{W}(\text{N}_2)(\text{P}_2^{\text{Me}}\text{PP}_2^{\text{Ph}})]$ complex compared to its molybdenum analogue. The investigations were based around the assumption that the complexes have different redox potentials, why the main focus evolved around electrochemistry. The second study provides an in-depth investigation regarding the coordination behavior of different tridentate PNP ligands. All PNP ligands were coordinated to molybdenum tricarbonyl complexes, due to their excellent spectroscopic properties. Gaining a better understanding of these systems is beneficial for the final project of this thesis, which deals with the synthesis and characterization of molybdenum tricarbonyl complexes bearing tridentate PNP ligands with functionalization for surface deposition. This project aims to continue the work of STUCKE, SCHLIMM and PETERSEN *et al.*, which already demonstrated the deposition of molybdenum tricarbonyl complexes with pincer and tripodal ligands on surfaces.^[261,262]

6.1 Project 1

The first project was focused on synthetic nitrogen fixation with the pentaPod ligand and a continuation of a prior study by ENGESSER *et al.*, which demonstrated the catalytic activity of the molybdenum dinitrogen complex bearing the pentaPod and its superiority compared to the regular dinitrogen complexes with pentaphosphine coordination spheres provided by tri- and bidentate phosphine ligands. As the molybdenum complex was catalytically active, the next step in testing the capability of the ligand was the coordination to alternative metal center. As tungsten is usually the metal of choice when exchanging molybdenum, the pentaPod was coordinated on tungsten and investigated regarding its activity towards derivatization and ammonia formation. This project was executed in collaboration with JUNGE and the pentaPod ligand was successfully coordinated and the tungsten mono-dinitrogen complex isolated. The resulting $[\text{WN}_2(\text{pentaPod})]$ complex was characterized using IR, Raman and NMR spectroscopy. Besides an expected shift to lower wavenumbers of the N_2 -stretch and additional satellites in the ^{31}P -NMR spectrum, the spectra as well as the crystal structure were surprisingly similar to the molybdenum analogue. Investigations regarding the catalytic activity towards ammonia formation of the $[\text{W}(\text{N}_2)(\text{P}_2^{\text{Me}}\text{PP}_2^{\text{Ph}})]$ complex in the presence of samarium diiodide / water resulted in 2.75 equiv. Although the activity was found to be well below the results of the molybdenum complex, this is the first example of a tungsten

dinitrogen complex capable of generating more than two equivalents of ammonia. In order to investigate the differences of the complexes, electrochemical and spectroelectrochemical studies were performed. The molybdenum as well as the tungsten complex were investigated by cyclic voltammetry. The cvs found for the complexes were very similar. $E_{1/2}$ of the first redox systems were determined at -1.16 V for the tungsten and at -1.13 V for the molybdenum complex, respectively. Nonetheless the reversibility of the $0 \rightleftharpoons +I$ system differs, as the tungsten complex was found to be fully reversible unlike the molybdenum complex, which was only partly reversible. For the second oxidation systems very similar $E_{1/2}$ values were found as well, yet the reversibility differed. Both systems were irreversible at low scan rates, but an increase in reversibility was observed for the tungsten complex as the scan rate was increased. Further analysis of the peak current function using Randles-Sevcik equation revealed an ECE type mechanism for the tungsten complex. Deeper investigations into the species formed upon oxidation were carried out by means of IR-spectroelectrochemical investigations. It was found that the $[W(N_2)(P_2^{Me}PP_2^{Ph})]^+$ complex was more stable than the molybdenum analogue, which released the dinitrogen ligand upon oxidation. Due to the higher stability of the oxidized complex the tungsten- N_2 complex was observed.

Following this project JUNGE *et al.* presented an extensive theoretical study regarding possible mechanisms of the NH_3 formation and the competing hydrogen evolution reaction.^[230] From previous attempts within the framework of this thesis, it was found that no significant amounts of ammonia were generated electrocatalytically upon addition of acids (cf. section 3.2). Further experimental investigations regarding this topic could be based on the success in electrocatalytic ammonia formation presented by the PETERS group.^[173] They demonstrated that the catalytic activity of a tungsten complex can be achieved by adding a mediator that acts as a PCET agent.

6.2 Project 2

The second and main project of this thesis was the investigation of the coordination behavior of tridentate PNP ligands on molybdenum tricarbonyl systems. The scope was to investigate the influence of phosphines and their substitutes on coordination behavior and stability. For this, a tridentate ligand with central aniline donor was chosen in reference to the well studied pincer ligands. A series of tridentate $PN^{Ph}P^R$ ligands ($R = Ph, Me, Et, Pln, Cyp, ^iPr, Cy, ^tBu$) was synthesized and coordinated to the $[Mo(CO)_3(cht)]$ precursor. All ligands were successfully synthesized but not all complexes could be obtained. Complexes bearing the $PN^{Ph}P^{Me}$, $PN^{Ph}P^{Pln}$ and $PN^{Ph}P^{tBu}$ could not be isolated. All other complexes were isolated and thoroughly characterized. From IR- and Raman spectra it became apparent that all complexes adapted a facial geometry in the solid state. This was expected as the precursor

predefined a facial coordination geometry. The facial geometry was also found in solution for all complexes, which was determined from the shift of the signals in the ^{31}P NMR spectra as well as the ABX pattern found for the equatorial CO ligands in the ^{13}C NMR spectra. Nonetheless, the meridional isomer was found as minor byproduct (<1%).

Comparison to similar systems (NH instead of NPh) in the literature revealed that the geometry of the complexes shifted from a facial to a meridional geometry with increasing steric demand of the phosphines substituents. DFT studies were performed in order to gain insights into the isomerization mechanism and the discrepancies between the two systems. Isodesmic calculations of the relative ligand exchange energies revealed a contradiction to the experimental results for the systems containing NPh as the meridional isomer is energetically favored for bulky phosphines. For the systems with NH, the calculations agree well with the experimental observations. What became clear, however, is that the molybdenum tricarbonyl complex bearing the $\text{PN}^{\text{Ph}}\text{P}^{\text{tBu}}$ ligand was energetically unfavorable in the facial and meridional geometry. Nonetheless, in the calculations no salient difference crystallized between the NPh and NH systems that would explain the different behavior, excluding thermodynamics as the cause for the observed geometries. Further calculations regarding the kinetics were performed in order to investigate the isomerization mechanism. Two possible pathways were found. The first is a direct isomerization in which one isomer transforms into the other over a transition state. The transition state during direct isomerization proved to be energetically unfavorable and also showed no significant differences. The second pathway involves the dissociation of a CO ligand prior to the isomeric transformation. This pathway indeed revealed differences between the two systems. For the transformation of the NH system the transition state between the facial and meridional state (starting from the dicarbonyl variant) was found to be energetically lower compared to the NPh complex. Furthermore, a second, low lying transition state between two conformers of the meridional isomer was found for the NH system. Of these two only one belongs to the conversion of the facial and the meridional isomers into each other. The higher energies of the NPh system can be explained by the formation of an agostic hydrogen bond between the phenylring and the molybdenum, stabilizing the pentacoordinated species, which needs to be broken during the isomerization, therefore leading to an higher energy barrier, hence inhibiting the isomeric transformation.

The experimental results of the complexes bearing $\text{PN}^{\text{Ph}}\text{P}$ ligands were obtained due to the fac-preorientation caused by the cycloheptatriene precursor. Subsequent investigations include the substitution of this precursor by a complex with prior meridional ligand arrangement or no predetermined orientation like the utilization of molybdenum hexacarbonyl as demonstrated by BELLER *et al.*^[285,286] Although high temperatures are required for this synthesis, $\text{Mo}(\text{CO})_6$ does not dictate a preferred coordination geometry, which could allow for the formation of the meridional isomers for ligands with bulky phosphines. Another possibility would be to coordinate the ligands to a molybdenum dicarbonyl complex, generating the

pentacoordinated species used during the calculations and expose them to a CO atmosphere, occupying the last coordination site of the complex. The synthesis of the pentacoordinated molybdenum complex was attempted by BELLER *et al.* as well with a promising indications towards successful synthesis.^[286]

6.3 Project 3

The final project of this thesis can be described as the next step to the second project. Aim of this part was the synthesis and characterization of molybdenum tricarbonyl complexes bearing tridentate PEP ligands (E = N, P). Our group already demonstrated the successful surface deposition of tricarbonyl complexes with a pincer and a tripodal pincer.^[261,262] The last complex within the series supported by ligands with three donors are the tridentate ligands. Attaching and studying the behavior of the complexes on the surface as well as the influence of the substrate on the complex is the first step towards heterogeneous catalysis. The first concept investigated for this purpose was closely related to the already successfully demonstrated pincer and tripod systems. These were attached to a TATA-platform and deposited onto a gold surface. In order to connect the ligand to a TATA-platform an acetylene group is required. Starting from *N,N*-bis(2-chloroethyl)aniline (**1**), which was the starting point for all PNP ligands (cf. Project 2), this function was introduced in a two step synthesis. Subsequent phosphination with diphenyl phosphine was successful. PPh₂ was chosen as donor because of its relatively high oxygen resistance compared to all other alkyl phosphines. Unfortunately, the coordination to the molybdenum tricarbonyl precursor was not successful. The precursor ([Mo(CO)₃(η^6 -toluene)]) was chosen because the [Mo(CO)₃(cht)] precursor was not available at the time and the relative stability of the toluene complex is supposedly lower than the cht complex.^[271] Although multiple attempts were made, the desired complex could not be isolated. A successful coordination should be possible when using the well established [Mo(CO)₃(cht)] precursor. This route was not repeated as the focus shifted from acetylene functionalized ligands to sulfur/thiofunctionalized PNP ligands.

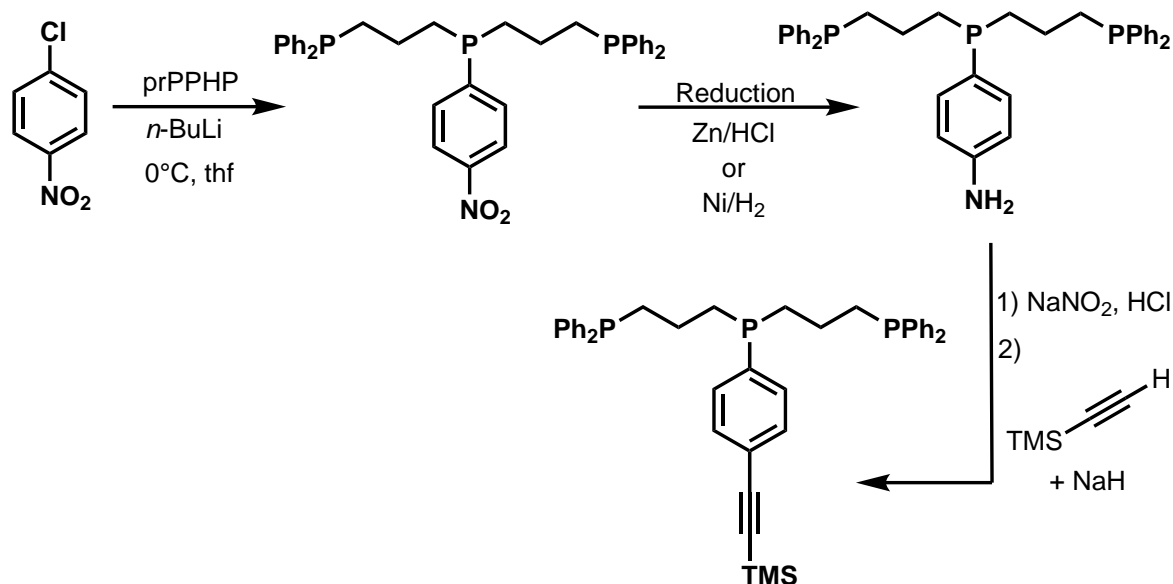
The TATA approach relies on physisorption of the platform to the surface. Using thiol groups, which are a part of the ligand system, a stronger covalent Au-S bond can be expressed, drastically improving the stability of the adsorbed molecules. The introduction of a thio function into the PNP ligand was demonstrated by selective substitution of the *para*-hydrogen of the aniline ring by a thiocyanate. This step was achieved in two ways: in a two step synthesis and a onepot synthesis both starting from the *N,N*-bis(2-chloroethyl)aniline (**1**). The resulting *N,N*-bis(2-chloroethyl)-*p*-thiocyanate-aniline (**5**) is an ideal dummy molecule to explore different and the best suited condition for the surface deposition as it is easy and quickly synthesized, air stable and obtainable in high yields. Attempts were made to directly

bind the compound **5** to the surface without prior reduction to a thiol. Due to the aurophilic character of the sulfur, the SCN group is split under the formation of a Au-S bond. The resulting CN⁻ ion is deposited as a byproduct on the surface. In a first attempt the formation of a Au-S bond was found in the monolayer as well as in the bulk. Unfortunately multiple byproducts were found but with further improvements to the method it should be possible to eliminate those.

The first issue during the ligand synthesis arose with the introduction of the phosphine donors, because the thiocyanate acts as a pseudo halogenide and apparently coupling parts of the phosphine to the aniline ring. In order to bypass this problem, the route was inverted. After synthesis of the PN^{Ph}P^{Ph} ligand, the SCN group was introduced. This reaction can be executed selectively, due to insufficient activation of the phenylring by the phosphorus compared to the amine. During the introduction of the SCN group, elemental bromine is released. This reacted with the phosphines leading to a halogenation. Nonetheless, the SCN was introduced successfully. Attempts to remove the bromine from the phosphorus via. reduction with LiAlH₄ and reducing the SCN function to the desired SH group in the same step proved to be unsuccessful, as no product was isolated. Based on these results, the synthesis route was modified again. In the final attempt, borane was introduced as protective group for the phosphine donors prior to the SCN introduction. The borane groups successfully inhibited the formation of phosphorus halogenides and allowed for the introduction of the thiocyanate group. The final step in the ligand synthesis was the removal of the protective group. Unfortunately, this lead to the formation of oxidized species probably due to insufficient degassing of the morpholine used for this reaction. The morpholine was degassed for 24 h which proved to be insufficient and should be extended or done using the freeze-pump-thaw method. Nonetheless, this route is very promising and should be repeated in the future. The removal of the protective borane group can also be accomplished by diethylamine, which itself is sensitive to air and can be acquired as oxygen free substance.

Alternative approaches for the introduction of a sulfur based anchor group would be the utilization of thiocarbamates or thioacetates. In addition to PNP systems, an attempt was made to develop a tridentate PPP system for surface fixation based on a modular system with known components. The experiments were based on the tridentate prPPHP ligand, which is a known intermediate during the pentaPod synthesis. This first building block should then be reacted with the commercially available ((4-chlorophenyl)ethynyl)trimethylsilane. The reaction in thf with *n*-BuLi resulted in a mixture of several products, but also in the formation of the desired product. Although most of the by-products were removed by column chromatography, the purity was insufficient, and a subsequent coordination experiment did not yield the desired complex. Multiple attempts to modify the reaction conditions and reagents did not yield the intended suppression of byproduct formation. In addition, substitution of the chlorine based building block by the bromine or fluorine variant was tested, but no formation of the desired product was observed. Due to this reason and the findings of MICHAELIS^[284]

the concept of a modular PPP ligand for surface functionalization was discontinued. In order to obtain ligand **13** a new route has to be developed either with regards to the findings of MICHAELIS or an entirely new route like the one presented in scheme 7.



Scheme 7: Alternative reaction pathway intended for the surface modification of the prPPHP ligand.

As an alternative for the route demonstrated by MICHAELIS, the prPPHP could be connected to a 1-chloro-4-nitro-benzene using *n*-BuLi. The release of the chloride should be favored in comparison to the ((4-chlorophenyl)ethynyl)trimethylsilane due to the mesomeric effect of the nitro group. Reduction of the nitro group to an amine allows subsequent conversion of the amine to a leaving group by diazotization, which can be substituted by deprotonated trimethylsilylacetylene. Due to the elimination of dinitrogen, it should be possible to obtain the ligand without side products and therefore without subsequent column chromatographic purification.

Experimental Section

7.1 Materials and Methods

All chemicals used were of commercially available grade and used as purchased with the exception of some solvents. The solvents were dried with appropriate drying agents. Hydrolysis and oxygen-sensitive reactions were carried out under Schlenk conditions (N₂- or Ar-atmosphere).

NMR spectroscopy

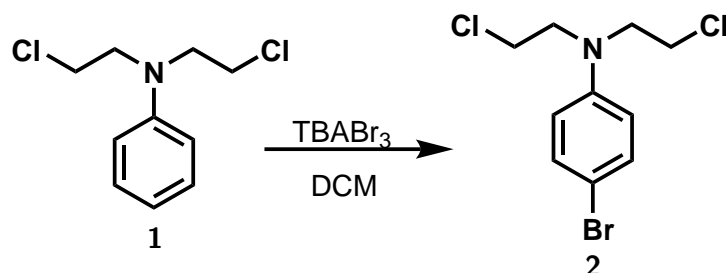
Nuclear magnetic resonance spectra were recorded using a Bruker AVANCE III HD 400 Pulse Fourier Transform spectrometer. Nuclei were measured at different frequencies against a reference (Table 7.1). Compounds susceptible to oxygen or hydrolysis were performed under Schlenk conditions. Spectra measured at higher frequencies were recorded using a Bruker Avance DRX 500 spectrometer.

Tab. 7.1: Frequencies and references of the measured nuclei.

Nucleus	Frequency / MHz	Reference
¹ H	400.13	TMS
¹ H	500.13	TMS
¹³ C	100.62	TMS
¹³ C	125.77	TMS
³¹ P	161.98	H ₃ PO ₄
¹¹ B	128.38	BF ₃

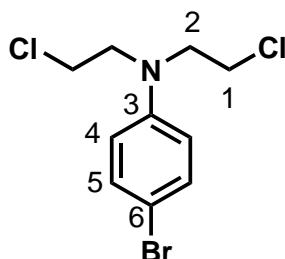
The deuterated solvents used were purchased from *Deutero* and *Sigma Aldrich*.

7.2 4-Bromo-*N,N*-bis(2-chloroethyl)aniline



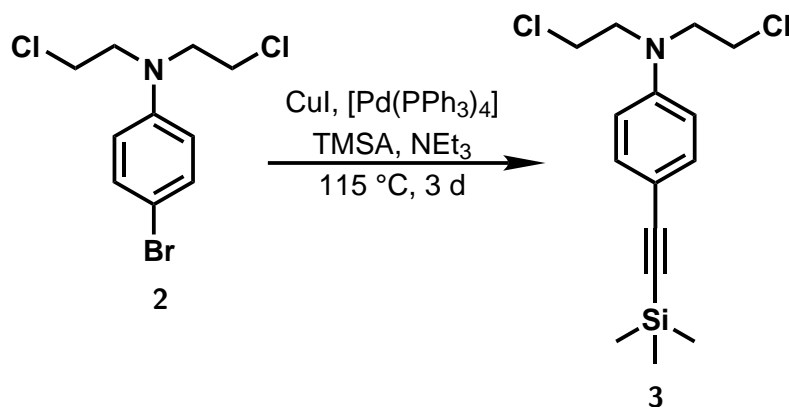
N,N-Bis(2-chloroethyl)aniline (**1**, 2.00 g, 9.17 mmol) were dissolved in dichloromethane (20 mL) and cooled to 0 °C. Over the course of 20 min, 4.44 g (9.21 mmol) of tetrabutylammonium tribromide were added and stirred for 30 min. The resulting reddish solution was subsequently extracted twice with 100 mL of sodium thiosulfate solution each time. The aqueous solution was in turn extracted with dichloro methane, the organic phases combined and dried over anhydrous sodium sulfate. After filtration the solvent was removed under vacuum. The resulting crude product was dissolved in methanol and put in the freezer (-32 °C) for 5 h. The precipitated rose crystalline solid was filtered of and dried under vacuum.

Yield: 1.64 g (5.52 mmol) 60 %



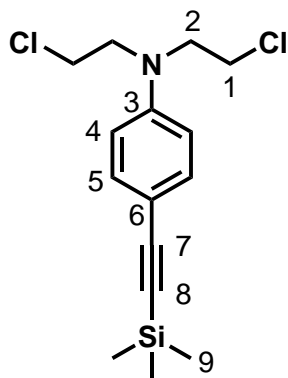
$^1\text{H-NMR}$ (500 MHz, CDCl_3 , 300 K): δ = 7.28-7.23 (m, 2 H, *H*-5), 6.52-6.47 (m, 2 H, *H*-4), 3.65-3.60 (m, 4 H, *H*-2), 3.57-3.52 (m, 4 H, *H*-1) ppm.

$^{13}\text{C-NMR}$ (125 MHz, CDCl_3 , 300 K): δ = 145 (s, 1 C, *C*-3), 132 (s, 2 C, *C*-4), 113 (s, 2 C, *C*-5), 110 (s, 1 C, *C*-6), 53.5 (s, 2 C, *C*-1), 40.2 (s, 2 C, *C*-2) ppm.

7.3 *N,N*-Bis(2-chloroethyl)-4-((trimethylsilyl)ethynyl)aniline

4-Bromo-*N,N*-bis(2-chloroethyl)aniline (**2**, 800 mg, 2.69 mmol), copper(I) iodide (108 mg, 0.57 mmol) and $[\text{Pd}(\text{PPh}_3)_4]$ (218 mg, 0.19 mmol) were dissolved in triethylamine (25 mL), and 0.7 mL (4.04 mmol) of TMS-acetylene was added. The black solution was heated at $100\text{ }^\circ\text{C}$ for 3 days under reflux. The solution was filtered over basic alumina and Celite[®] and washed with thf (20 mL). The solvent was removed in vacuo resulting a viscous dark orange oil. The crude product was purified via column chromatography using a mixture of *n*-hexane and ethyl acetate (4:1).

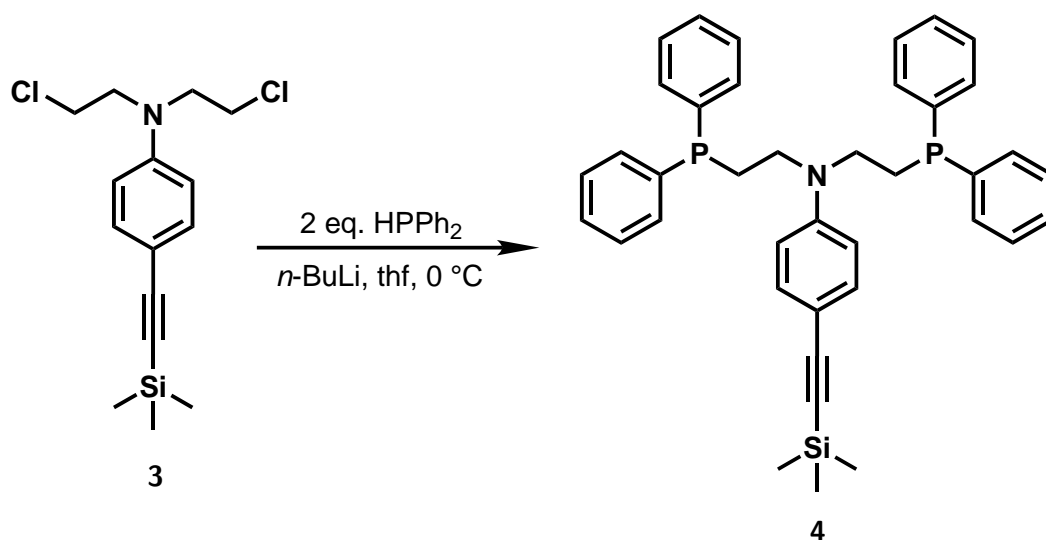
Yield: 506 mg (1.61 mmol) 60 %



¹H-NMR (500 MHz, CDCl₃, 300 K): δ = 7.29-7.27 (m, 2H, *H*-5), 6.52-6.49 (m, 2H, *H*-4), 3.68-3.62 (m, 4H, *H*-2), 3.57-3.52 (m, 4H, *H*-1), 0.16 (m, 9H, *H*-9) ppm.

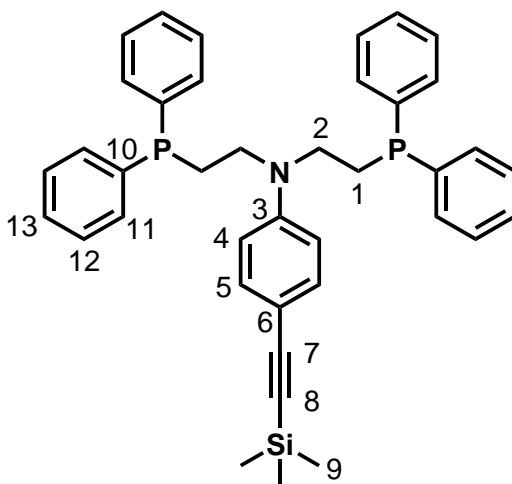
^{13}C -NMR (125 MHz, CDCl_3 , 300 K): δ = 146 (s, 1 C, C- β), 134 (s, 2 C, C- α), 114 (s, 2 C, C-5), 111 (s, 1 C, C-6), 106 (s, 1 C, C-10), 92.2 (s, 1 C, C-9), 53.4 (s, 2 C, C-1), 40.4 (s, 2 C, C-2), 0.30 (s, 3 C, C-11) ppm.

7.4 *N,N*-Bis(2-(diphenylphosphanyl)ethyl)-4-((trimethylsilyl)ethynyl)aniline



N,N-bis(2-chloroethyl)-4-((trimethylsilyl)ethynyl)aniline (**3**, 440 mg, 1.34 mmol) was dissolved in thf (10 mL). In a second vessel, diphenyl phosphine (521 mg, 2.80 mmol) was dissolved in thf (10 mL) as well and both solutions cooled to $0\text{ }^\circ\text{C}$. To the diphenyl phosphine solution, $n\text{-buli}$ (1.2 mL, 3.14 mmol) was added dropwise and stirred for 30 min. Afterwards, the solution with the ligand precursor **3** was added slowly to the phosphine solution and stirred for 4 d at room temperature. The solvent as well as excess $n\text{-buli}$ were removed in vacuo. The residue was dissolved in diethyl ether and filtered through basic aluminum oxid and Celite[®]. The product was obtained as viscous orange oil.

Yield: 360 mg (0.59 mmol) 44 %

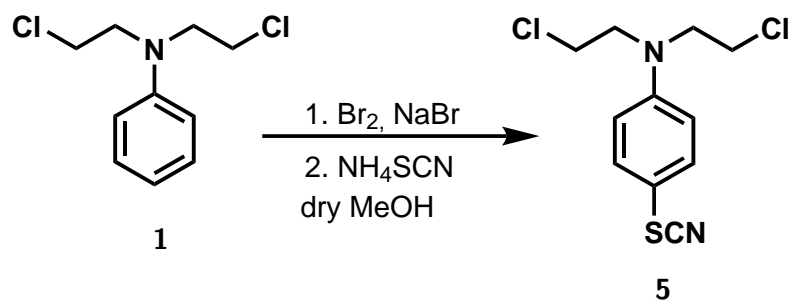


^1H -NMR (400 MHz, CDCl_3 , 300 K): δ = 7.31-7.26 (m, 8 H, *H*-11), 7.22-7.16 (m, 12 H, *H*-12/*H*-13), 7.09-7.05 (m, 2 H, *H*-5), 7.02-7.00 (m, 2 H, *H*-4), 3.25-3.17 (m, 4 H, *H*-2), 2.17-2.12 (m, 4 H, *H*-1), 0.12 (m, 9 H, *H*-9) ppm.

^{13}C -NMR (100 MHz, CDCl_3 , 300 K): δ = 147.7 (s, 1 C, *C*-3), 138.8 (d, J_{CP} = 12.3 Hz, 4 C, *C*-10), 133.3 (s, 2 C, *C*-4), 132.8 (d, J_{CP} = 18.9 Hz, 8 C, *C*-11), 128.9 (s, 4 C, *C*-13), 128.6 (d, J_{CP} = 6.76 Hz, 8 C, *C*-12), 111.5 (s, 2C, *C*-5), 109.8 (s, 1 C, *C*-6), 106.5 (s, 1 C, *C*-7), 91.3 (s, 1 C, *C*-8), 47.7 (d, J_{CP} = 25.6 Hz, 2 C, *C*-2), 26.2 (d, J_{CP} = 14.4 Hz, 2 C, *C*-1), 0.37 (s, 3 C, *C*-9) ppm.

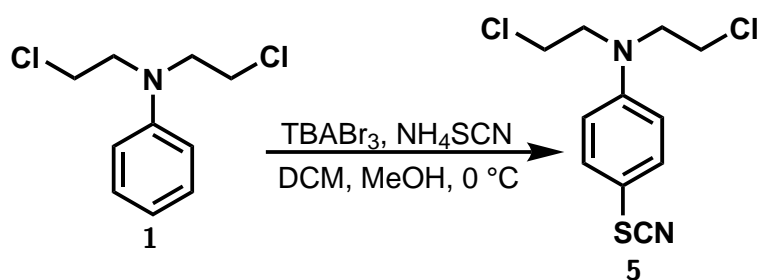
^{31}P -NMR (162 MHz, CDCl_3 , 300 K, H_3PO_4): -21.9 (s, 2P, *PPh*₂) ppm.

7.5 *N,N*-Bis(2-chloroethyl)-4-thiocyanatoaniline



N,N-Bis(2-chloroethyl)aniline (**1**, 2.00 g, 9.17 mmol) and ammonium thiocyanate (1.5 g, 19.7 mmol) were dissolved in methanol (30 mL). The solution was cooled to 0 °C and a second solution of bromine (0.5 mL) and sodium bromide (0.5 g) dissolved in methanol (5 mL), was added drop wise. The solution was stirred for 10 min at 0 °C, before poured into deionized water (100 mL). This step was supposed to precipitate the desired product, however, the crude product immediately dissolved again. Due to this, the solution was extracted with diethyl ether (3x 100 mL) and washed with sodium thiosulfate to remove excess bromine. The organic layer was dried over anhydrous magnesium sulfate and the solvent removed. The resulting dark oil was recrystallized from ethanol yielding the desired product as white solid.

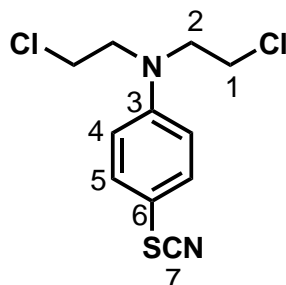
Yield: 1.39 (5.05 mmol) 55 %



A second method was used in order to synthesize the *N,N*-Bis(2-chloroethyl)-4-thiocyanatoaniline (**5**). For this, *N,N*-Bis(2-chloroethyl)aniline (**1**, 2.00 g, 9.17 mmol) and ammonium thiocyanate (1.5 g, 19.7 mmol) were dissolved in a mixture of methanol (30 ml) and dichloromethane (10 mL). The solution was cooled to 0 °C and a solution of TBABr₃ (4.42 g, 9.17 mmol) dissolved in DCM (10 mL) was added. The solution was stirred for 10 min at 0 °C and another 30 min at room temperature. The solution was washed with sodium thiosulfate solution and dried using magnesium sulfate. The solvent was removed and the crude product recrystallized

from methanol. The recrystallization was repeated twice in order to remove all ammonium salts.

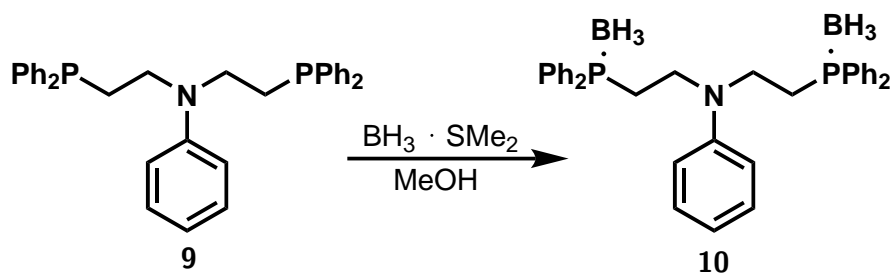
Yield: 1.44 g (5.23 mmol) 57 %



$^1\text{H-NMR}$ (400 MHz, CDCl_3 , 300 K): δ = 7.48-7.44 (m, 2 H, *H*-4), 6.72-6.68 (m, 2 H, *H*-5), 3.79-3.75 (m, 4 H, *H*-2), 3.66-3.62 (m, 4 H, *H*-1) ppm.

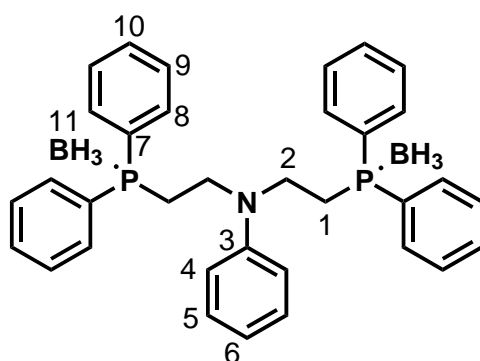
$^{13}\text{C-NMR}$ (125 MHz, CDCl_3 , 300 K): δ = 148 (s, 1 C, *C*-3), 135 (s, 2 C, *C*-4), 113 (s, 2 C, *C*-5), 112 (s, 1 C, *C*-6), 112 (s, 1 C, *C*-7), 53.4 (s, 2 C, *C*-2), 40.2 (s, 2 C, *C*-1) ppm.

7.6 *N,N*-Bis(2-(diphenylphosphino)ethyl)aniline-borane-complex



The $\text{PN}^{\text{Ph}}\text{P}^{\text{Ph}}$ (**9**, 604 mg, 1.17 mmol) was dissolved in DCM (15 mL) and the borane dimethyl sulfide complex (340 mg, 4.47 mmol) was added. The solution was stirred for 2 h at room temperature and all volatile compounds removed in vacuo. The product was obtained as colorless solid.

Yield: 578 mg (1.06 mmol) 91 %



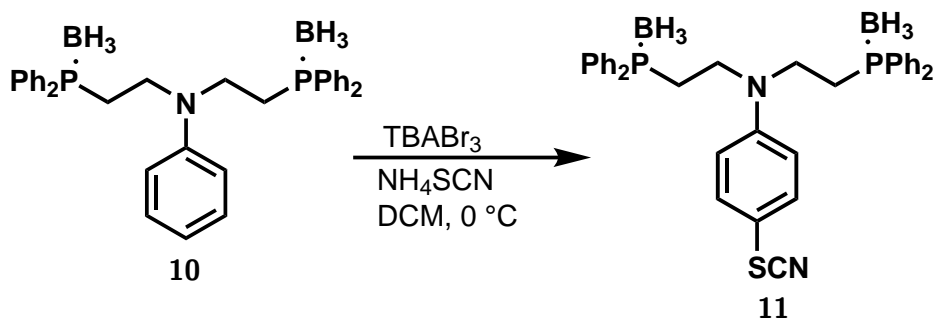
$^1\text{H-NMR}$ (400 MHz, CDCl_3 , 300 K): δ = 7.69-7.64 (m, 8 H, $H-8$), 7.60-7.58 (m, 2 H, $H-4$), 7.53-7.41 (m, 12 H, $H-9/H-10$), 7.39-7.34 (m, 3 H, $H-5/H-6$), 3.47-3.38 (m, 4 H, $H-2$), 1.85-1.74 (m, 4 H, $H-1$), 1.24-0.50 (m, 6 H, $H-11$) ppm.

$^{13}\text{C-NMR}$ (100 MHz, CDCl_3 , 300 K): δ = 147.7 (s, 4 C, $C-7$), 145.7 (s, 1 C, $C-3$), 131.2-130.7 (m, 8 C, $C-8$), 128.5 (s, 2 C, $C-4$), 128.1-127.8 (m, 8 C, $C-9$), 127.4 (s, 2 C, $C-5$), 123.2 (s, 4 C, $C-10$), 111.7 (s, 1 C, $C-6$), 60.7 (d, J_{CP} = 9.27 Hz, 2 C, $C-2$), 20.1 (d, J_{CP} = 38.1 Hz, 2 C, $C-1$) ppm.

$^{31}\text{P-NMR}$ (162 MHz, CDCl_3 , 300 K, H_3PO_4): 12.5 (s, 2P, $\text{PPh}_2 \cdot \text{BH}_3$) ppm.

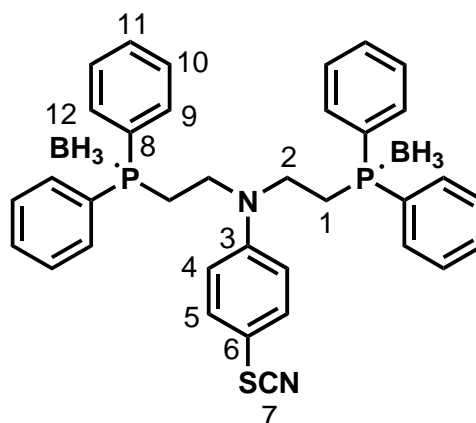
$^{11}\text{B-NMR}$ (128 MHz, CDCl_3 , 300 K, BF_3): -41.3 (s, 2 B, BH_3) ppm.

7.7 *N,N*-Bis(2-(diphenylphosphaneyl)ethyl)-4-thiocyanatoaniline-borane-complex



$\text{PN}^{\text{Ph}}\text{P}^{\text{Ph}} \cdot \text{BH}_3$ (**10**, 200 mg, 0.37 mmol) and ammonium thiocyanate (56.3 mg, 0.74) were dissolved in a mixture of DCM (5 mL) and methanol (5 mL). In a second vessel TBABr_3 (177 mg, 0.37 mmol) was dissolved using the same mixture. The ligand solution was cooled to 0 °C and the TBABr_3 solution was added, changing the color to a deep purple color. After stirring for 10 min, sodium thiocyanate solution (5 drops) were added. All volatile components were removed in vacuo and the crude product isolated using diethyl ether. The product was obtained as colorless solid.

Yield: 84.2 mg (0.14 mmol) 37 %



^1H -NMR (400 MHz, CDCl_3 , 300 K): δ = 7.68-7.61 (m, 8 H, *H*-9), 7.55-7.34 (m, 12 H, *H*-10/*H*-11), 7.34-7.32 (m, 2 H, *H*-4), 7.19-7.15 (m, 2 H, *H*-5), 3.45-3.39 (m, 4 H, *H*-2), 2.44-2.36 (m, 4 H, *H*-1), 1.73-0.82 (m, 6 H, *H*-12) ppm.

^{13}C -NMR (100 MHz, CDCl_3 , 300 K): δ = 147.7 (s, 1 C, *C*-3), 135.0 (s, 4 C, *C*-8), 132.2 (m, 2 C, *C*-4), 132.1 (s, 8 C, *C*-9), 131.8 (m, 8 C, *C*-10), 129.6 (s, 2 C, *C*-5), 129.2 (s, 4 C, *C*-11), 129.6 (s, 1 C, *C*-6), 108.3 (s, 1 C, *C*-7), 45.3 (d, J_{CP} = 5.80 Hz, 2 C, *C*-2), 23.4 (d, J_{CP} = 33.4 Hz, 2 C, *C*-1) ppm.

^{31}P -NMR (162 MHz, CDCl_3 , 300 K, H_3PO_4): 12.5 (s, 2P, $\text{PPh}_2 \cdot \text{BH}_3$) ppm.

^{11}B -NMR (128 MHz, CDCl_3 , 300 K, BF_3): -41.3 (s, 2 B, BH_3) ppm.

References

- [1] S. Tong, H. Bambrick, P. J. Beggs, L. Chen, Y. Hu, W. Ma, W. Steffen, J. Tan, *Environ.* **2022**, *158*, 106892.
- [2] P. Dasgupta, A. Dasgupta, S. Barrett, *Environ Resource Econ* **2021**.
- [3] J. Tyagi, S. Ahmad, M. Malik, *Int. J. Environ. Sci. Technol.* **2022**.
- [4] W. M. Stewart, D. W. Dibb, A. E. Johnston, T. J. Smyth, *Agron. J.* **2005**, *97*, 1–6.
- [5] V. Smil, *Ambio* **2002**, *31*, 126–131.
- [6] J. Erisman, M. Sutton, J. Galloway, et al., *Nature Geosci* **2008**, *1*, 636–639.
- [7] J. Humphreys, R. Lan, S. Tao, *Adv. Energy and Sustainability Res.* **2021**, *2*, 2000043.
- [8] A. Mittasch, *Bemerkungen zur Katalyse*, **1926**.
- [9] B. Wilk, R. Pelka, W. Arabczyk, *J. Phys. Chem. C* **2017**, *121*, 8548–8556.
- [10] S. Giddey, S. Badwal, A. Kulkarni, *Int. J. Hydrog. Energy* **2013**, *38*, 14576–14594.
- [11] T. Kandemir, M. E. Schuster, A. Senyshyn, M. Behrens, R. Schloegl, *Angew. Chem. Int. Ed.* **2013**, *52*, 12723–12726.
- [12] C. Smith, A. K. Hill, L. Torrente-Murciano, *Energy Environ. Sci* **2020**, *13*, 331–344.
- [13] N. Lehnert, B. W. Musselman, L. C. Seefeldt, *Chem Soc Rev* **2021**, *50*, 3640–3646.
- [14] B. S. Shridhar, *Int. J. Microbiol. Res.* **2012**, *3*, 46–52.
- [15] J. P. Bellenger, R. Darnajoux, X. Zhang, A. M. Kraepiel, *Biogeochemistry* **2020**, *149*, 53–73.
- [16] K. E. Luxem, A. M. Kraepiel, L. Zhang, J. R. Waldbauer, X. Zhang, *Environ. Microbiol.* **2020**, *22*, 1397–1408.
- [17] R. Darnajoux, R. Bradley, J. P. Bellenger, *Environ. Sci. Technol.* **2022**, *56*, 2760–2769.
- [18] P. C. D. Santos, R. Y. Igarashi, H. I. Lee, B. M. Hoffman, L. C. Seefeldt, D. R. Dean, *Acc. Chem. Res.* **2005**, *38*, 208–214.
- [19] Y. Tanabe, Y. Nishibayashi, *Chem. Soc. Rev.* **2021**, *50*, 5201–5242.
- [20] S. J. Forrest, B. Schluschaß, E. Y. Yuzik-Klimova, S. Schneider, *Chem. Rev.* **2021**, *121*, 6522–6587.
- [21] S. Hinrichsen, H. Broda, C. Gradert, L. Söncksen, F. Tuczek, *Annu. rep. prog. chem. Sect. A: Inorg. Chem.* **2012**, *108*, 17–47.

- [22] A. J. Martín, T. Shinagawa, J. Pérez-Ramírez, *Chem* **2019**, *5*, 263–283.
- [23] F. Haber, The synthesis of ammonia from its elements, **1920**.
- [24] C. Bosch, The development of the chemical high pressure method during the establishment of the new ammonia industry, **1932**.
- [25] G. Soloveichik, *Nat. Catal.* **2019**, *2*, 377–380.
- [26] K. H. R. Rouwenhorst, A. S. Travis, L. Lefferts, *Sustain. Chem.* **2022**, *3*, 149–171.
- [27] G. J. Leigh in *Vol. 1*, **2004**, pp. 33–54.
- [28] B. Steininger, *Anthr. Rev.* **2021**, *8*, 262–279.
- [29] T. Kandemir, M. E. Schuster, A. Senyshyn, M. Behrens, R. Schlögl, *Angew. Chem. Int. Ed.* **2013**, *52*, 12723–12726.
- [30] A. Holleman, N. Wiberg, *Anorganische Chemie, Vol. 103*, **2017**, pp. 751–754.
- [31] G. Marnellos, M. Stoukides, *Science* **1998**, *282*, 98–100.
- [32] G. Ertl, *Angew. Chem. Int. Ed.* **2008**, *47*, 3524–3535.
- [33] M. Appl in John Wiley and Sons, Ltd, **1999**, pp. 9–63.
- [34] P. H. Emmett in (Eds.: R. I. D. Edmund, Jaffee), Springer US, **1975**, pp. 3–34.
- [35] G. Ertl, *Adv. Catal.* **2000**, *45*, 1–69.
- [36] G. Ertl, *Catal. Rev. Sci. Eng.* **1980**, *21*, 201–223.
- [37] H.-P. Jia, E. A. Quadrelli, *Chem. Soc. Rev.* **2014**, *43*, 547–564.
- [38] G. Ertl, *J. Vac. Sci. Technol.* **1983**, *1*, 1247–1253.
- [39] G. Ertl, *Angew. Chem.* **1990**, *102*, 1258–1266.
- [40] I. I. Cheema, U. Krewer, *RSC Advances* **2018**, *8*, 34926–34936.
- [41] R. Shi, X. Zhang, G. I. Waterhouse, Y. Zhao, T. Zhang, *Adv. Energy Mater.* **2020**, *10*.
- [42] A. Vojvodic, A. J. Medford, F. Studt, F. Abild-Pedersen, T. S. Khan, T. Bligaard, J. K. Nørskov, *Chem. Phys. Lett.* **2014**, *598*, 108–112.
- [43] V. Kyriakou, I. Garagounis, A. Vourros, E. Vasileiou, M. Stoukides, *Joule* **2020**, *4*, 142–158.
- [44] S. Giddey, S. P. Badwal, A. Kulkarni, *Int. J. Hydrog. Energy* **2013**, *38*, 14576–14594.
- [45] D. Fowler, M. Coyle, U. Skiba, M. A. Sutton, J. N. Cape, S. Reis, L. J. Sheppard, A. Jenkins, B. Grizzetti, J. N. Galloway, P. Vitousek, A. Leach, A. F. Bouwman, K. Butterbach-Bahl, F. Dentener, D. Stevenson, M. Amann, M. Voss, *Philos. Trans. R. Soc. Lond.* **2013**, *368*.
- [46] L. Y. Stein, M. G. Klotz, *Curr. Biol.* **2016**, *26*, R94–R98.
- [47] G. J. D. Kirk, H. J. Kronzucker, *Annals of Botany* **2005**, *96*, 639–646.

-
- [48] H. Daims, E. V. Lebedeva, P. Pjevac, P. Han, C. Herbold, M. Albertsen, N. Jehmlich, M. Palatinszky, J. Vierheilig, A. Bulaev, R. H. Kirkegaard, M. V. Bergen, T. Rattei, B. Bendinger, P. H. Nielsen, M. Wagner, *Nature* **2015**, *528*, 504–509.
- [49] S. Lax, D. P. Smith, J. Hampton-Marcell, S. M. Owens, K. M. Handley, N. M. Scott, S. M. Gibbons, P. Larsen, B. D. Shogan, S. Weiss, J. L. Metcalf, L. K. Ursell, Y. Vázquez-Baeza, W. V. Treuren, N. A. Hasan, M. K. Gibson, R. Colwell, G. Dantas, R. Knight, J. A. Gilbert, *Science* **2014**, *345*, 1048–1052.
- [50] M. Könneke, A. E. Bernhard, J. R. D. L. Torre, C. B. Walker, J. B. Waterbury, D. A. Stahl, *Nature* **2005**, *437*, 543–546.
- [51] M. Palatinszky, C. Herbold, N. Jehmlich, M. Pogoda, P. Han, M. V. Bergen, I. Lagkouvardos, S. M. Karst, A. Galushko, H. Koch, D. Berry, H. Daims, M. Wagner, *Nature* **2015**, *524*, 105–108.
- [52] N. von Wirén, S. Gazzarrini, A. Gojon, W. B. Frommer, *Curr. Opin. Plant Biol.* **2000**, *3*, 254–261.
- [53] E. J. Bedmar, E. F. Robles, M. J. Delgado, The complete denitrification pathway of the symbiotic, nitrogen-fixing bacterium *Bradyrhizobium japonicum*, **2004**.
- [54] H. Cypionka, *Grundlagen der Mikrobiologie, Vol. 4*, Springer Berlin Heidelberg, **2010**, pp. 197–201.
- [55] W. G. Zumft, *Microbiol. Mol. Biol. Rev.* **1997**, *61*, 533–616.
- [56] J. J. G. Moura, P. Gonzalez, I. Moura, G. Fauque in *Vol. 1*, **2007**, pp. 241–264.
- [57] J. P. Zehr, D. G. Capone, *Science* **2020**, *368*.
- [58] S. D. Threatt, D. C. Rees, *FEBS Letters* **2022**, *597*, 45–58.
- [59] A. M. Marcarelli, R. W. Fulweiler, J. T. Scott, *Limnol. Oceanogr. Lett* **2022**, *7*, 1–10.
- [60] B. Bergman, G. Sandh, S. Lin, J. Larsson, E. J. Carpenter, *FEMS Microbiol. Rev.* **2013**, *37*, 286–302.
- [61] D. G. Capone, J. A. Burns, J. P. Montoya, A. Subramaniam, C. Mahaffey, T. Gunderson, A. F. Michaels, E. J. Carpenter, *Global Biogeochem Cycles* **2005**, *19*, 1–17.
- [62] H. W. Paerl, *Phycologia* **1996**, *35*, 25–35.
- [63] J. D. Noar, J. M. Bruno-Bárcena, *Microbiology* **2018**, *164*, 421–436.
- [64] W. A. Bulen, J. R. Lecomte, *PNAS* **1966**, *56*, 979–986.
- [65] Y. Hu, M. W. Ribbe, *J. Biol. Inorg. Chem.* **2014**, *19*, 731–736.
- [66] H. Paerl, *F1000Research* **2017**, *6*.
- [67] G. W. Niven, N. W. Kerby, P. Rowell, R. H. Reed, W. D. Stewart, *J. Phycol.* **1987**, *22*, 411–416.

- [68] K. M. Lancaster, Y. Hu, U. Bergmann, M. W. Ribbe, S. Debeer, *J. Am. Chem. Soc.* **2013**, *135*, 610–612.
- [69] M. M. Georgiadis, H. Komiya, P. Chakrabarti, D. Woo, J. J. Kornuc, D. C. Rees, *Science* **1992**, *257*, 1653–1659.
- [70] J. Kirn, D. C. Rees, *Nature* **1992**, *360*, 553–560.
- [71] H. Schindelin, C. Kisker, J. L. Schlessman, J. B. Howard, D. C. Rees, *Nature* **1997**, *387*, 370–376.
- [72] E. F. Pettersen, T. D. Goddard, C. C. Huang, E. C. Meng, G. S. Couch, T. I. Croll, J. H. Morris, T. E. Ferrin, *Protein Sci.* **2021**, *30*, 70–82.
- [73] T. D. Goddard, C. C. Huang, E. C. Meng, E. F. Pettersen, G. S. Couch, J. H. Morris, T. E. Ferrin, *Protein Sci.* **2018**, *27*, 14–25.
- [74] R. Bjornsson, F. Neese, R. R. Schrock, O. Einsle, S. Debeer, *J. Biol. Inorg. Chem.* **2015**, *20*, 447–460.
- [75] V. K. Shah, W. J. Brill, *Biochem.* **1977**, *74*, 3249–3253.
- [76] S. P. Cramer, K. O. Hodgson, W. O. Gillum, L. E. Mortenson, *J. Am. Chem. Soc.* **1978**, *100*, 11.
- [77] J. Kim, D. C. Rees, *Science* **1982**, *257*, 1677–1682.
- [78] O. Einsle, F. A. Tezcan, S. L. A. Andrade, B. Schmid, M. Yoshida, J. B. Howard, D. C. Rees, *Science* **2002**, *297*, 1696–1700.
- [79] M. K. Lancaster, M. Roemelt, P. Ettenhuber, Y. Hu, M. W. Ribbe, F. Neese, U. Bergmann, S. DeBeer, *Science* **2011**, *334*, 974–977.
- [80] T. Spatzal, M. Aksoyoglu, L. Zhang, S. L. Andrade, E. Schleicher, S. Weber, D. C. Rees, O. Einsle, *Science* **2011**, *334*, 940.
- [81] K. Danyal, D. R. Dean, B. M. Hoffman, L. C. Seefeldt, *Biochem.* **2011**, *50*, 9255–9263.
- [82] Y. Hu, M. W. Ribbe, *Biochim Biophys Acta Bioenerg* **2013**, *1827*, 1112–1122.
- [83] D. R. Dean, J. T. Bolin, L. Zheng', *J. Bacteriol.* **1993**, *175*, 6737–6744.
- [84] M. A. Blank, C. C. Lee, Y. Hu, K. O. Hodgson, B. Hedman, M. W. Ribbe, *Inorg. Chem.* **2011**, *50*, 7123–7128.
- [85] J. B. Solomon, K. Tanifuji, C. C. Lee, A. J. Jasniewski, B. Hedman, K. O. Hodgson, Y. Hu, M. W. Ribbe, *Angew. Chem. Int. Ed.* **2022**, *61*.
- [86] N. S. Sickerman, M. W. Ribbe, Y. Hu, *Acc. Chem. Res.* **2017**, *50*, 2834–2841.
- [87] R. N. F. Thorneley, D. J. Lowe, Nitrogenase: substrate binding and activation, **1996**.
- [88] B. K. Burgess, D. J. Lowe, *Chem. Rev.* **1996**, *96*, 2983–3011.
- [89] O. Einsle, D. C. Rees, *Chem. Rev.* **2020**, *120*, 4969–5004.

- [90] R. Thorneley, D. J. Lowe in *Vol. 7*, **1985**, pp. 89–116.
- [91] J. Chatt, J. R. Dilworth, R. L. Richards, *Chemical Reviews* **1978**, *78*, 589–625.
- [92] Z.-Y. Yang, K. Danyal, L. C. Seefeldt in *Vol. 766*, **2011**, pp. 9–29.
- [93] F. A. Tezcan, J. T. Kaiser, D. Mustafi, M. Y. Walton, J. B. Howard, D. C. Rees, *Science* **2005**, *309*, 1377–1380.
- [94] H. L. Rutledge, F. A. Tezcan, *Chem. Rev.* **2020**, *120*, 5158–5193.
- [95] F. E. Katz, C. P. Owens, F. A. Tezcan, *Isr. J. Chem.* **2016**, *56*, 682–692.
- [96] S. Duval, K. Danyal, S. Shaw, A. K. Lytle, D. R. Dean, B. M. Hoffman, E. Antony, L. C. Seefeldt, *Proc. Natl. Acad. Sci. USA* **2013**, *110*, 16414–16419.
- [97] D. Y. Jeng, J. A. Morris, L. E. Mortenson, *J. Biol. Chem.* **1970**, *245*, 2809–2813.
- [98] T. L. Jones, R. H. Burris, *Biochim Biophys Acta Bioenerg* **1972**, *275*, 93–101.
- [99] R. R. Eady, J. R. Postgate, *Nature* **1974**, *249*, 805–810.
- [100] S. Imam, R. R. Eady, *FEBS Letters* **1980**, *110*, 35–38.
- [101] J. B. Howard, D. C. Rees, *Chem. Rev.* **1996**, *96*, 2965–2982.
- [102] J. B. Howard, D. C. Rees, *Annu. Rev. Biochem.* **1994**, *63*, 235–264.
- [103] R. V. Hageman, R. H. Burris, *Proc. Natl. Acad. Sci. USA* **1978**, *75*, 2699–2702.
- [104] P. E. Siegbahn, *Phys. Chem. Chem. Phys.* **2019**, *21*, 15747–15759.
- [105] D. Lukoyanov, Z. Y. Yang, N. Khadka, D. R. Dean, L. C. Seefeldt, B. M. Hoffman, *J. Am. Chem. Soc.* **2015**, *137*, 3610–3615.
- [106] D. Lukoyanov, N. Khadka, D. R. Dean, S. Raugei, L. C. Seefeldt, B. M. Hoffman, *Inorg. Chem.* **2017**, *56*, 2233–2240.
- [107] B. M. Hoffman, D. Lukoyanov, D. R. Dean, L. C. Seefeldt, *Acc. Chem. Res.* **2013**, *46*, 587–595.
- [108] W. J. Wei, P. E. Siegbahn, *Chem. Eur. J.* **2022**, *28*.
- [109] P. E. Siegbahn, M. R. Blomberg, *Front. Chem.* **2018**, *6*.
- [110] P. E. Siegbahn, *Inorg. Chem.* **2018**, *57*, 1090–1095.
- [111] W. Kang, C. C. Lee, A. J. Jasniewski, M. W. Ribbe, Y. Hu, *Science* **2020**, *368*, 1381–1385.
- [112] J. Kästner, P. E. Blöchl, *J. Am. Chem. Soc.* **2007**, *129*, 2998–3006.
- [113] I. Djurdjevic, O. Einsle, L. Decamps, Nitrogenase Cofactor: Inspiration for Model Chemistry, **2017**.
- [114] M. J. Dilworth, R. R. Eadyt, *Biochem. J* **1991**, *277*, 465–468.

- [115] B. M. Barney, M. Laryukhin, R. Y. Igarashi, H. I. Lee, P. C. D. Santos, T. C. Yang, B. M. Hoffman, D. R. Dean, L. C. Seefeldt, *Biochem.* **2005**, *44*, 8030–8037.
- [116] R. D. Coucouvanis, P. E. Mosier, K. D. Demadis, S. Patton, S. M. Malinak, C. G. Kim, M. A. Tyson, *J. Am. Chem. Soc.* **1993**, *115*, 12193.
- [117] N. Stucke, T. Weyrich, M. Pfeil, K. Grund, A. Kindjajev, F. Tucek in *Vol. 60*, Springer Verlag, **2017**, pp. 113–152.
- [118] C. J. Pickett, *JBIC* **1996**, *1*, 601–606.
- [119] A. D. Allen, C. V. Senoff, *Chem. Commun. (London)* **1965**, *156*, 621–622.
- [120] A. Yamamoto, S. Kitazume, L. S. Pu, S. Ikeda, *Chem. Commun. (London)* **1967**, 79–80.
- [121] B. A. MacKay, M. D. Fryzuk, *Chem. Rev.* **2004**, *104*, 385–401.
- [122] G. J. Kubas, *J. Organomet. Chem.* **2001**, *635*, 37–68.
- [123] R. J. Burford, M. D. Fryzuk, *Nat Rev Chem* **2017**, *1*.
- [124] G. J. Leigh, *Acc. Chem. Res.* **1992**, *25*, 177–181.
- [125] T. A. Bazhenova, A. E. Shilov, *Coord. Chem. Rev.* **1995**, *144*, 69–145.
- [126] J. Chatt, *Pure Appl. Chem.* **1970**, *24*, 425–441.
- [127] Q. J. Bruch, G. P. Connor, N. D. McMillion, A. S. Goldman, F. Hasanayn, P. L. Holland, A. J. Miller, *ACS Catal.* **2020**, *10*, 10826–10846.
- [128] H. P. Jia, E. A. Quadrelli, *Chem. Soc. Rev.* **2014**, *43*, 547–564.
- [129] L. S. Yamout, M. Ataya, F. Hasanayn, P. L. Holland, A. J. Miller, A. S. Goldman, *J. Am. Chem. Soc.* **2021**, *143*, 9744–9757.
- [130] F. Hasanayn, P. L. Holland, A. S. Goldman, A. J. M. Miller, *J. Am. Chem. Soc.* **2023**, *145*, 4326–4342.
- [131] F. Studt, F. Tucek, *J. Comput. Chem.* **2006**, *27*, 1278–1291.
- [132] M. P. Shaver, M. D. Fryzuk, *Adv. Synth. Catal.* **2003**, *345*, 1061–1076.
- [133] P. L. Holland, *Dalton Trans.* **2010**, *39*, 5415–5425.
- [134] J. Chatt, C. M. Elson, N. E. Hooper, J. G. Leigh, *J. Chem. Soc. Dalton Trans.* **1975**, 2392–2401.
- [135] R. J. Deeth, C. N. Field, *J. Chem. Soc. Dalton Trans.* **1994**, 1943–1948.
- [136] M. D. Walter in *Vol. 65*, Academic Press Inc., **2016**, pp. 261–377.
- [137] C. Köthe, C. Limberg, *Z. anorg. allg. Chem.* **2015**, *641*, 18–30.
- [138] M. J. Bezdek, S. Guo, P. J. Chirik, *Inorg. Chem.* **2016**, *55*, 3117–3127.

- [139] K. Arashiba, K. Sasaki, S. Kuriyama, Y. Miyake, H. Nakanishi, Y. Nishibayashi, *Organometallics* **2012**, *31*, 2035–2041.
- [140] J. Junge, S. Froitzheim, T. A. Engesser, J. Krahmer, C. Näther, N. L. Poul, F. Tuczek, *Dalton Trans.* **2022**, *51*, 6166–6176.
- [141] W. Strohmeier, F.-J. Müller, *Chem. Ber.* **1967**, *100*, 2812–2821.
- [142] C. A. Tolman, *Chem. Rev.* **1977**, *77*, 313–348.
- [143] C. A. Tolman, *J. Am. Chem. Soc.* **1970**, *92*, 2953–2956.
- [144] J. L. Crossland, D. R. Tyler, *Coord. Chem. Rev.* **2010**, *254*, 1883–1894.
- [145] S. Hinrichsen, A. C. Schnoor, K. Grund, B. Flöser, A. Schlimm, C. Näther, J. Krahmer, F. Tuczek, *Dalton Trans.* **2016**, *45*, 14801–14813.
- [146] L. J. Murray, W. W. Weare, J. Shearer, A. D. Mitchell, K. A. Abboud, *J. Am. Chem. Soc.* **2014**, *136*, 13502–13505.
- [147] M. D. Fryzuk, *Acc. Chem. Res.* **2009**, *42*, 127–133.
- [148] I. Klopsch, E. Y. Yuzik-Klimova, S. Schneider in *Vol. 60*, Springer Verlag, **2017**, pp. 71–112.
- [149] G. A. Silantyev, M. Förster, B. Schluschaß, J. Abbenseth, C. Würtele, C. Volkmann, M. C. Holthausen, S. Schneider, *Angew. Chem.* **2017**, *129*, 5966–5970.
- [150] J. F. Berry, *Comments Inorg Chem* **2009**, *30*, 28–66.
- [151] J. Chatt, R. L. Pearman, R. L. Richards, *Nature* **1975**, *253*, 39–40.
- [152] C. J. Pickett, J. Talarmin, *Nature* **1985**, 652–653.
- [153] C. J. Pickett, K. S. Ryder, J. Talarmin, *J. Chem. Soc. Dalton Trans.* **1986**, 1453–1457.
- [154] G. C. Stephan, C. Sivasankar, F. Studt, F. Tuczek, *Eur. J. Chem.* **2008**, *14*, 644–652.
- [155] A. Dreher, G. Stephan, F. Tuczek, *Adv Inorg Chem* **2009**, *61*, 367–405.
- [156] K. Mersmann, A. Hauser, N. Lehnert, F. Tuczek, *Inorg. Chem.* **2006**, *45*, 5044–5056.
- [157] F. Tuczek in **2022**.
- [158] D. V. Yandulov, R. R. Schrock, *Science* **2003**, *301*, 71–76.
- [159] R. R. Schrock, *Acc. Chem. Res.* **2005**, *38*, 955–962.
- [160] R. R. Schrock, *Angew. Chem. Int. Ed.* **2008**, *47*, 5512–5522.
- [161] F. Studt, F. Tuczek, *Angew. Chem. Int. Ed.* **2005**, *44*, 5639–5642.
- [162] A. Magistrato, A. Robertazzi, P. Carloni, *J. Chem. Theory Comput.* **2007**, *3*, 1708–1720.
- [163] J. M. Chin, R. R. Schrock, P. Müller, *Inorg. Chem.* **2010**, *49*, 7904–7916.
- [164] D. V. Yandulov, R. R. Schrock, *Can. J. Chem.* **2005**, *83*, 341–357.

- [165] L. A. Wickramasinghe, T. Ogawa, R. R. Schrock, P. Müller, *J. Am. Chem. Soc.* **2017**, *139*, 9132–9135.
- [166] J. S. Anderson, J. Rittle, J. C. Peters, *Nature* **2013**, *501*, 84–87.
- [167] T. J. D. Castillo, N. B. Thompson, J. C. Peters, *J. Am. Chem. Soc.* **2016**, *138*, 5341–5350.
- [168] T. M. Buscagan, P. H. Oyala, J. C. Peters, *Angew. Chem. Int. Ed.* **2017**, *129*, 7025–7030.
- [169] M. J. Chalkley, T. J. D. Castillo, B. D. Matson, J. P. Roddy, J. C. Peters, *ACS Cent. Sci.* **2017**, *3*, 217–223.
- [170] M. J. Chalkley, T. J. D. Castillo, B. D. Matson, J. C. Peters, *J. Am. Chem. Soc.* **2018**, *140*, 6122–6129.
- [171] J. Y. Becker, S. Avraham, *J. Electroanal. Chem* **1990**, *280*, 119–127.
- [172] M. A. Shipman, M. D. Symes, *Catal.* **2017**, *286*, 57–68.
- [173] P. Garrido-Barros, J. Derosa, M. J. Chalkley, J. C. Peters, *Nature* **2022**, *609*, 71–76.
- [174] A. F. Ibrahim, P. Garrido-Barros, J. C. Peters, *ACS Catal.* **2023**, *13*, 72–78.
- [175] A. Takaoka, L. C. H. Gerber, J. C. Peters, *Angew. Chem.* **2010**, *122*, 4182–4185.
- [176] J. Fajardo, J. C. Peters, *J. Am. Chem. Soc.* **2017**, *139*, 16105–16108.
- [177] M. Albrecht, G. van Koten, *Angew. Chem. Int. Ed.* **2001**, *40*, 3750–3781.
- [178] J. I. V. D. Vlugt, J. N. Reek, *Angew. Chem. Int. Ed.* **2009**, *48*, 8832–8846.
- [179] L. Piccirilli, D. L. J. Pinheiro, M. Nielsen, *Catalysts* **2020**, *10*.
- [180] A. Agapova, E. Alberico, A. Kammer, H. Junge, M. Beller, *ChemCatChem* **2019**, *11*, 1910–1914.
- [181] C. Gunanathan, D. Milstein, *Chem. Rev.* **2014**, *114*, 12024–12087.
- [182] S. Schneider, J. Meiners, B. Askevold, *Eur. J. Inorg. Chem.* **2012**, 412–429.
- [183] E. Peris, R. H. Crabtree, *Chem. Soc. Rev.* **2018**, *47*, 1959–1968.
- [184] G. Herzberg, ; I. Nakagawa, T. Simanouchi, ; T. Shida, Y. Egawa, J. Kubodera, T. K. ; Cotton, F. A. Wilkinson, *J. Organomet. Chem* **1981**, *103*, 133.
- [185] C. Hou, Y. Li, Z. Ke, *Inorg. Chim. Acta* **2020**, *511*.
- [186] K. Arashiba, Y. Miyake, Y. Nishibayashi, *Nat. Chem.* **2011**, *3*, 120–125.
- [187] E. Kinoshita, K. Arashiba, S. Kuriyama, Y. Miyake, R. Shimazaki, H. Nakanishi, Y. Nishibayashi, *Organometallics* **2012**, *31*, 8437–8443.
- [188] S. Kuriyama, K. Arashiba, K. Nakajima, H. Tanaka, N. Kamaru, K. Yoshizawa, Y. Nishibayashi, *J. Am. Chem. Soc.* **2014**, *136*, 9719–9731.

- [189] S. Kuriyama, K. Arashiba, K. Nakajima, H. Tanaka, K. Yoshizawa, Y. Nishibayashi, *Chem. Sci.* **2015**, *6*, 3940–3951.
- [190] A. Eizawa, K. Arashiba, H. Tanaka, S. Kuriyama, Y. Matsuo, K. Nakajima, K. Yoshizawa, Y. Nishibayashi, *Nat. Commun.* **2017**, *8*.
- [191] H. Tanaka, K. Arashiba, S. Kuriyama, A. Sasada, K. Nakajima, K. Yoshizawa, Y. Nishibayashi, *Nat. Commun.* **2014**, *5*.
- [192] K. Arashiba, E. Kinoshita, S. Kuriyama, A. Eizawa, K. Nakajima, H. Tanaka, K. Yoshizawa, Y. Nishibayashi, *J. Am. Chem. Soc.* **2015**, *137*, 5666–5669.
- [193] K. Arashiba, A. Eizawa, H. Tanaka, K. Nakajima, K. Yoshizawa, Y. Nishibayashi, *Bull. Chem. Soc. Jpn.* **2017**, *90*, 1111–1118.
- [194] Y. Ashida, K. Arashiba, K. Nakajima, Y. Nishibayashi, *Nature* **2019**, *568*, 536–540.
- [195] Y. Ashida, T. Mizushima, K. Arashiba, A. Egi, H. Tanaka, K. Yoshizawa, Y. Nishibayashi, *Nat. Synth.* **2023**, *2*, 635–644.
- [196] Y. Ashida, K. Arashiba, H. Tanaka, A. Egi, K. Nakajima, K. Yoshizawa, Y. Nishibayashi, *Inorg. Chem.* **2019**, *58*, 8927–8932.
- [197] Y. Ashida, Y. Nishibayashi, *Chem. Comm.* **2021**, *57*, 1176–1189.
- [198] K. Arashiba, H. Tanaka, K. Yoshizawa, Y. Nishibayashi, *Chem. Eur. J.* **2020**, *26*, 13383–13389.
- [199] A. Yamamoto, X. Liu, K. Arashiba, A. Konomi, H. Tanaka, K. Yoshizawa, Y. Nishibayashi, H. Yoshida, *Inorg. Chem.* **2022**.
- [200] Y. Ashida, Y. Onozuka, K. Arashiba, A. Konomi, H. Tanaka, S. Kuriyama, Y. Yamazaki, K. Yoshizawa, Y. Nishibayashi, *Nat. Commun.* **2022**, *13*.
- [201] S. Kuriyama, T. Kato, H. Tanaka, A. Konomi, K. Yoshizawa, Y. Nishibayashi, *Bull. Chem. Soc. Jpn.* **2022**, *95*, 683–692.
- [202] S. Kuriyama, S. Wei, H. Tanaka, A. Konomi, K. Yoshizawa, Y. Nishibayashi, *Inorg. Chem.* **2022**, *61*, 5190–5195.
- [203] Y. Ashida, A. Egi, K. Arashiba, H. Tanaka, T. Mitsumoto, S. Kuriyama, K. Yoshizawa, Y. Nishibayashi, Y. Nishibayashi, A. Egi, K. Yoshizawa, H. Tanaka, *Chem. Eur. J.* **2022**, *2022*, 202200557–202200558.
- [204] Y. Sekiguchi, K. Arashiba, H. Tanaka, A. Eizawa, K. Nakajima, K. Yoshizawa, Y. Nishibayashi, *Angew. Chem. Int. Ed.* **2018**, *130*, 9202–9206.
- [205] Y. Tanabe, Y. Nishibayashi, *Coord. Chem. Rev.* **2019**, *381*, 135–150.
- [206] F. Meng, S. Kuriyama, A. Egi, H. Tanaka, K. Yoshizawa, Y. Nishibayashi, *Organometallics* **2022**.

- [207] F. Meng, S. Kuriyama, H. Tanaka, A. Egi, K. Yoshizawa, Y. Nishibayashi, *Angew. Chem. Int. Ed.* **2021**, *60*, 13906–13912.
- [208] S. Kuriyama, S. Wei, T. Kato, Y. Nishibayashi, *Molecules* **2022**, *27*.
- [209] J. Krahmer, H. Broda, C. Näther, G. Peters, W. Thimm, F. Tuczek, *Eur. J. Inorg. Chem.* **2011**, 4377–4386.
- [210] L. Söncksen, C. Gradert, J. Krahmer, C. Näther, F. Tuczek, *Inorg. Chem.* **2013**, *52*, 6576–6589.
- [211] L. Söncksen, Dissertation, **2013**.
- [212] T. Weyrich, J. Krahmer, T. A. Engesser, C. Näther, F. Tuczek, *Dalton Trans.* **2019**, *48*, 6019–6025.
- [213] H. Broda, S. Hinrichsen, J. Krahmer, C. Näther, F. Tuczek, *Dalton Trans.* **2014**, *43*, 2007–2012.
- [214] T. Weyrich, Dissertation, **2018**.
- [215] H. Broda, Dissertation, **2013**.
- [216] M. Pfeil, T. A. Engesser, J. Krahmer, C. Näther, F. Tuczek, *Z. anorg. allg. Chem.* **2021**, *647*, 1778–1788.
- [217] M. Pfeil, T. A. Engesser, A. Koch, J. Junge, J. Krahmer, C. Näther, F. Tuczek, *Eur. J. Inorg. Chem.* **2020**, *2020*, 1437–1448.
- [218] M. Pfeil, Dissertation, **2020**.
- [219] J. Krahmer, Dissertation, **2011**.
- [220] K. Klatt, Dissertation, **2008**.
- [221] A.-C. Schnoor, Dissertation, **2015**.
- [222] S. Dommaschk, Dissertation, **2016**.
- [223] K. Grund, Unpublished Results, **2017**.
- [224] K. Klatt, G. Stephan, G. Peters, F. Tuczek, *Inorg. Chem.* **2008**, *47*, 6541–6550.
- [225] T. A. George, M. A. Jackson, B. B. Kaul, *Polyhedron* **1991**, *10*, 467–470.
- [226] T. A. George, M. A. Jackson, *Inorg. Chem.* **1988**, *27*, 924–926.
- [227] S. Hinrichsen, A. Kindjajev, S. Adomeit, J. Krahmer, C. Näther, F. Tuczek, *Inorg. Chem.* **2016**, *55*, 8712–8722.
- [228] A. Kinjajev, Unpublished Results, **2017**.
- [229] N. Stucke, J. Krahmer, C. Näther, F. Tuczek, *Eur. J. Inorg. Chem.* **2018**, *2018*, 5108–5116.
- [230] J. Junge, T. A. Engesser, J. Krahmer, C. Näther, F. Tuczek, *Z. anorg. allg. Chem.* **2021**, *647*, 822–831.

- [231] T. A. Engesser, A. Kindjajev, J. Junge, J. Krahmer, F. Tuczek, *Chem. Eur. J.* **2020**, *26*, 14807–14812.
- [232] L. Alig, M. Fritz, S. Schneider, First-Row Transition Metal (De)Hydrogenation Catalysis Based on Functional Pincer Ligands, **2019**.
- [233] S. Hinrichsen, A. C. Schnoor, K. Grund, B. Flöser, A. Schlimm, C. Näther, J. Krahmer, F. Tuczek, *Dalton Trans.* **2016**, *45*, 14801–14813.
- [234] H. Zhang, R. Yuan, W. Wu, Y. Mo, *Chem. Eur. J.* **2020**, *26*, 2619–2625.
- [235] A. G. Orpen, N. G. Connelly, *Organometallics* **1990**, *9*, 1206–1210.
- [236] R. H. Crabtree, *The Organometallic Chemistry of the Transition Metals*, Vol. 6. Edition, John Wiley and Sons, **2013**, pp. 19–36.
- [237] C. Gradert, J. Krahmer, F. D. Sönnichsen, C. Näther, F. Tuczek, *Eur. J. Inorg. Chem.* **2013**, 3943–3955.
- [238] P. Dawson, *Phyr. Chem. So Ud* **1975**, *36*, 1401–1402.
- [239] S. Bruderer, A. O. Benz, P. Stäuber, A. S. Davydov, *Sov. Phys. Usp* **1964**, *7*, 393–448.
- [240] P. Ghosh, *Solid State Commun.* **1976**, *19*, 639–642.
- [241] T. A. Gavrilko, G. O. Puchkovska, V. I. Styopkin, T. V. Bezrodna, J. Baran, M. Drozd, *Ukr. J. Phys.* **2013**, *58*, 637–646.
- [242] K. Wang, D. Smith, Y. Zheng, *Carbon Resour. Convers* **2018**, *1*, 2–31.
- [243] I. A. Amar, R. Lan, C. T. Petit, S. Tao, *J Solid State Electrochem* **2011**, *15*, 1845–1860.
- [244] H. Miessner, *J. Am. Chem. Soc* **1994**, *116*, 11522–11530.
- [245] H. Miessner, K. Richter, *J Mol Catal A Chem* **1999**, *146*, 107–115.
- [246] D. L. Dubois, *Inorg. Chem* **1984**, *23*, 2047–2052.
- [247] S. Ossinger, H. Naggert, L. Kipgen, T. Jasper-Toennies, A. Rai, J. Rudnik, F. Nickel, L. M. Arruda, M. Bernien, W. Kuch, R. Berndt, F. Tuczek, *J. Phys. Chem. C* **2017**, *121*, 1210–1219.
- [248] T. Knaak, C. González, Y. J. Dappe, G. D. Harzmann, T. Brandl, M. Mayor, R. Berndt, M. Gruber, *J. Phys. Chem. C* **2019**, *123*, 4178–4185.
- [249] T. G. Gopakumar, F. Matino, H. Naggert, A. Bannwarth, F. Tuczek, R. Berndt, *Angew Chem. Int. Ed.* **2012**, *51*, 6262–6266.
- [250] E. Ludwig, H. Naggert, M. Kalläne, S. Rohlf, E. Kröger, A. Bannwarth, A. Quer, K. Rossnagel, L. Kipp, F. Tuczek, *Angew. Chem.* **2014**, *126*, 3063–3067.
- [251] A. Ulman, *Chem. Rev.* **1996**, *96*, 1533–1554.
- [252] A. Badia, R. B. Lennox, L. Reven, *Acc. Chem. Res* **2000**, *33*, 475–481.

- [253] M. Singh, N. Kaur, E. Comini, *J. Mater. Chem. C* **2020**, *8*, 3938–3955.
- [254] J. Sánchez-Bodón, J. A. D. Olmo, J. M. Alonso, I. Moreno-Benítez, J. L. Vilas-Vilela, L. Pérez-Álvarez, *Polymers* **2022**, *14*, 165.
- [255] S. P. Pujari, L. Scheres, A. T. Marcelis, H. Zuilhof, *Angew. Chem. Int. Ed.* **2014**, *53*, 6322–6356.
- [256] S. A. Jadhav, *Cent. Eur. J. Chem.* **2011**, *9*, 369–378.
- [257] E. Fast, A. Schlimm, I. Lautenschläger, K. U. Clausen, T. Strunskus, C. Spormann, T. K. Lindhorst, F. Tuczek, *Chem. Eur. J.* **2020**, *26*, 485–501.
- [258] B. Baisch, D. Raffa, U. Jung, O. M. Magnussen, C. Nicolas, J. Lacour, J. Kubitschke, R. Herges, *J. Am. Chem. Soc.* **2009**, *131*, 442–443.
- [259] R. Löw, T. Rusch, F. Röhricht, O. Magnussen, R. Herges, *Beilstein J. Org. Chem.* **2019**, *15*, 1485–1490.
- [260] H. Jacob, S. Ulrich, U. Jung, S. Lemke, T. Rusch, C. Schütt, F. Petersen, T. Strunskus, O. Magnussen, R. Herges, F. Tuczek, *Phys. Chem. Chem. Phys.* **2014**, *16*, 22643–22650.
- [261] A. Schlimm, N. Stucke, B. M. Flöser, T. Rusch, J. Krahmer, C. Näther, T. Strunskus, O. M. Magnussen, F. Tuczek, *Chem. Eur. J.* **2018**, *24*, 10732–10744.
- [262] F. Petersen, I. Lautenschläger, A. Schlimm, B. M. Flöser, H. Jacob, R. Amirbeigiariab, T. R. Rusch, T. Strunskus, O. Magnussen, F. Tuczek, *Dalton Trans.* **2021**, *50*, 1042–1052.
- [263] R. Huisgen, *1,3-Dipolar cycloaddition chemistry*. A. Padwa, Ed., Wiley, **1984**, pp. 1–176.
- [264] E. Hrishikesan, R. Manjunath, P. Kannan, *J. Solution Chem.* **2016**, *45*, 907–919.
- [265] L. R. Hoover, T. Pryor, J. A. Weitgenant, P. E. Williams, B. N. Storhoff, J. C. Huffman, *Phosphorus Sulfur Silicon Relat. Elem.* **1997**, *122*, 155–166.
- [266] K. Sonogashira, Y. Tohda, N. Hagihara, *Tetrahedron Letters* **1975**, 4467–4470.
- [267] K. Leonard, M. Nelen, M. Raghu, M. R. Detty, *J. Heterocycl. Chem.* **1999**, *36*, 707–717.
- [268] G. Wittig, W. Böll, *Chem. Ber.* **1962**, *95*, 2526–2534.
- [269] A. N. Nesmeyanov, V. V. Krivykh, V. S. Kaganovich, M. L. Rybinskaya, *J. Organomet. Chem.* **1975**, *102*, 185–193.
- [270] B. B. Nicholls, M. C. Whiting, *J. Chem. Soc.* **1959**, *69*, 551–556.
- [271] C. D. Hoff, *J. Organomet. Chem.* **1985**, *282*, 201–214.
- [272] F. A. Cotton, J. E. McCleverty, J. E. White, R. B. King, A. F. Fronzaglia, M. A. Bisnette in Academic Press, **1967**, pp. 45–47.
- [273] K. U. Clausen, Current Works, **2023**.

-
- [274] S. G. Keskin, J. M. Stanley, A. H. Cowley, *Polyhedron* **2017**, *138*, 206–217.
- [275] C. Vericat, M. E. Vela, G. Benitez, P. Carro, R. C. Salvarezza, *Chem. Soc. Rev.* **2010**, *39*, 1805–1834.
- [276] J. W. Ciszek, M. P. Stewart, J. M. Tour, *J. Am. Chem. Soc.* **2004**, *126*, 13172–13173.
- [277] J. W. Ciszek, M. P. Stewart, J. M. Tour, *J. Am. Chem. Soc.* **2004**, *126*, 13172–13173.
- [278] K. Bourumeau, A.-C. Gaumont, J.-M. Denis, *J. Organomet. Chem.* **1997**, *529*, 205–213.
- [279] K. Zhu, P. D. Achord, X. Zhang, K. Krogh-Jespersen, A. S. Goldman, *J. Am. Chem. Soc.* **2004**, *126*, 13044–13053.
- [280] P. Stössel, H. A. Mayer, C. Maichle-Mössmer, R. Fawzi, M. Steimann, *Inorg. Chem.* **1996**, *35*, 5860–5867.
- [281] M. Ohff, J. Holz, M. Quirnbach, A. Börner, *Synthesis* **1998**, *10*, 1391–1415.
- [282] B. Rapp, J. E. Drake, *Inorg. Chem.* **1973**, *12*, 2868.
- [283] N. A. Bondarenko, K. V. Tcarkova, S. K. Belus', O. I. Artyushin, *Phosphorus Sulfur Silicon Relat. Elem.* **2021**, *196*, 902–910.
- [284] N. Michaelis, Masterthesis, **2021**.
- [285] T. Leischner, A. Spannenberg, K. Junge, M. Beller, *Organometallics* **2018**, *37*, 4402–4408.
- [286] N. F. Both, A. Spannenberg, K. Junge, M. Beller, *Organometallics* **2022**, *41*, 1797–1805.

Appendix

Electronic Supplementary Material (ESI) for Dalton Transactions.
This journal is © The Royal Society of Chemistry 2022

Supporting Information

Tungsten and Molybdenum Dinitrogen Complex Supported by a Pentadentate Tetrapodal Phosphine Ligand: Comparative Spectroscopic, Electrochemical and Reactivity Studies

Jannik Junge^{†a}, Sven Froitzheim^{†a}, Tobias A. Engesser^a, Jan Krahmer^a, Christian Näther^a, Nicolas Le Poul^{*b}, Felix Tuczek^{*a}

Content	page
$[\text{WCl}_3(\kappa^3\text{-P}_2^{\text{Me}}\text{PP}_2^{\text{Ph}})]$	2
$[\text{W}(\text{N}_2)(\text{P}_2^{\text{Me}}\text{PP}_2^{\text{Ph}})]$ (2)	4
Electrochemistry of $[\text{Mo}(\text{N}_2)(\text{P}_2^{\text{Me}}\text{PP}_2^{\text{Ph}})]$ (1) and $[\text{W}(\text{N}_2)(\text{P}_2^{\text{Me}}\text{PP}_2^{\text{Ph}})]$ (2)	12
^1H -DOSY NMR spectrum of $[\text{W}(\text{N}_2)(\text{P}_2^{\text{Me}}\text{PP}_2^{\text{Ph}})]$ (2)	13
$[\text{W}(\text{NNH}_2)(\text{P}_2^{\text{Me}}\text{PP}_2^{\text{Ph}})](\text{BAR}^{\text{F}})_2$ (3-BAR^F)	14
$[\text{W}(\text{NNH}_2)(\text{P}_2^{\text{Me}}\text{PP}_2^{\text{Ph}})][\text{Al}(\text{pftb})_4]_2$ (3-Al(pftb)₄)	24
Catalytic experiments	24
Cartesian coordinates of $[\text{W}(\text{N}_2)(\text{P}_2^{\text{Me}}\text{PP}_2^{\text{Ph}})]$ (2) and $[\text{W}(\text{NNH}_2)(\text{P}_2^{\text{Me}}\text{PP}_2^{\text{Ph}})]^{2+}$ (3)	25

^aInstitut für Anorganische Chemie,
CAU Kiel, Max-Eyth-Str. 2, 24118 Kiel.
Email: ftuczek@ac.uni-kiel.de

^bLaboratoire de Chimie, Electrochimie Moléculaires et Chimie Analytique (UMR CNRS 6521)
Université de Bretagne Occidentale, 6 Avenue Le Gorgeu, 29238 Brest, France
Email: Lepoul@univ-brest.fr

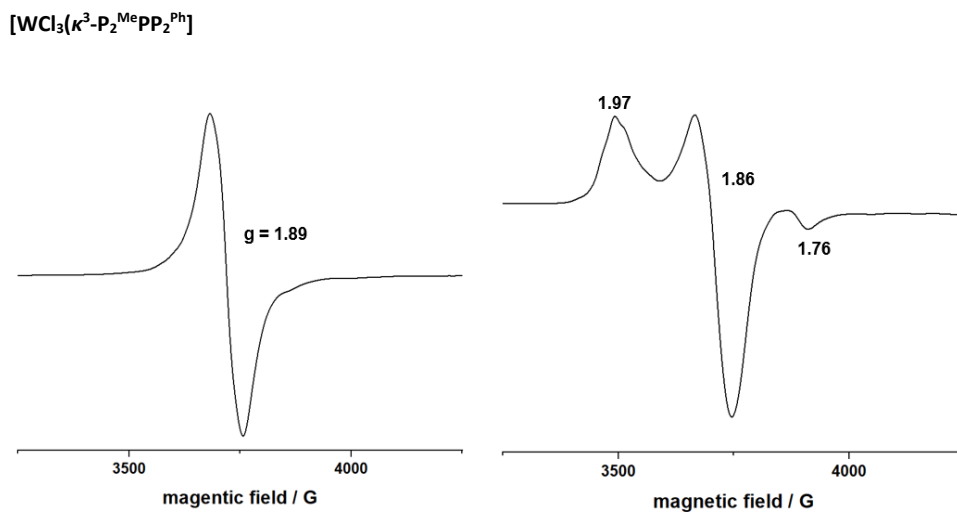


Figure S1. X-band (9.8 GHz) EPR spectra of thf solutions of $[\text{WCl}_3(\kappa^3\text{-P}_2^{\text{Me}}\text{PP}_2^{\text{Ph}})]$ at room temperature (left) and 77 K (right). The X-band EPR spectra were recorded on a Bruker EMX Plus spectrometer with dual mode cavity, 2.0 mW microwave power and modulation amplitude of 1 mT.

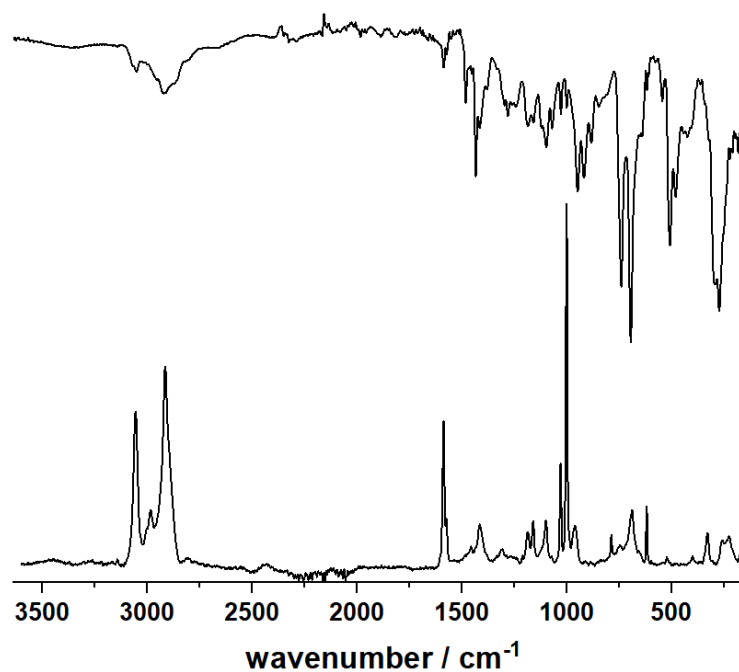


Figure S2. IR and Raman spectrum of $[\text{WCl}_3(\kappa^3\text{-P}_2^{\text{Me}}\text{PP}_2^{\text{Ph}})]$.

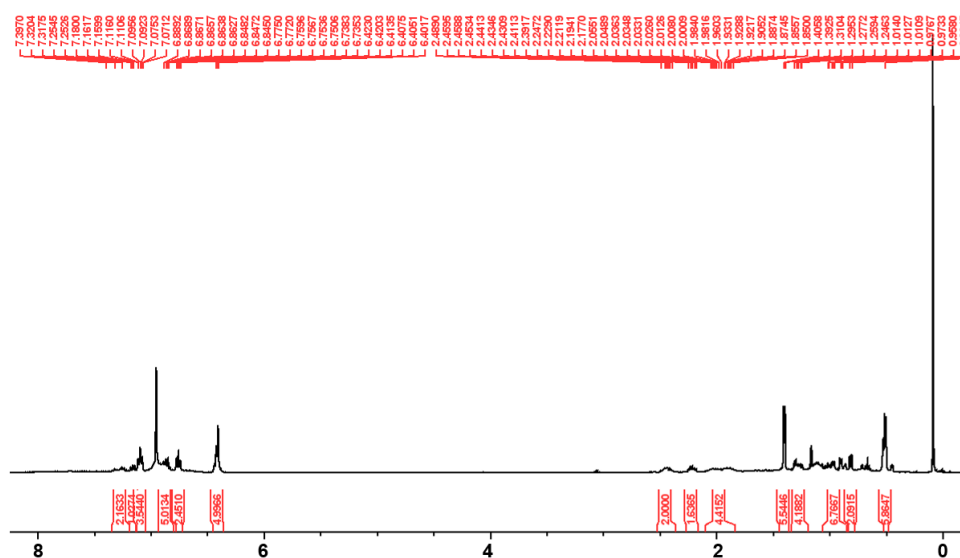
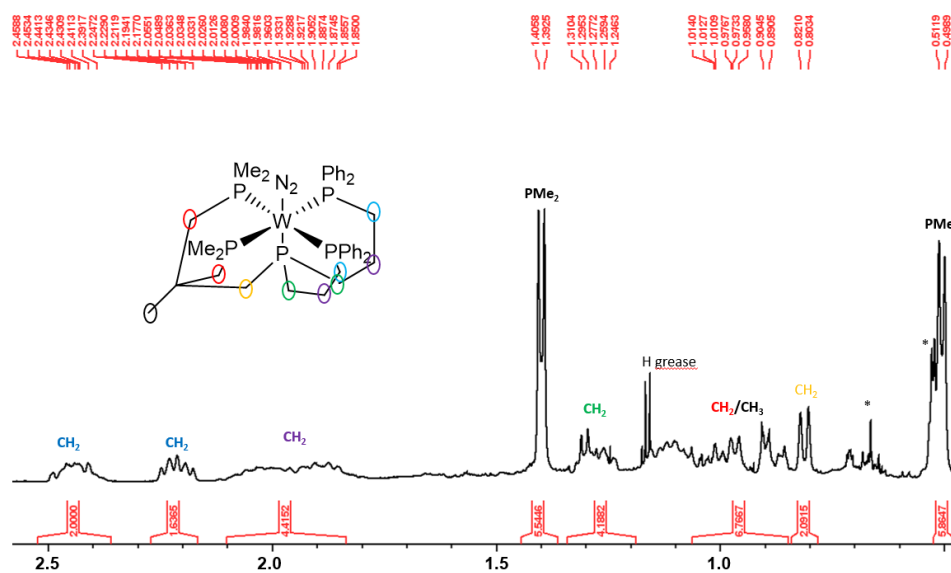
Table S1. Experimental frequencies of the Raman and IR bands of $[\text{WCl}_3(\kappa^3\text{-P}_2^{\text{Me}}\text{PP}_2^{\text{Ph}})] [\text{cm}^{-1}]$.

$[\text{WCl}_3(\kappa^3\text{-P}_2^{\text{Me}}\text{PP}_2^{\text{Ph}})] (\mathbf{2})$					
Raman	IR	Assignment	Raman	IR	Assignment
-	3067 (w)	-	-	945 (m)	CC
3054 (m)	3051 (w)	$\nu(\text{CH})$	-	917 (m)	CC
2982 (w)	-	$\nu_{\text{as}}(\text{CH}_3/\text{CH}_2)$	-	880 (m)	-
-	2954 (sh)	-	-	843 (w)	-
2913 (s)	2919 (m)	$\nu_s(\text{CH}_3/\text{CH}_2)$	-	805 (vw)	-
-	2867 (sh)	-	786 (w)	-	-
-	2801 (w)	-	-	739 (s)	-
1586 (s)	1589 (m)	CC	688 (w)	693 (vs)	-
1573 (w)	1568 (w)	-	-	639 (vw)	-
-	1551 (vw)	-	619 (w)	617 (w)	-
-	1480 (m)	-	-	577 (vw)	-
1455 (vw)	1455 (vw)	-	-	543 (w)	-
-	1430 (m)	PC	-	508 (s)	-
1414 (w)	1412 (w)	PC	-	479 (m)	-
-	1381 (w)	-	-	442 (vw)	-
-	1330 (vw)	-	-	425 (w)	-
1306 (vw)	1297 (w)	-	400 (vw)	404 (vw)	-
-	1279 (w)	-	-	362 (vw)	-
-	1260 (vw)	-	-	340 (sh)	-
-	1241 (w)	-	328 (w)	323 (sh)	-
1210 (vw)	-	-	-	294 (s)	-
1186 (w)	1182 (w)	-	-	271 (vs)	-
1160 (w)	1156 (w)	-	258 (w)	252 (sh)	-
-	1119 (w)	-	-	221 (vw)	-
1100 (w)	1096 (m)	-	-	208 (vw)	-
1073 (vw)	1069 (w)	-	-	178 (w)	-
1028 (m)	1025 (w)	-	150 (vw)	158 (w)	-
1000 (vs)	1000 (w)	CC	-	133 (m)	-
960 (w)	-	-	-	120 (w)	-

vw = very weak, w = weak, m = medium, s = strong, vs = very strong; ν = valence, δ = deformation

$$[\text{W}(\text{N}_2)(\text{P}_2^{\text{Me}}\text{PP}_2^{\text{Ph}})] \text{ (2)}$$

NMR spectroscopy

Figure S3. ^1H NMR spectrum of **2** in benzene- d_6 .Figure S4. Enlargement of the aliphatic region of the ^1H NMR spectrum of **2** in benzene- d_6 and assignment of the signals.

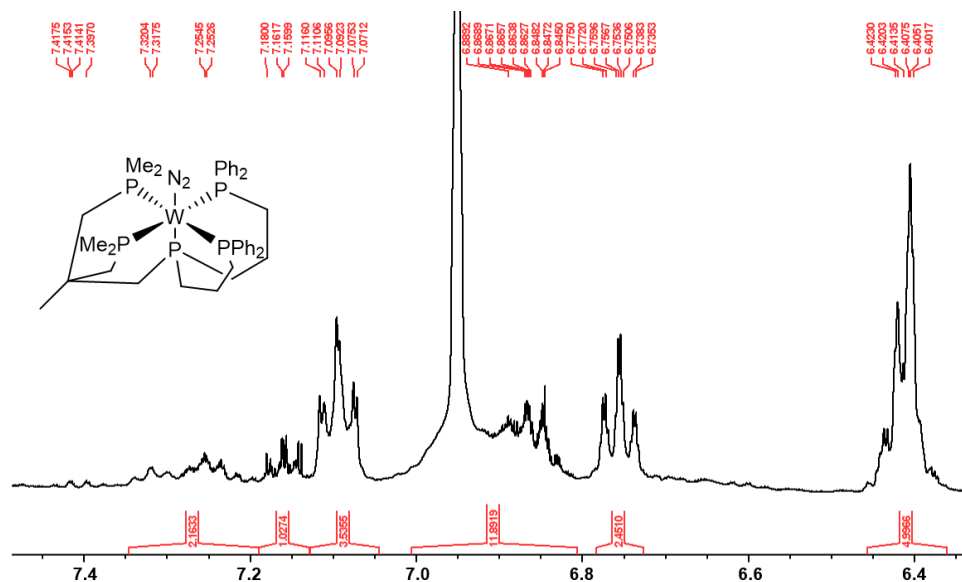


Figure S5. Enlargement of the aromatic region of the ¹H NMR spectrum of **2** in benzene-*d*₆.

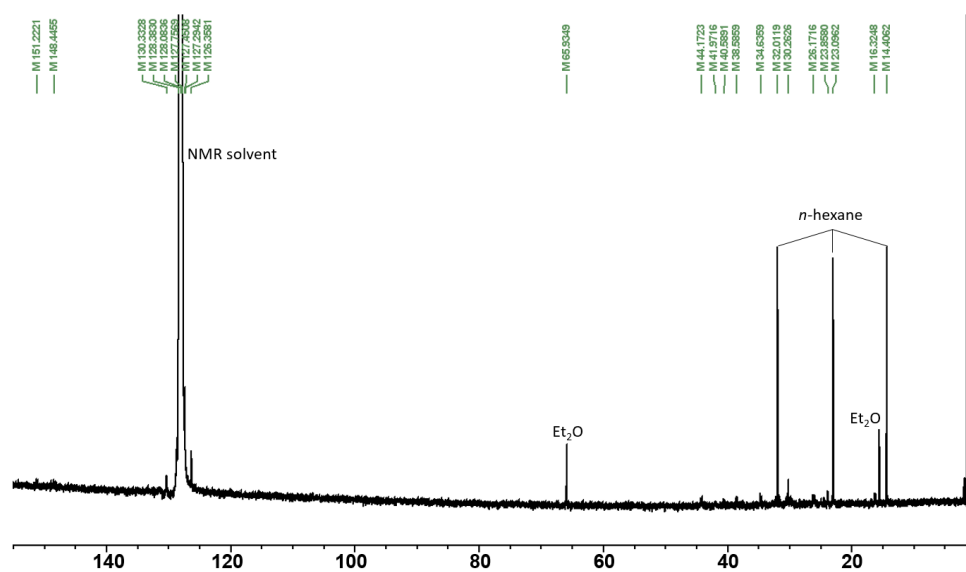


Figure S6. ¹³C NMR spectrum of **2** in benzene-*d*₆.

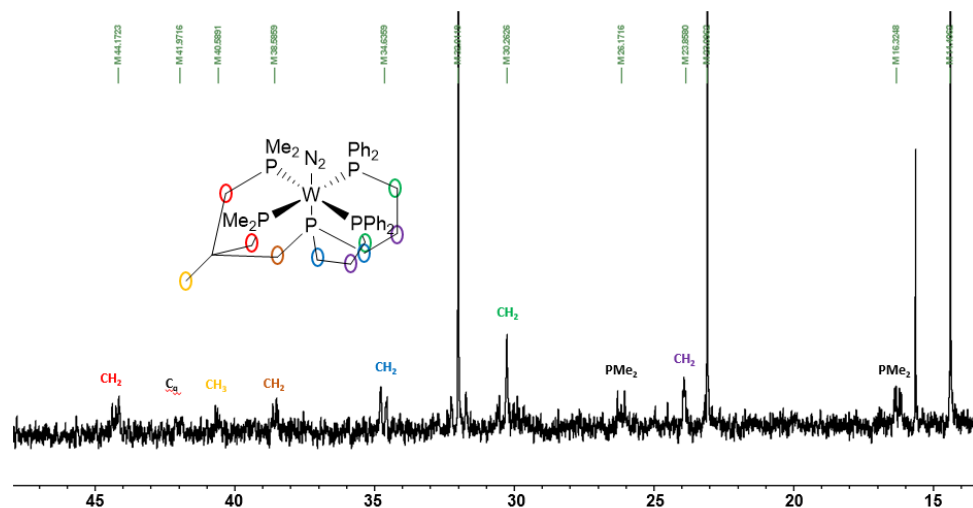


Figure S7. Enlargement of the aliphatic region of the ^{13}C NMR spectrum of **2** in benzene- d_6 and assignment of the signals.

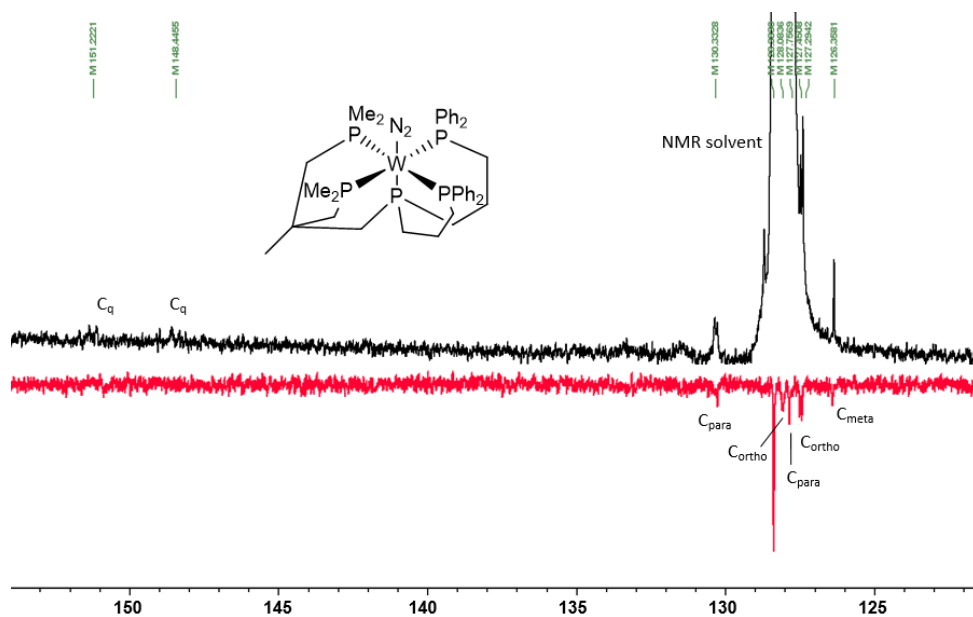


Figure S8. Enlargement of the aromatic region of the ^{13}C NMR and ^{13}C DEPT NMR spectrum of **2** in benzene- d_6 and assignment of the signals. The DEPT spectrum was plotted with the CH signals pointing downwards.

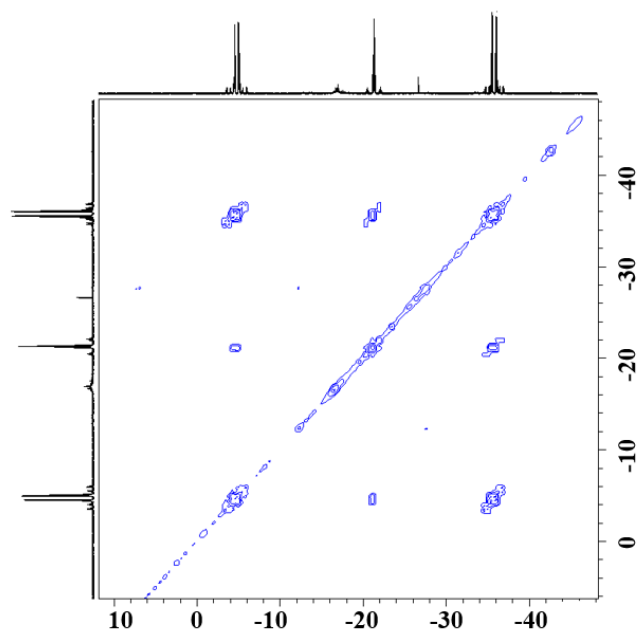


Figure S9. ^{31}P - ^{31}P -COSY spectrum of **2** in benzene- d_6 .

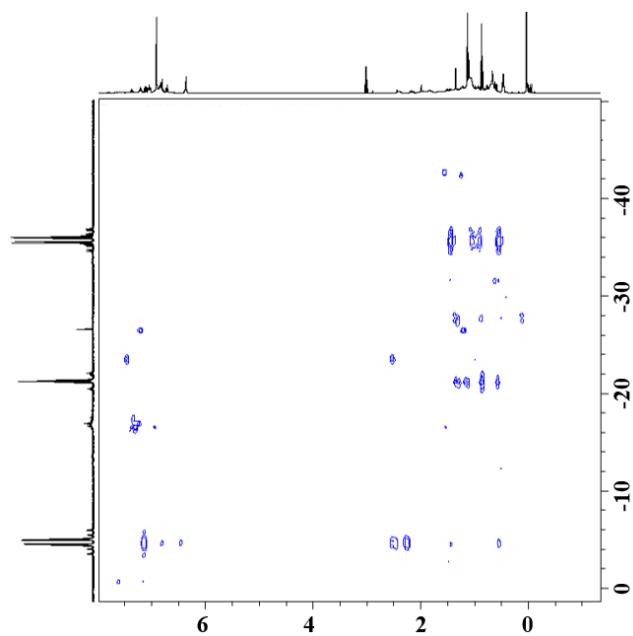


Figure S10. ^{31}P - ^1H -HMBC spectrum of **2** in benzene- d_6 .

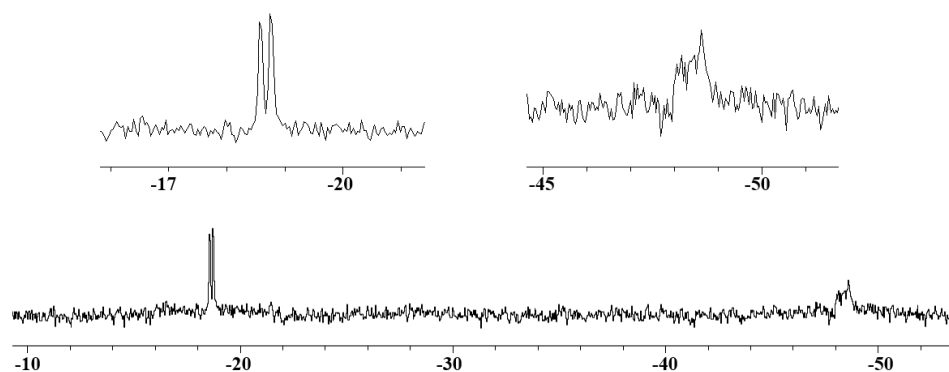


Figure S11. ^{15}N NMR spectrum of $^{15}\text{N-2}$ in benzene- d_6 .

Table S2. Comparison of $^{15}\text{N-}^{31}\text{P}$ and $^{15}\text{N-}^{15}\text{N}$ coupling constants of $^{15}\text{N-}[\text{Mo}(\text{N}_2)(\text{P}_2^{\text{Me}}\text{P}_2^{\text{Ph}})]$ ($^{15}\text{N-1}$)^[1] and $^{15}\text{N-}[\text{W}(\text{N}_2)(\text{P}_2^{\text{Me}}\text{P}_2^{\text{Ph}})]$ ($^{15}\text{N-2}$).

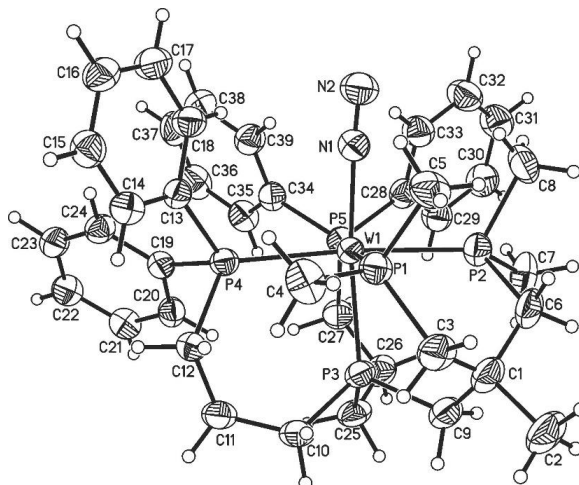
Complex	J/Hz						
	$J(\text{P}_\text{A}-\text{N}_\alpha)$	$J(\text{P}_\text{A}-\text{N}_\beta)$	$J(\text{P}_\text{X}-\text{N}_\alpha)$	$J(\text{P}_\text{X}-\text{N}_\beta)$	$J(\text{P}_\text{M}-\text{N}_\alpha)$	$J(\text{P}_\text{M}-\text{N}_\beta)$	$J(\text{N}_\alpha-\text{N}_\beta)$
$^{15}\text{N-1}$ ^[1]	3.0	-	3.4	0.8	13.1	1.3	6.9
$^{15}\text{N-2}$	2.7	0.3	2.6	0.7	13.9	1.6	7.4

Vibrational spectroscopy of $[W(N_2)(P_2^{Me}PP_2^{Ph})] (2)$

Table S3. Experimental frequencies of the Raman and IR bands of $[W(N_2)(P_2^{Me}PP_2^{Ph})] (2)$ [cm^{-1}].

$[W(N_2)(P_2^{Me}PP_2^{Ph})] / [W(^{15}N_2)(P_2^{Me}PP_2^{Ph})]$					
Raman	IR	Assignment	Raman	IR	Assignment
-	3139 (vw)	-	-	1072 (m)	-
-	3069 (w)	-	-	1048 (m)	-
3053 (s)	3049 (w)	v(CH)	1029 (m)	1025 (s)	-
-	2994 (vw)	-	1001 (vs)	-	-
2963 (w)	2959 (m)	$\nu_{as}(CH_3/CH_2)$	-	970 (w)	-
-	2920 (sh)	-	933 (vw)	925 (m)	-
2912 (vs)	2906 (m)	$\nu_s(CH_3/CH_2)$	910 (vw)	905 (s)	-
2888 (s)	-	-	-	875 (m)	-
2863 (sh)	2855 (m)	-	-	832 (w)	-
-	2812 (sh)	-	-	798 (s)	CC
-	1982 (w)	-	-	737 (s)	CC
1903 (s)/1840 (s)	1901 (vs)/1840 (vs)	v(N-N)	-	693 (vs)	CC
-	1805 (vw)	-	670 (w)	662 (s)	CC
-	1750 (vw)	-	637 (vw)	-	-
1587 (s)	1585 (w)	CC	-	625 (s)	-
1572 (w)	1571 (w)	-	618 (w)	612 (s)	-
-	1481 (m)	-	-	544 (vw)	-
1451 (vw)	1448 (w)	-	505 (vw)	506 (vs)	-
1434 (vw)	1431 (s)	PC	-	475 (m)	-
1418 (vw)	1418 (sh)	-	431 (w)/419 (w)	429 (w)/421 (w)	v(W-N)
1405 (vw)	-	-	403 (vw)	402 (s)	-
-	1373 (w)	-	364 (vw)	372 (vw)	-
-	1328 (vw)	-	350 (vw)	345 (m)	-
1297 (vw)	1293 (w)	-	315 (vw)	313 (w)	-
1274 (vw)	-	-	292 (vw)	290 (w)	-
-	1258 (s)	-	257 (vw)	263 (vw)	-
-	1218 (vw)	-	-	-	-
1186 (w)	1184 (vw)	-	242 (w)	240 (m)	-
1156 (w)	1153 (w)	-	193 (w)	191 (vw)	-
1093 (m)	1089 (s)	-	-	-	-

vw = very weak, w = weak, m = medium, s = strong, vs = very strong; v = valence, δ = deformation

Crystal Data for $[\text{W}(\text{N}_2)(\text{P}_2^{\text{Me}}\text{PP}_2^{\text{Ph}})]$ (2**)****Figure S12.** ORTEP plot of **2** with labelling and displacement ellipsoids drawn at the 50% probability level.**Table S4.** Crystal data and structure refinement for $[\text{W}(\text{N}_2)(\text{P}_2^{\text{Me}}\text{PP}_2^{\text{Ph}})]$ (**2**)

Empirical formula	$\text{C}_{39}\text{H}_{53}\text{N}_2\text{P}_5\text{W}$	
Formula weight	888.53	
Temperature	200(2) K	
Wavelength	0.71073 Å	
Crystal system	Monoclinic	
Space group	$\text{P}2_1/\text{n}$	
Unit cell dimensions	$a = 19.2033(8)$ Å	$a = 90^\circ$
	$b = 9.4433(3)$ Å	$b = 107.168(3)^\circ$
	$c = 21.9208(10)$ Å	$c = 90^\circ$
Volume	$3798.1(3)$ Å ³	
Z	4	
Density (calculated)	1.554 Mg/m ³	
Absorption coefficient	3.283 mm^{-1}	
F(000)	1800	
Crystal size	$0.07 \times 0.12 \times 0.17 \text{ mm}^3$	
Theta range for data collection	1.678 to 28.003°	
Index ranges	$-24 \leq h \leq 25$, $-12 \leq k \leq 12$, $-28 \leq l \leq 28$	
Reflections collected	59003	
Independent reflections	9164	
[R(int)]	0.0542]	
Reflections with $I > 2\sigma(I)$	8455	
Completeness to $\theta = 25.242^\circ$	99.7 %	
Refinement method	Full-matrix least-squares on F^2	
Data / restraints / parameters	9164 / 0 / 430	
Goodness-of-fit on F^2	1.076	
Final R indices [$I > 2\sigma(I)$]	$R1 = 0.0365$, $wR2 = 0.0899$	
R indices (all data)	$R1 = 0.0402$, $wR2 = 0.0921$	
Extinction coefficient	0.00220(19)	
Largest diff. peak and hole	1.096 and -1.154 e.Å^{-3}	

Table S5. Bond lengths [\AA] and angles [$^\circ$] of $[\text{W}(\text{N}_2)(\text{P}_2^{\text{Me}}\text{PP}_2^{\text{Ph}})]$ (**2**)

W(1)-N(1)	2.020(3)	W(1)-P(2)	2.4365(10)
W(1)-P(3)	2.3827(10)	W(1)-P(1)	2.4374(10)
W(1)-P(4)	2.4361(9)	W(1)-P(5)	2.4399(10)
N(1)-N(2)	1.084(5)	P(3)-W(1)-P(1)	84.31(3)
N(1)-W(1)-P(3)	170.65(9)	P(4)-W(1)-P(1)	90.32(3)
N(1)-W(1)-P(4)	95.25(9)	P(2)-W(1)-P(1)	81.97(4)
P(3)-W(1)-P(4)	89.64(3)	N(1)-W(1)-P(5)	94.90(10)
N(1)-W(1)-P(2)	88.16(9)	P(3)-W(1)-P(5)	92.57(3)
P(3)-W(1)-P(2)	85.93(3)	P(4)-W(1)-P(5)	95.37(3)
P(4)-W(1)-P(2)	171.45(3)	P(2)-W(1)-P(5)	92.14(3)
N(1)-W(1)-P(1)	87.69(10)	P(1)-W(1)-P(5)	173.50(3)
N(2)-N(1)-W(1)	175.0(3)	C(25)-P(3)-W(1)	121.11(13)
C(4)-P(1)-W(1)	128.22(14)	C(9)-P(3)-W(1)	114.35(14)
C(5)-P(1)-W(1)	115.16(15)	C(13)-P(4)-W(1)	117.09(11)
C(3)-P(1)-W(1)	115.03(15)	C(12)-P(4)-W(1)	116.36(12)
C(7)-P(2)-W(1)	125.70(16)	C(19)-P(4)-W(1)	126.31(12)
C(8)-P(2)-W(1)	117.39(16)	C(27)-P(5)-W(1)	118.05(14)
C(6)-P(2)-W(1)	115.25(15)	C(34)-P(5)-W(1)	120.24(12)
C(10)-P(3)-W(1)	119.34(13)	C(28)-P(5)-W(1)	117.26(13)

Table S6. Comparison of bond lengths of molybdenum (**1**) und tungsten (**2**) dinitrogen complexes and calculated bond length of hydrazido(2-) complexes of molybdenum and tungsten (**3**).

Bond length/ \AA	$[\text{Mo}(\text{N}_2)(\text{P}_5)]$ (1)	$[\text{W}(\text{N}_2)(\text{P}_5)]$ (2)	$[\text{Mo}(\text{NNH}_2)(\text{P}_5)]^{2+ \text{ a}}$	$[\text{W}(\text{NNH}_2)(\text{P}_5)]^{2+ \text{ a}}$ (3)
N-N	1.099(5)	1.084(5)	1.30693	1.31330
M-N	2.033(5)	2.020(3)	1.74663	1.76704
M-P _{ax.}	2.3868(12)	2.3827(10)	2.61968	2.62834
M-PMe ₂ (1)	2.4433(14)	2.4365(10)	2.51442	2.51872
M-PMe ₂ (2)	2.4440(13)	2.4374(10)	2.52547	2.52766
M-PPh ₂ (1)	2.4518(13)	2.4361(10)	2.56995	2.56758
M-PPh ₂ (2)	2.4536(13)	2.4399(10)	2.51545	2.51952

P₅ = P₂^{Me}PP₂^{Ph}, ^aAll calculations on PBE0/def2-TZVP level

Supplementary electrochemical and spectroelectrochemical data for $[\text{W}(\text{N}_2)(\text{P}^{\text{Me}}_2\text{PP}_2^{\text{Ph}})]$ (2) and $[\text{Mo}(\text{N}_2)(\text{P}^{\text{Me}}_2\text{PP}_2^{\text{Ph}})]$ (1).

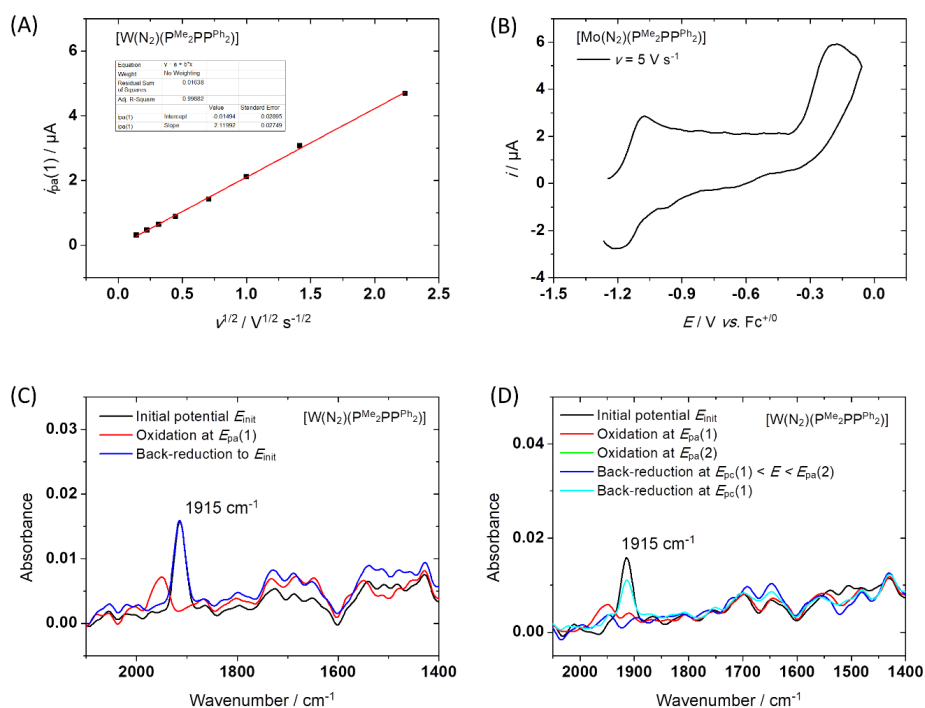


Figure S13. A) Plot of $i_{\text{pa}}(1)$ vs. $v^{1/2}$ from CV data obtained for $[\text{W}(\text{NNH}_2)(\text{P}_2^{\text{Me}}\text{PP}_2^{\text{Ph}})]$ (0.4 mM) in THF/NaBPh₄ 20 mM, red curve: linear fit; B) CV of $[\text{Mo}(\text{N}_2)(\text{P}^{\text{Me}}_2\text{PP}_2^{\text{Ph}})]$ (1 mM) at Pt working electrode (diam. 1 mm) for $\nu = 05 \text{ V s}^{-1}$ in THF/NaBPh₄ 20 mM.; C) Infrared spectra of $[\text{W}(\text{N}_2)(\text{P}^{\text{Me}}_2\text{PP}_2^{\text{Ph}})]$ (15 mM) in THF/NaBPh₄ 20 mM recorded during *in-situ* spectroelectrochemical measurements before (black) and after oxidation at $E_{\text{pa}}(1)$ (red), then returning back to the initial potential (blue); (D) The same as (C) except that oxidation at $E_{\text{pa}}(1)$ (red) is followed by oxidation at $E_{\text{pa}}(2)$ (green), then back-reduction to $E_{\text{pc}}(1) < E < E_{\text{pa}}(2)$ (blue) and finally $E_{\text{pc}}(1)$ (cyan).

^1H -DOSY NMR experiment of $[\text{W}(\text{N}_2)(\text{P}_2^{\text{Me}}\text{PP}_2^{\text{Ph}})]$ (2**)**

The ^1H -DOSY NMR was measured with 13 mg (14.6 μmol) of $[\text{W}(\text{N}_2)(\text{P}_2^{\text{Me}}\text{PP}_2^{\text{Ph}})]$ (**2**) and 17 mg (49.7 μmol) NaBPh_4 in 0.5 ml deuterated THF. The resulting value for the diffusion coefficient was $9.5 \cdot 10^{-6} \text{ cm}^2 \text{ s}^{-1}$.

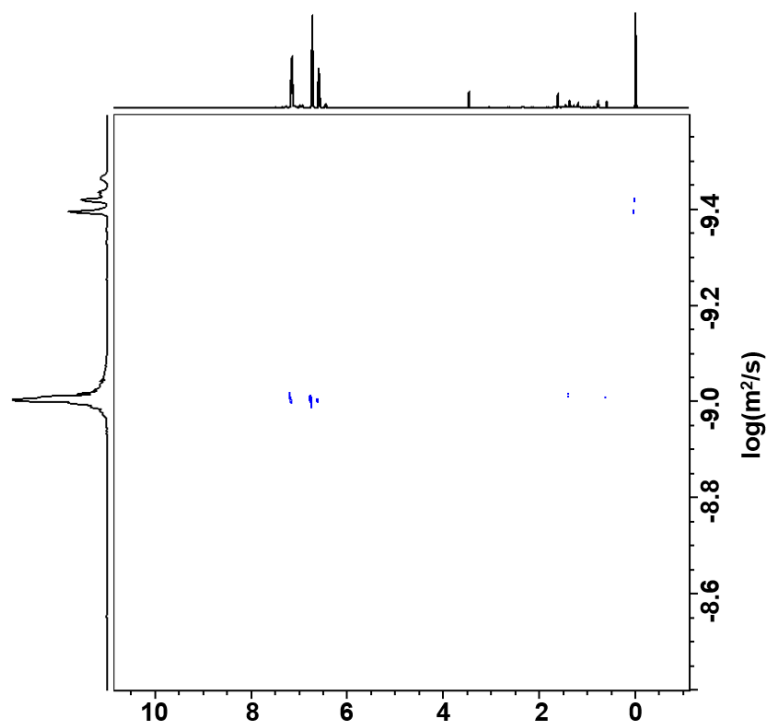


Figure S14. ^1H -DOSY NMR spectrum of $[\text{W}(\text{N}_2)(\text{P}_2^{\text{Me}}\text{PP}_2^{\text{Ph}})]$ (**2**).

Vibrational spectroscopy of $[\text{W}(\text{NNH}_2)(\text{P}_2^{\text{Me}}\text{PP}_2^{\text{Ph}})](\text{BAr}^{\text{F}})_2$ (**3-BAr^F**)

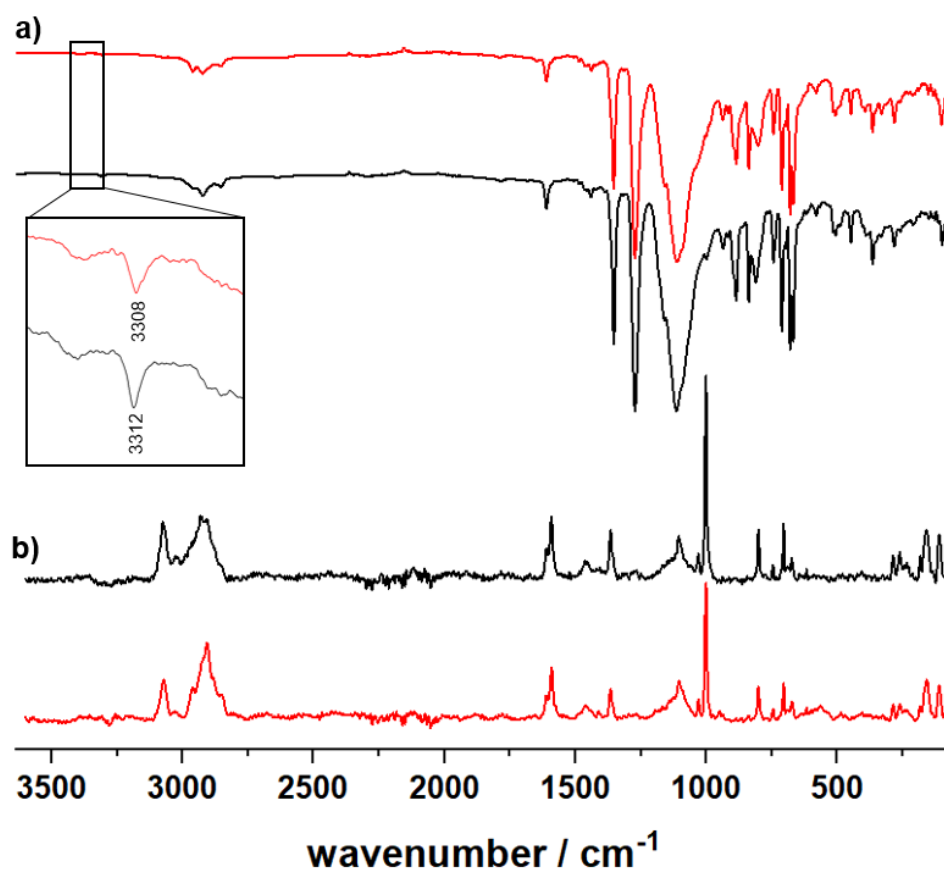


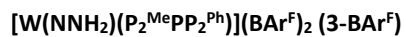
Figure S15. a) IR and b) Raman spectra of (**3-BAr^F**) (black) and $^{15}\text{N}_2$ -**3-BAr^F** (red). The enlargement shows the N-H vibrational frequency and its shift when labelling with ^{15}N isotope.

Table S7. Experimental frequencies of the Raman and IR bands of $[\text{W}(\text{NNH}_2)(\text{P}_2^{\text{Me}}\text{PP}_2^{\text{Ph}})](\text{BAr}^{\text{F}})_2$ (**3-BAr^F**) [cm^{-1}].

$[\text{W}(\text{NNH}_2)(\text{P}_2^{\text{Me}}\text{PP}_2^{\text{Ph}})](\text{BAr}^{\text{F}})_2 /$ $[\text{W}({}^{15}\text{N}^{15}\text{NH}_2)(\text{P}_2^{\text{Me}}\text{PP}_2^{\text{Ph}})](\text{BAr}^{\text{F}})_2$		NaBAr ^F		Assignment
Raman	IR	Raman	IR	
-	3312 (w) / 3308 (w)	-	-	N-H
3074 (w)	3076 (vw)	3084 (m)	-	$\nu(\text{CH})$
3023 (vw)	-	3029 (w)	-	$\nu_{\text{as}}(\text{CH}_3/\text{CH}_2)$
2960 (w)	2960 (w)	-	2967 (vw)	-
2932 (m)	2924 (m)	-	-	$\nu_{\text{s}}(\text{CH}_3/\text{CH}_2)$
2906 (m)	-	-	-	-
2882 (sh)	-	2885 (w)	-	-
2852 (w)	2853 (w)	-	-	-
-	-	2637 (vw)	2641 (vw)	-
-	-	2592 (vw)	-	-
-	-	2541 (vw)	-	-
-	1790 (vw)	-	-	-
-	-	-	1629 (w)	-
1611 (m)	1611 (m)	1611 (m)	1612 (m)	CC
1593 (s)	-	1596 (s)	-	CC
1523 (vw)	-	-	-	-
1464 (w)	-	1467 (vw)	-	-
-	1443 (w)	-	-	-
-	-	1422 (vw)	-	-
1364 (s)	1352 (s)	1367 (s)	1355 (s)	CF
-	-	1323 (vw)	-	-
-	1272 (vs)	1272 (w)	1277 (vs)	CC, CF
-	-	1197 (w)	1190 (sh)	-
-	1159 (m)	1161 (w)	1170 (m)	CC, CF
-	-	-	1139 (sh)	-
1107 (w)	1114 (vs)	1113 (w)	1115 (vs)	CC, CF
-	1092 (sh)	-	-	-
-	-	-	1063 (s)	-
1030 (w)	-	1043 (w)	-	-
1003 (vs)	998 (w)	1000 (vs)	1000 (w)	BC

-	-	-	964 (w)	-
952 (w)	-	-	-	-
939 (vw)	934 (w)	935 (w)	945 (m)	-
-	-	-	933 (m)	-
914 (vw)	918 (vw)	-	-	-
-	886 (s)	892 (w)	886 (vs)	CC
840 (vw)	838 (s)	837 (vw)	838 (s)	CC
-	809 (m)	-	-	-
801 (s)	-	801 (s)	-	CC
745 (w)	743 (m)	744 (m)	742 (m)	-
704 (s)	711 (s)	702 (s)	708 (vs)	CC
-	698 (w)	-	-	-
689 (w)	680 (s)	-	678 (vs)	CC
675 (w)	669 (s)	673 (m)	670 (vs)	-
617 (vw)	617 (vw)	-	-	-
-	609 (vw)	-	609 (vw)	-
-	580 (w)	583 (w)	582 (w)	-
-	568 (vw) / 554 (w)	-	-	W-N
-	516 (w)	-	-	-
-	507 (w)	-	505 (vw)	-
-	488 (w)	-	-	-
-	449 (m)	-	449 (m)	-
-	403 (w)	410 (m)	401 (w)	-
-	392 (w)	389 (w)	386 (w)	-
-	380 (vw)	-	-	-
-	366 (m)	-	366 (m)	CC, CF
-	353 (sh)	354 (w)	-	-
-	331 (vw)	-	-	-
-	-	321 (w)	317 (vw)	-
287 (w)	283 (w)	293 (m)	287 (w)	CC
262 (w)	259 (w)	261(w)	259 (w)	-
244 (vw)	246 (vw)	-	-	-
235 (w)	-	238 (s)	-	-
-	-	216 (w)	-	-

vw = very weak, w = weak, m = medium, s = strong, vs = very strong; v = valence, δ = deformation



NMR spectroscopy

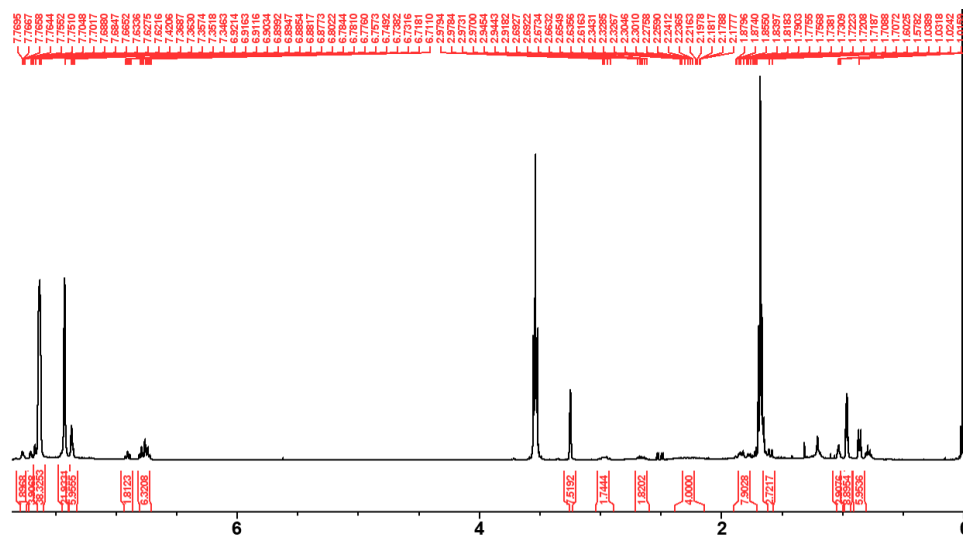


Figure S16. 1H NMR spectrum of **3-BAr^F** in diethylether- d_{10} .

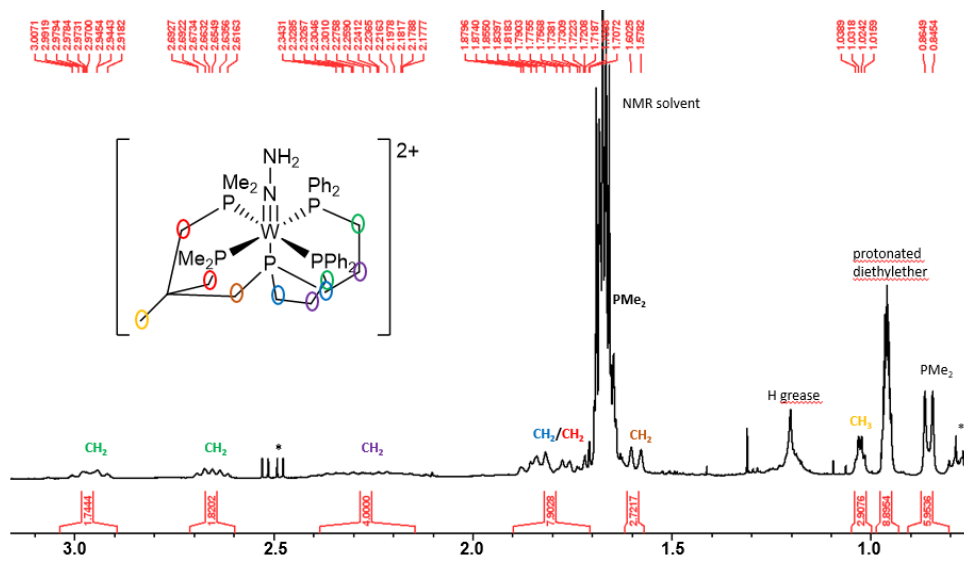


Figure S17. Enlargement of the aliphatic region of the 1H NMR spectrum of **3-BAr^F** in diethylether- d_{10} and assignment of the signals.

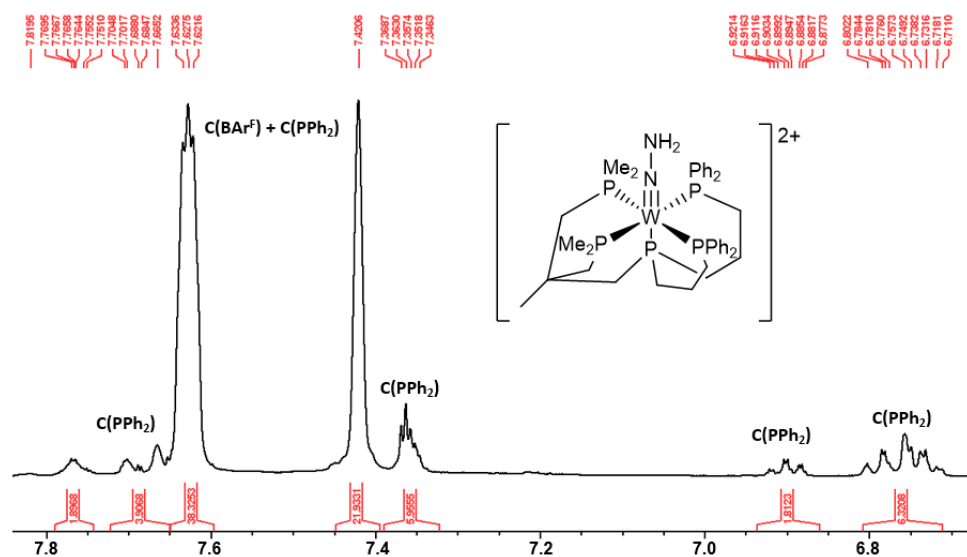


Figure S18. Enlargement of the aromatic region of the ^1H NMR spectrum of **3-BarF** in diethylether- d_{10} and assignment of the signals

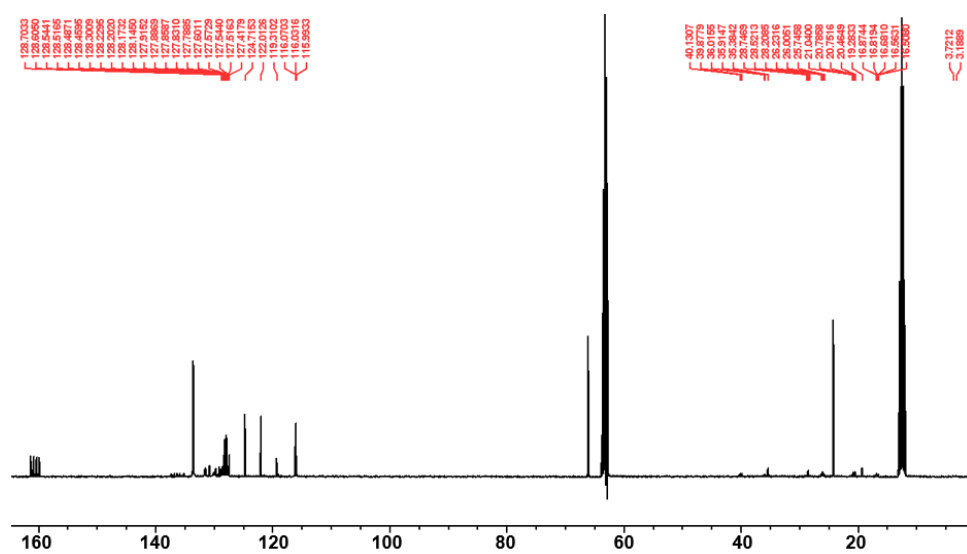


Figure S19. ^{13}C NMR spectrum of **3-BarF** in diethylether- d_{10} .

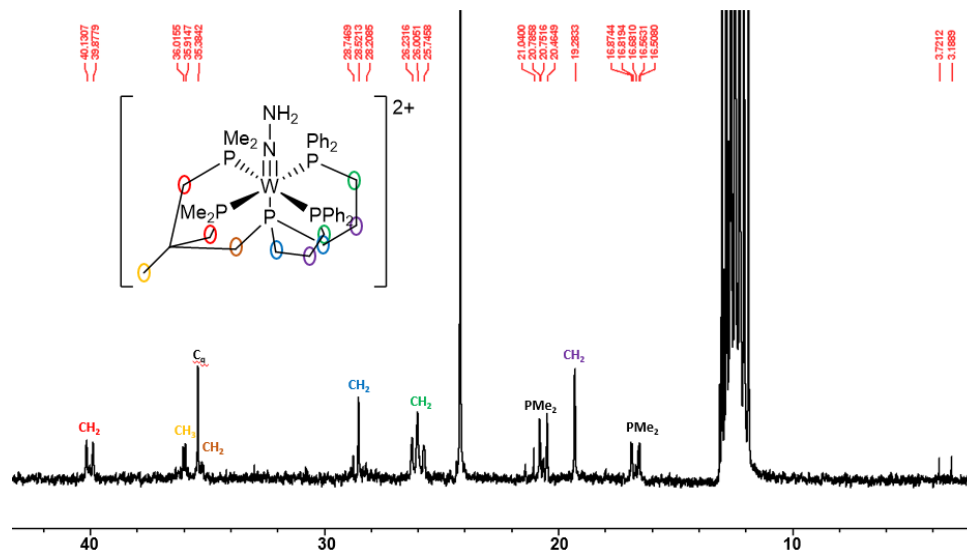


Figure S20. Enlargement of the aliphatic region of the ¹³C NMR spectrum of **3-BAr^F** in diethylether-*d*₁₀ and assignment of the signals.

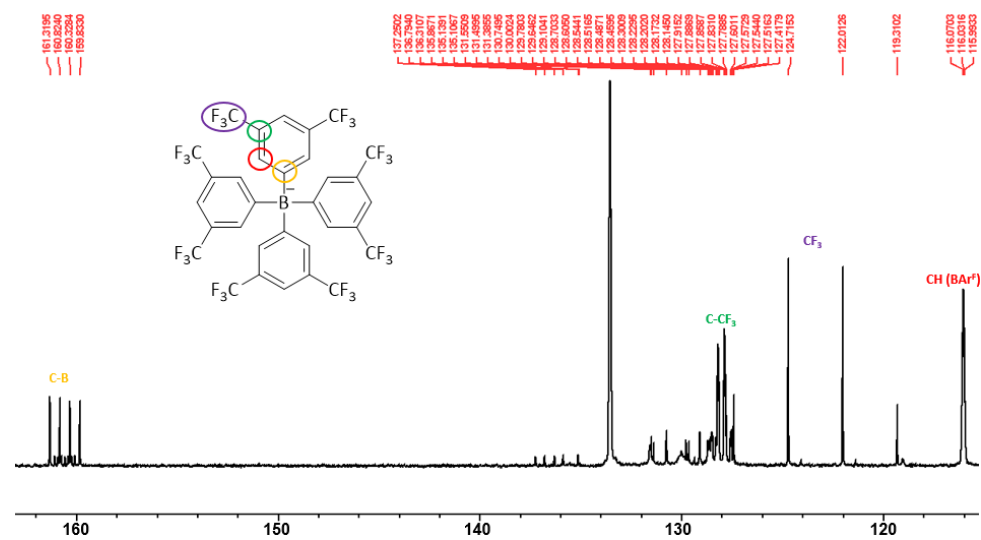


Figure S21. Enlargement of the aromatic region of the ¹³C NMR spectrum of **3-BAr^F** in diethylether-*d*₁₀ and assignment of the BAr^F-signals.

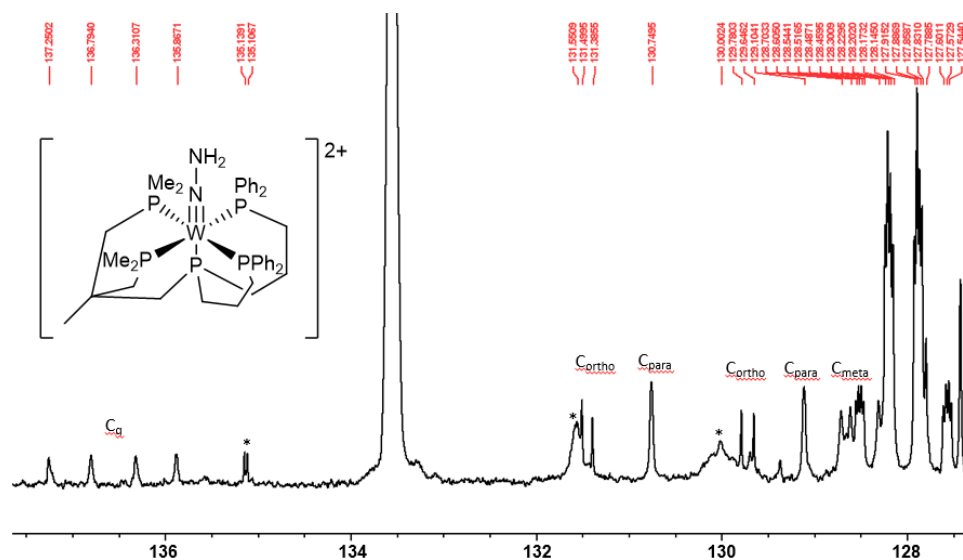


Figure S22. Enlargement of the aromatic region of the ^{13}C NMR spectrum of **3-Bar^F** in diethylether- d_{10} and assignment of the diphenylphosphine signals.

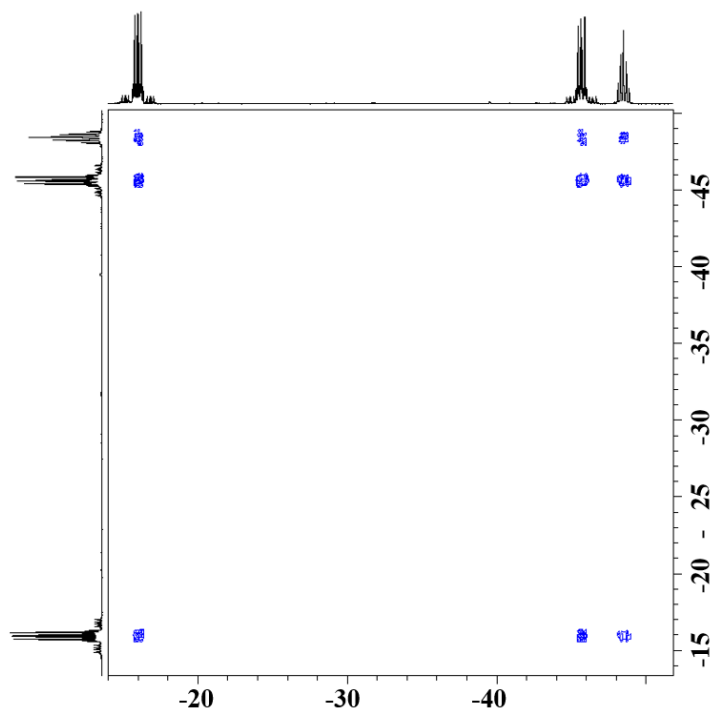


Figure S23. ^{31}P - ^{31}P -COSY spectrum of **3-BAr^F** in diethylether- d_{10} .

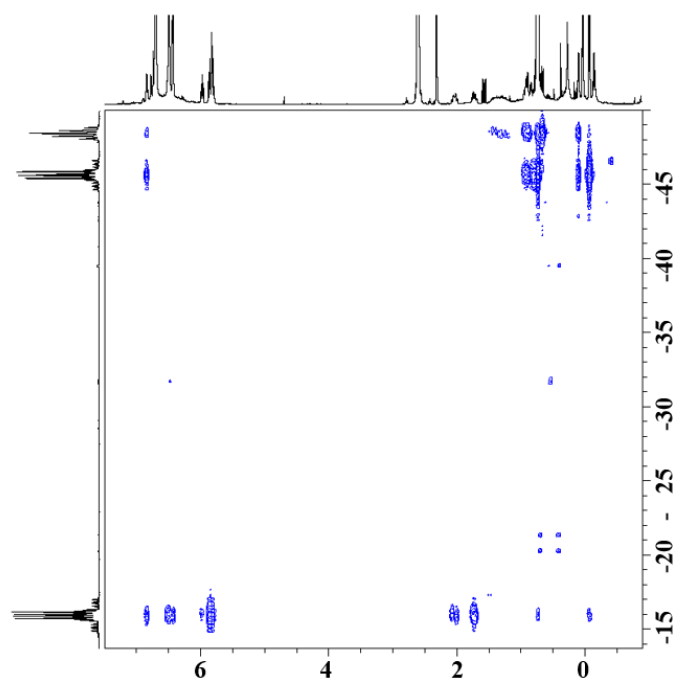


Figure S24. ^1H - ^{31}P -HMBC spectrum of **3-BAr^F** in diethylether- d_{10} .

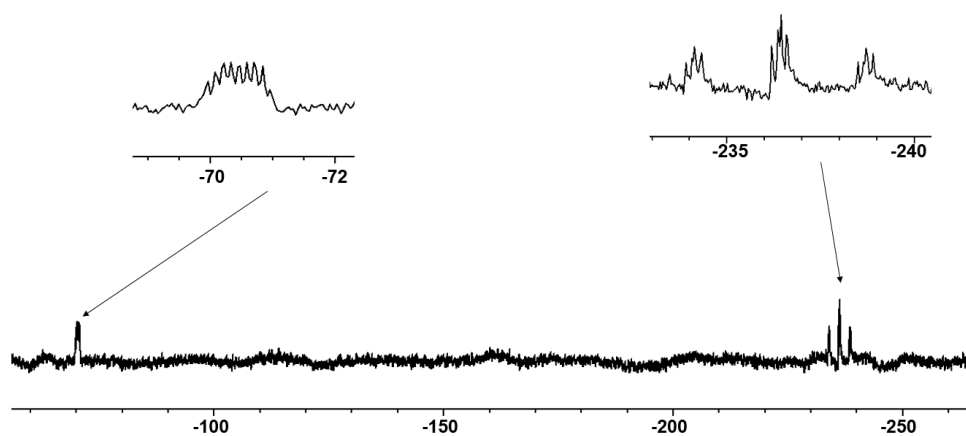


Figure S25. ^{15}N NMR spectrum of **3-BAr^F** in diethylether- d_{10} .

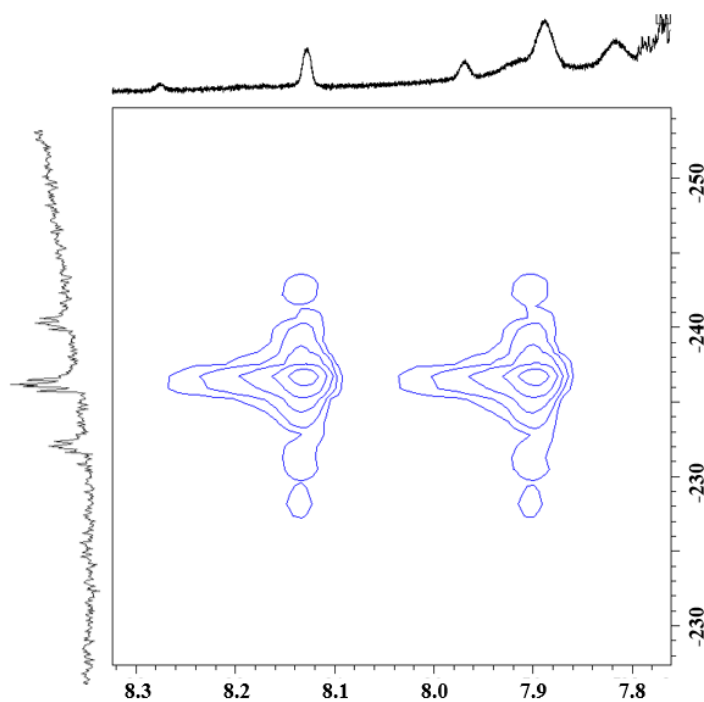


Figure S26. ^1H - ^{15}N -HMBC spectrum of **3-BAr^F** in diethylether- d_{10} .

Table S8. Comparison of ^{15}N - ^{31}P , ^{15}N - ^{15}N and ^1H - ^{15}N coupling constants of $[\text{Mo}(^{15}\text{N}^{15}\text{NH}_2)(\text{P}_2^{\text{Me}}\text{P}_2^{\text{Ph}})][\text{BAr}^{\text{F}}]_2$ ^[2] and $[\text{W}(^{15}\text{N}^{15}\text{NH}_2)(\text{P}_2^{\text{Me}}\text{P}_2^{\text{Ph}})][\text{BAr}^{\text{F}}]_2$ (**^{15}N -3-BArF**). The A, X and M designations of the phosphorus nuclei refer to Fig. 6

Complex	<i>J</i> /Hz							
	<i>J</i> (P _A -N _α)	<i>J</i> (P _A -N _β)	<i>J</i> (P _X -N _α)	<i>J</i> (P _X -N _β)	<i>J</i> (P _M -N _α)	<i>J</i> (P _M -N _β)	<i>J</i> (N _α -N _β)	<i>J</i> (H-N _β)
[Mo¹⁵N¹⁵NH₂]	5.9	-	6.3	-	23.2	7.6	11.2	94.6
¹⁵N-3-BAr^F	5.0	0.5	5.5	0.5	20.4	6.6	10.5	92.0

[Mo¹⁵N¹⁵NH₂] = $[\text{Mo}(^{15}\text{N}^{15}\text{NH}_2)(\text{P}_2^{\text{Me}}\text{P}_2^{\text{Ph}})][\text{BAr}^{\text{F}}]_2$



NMR spectroscopy

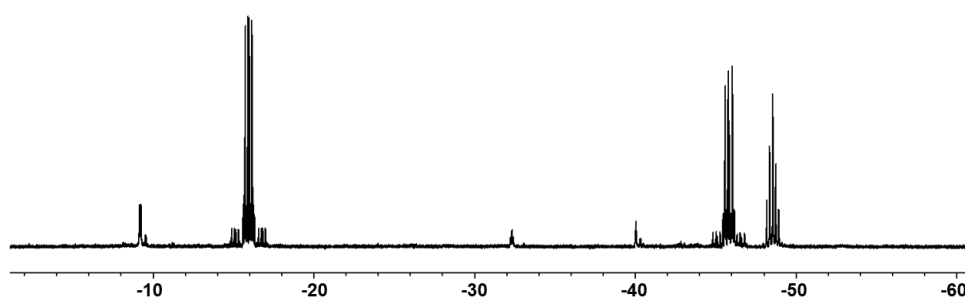


Figure S27. ^{31}P NMR spectrum of **3-Al(pftb)₄** in diethylether- d_{10} .

Catalytic Experiments

To a mixture of 3.6 ml 0.1 M $\text{SmI}_2(\text{THF})_2$ solution (360 μmol) in THF and 1.4 mL of 0.26 M H_2O (360 μmol) in THF was added 2 μmol of $[\text{W}(\text{N}_2)(\text{P}^{\text{Me}}_2\text{PP}^{\text{Ph}}_2)]$ (**2**) dissolved in 1 ml of THF and stirred until the dark blue solution turned yellow. Ammonia present in the reaction solution was driven with a stream of N_2 through a glass bridge into a cold trap (cooled with acetone/ N_2) filled with 15 mL 2 M ethereal HCl solution. To drive off remaining ammonia 20 mL of a 0.125 M solution of NaOH in methanol was added to the reaction solution. Thereby the reaction solution was heated to 60° C. After expulsion of all NH_3 the solvent was removed from the cold trap *in vacuo*. The resulting NH_4Cl was quantified by the Berthelot reaction.

DFT calculations

Cartesian coordinates of $[W(N_2)(P_2^{Me}PP_2^{Ph})]$ (**2**). Units are presented in Å.

Atom	Coordinates (Å)		
	X	Y	Z
H	-6.61769237943842	-3.55589612095695	2.09109886691751
C	-6.51553701941306	-2.48048063844388	2.00057949031877
C	-7.35454725287299	-1.63760298042026	2.71623650354543
H	-8.10980573611169	-2.05255630128992	3.37439743395388
C	-7.22472443954043	-0.26392866883899	2.59669522235916
H	-7.87315455240053	0.37544369997916	3.18395620912508
C	-6.26976157669984	0.28896521555142	1.74567352796594
C	-5.42952500283083	-0.56445402897565	1.04254661508719
H	-4.69105324852686	-0.13583757858759	0.37571395159931
C	-5.54744418711505	-1.94010312595627	1.16969711495411
H	-4.88930471879246	-2.58967916978783	0.60440439829226
H	-9.00001852762539	-2.86897620537550	-1.15967014810372
C	-8.34510249317739	-2.02422082896486	-1.33841520300985
C	-8.67737402030631	-0.76715992835512	-0.85486757446903
H	-9.59213583514926	-0.62455066737744	-0.29102158737361
C	-7.82698122990991	0.30314333857141	-1.06938748146425
H	-8.07537302383302	1.27373774051868	-0.66037627458174
C	-6.63686307529212	0.15269644364817	-1.77584576885737
C	-6.31856113898773	-1.11254680625014	-2.26142849076683
H	-5.39796148683469	-1.26755806737154	-2.80887975166288
C	-7.16325919080892	-2.19126065134605	-2.04079924072346
H	-6.88831312535339	-3.17045675580827	-2.41689426268507
C	-4.33662549271118	0.87968053297606	-3.17368856730828
C	-3.13368228994258	0.42394148836476	-2.64036548073945
H	-2.94866727931480	0.52757410606127	-1.58176024993208
C	-2.16066121673825	-0.14539072389062	-3.44828468574658
H	-1.23229688056975	-0.48852639457724	-3.00599482885942
C	-2.37119384397537	-0.26387971495906	-4.81402191018667
H	-1.60801168690625	-0.69613439039059	-5.45093724632249
C	-3.56981033173938	0.17357548571053	-5.35768568112064
H	-3.74958564715962	0.08075912513737	-6.42296438517687
C	-4.54531152500091	0.73053416210821	-4.54396549156972
H	-5.47316610184209	1.05355135672042	-4.99696798091939
C	-5.49884396336963	2.99045198117306	5.63716147332622
C	-6.07737106525697	2.85927954917004	4.38088641261548
H	-7.08592450245652	3.22575331204655	4.23652140175442
C	-5.36705445593536	2.30189920310580	3.32163341442670
C	-4.06905007693688	1.85020231921068	3.56236613747005
H	-3.50023816378950	1.40304403239283	2.75568219537401
C	-3.49472620830462	1.96835068098132	4.81637719426579
H	-2.48530823371728	1.60735065402186	4.97907969385821
C	-4.20447524347541	2.55026630870514	5.85912285323487
H	-3.75210719331759	2.65384271855211	6.83848299343066
H	-6.06527364645254	3.44393609926177	6.44301056024351
P	-6.00486050012249	2.10926304648966	1.59760584125503

P	-5.56683613123230	1.64188952885101	-2.02470874829756
W	-4.68091869378206	3.05797114393275	-0.22369205572781
P	-6.34648317883831	4.71145743107627	-0.66758702940202
C	-7.72741255055597	2.73941345530844	1.79431703067911
C	-7.84832467096710	4.26074313773150	1.74081906932185
H	-8.14945376876445	2.36376534671908	2.72777335890347
H	-8.32068376121900	2.29118158552777	0.99513150105695
C	-7.90637741149028	4.82555606222422	0.32929593482439
H	-7.02917623981423	4.71839618789684	2.29909293368552
H	-8.76647807338264	4.55266643493717	2.26194188212797
H	-8.21852148585068	5.87540897551788	0.34917216701177
H	-8.67595091501194	4.28659662016342	-0.23270611345029
C	-7.14752855912238	4.78053370312396	-2.32856844847091
C	-7.71058689026087	3.43788843020562	-2.77010862010769
H	-6.40430482684841	5.12450825494646	-3.05334741864091
H	-7.93767771707569	5.53921795363826	-2.29753026803488
C	-6.65823347715667	2.46910638392894	-3.28826095767288
H	-8.43421226674406	3.60842802604769	-3.57395283049663
H	-8.28168010699860	2.97929424724666	-1.95664645946940
H	-6.00318621876832	3.00169945928348	-3.98069080227010
H	-7.14848701563092	1.67481778882867	-3.85547977024483
P	-3.71333770792500	4.77129524029579	1.22109838029220
P	-3.36097043834920	4.21515472941073	-1.90075723797010
C	-3.26499527035780	3.87861785732611	-3.70907660991184
H	-4.25317278491693	3.87862907986290	-4.16544327027465
H	-2.80333099397373	2.90893481562719	-3.88921838309855
H	-2.66157198152750	4.65470389592459	-4.18717336068717
C	-1.54044749145397	4.21943759830546	-1.63195069079055
H	-1.28090175152940	4.65415658295462	-0.66959778541807
H	-1.02291181014253	4.76731121812404	-2.42310215957001
H	-1.19664681715231	3.18299930018391	-1.63330652605773
C	-2.07520395795524	4.43492775750185	1.97755077497380
H	-1.40374408004217	3.94157234468041	1.27723027235265
H	-2.22774324912922	3.75926493079087	2.82057183413561
H	-1.61746126043243	5.35702873949799	2.34329474893360
C	-4.49736452150748	5.47200878305762	2.73340143946669
H	-5.43082153214684	5.97496734491007	2.48100131083181
H	-3.82242917723817	6.20580544842248	3.18099166859077
H	-4.70511618625721	4.69245917752798	3.46182282273746
C	-3.73718445628500	6.02305108486650	-2.06251023197807
C	-4.25820952087494	6.74885760939306	-0.81840365706868
H	-4.46260875924427	6.12508513133831	-2.87590137623900
H	-2.82186706051670	6.51834244874750	-2.40763207929942
C	-3.38121153553309	6.40131929455201	0.39071301334541
H	-3.49025117290810	7.18016543905913	1.15195536479070
H	-2.33334443652139	6.42547074785151	0.07836658177717
C	-5.74987943613399	6.46802101280744	-0.54906476852002
H	-6.35603304514243	7.06631535482142	-1.23974309194804
H	-5.99274417290129	6.83042743098403	0.45496966093072
C	-4.12269187784869	8.25217030591906	-1.06961679158340
H	-3.07088326032924	8.53621095299057	-1.16391296231700
H	-4.55611136289402	8.82524128852779	-0.24502936282674

H	-4.63652269109007	8.54145421157537	-1.99074064007066
N	-3.10934012682751	1.90378320277536	0.25302384229692
N	-2.18819330334162	1.33204662971555	0.55468770105485

Cartesian coordinates of $[W(NNH_2)(P_2^{Me}PP_2^{Ph})]^{2+}$ (3**). Units are presented in Å.**

Atom	Coordinates (Å)		
	X	Y	Z
H	-6.44611592751000	-3.56001051906125	2.27875716728885
C	-6.38385986394194	-2.48782909642135	2.13774141233729
C	-7.16491389462714	-1.63866531297679	2.90975859024004
H	-7.83490136524710	-2.04535171943689	3.65748716830348
C	-7.07821304508500	-0.26805385047996	2.73887793873879
H	-7.66669447196178	0.37684436911047	3.38095864745393
C	-6.22373322240910	0.27051550220756	1.77671984730274
C	-5.44788111065274	-0.58776020564825	1.00764059534234
H	-4.80755161727347	-0.18075632418805	0.23664140192632
C	-5.52435930721107	-1.96033668613495	1.18757756756771
H	-4.92218231307873	-2.61903296085495	0.57346376760251
H	-8.88507599532738	-2.95714545840823	-1.14435151297273
C	-8.25276524875633	-2.09634257243749	-1.32408392501407
C	-8.65392581211440	-0.83783598637946	-0.89810473034938
H	-9.59987317324336	-0.71291281249599	-0.38526907810306
C	-7.84142010394083	0.25805995187629	-1.12618717455043
H	-8.16024265625338	1.23303030184074	-0.78066202366713
C	-6.62449705442263	0.11848300005425	-1.78832400009129
C	-6.23206289585702	-1.14601304603268	-2.21789970101467
H	-5.29232283368914	-1.28108147677671	-2.73715904469657
C	-7.04408369085814	-2.24606956316916	-1.98400481286412
H	-6.72811748582786	-3.22494372572508	-2.32433706893053
C	-4.33894207801734	0.92811841803423	-3.24421385543259
C	-3.07039601673779	0.60486759418684	-2.76951688936536
H	-2.81973321410372	0.76601767754826	-1.73151672877849
C	-2.10806552746700	0.08386072118973	-3.62168698974437
H	-1.12682237433205	-0.16483731133430	-3.23495840781023
C	-2.39902270189256	-0.11630511909128	-4.96253486950568
H	-1.64581471648059	-0.51550833357952	-5.63088934584344
C	-3.66453928277813	0.18920246608500	-5.44244195292770
H	-3.90479276772317	0.02535071293638	-6.48597735387809
C	-4.63035690264280	0.69966917518519	-4.58957123817924
H	-5.61230754736382	0.91191316766994	-4.99127590977165
C	-5.71792819161504	3.09820764548655	5.65487563737754
C	-6.23300710400182	2.92804904847081	4.37633425324427
H	-7.24989850605206	3.24569981934598	4.18632154581655
C	-5.45008372107663	2.37383536503928	3.36741388698254
C	-4.15528399454860	1.95989322544099	3.67742346412000
H	-3.54776273086323	1.49041878196041	2.91246593519925
C	-3.64414180192499	2.11973873884216	4.95375194342781
H	-2.64005878210376	1.78168226676452	5.18225231458763

C	-4.42230761702164	2.70303394994940	5.94554060325168
H	-4.02422587264799	2.83399833869431	6.94420683238585
H	-6.33777509163393	3.53827957602065	6.42679555410785
P	-6.03750593923301	2.08019992801514	1.66099786114708
P	-5.60672972296713	1.59717966718270	-2.11429016115325
W	-4.56432862597741	2.94279735346837	-0.19201076710801
P	-6.36525656567961	4.80161682136784	-0.64984487487712
C	-7.75132240531194	2.71856953823488	1.70716199019126
C	-7.87970250773703	4.23954926061069	1.73268877102210
H	-8.23710133038714	2.28257266622508	2.58088957791039
H	-8.27257530655117	2.30497621874127	0.84289561763675
C	-7.90095048277641	4.87654156832761	0.35390793158262
H	-7.09731368694076	4.68192157262478	2.35096306139575
H	-8.82299457604507	4.49612021116494	2.22212054979281
H	-8.17203865090952	5.93448306830863	0.42360690259446
H	-8.68146218666456	4.40200498522843	-0.24734509785702
C	-7.08673118139648	4.82335530709216	-2.32910345694727
C	-7.71202204312294	3.50490720882680	-2.75719189686704
H	-6.31651391627986	5.12452448860981	-3.04233649376132
H	-7.83691742499310	5.62077627431689	-2.32380669285813
C	-6.71396324329782	2.49351023818142	-3.29301069686889
H	-8.42302049551804	3.71570427018786	-3.56008418047572
H	-8.31169339838887	3.07496043954083	-1.95017686893260
H	-6.07125585940574	2.97863388111126	-4.02870586423216
H	-7.25567710913040	1.70540628607714	-3.81865284347018
P	-3.68720356100495	4.79633945299553	1.27051100939035
P	-3.35153815535037	4.22957383656737	-1.99823143589010
C	-3.35619147978324	3.92552782522534	-3.79755652529189
H	-4.35983218021453	3.97288293743758	-4.21481068425610
H	-2.92504367244743	2.95353016468203	-4.02673446193288
H	-2.75209858332830	4.70387012457645	-4.26967894693823
C	-1.55545098362535	4.11706235302993	-1.70822350891113
H	-1.27729298260380	4.50353794829896	-0.73149535949387
H	-1.01856352763649	4.67524900817462	-2.47782309563546
H	-1.26425582488867	3.06686614787645	-1.76554475723915
C	-2.08661144769171	4.32302660584606	1.99664348998939
H	-1.41831486686645	3.90784319967835	1.24475467754604
H	-2.26963396169923	3.57682289901203	2.77022537177901
H	-1.61447191914245	5.19339392067607	2.45648092407760
C	-4.50872554516531	5.47292081802218	2.75191348311219
H	-5.44818927665925	5.96080039670723	2.49565248286042
H	-3.84850767456659	6.22019730249644	3.19709460887873
H	-4.70431045912619	4.69304722155812	3.48283974910240
C	-3.71113587421370	6.03745321104187	-2.05469772694204
C	-4.18591345780953	6.75292926520183	-0.78865193829543
H	-4.43528952023833	6.19168810642375	-2.85947577751060
H	-2.78542786282497	6.50892565260267	-2.40165293194641
C	-3.29781648223018	6.37133748825367	0.40108405472161
H	-3.34849531600462	7.15845261819973	1.15839084887691
H	-2.25643107140141	6.33767719704115	0.07175421430061
C	-5.67695514839105	6.50382661324668	-0.49571593869734
H	-6.28196824887330	7.12044744500046	-1.16918034599792

H	-5.90570050129491	6.85659998958415	0.51336667651865
C	-4.02505819316659	8.25725053413274	-1.02298852121873
H	-2.97057902945778	8.52206111027586	-1.12677590472053
H	-4.43438278086187	8.82889340943490	-0.18686453172525
H	-4.54275403036947	8.57032017472487	-1.93259771831382
N	-3.29248025860450	1.80098084724780	0.25640427836244
N	-2.34844451026759	0.95481237419498	0.59927638543027
H	-1.57128491858506	1.34962899603508	1.11402585361593
H	-2.67932040257316	0.06429381774471	0.95549017341570

References

- [1] S. Hinrichsen, A. Kindjajev, S. Adomeit, J. Krahmer, C. Näther, F. Tuczek, *Inorg. Chem.* **2016**, *55*, 8712.
- [2] T. A. Engesser, A. Kindjajev, J. Junge, J. Krahmer, F. Tuczek, *Chem. Eur. J.* **2020**, *26*, 14807.

Supplementary Material to:**Molybdenum tricarbonyl complexes supported by linear PNP ligands: Influence of P- and N-substituents on relative stability, stereoisomerism and on the activation of small molecules**

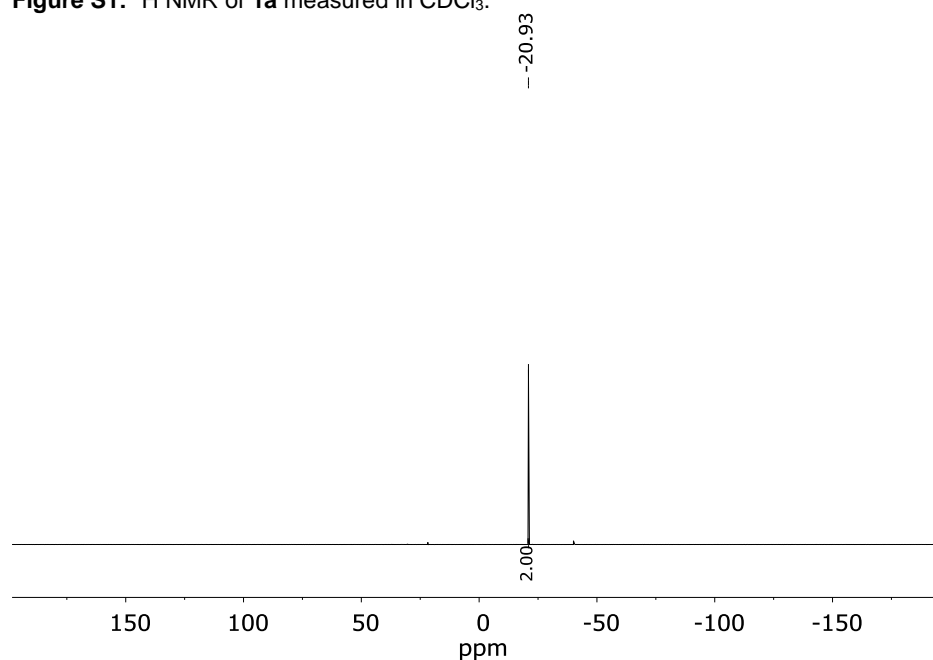
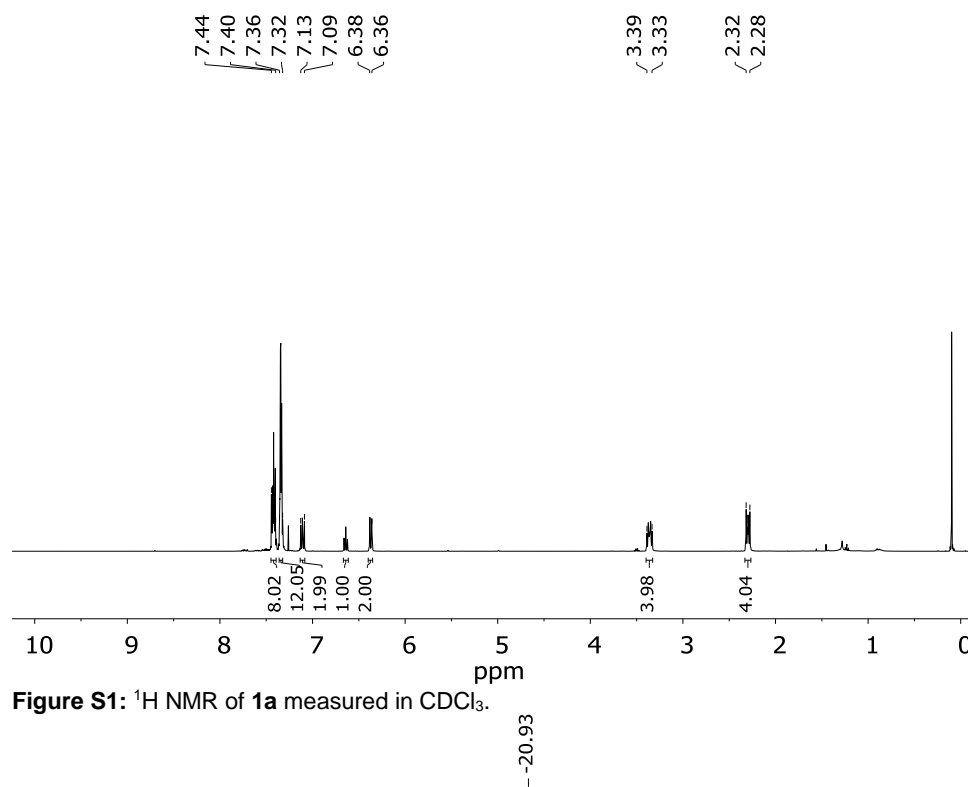
Sven Froitzheim,^[a] Jannik Junge,^[a] Christopher Barnehl,^[a] Tobias A. Engesser,^{*[a]} Jan Krahmer,^[a] Christian Näther^[a] and Felix Tuczek^{*[a]}

Contents

1. IR and NMR spectra of the ligands	2
1.1. Spectra of $\text{PN}^{\text{Ph}}\text{P}^{\text{Ph}}$ (1a).....	2
1.2. Spectra of $\text{PN}^{\text{Ph}}\text{P}^{\text{Me}}$ (1b)	4
1.3. Spectra of $\text{PN}^{\text{Ph}}\text{P}^{\text{Et}}$ (1d)	6
1.4. Spectra of $\text{PN}^{\text{Ph}}\text{P}^{\text{In}}$ (1d)	8
1.5. Spectra of $\text{PN}^{\text{Ph}}\text{P}^{\text{Cyp}}$ (1e)	10
1.6. Spectra of $\text{PN}^{\text{Ph}}\text{P}^{\text{iPr}}$ (1f).....	12
1.7. Spectra of $\text{PN}^{\text{Ph}}\text{P}^{\text{Cy}}$ (1g).....	14
1.8. Spectra of $\text{PN}^{\text{Ph}}\text{P}^{\text{tBu}}$ (1h)	16
2. IR, Raman and NMR spectra of the complexes	18
2.1. Spectra of $[\text{Mo}(\text{CO})_3(\text{PN}^{\text{Ph}}\text{P}^{\text{Ph}})]$ (2a).....	18
2.2. Spectra of $[\text{Mo}(\text{CO})_3(\text{PN}^{\text{Ph}}\text{P}^{\text{Et}})]$ (2c)	20
2.3. Spectra of $[\text{Mo}(\text{CO})_3(\text{PN}^{\text{Ph}}\text{P}^{\text{Cyp}})]$ (2e)	22
2.4. Spectra of $[\text{Mo}(\text{CO})_3(\text{PN}^{\text{Ph}}\text{P}^{\text{iPr}})]$ (2f).....	24
2.5. Spectra of $[\text{Mo}(\text{CO})_3(\text{PN}^{\text{Ph}}\text{P}^{\text{Cy}})]$ (2g).....	26
2.6. ABX Spin Systems of the Complexes.....	28
2.7. <i>fac-mer</i> -ratios of the complexes	31
3. Calculations	32
3.1. Optimized Structures of the Complexes	32
3.2. Metal-ligand bond lengths of the calculated facial and meridional $[\text{Mo}(\text{CO})_3(\text{PN}^{\text{Ph}}\text{P}^{\text{R}})]$ complexes (R = Ph, Et, ⁱ Pr, Cy, ^t Bu).....	38
3.3. Energy calculations for <i>fac</i> - and <i>mer</i> - $[\text{Mo}(\text{CO})_3(\text{PN}^{\text{R}}\text{P}^{\text{R}})]$ complexes	39
3.4. Relative free energies	41
3.5. Energy calculations of the relative Gibbs energies for the <i>fac-mer</i> -transformations.....	43
4. Crystal structure determination of $[\text{Mo}(\text{CO})_3(\text{PN}^{\text{Ph}}\text{P}^{\text{Et}})]$ (2c)	47
5. References	49

1. IR and NMR spectra of the ligands

1.1. Spectra of $\text{PN}^{\text{Ph}}\text{P}^{\text{Ph}}$ (**1a**)



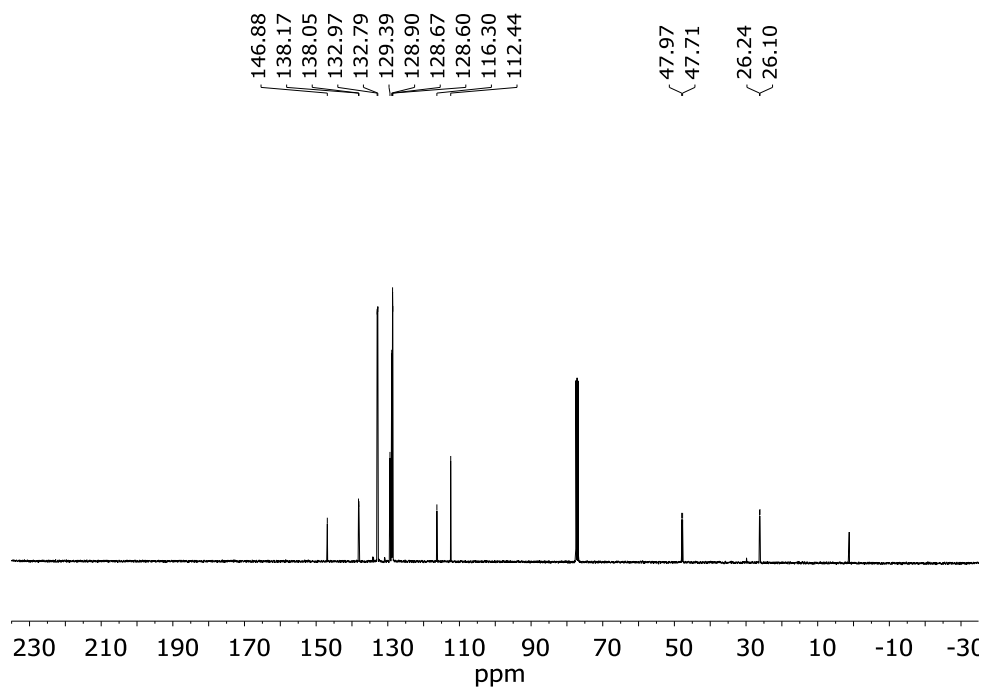


Figure S3: ^{13}C NMR of **1a** measured in CDCl_3 .

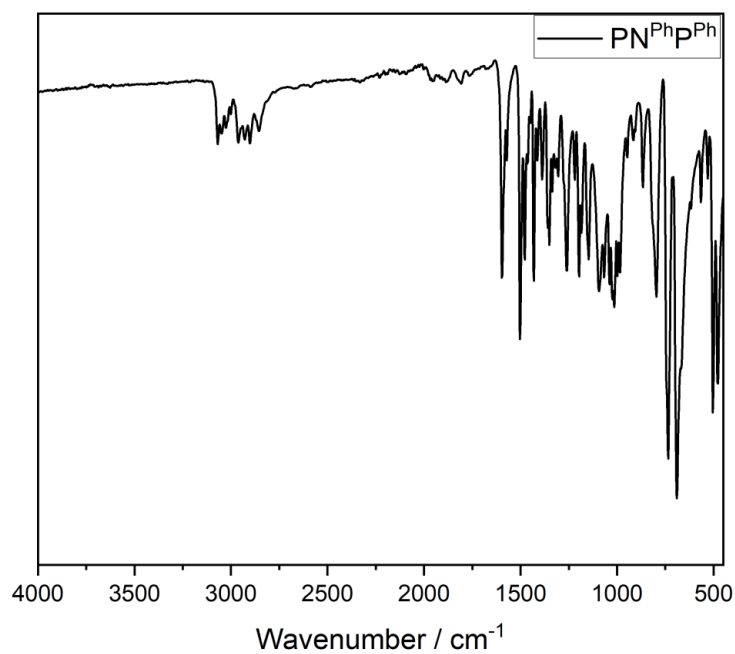


Figure S4: Solid state IR of **1a**.

1.2. Spectra of $\text{PN}^{\text{Ph}}\text{P}^{\text{Me}}$ (**1b**)

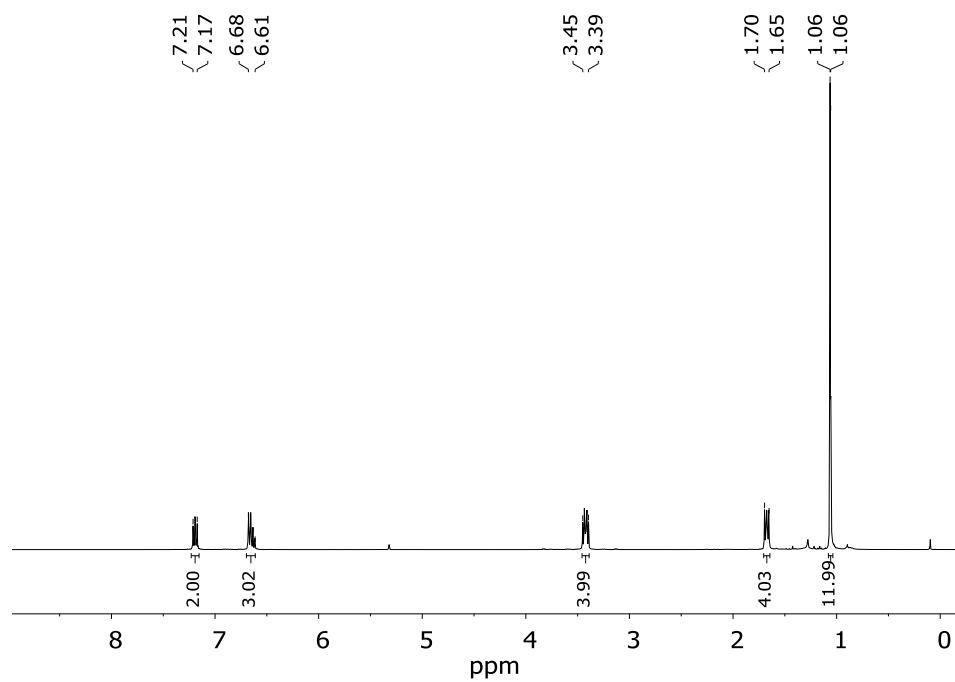


Figure S5: ^1H NMR of **1b** measured in CD_2Cl_2 .

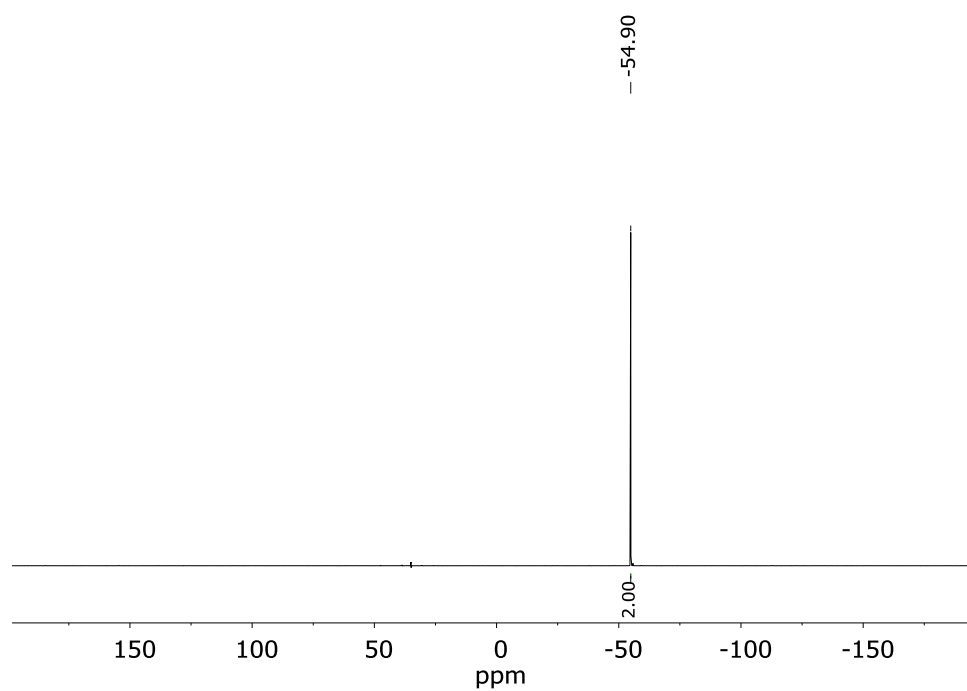


Figure S6: ^{31}P NMR of **1b** measured in CD_2Cl_2 .

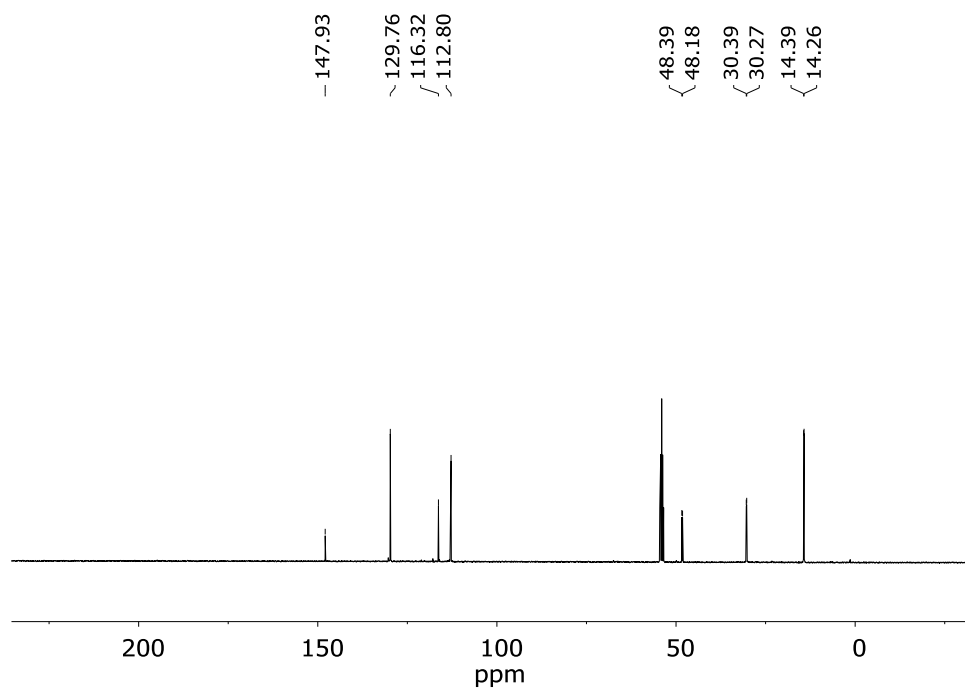


Figure S7: ^{13}C NMR of **1b** measured in CDCl_3 .

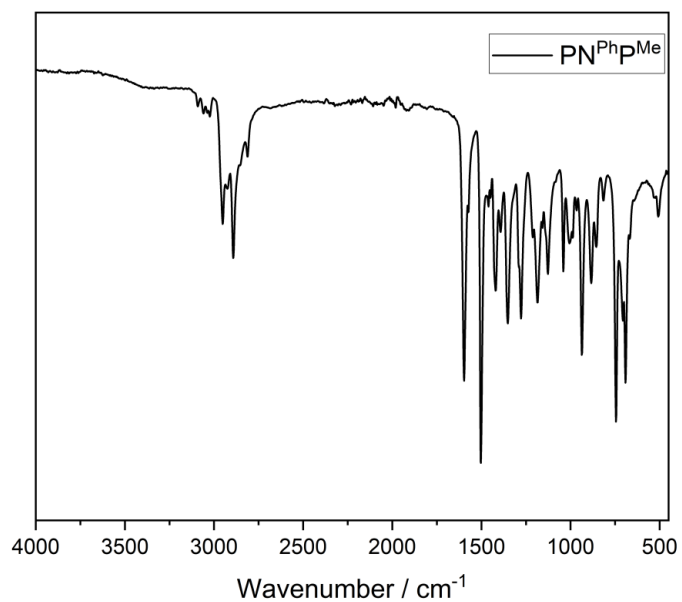


Figure S8: Solid state IR of **1b**.

1.3. Spectra of $\text{PN}^{\text{Ph}}\text{P}^{\text{Et}}$ (1d)

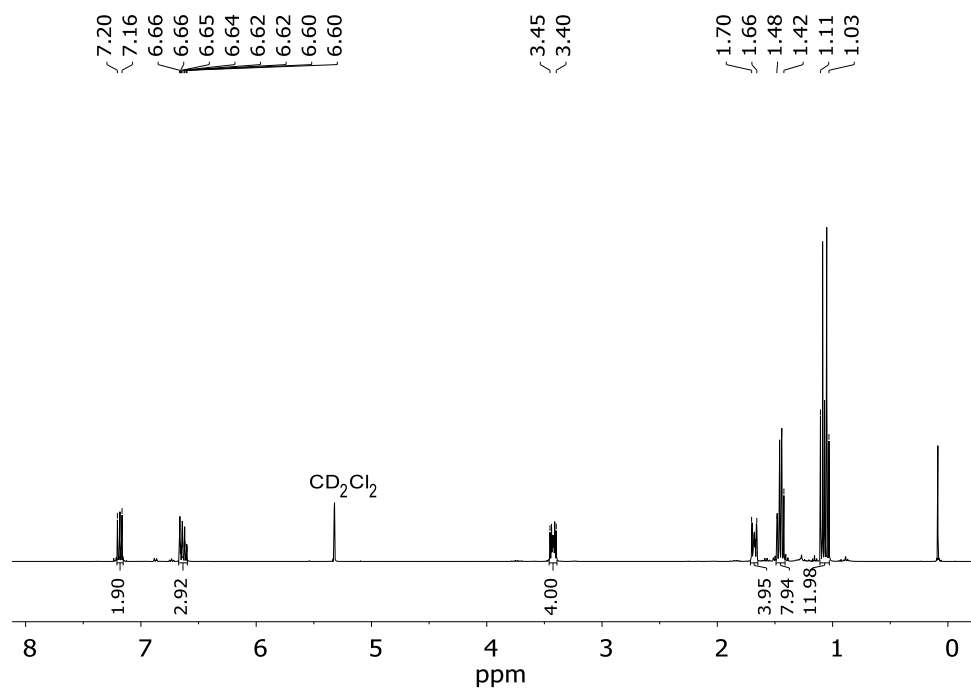


Figure S9: ^1H NMR of **1c** measured in CD_2Cl_2 .

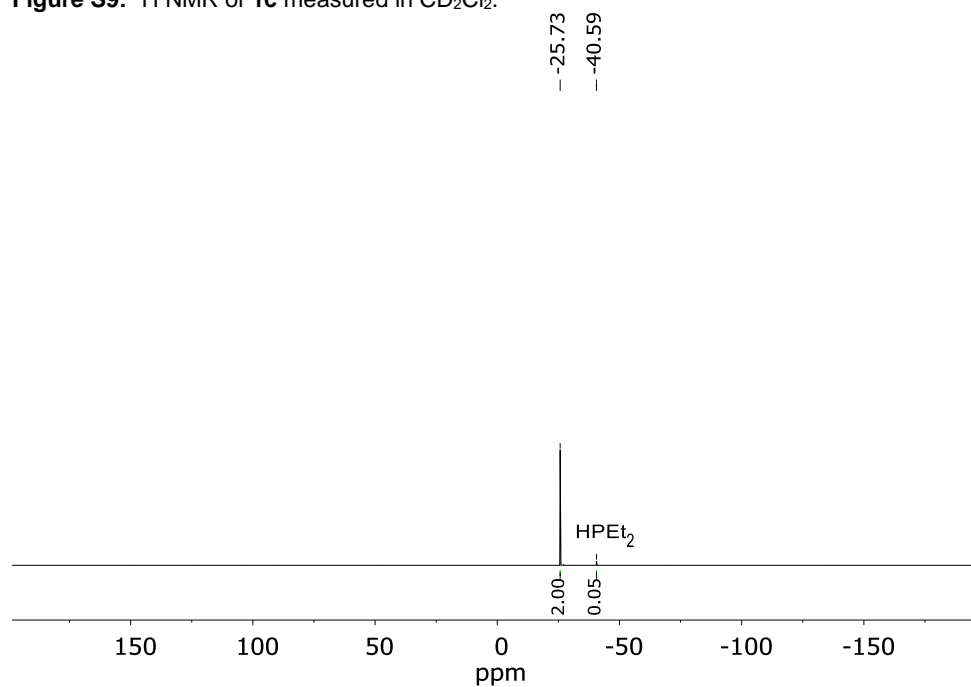


Figure S10: ^{31}P NMR of **1c** measured in CD_2Cl_2 .

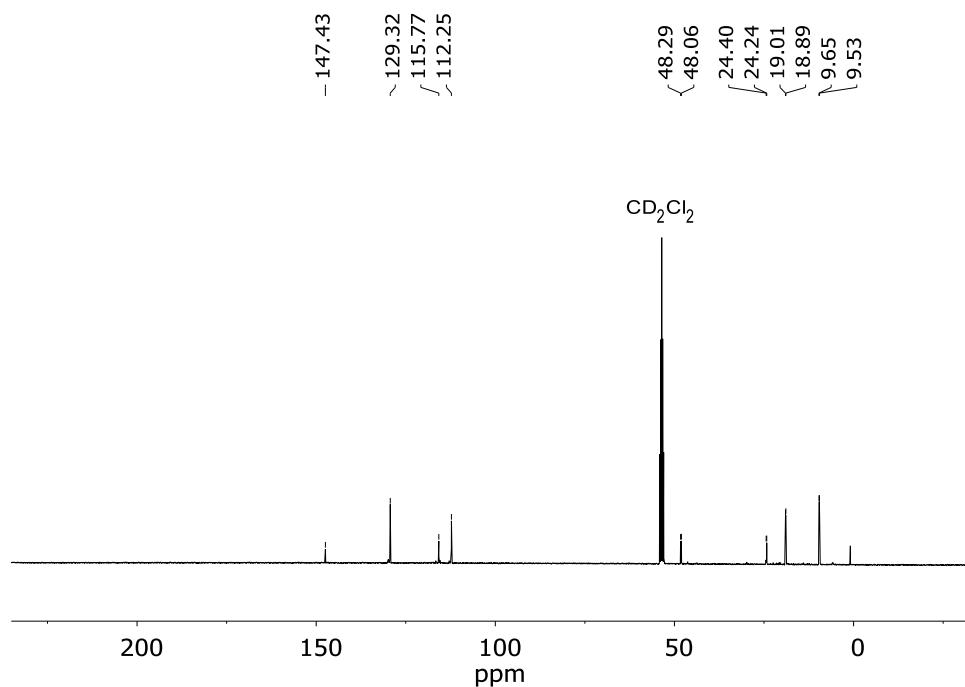


Figure S11: ¹³C NMR of **1c** measured in CD₂Cl₂.

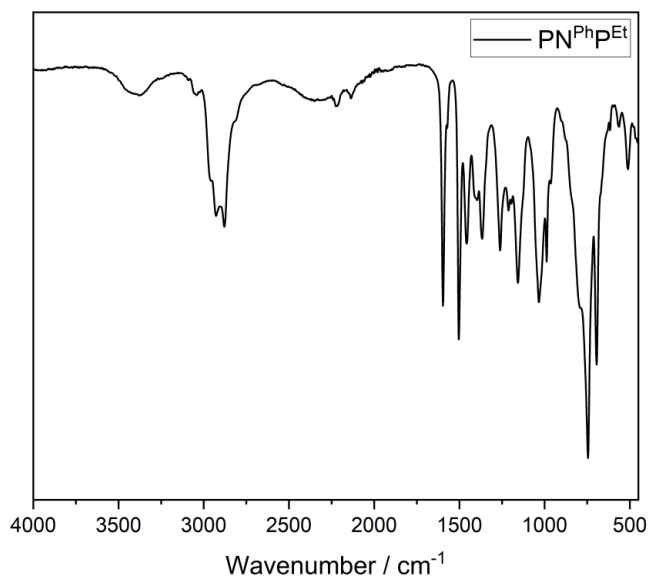


Figure S12: Solid state IR of **1c**.

1.4. Spectra of $\text{PN}^{\text{Ph}}\text{P}^{\text{Pln}}$ (**1d**)

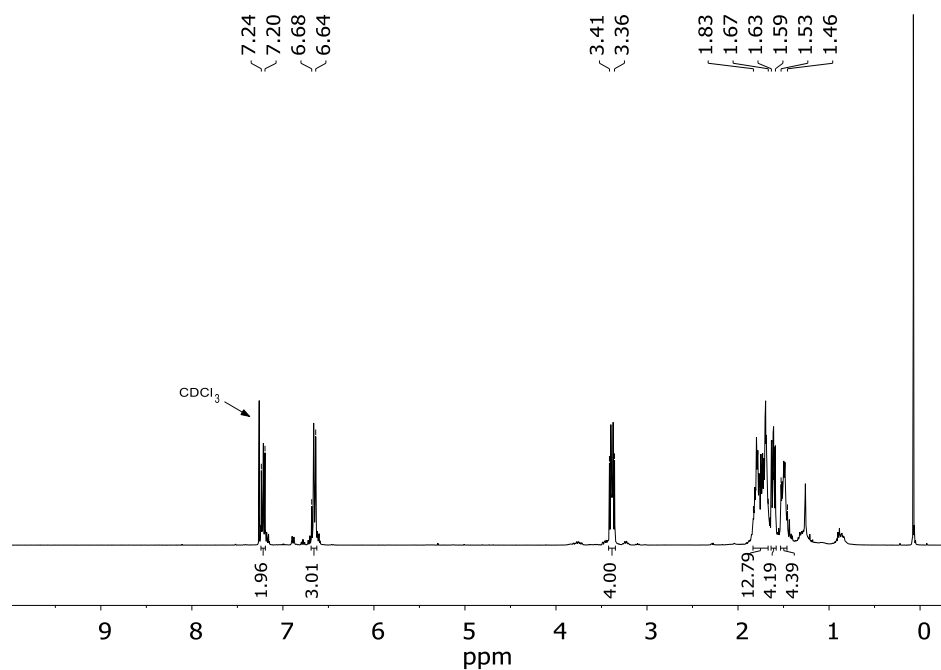


Figure S13: ^1H NMR of **1d** measured in CDCl_3 .

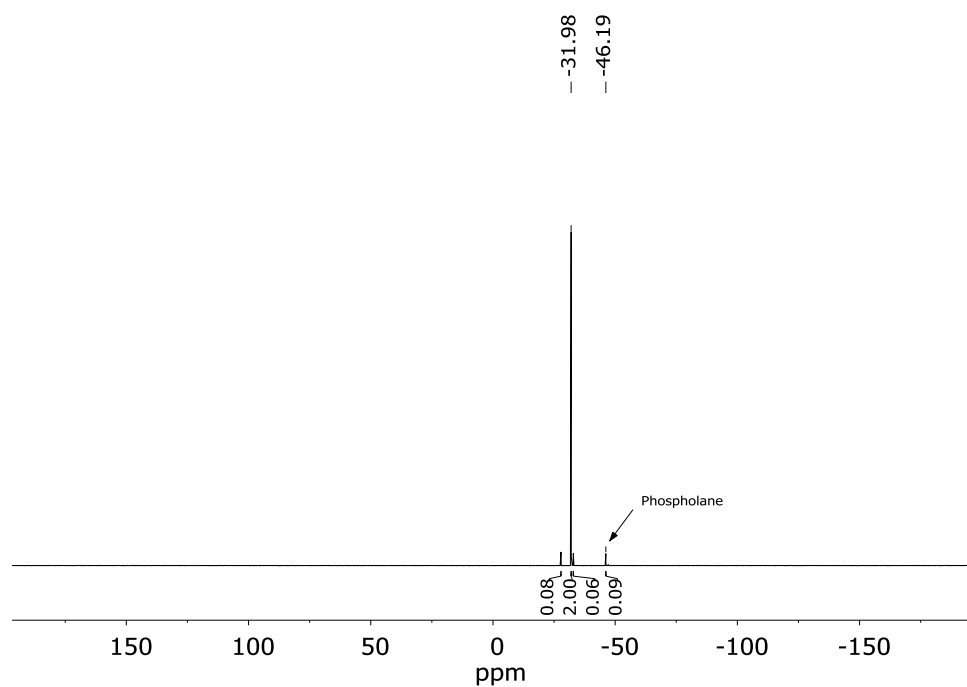


Figure S14: ^{31}P NMR of **1d** measured in CDCl_3 .

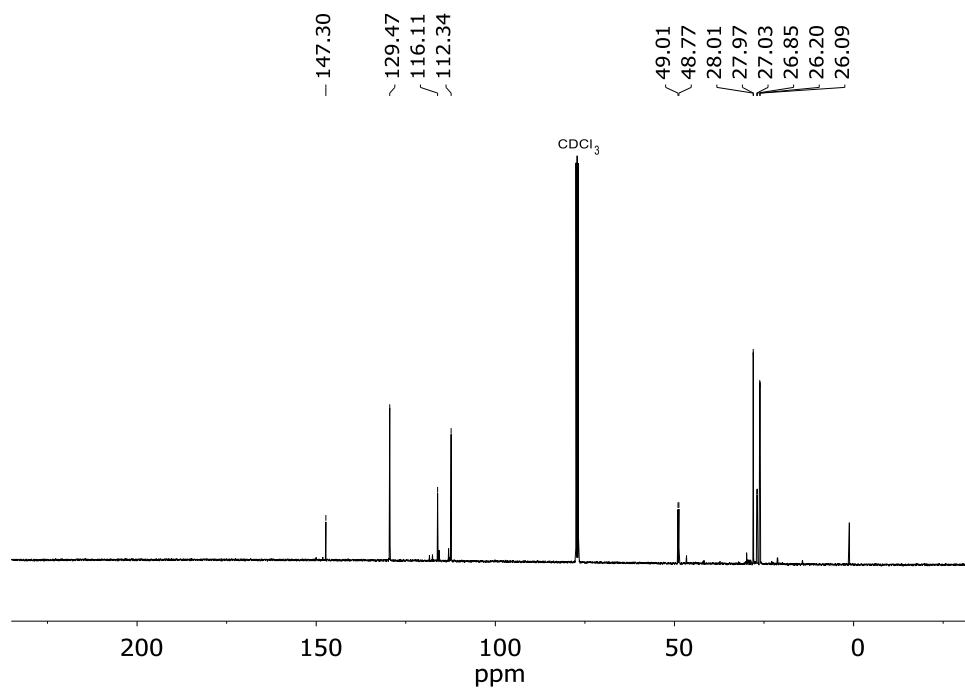


Figure S15: ^{13}C NMR of **1d** measured in CDCl_3 .

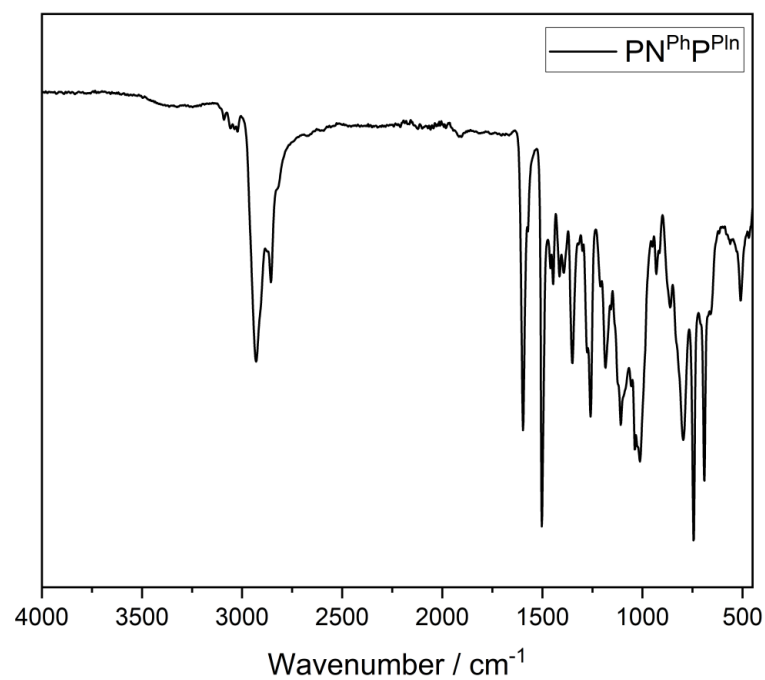


Figure S16: Solid state IR of **1d**.

1.5. Spectra of $\text{PN}^{\text{Ph}}\text{P}^{\text{Cyp}}$ (**1e**)

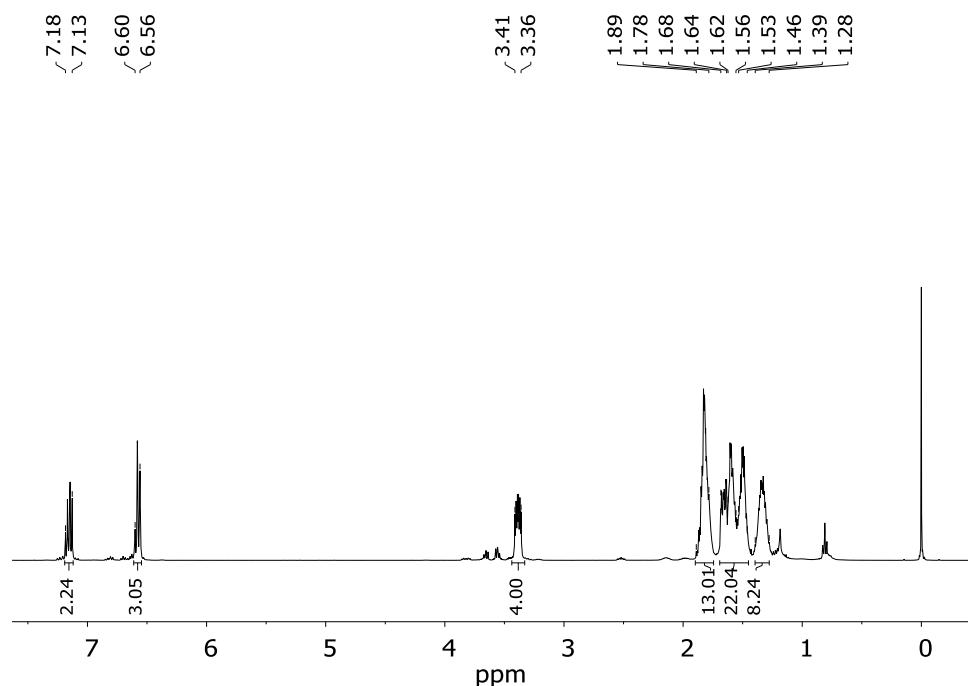


Figure S17: ^1H NMR of **1e** measured in CDCl_3 .

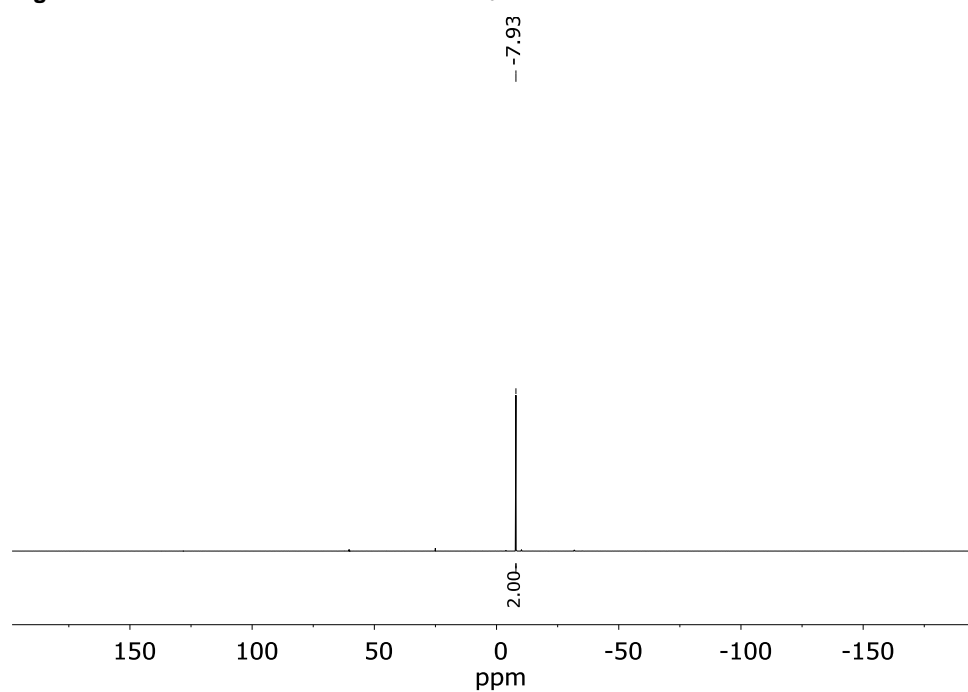
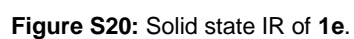
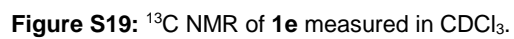


Figure S18: ^{31}P NMR of **1e** measured in CDCl_3 .



1.6. Spectra of $\text{PN}^{\text{Ph}}\text{P}^{\text{iPr}}$ (**1f**)

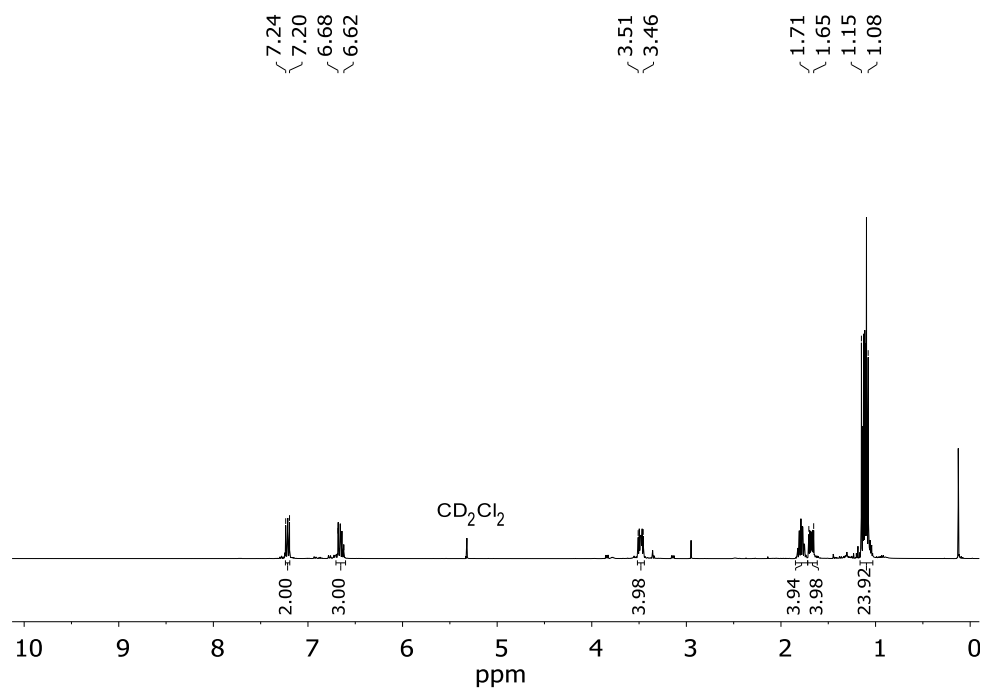


Figure S21: ^1H NMR of **1f** measured in CD_2Cl_2 .

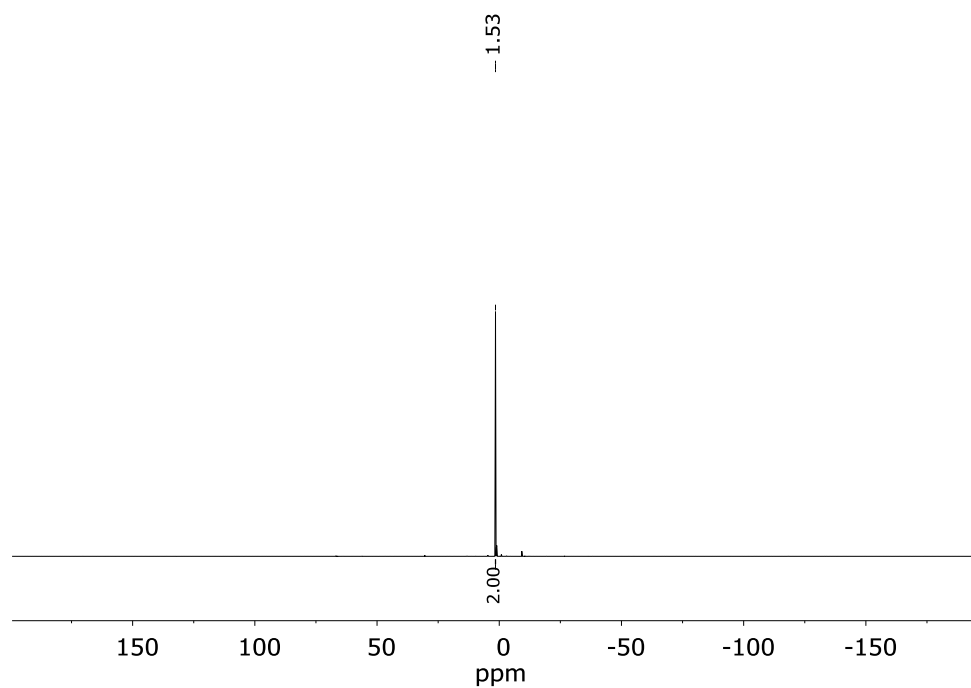


Figure S22: ^{31}P NMR of **1f** measured in CD_2Cl_2 .

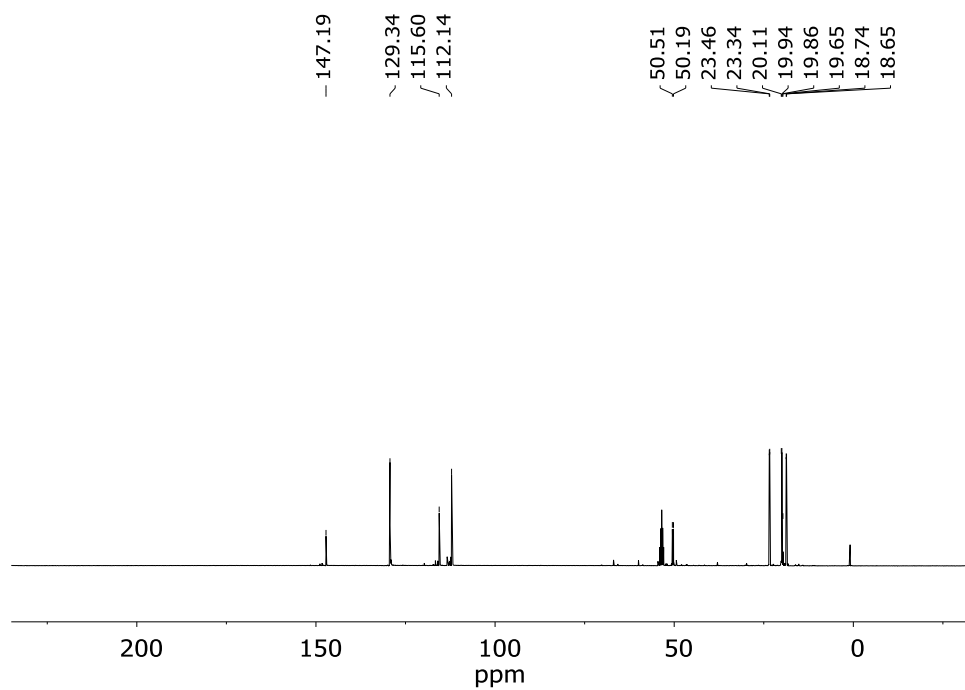


Figure S23: ^{13}C NMR of **1f** measured in CD_2Cl_2 .

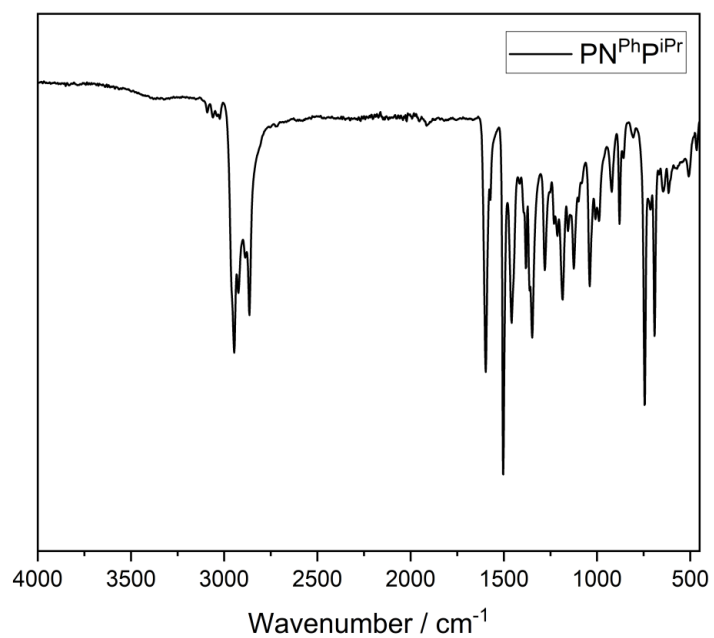


Figure S24: Solid state IR of **1f**.

1.7. Spectra of $\text{PN}^{\text{Ph}}\text{P}^{\text{Cy}}$ (**1g**)

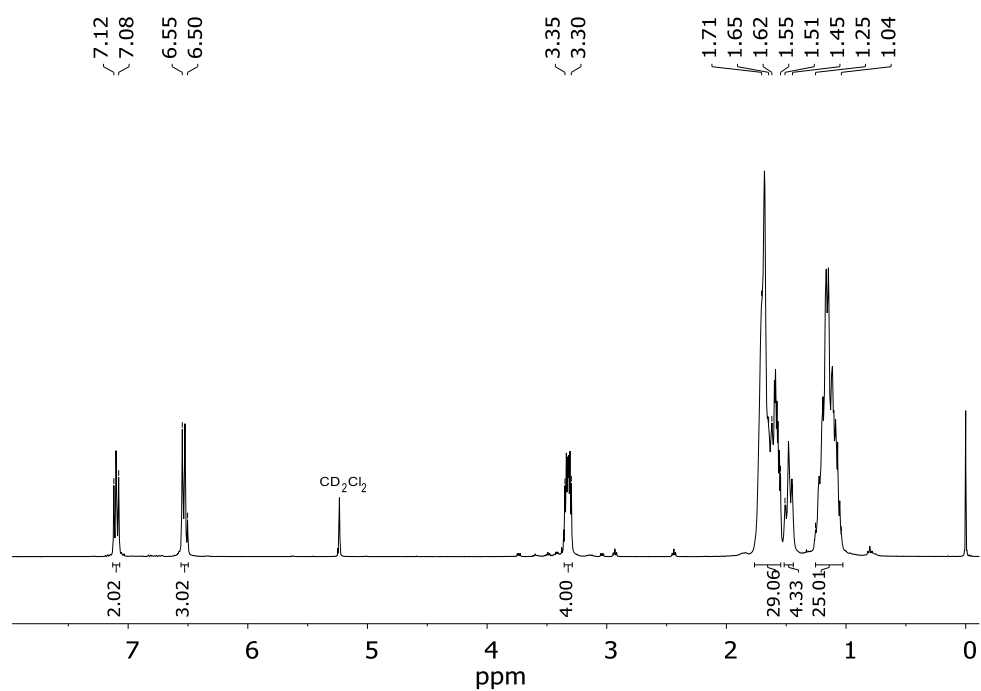


Figure S25: ^1H NMR of **1g** measured in CD_2Cl_2 .

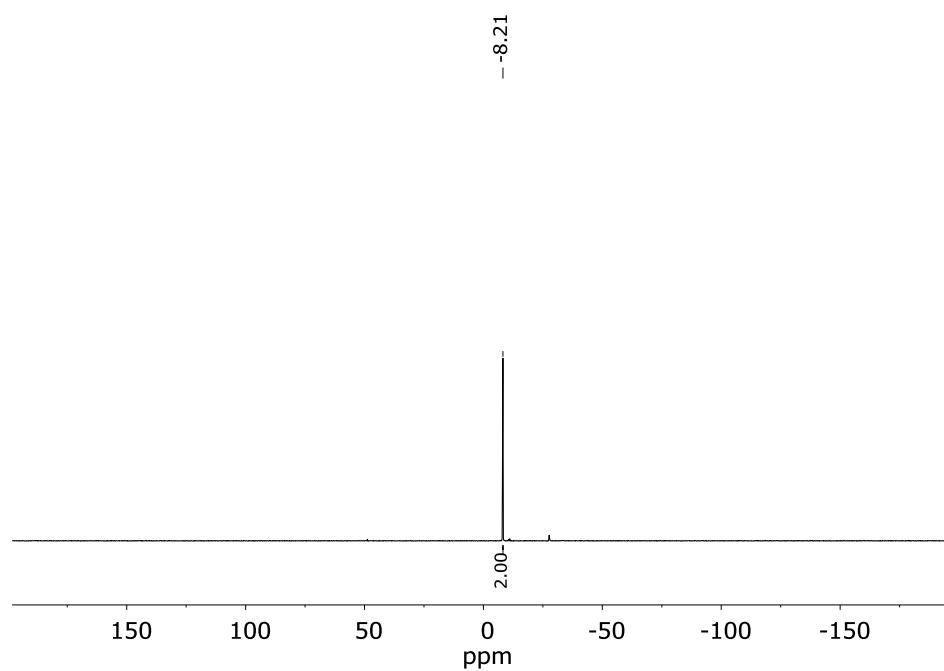


Figure S26: ^{31}P NMR of **1g** measured in CD_2Cl_2 .

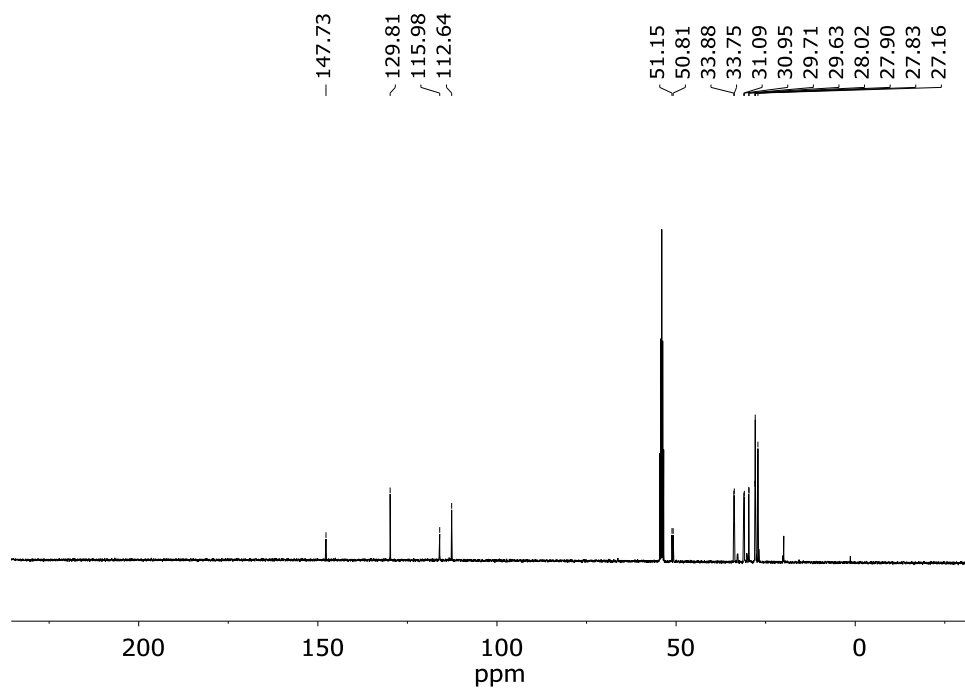


Figure S27: ^{13}C NMR of **1g** measured in CD_2Cl_2 .

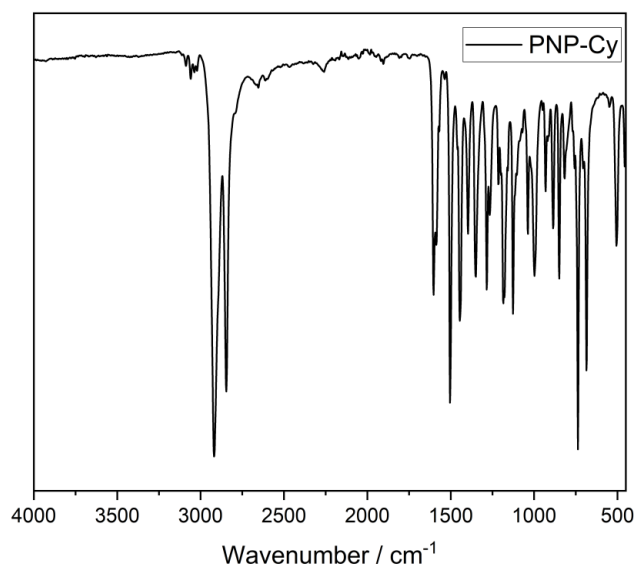


Figure S28: Solid state IR spectrum of **1g**.

1.8. Spectra of $\text{PN}^{\text{Ph}}\text{P}^{\text{tBu}}$ (**1h**)

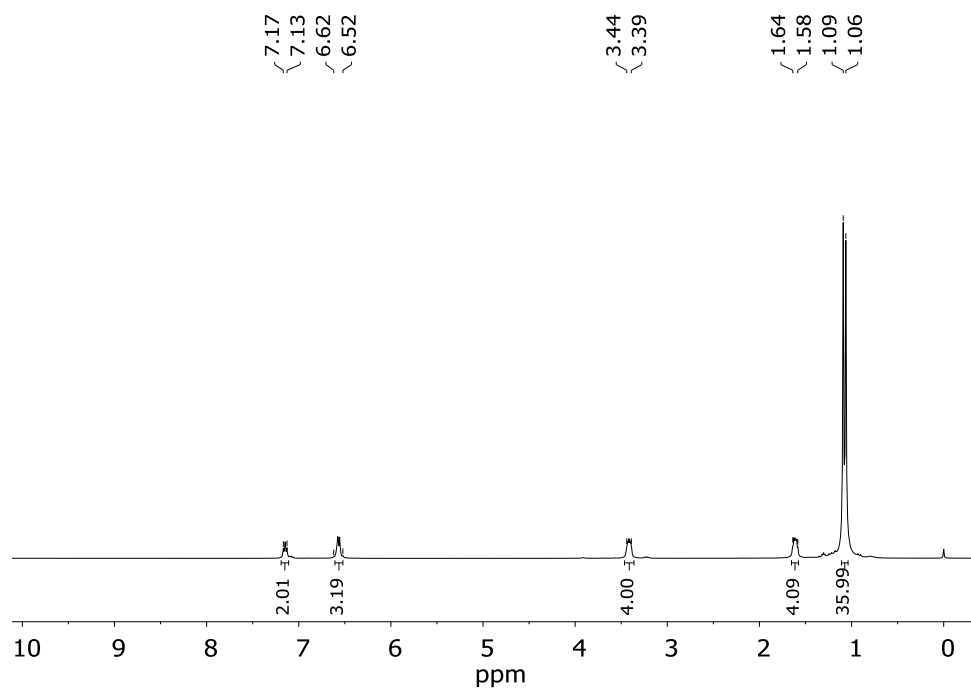


Figure S29: ^1H NMR of **1h** measured in CDCl_3 .

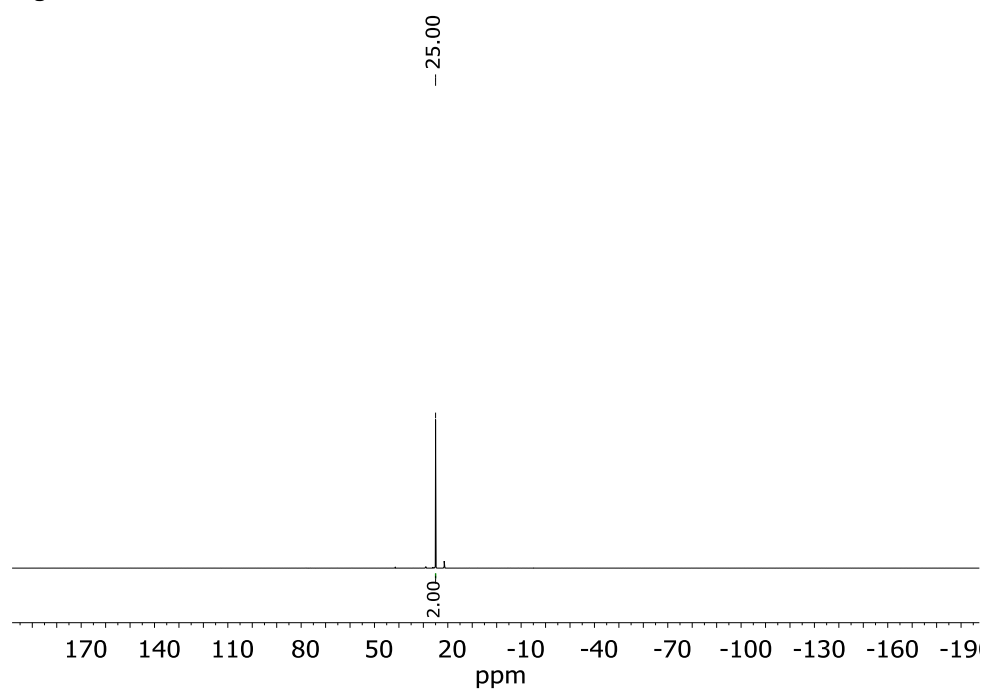


Figure S30: ^{31}P NMR of **1h** measured in CDCl_3 .

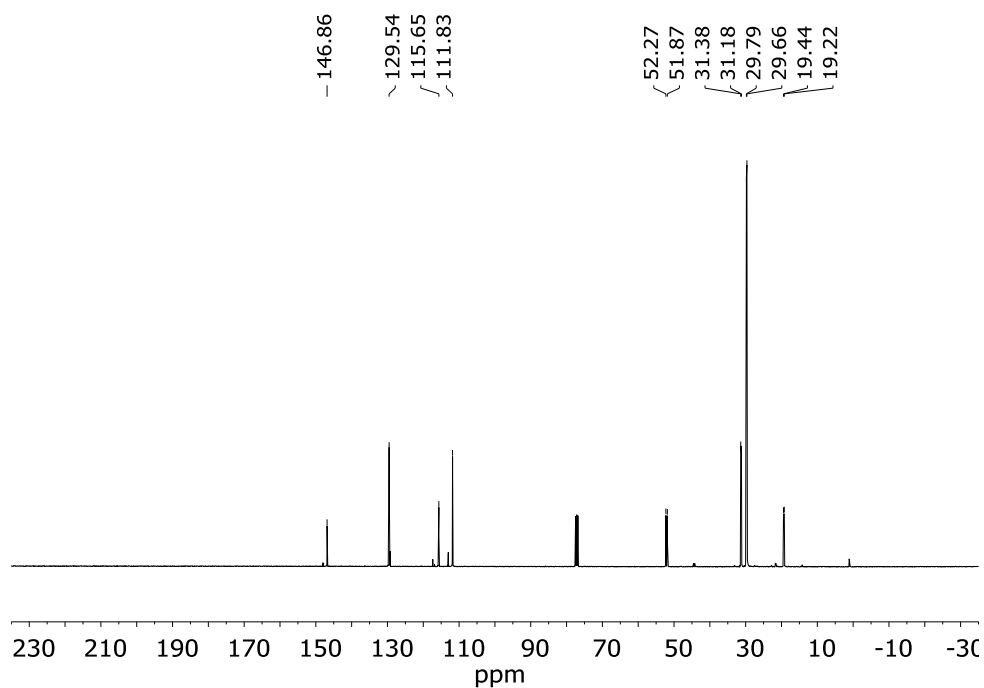


Figure S31: ^{13}C NMR of **1h** measured in CDCl_3 .

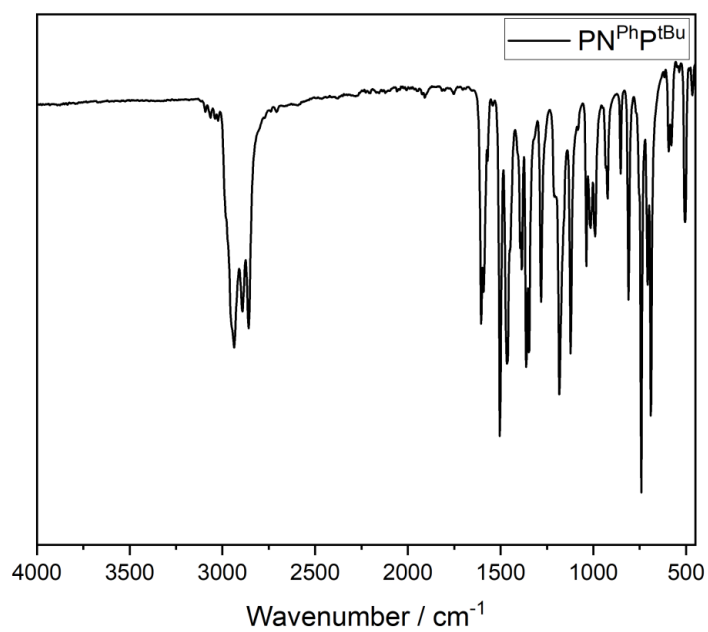


Figure S32: Solid state IR spectrum of **1g**.

2. IR, Raman and NMR spectra of the complexes

2.1. Spectra of $[\text{Mo}(\text{CO})_3(\text{PN}^{\text{Ph}}\text{P}^{\text{Ph}})]$ (**2a**)

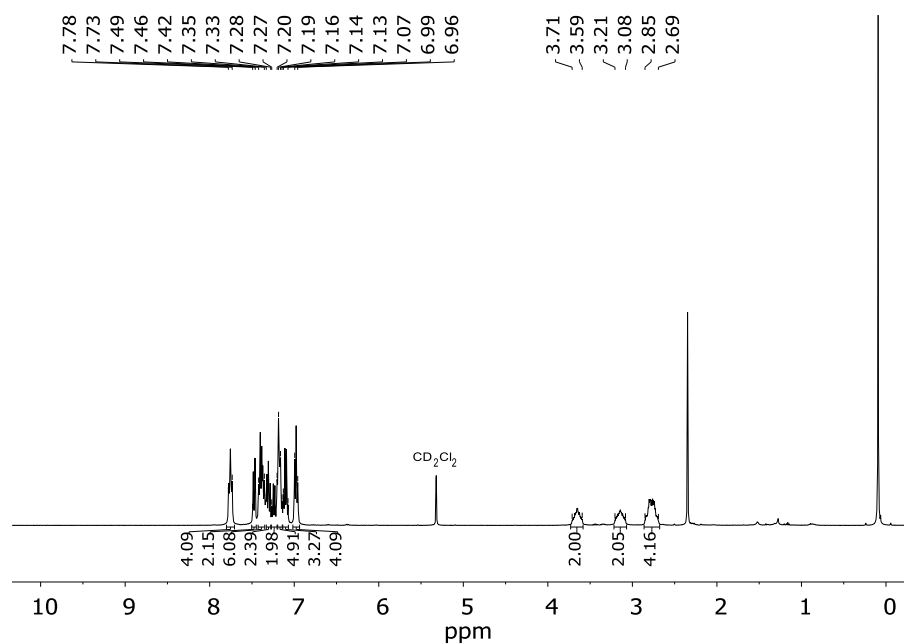


Figure S33: ^1H NMR of $[\text{Mo}(\text{CO})_3(\text{PN}^{\text{Ph}}\text{P}^{\text{Ph}})]$ (**2a**) measured in CD_2Cl_2 .

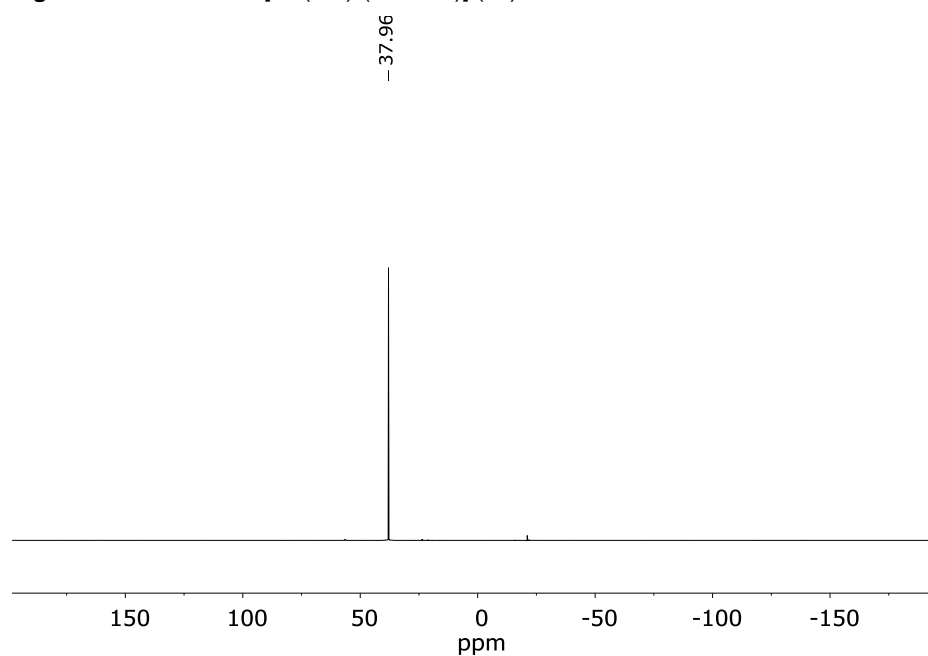


Figure S34: ^{31}P NMR of $[\text{Mo}(\text{CO})_3(\text{PN}^{\text{Ph}}\text{P}^{\text{Ph}})]$ (**2a**) measured in CD_2Cl_2 .

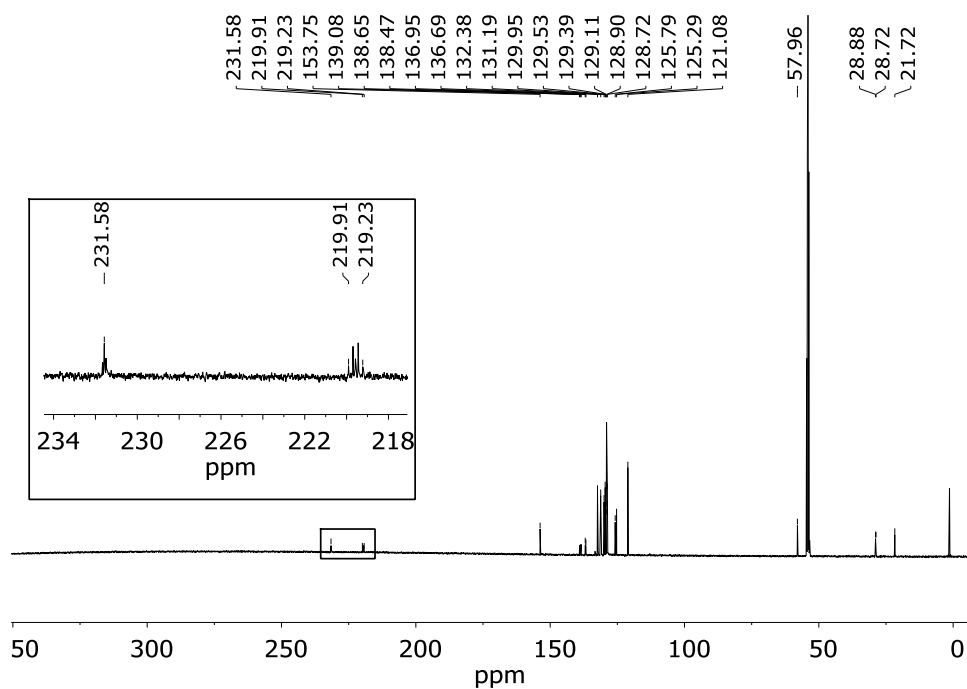


Figure S35: ^{13}C NMR of $[\text{Mo}(\text{CO})_3(\text{PN}^{\text{Ph}}\text{P}^{\text{Ph}})]$ (**2a**) measured in CD_2Cl_2 . The signals of the CO ligands are enlarged.

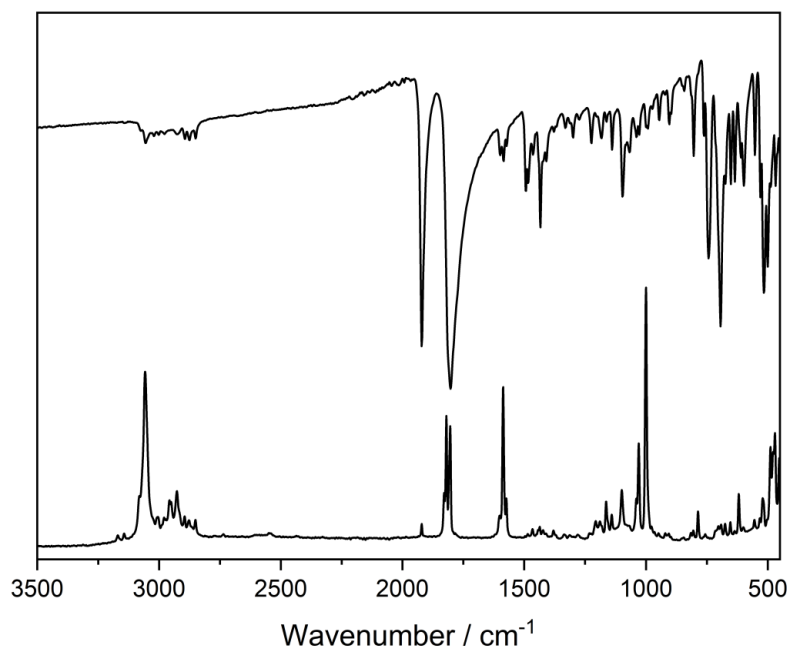


Figure S36: Solid state IR and Raman spectra of $[\text{Mo}(\text{CO})_3(\text{PN}^{\text{Ph}}\text{P}^{\text{Ph}})]$ (**2a**).

2.2. Spectra of $[\text{Mo}(\text{CO})_3(\text{PN}^{\text{Ph}}\text{P}^{\text{Et}})]$ (**2c**)

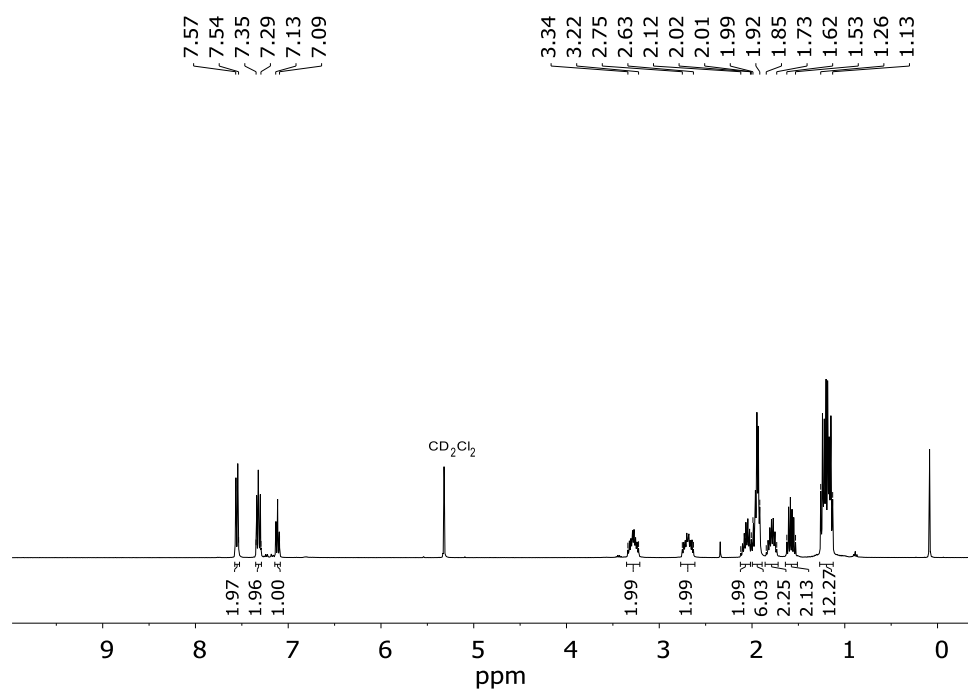


Figure S37: ^1H NMR of $[\text{Mo}(\text{CO})_3(\text{PN}^{\text{Ph}}\text{P}^{\text{Et}})]$ (**2c**) measured in CD_2Cl_2 .

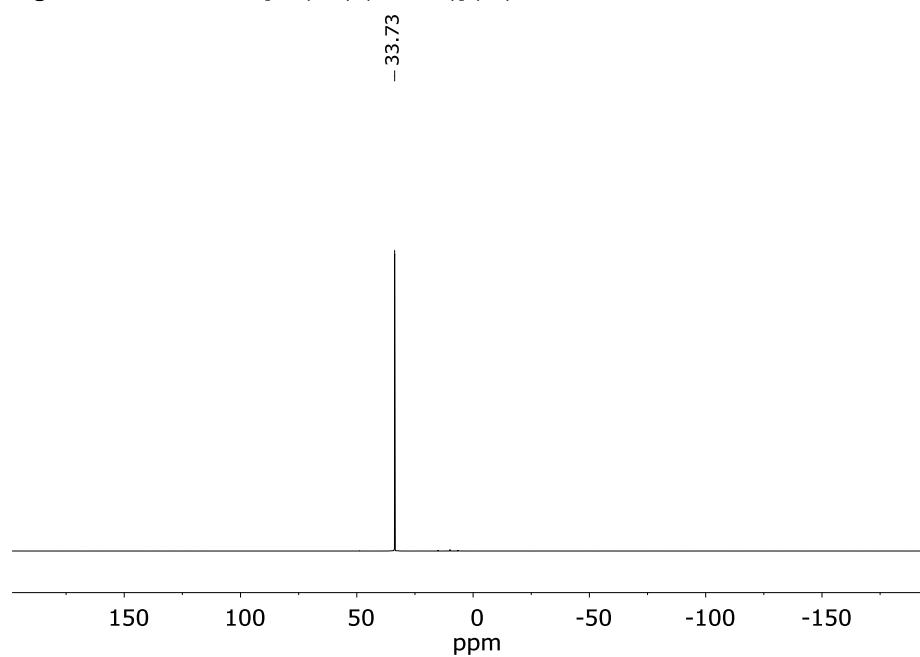


Figure S38: ^{31}P NMR of $[\text{Mo}(\text{CO})_3(\text{PN}^{\text{Ph}}\text{P}^{\text{Et}})]$ (**2c**) measured in CD_2Cl_2 .

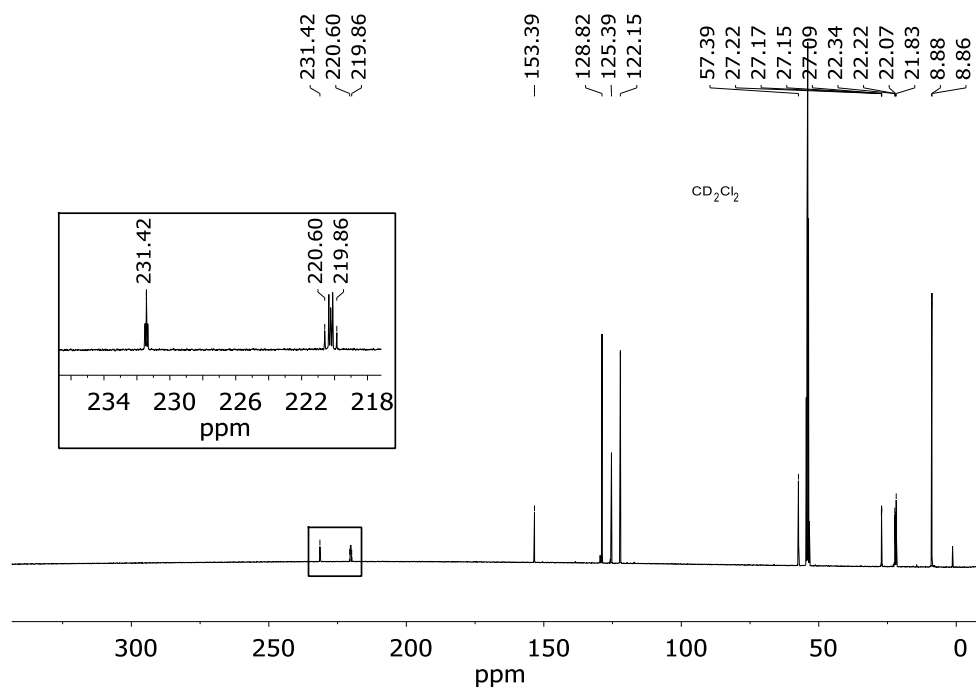


Figure S39: ^{13}C NMR of $[\text{Mo}(\text{CO})_3(\text{PN}^{\text{Ph}}\text{P}^{\text{Et}})]$ (**2c**) measured in CD_2Cl_2 . The signals of the CO ligands are enlarged.

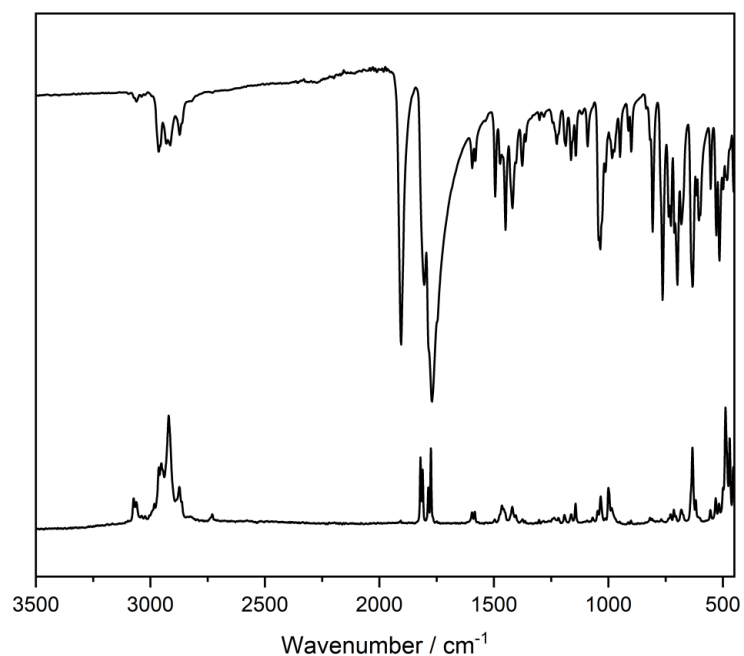


Figure S40: Solid state IR and Raman spectra of $[\text{Mo}(\text{CO})_3(\text{PN}^{\text{Ph}}\text{P}^{\text{Et}})]$ (**2c**).

2.3. Spectra of $[\text{Mo}(\text{CO})_3(\text{PN}^{\text{Ph}}\text{P}^{\text{Cyp}})]$ (**2e**)

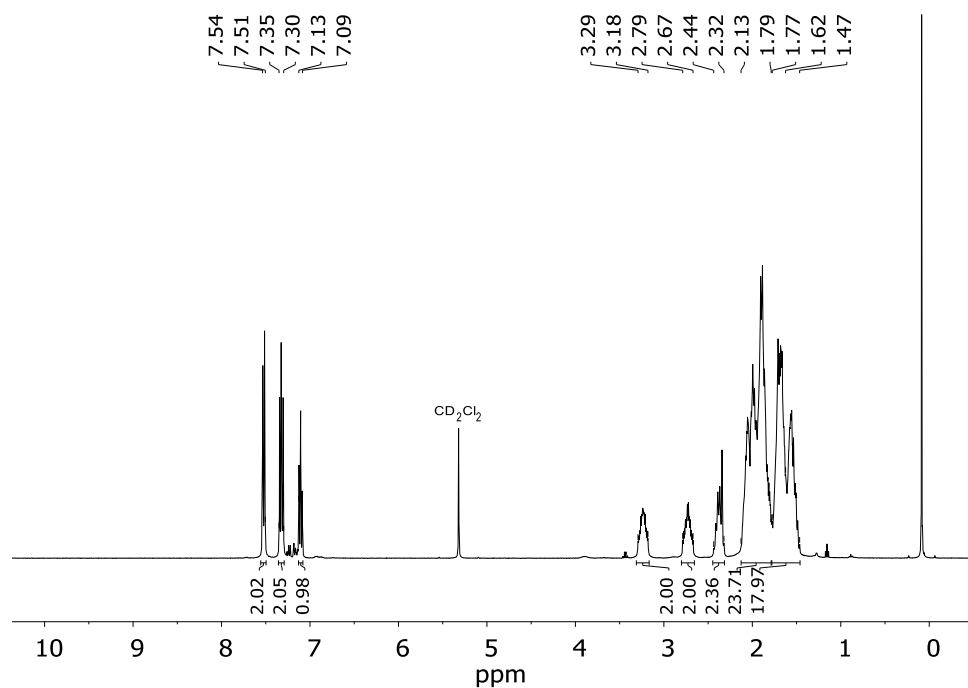


Figure S41: ^1H NMR of $[\text{Mo}(\text{CO})_3(\text{PN}^{\text{Ph}}\text{P}^{\text{Cyp}})]$ (**2e**) measured in CD_2Cl_2 .

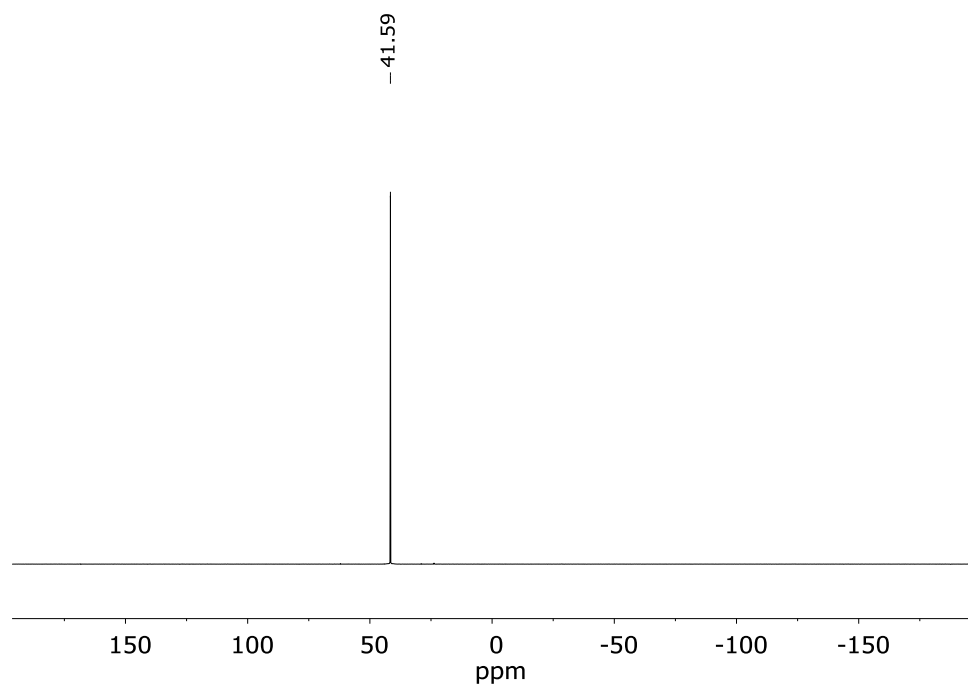


Figure S42: ^{31}P NMR of $[\text{Mo}(\text{CO})_3(\text{PN}^{\text{Ph}}\text{P}^{\text{Cyp}})]$ (**2e**) measured in CD_2Cl_2 .

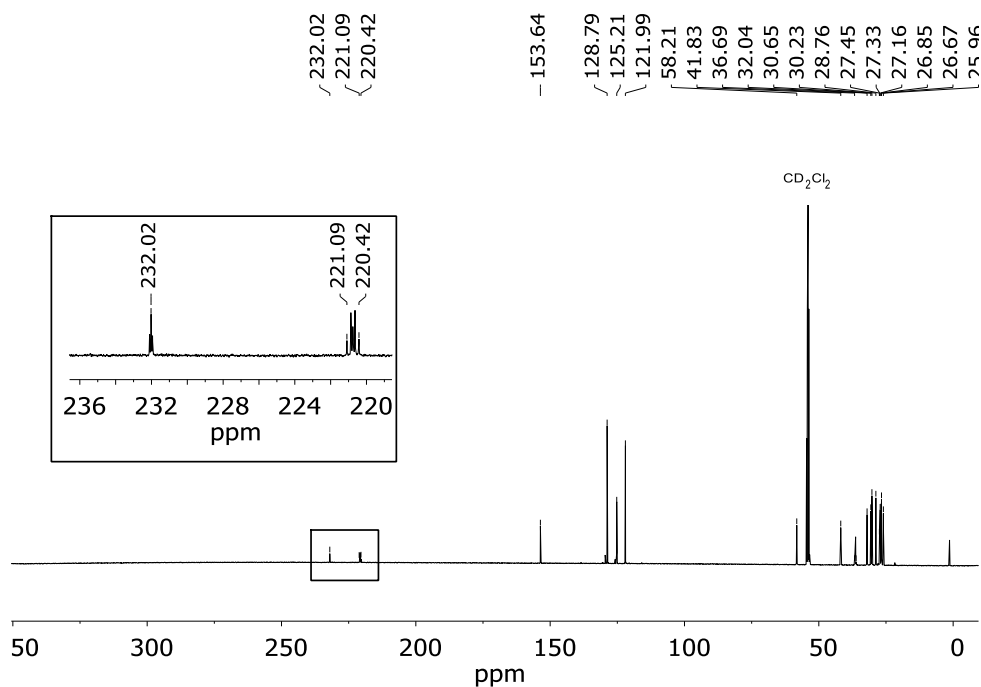


Figure S43: ^{13}C NMR of $[\text{Mo}(\text{CO})_3(\text{PN}^{\text{Ph}}\text{PCyp})]$ (**2e**) measured in CD_2Cl_2 . The signals of the CO ligands are enlarged.

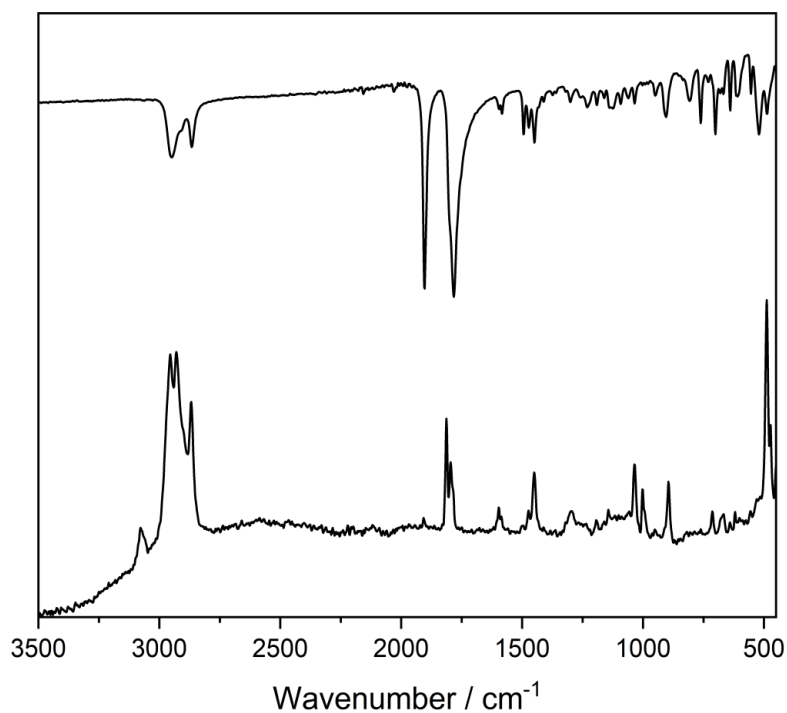


Figure S44: Solid state IR and Raman spectra of $[\text{Mo}(\text{CO})_3(\text{PN}^{\text{Ph}}\text{PCyp})]$ (**2e**).

2.4. Spectra of $[\text{Mo}(\text{CO})_3(\text{PN}^{\text{Ph}}\text{P}^{\text{iPr}})]$ (**2f**)

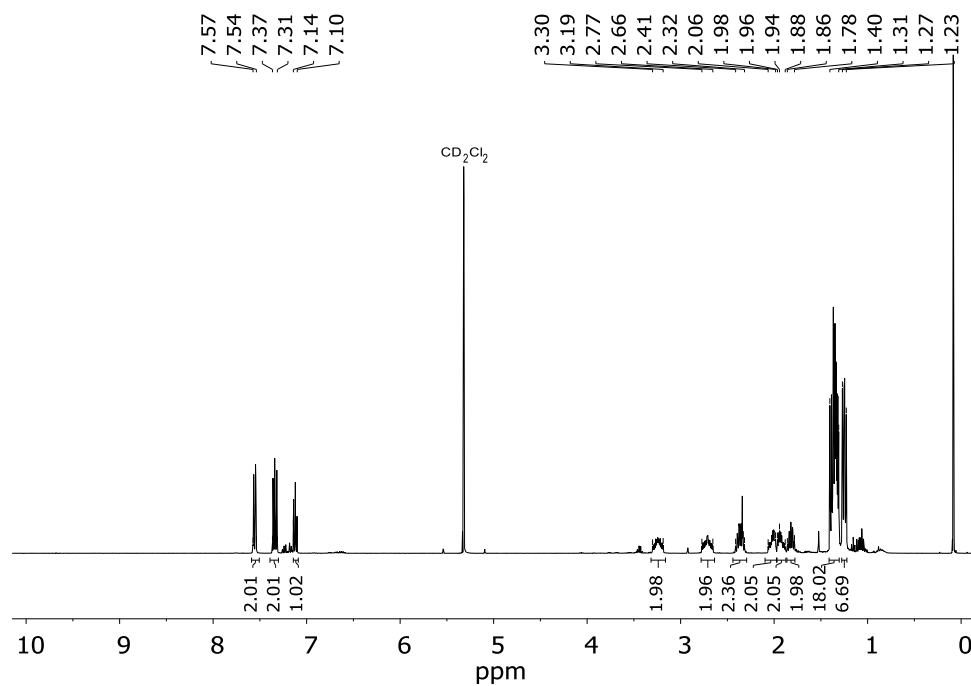


Figure S45: ^1H NMR of $[\text{Mo}(\text{CO})_3(\text{PN}^{\text{Ph}}\text{P}^{\text{iPr}})]$ (**2f**) measured in CD_2Cl_2 .

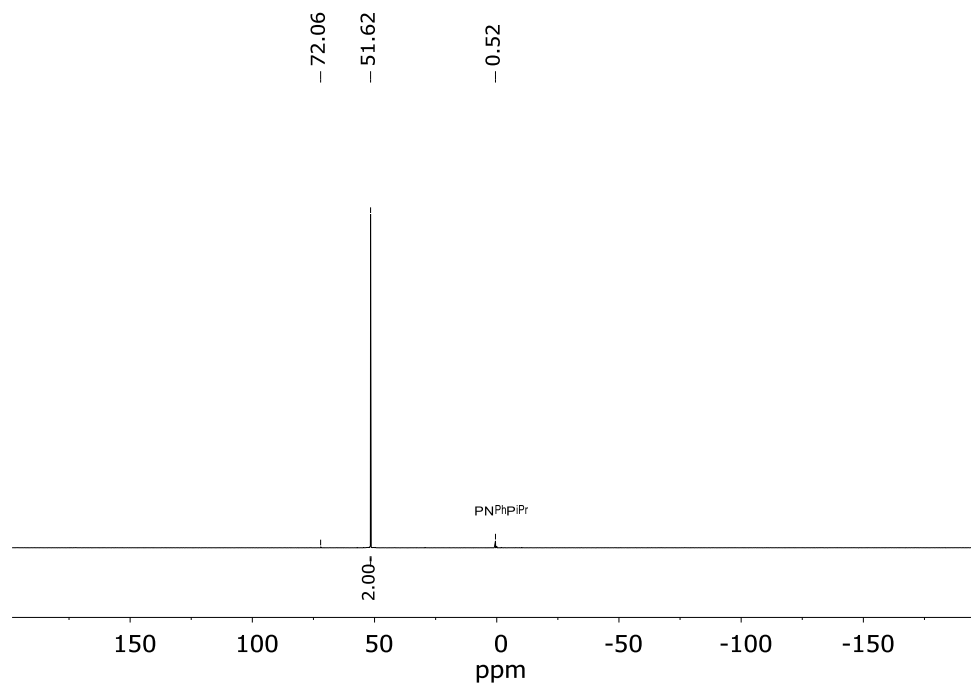


Figure S46: ^{31}P NMR of $[\text{Mo}(\text{CO})_3(\text{PN}^{\text{Ph}}\text{P}^{\text{iPr}})]$ (**2f**) measured in CD_2Cl_2 .

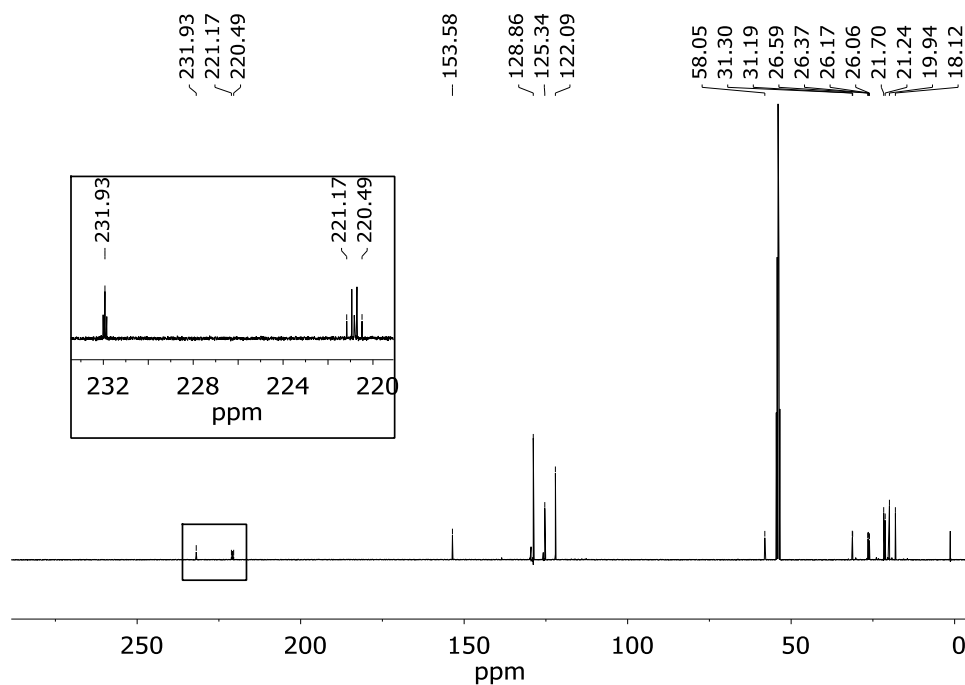


Figure S47: ^{13}C NMR of $[\text{Mo}(\text{CO})_3(\text{PN}^{\text{Ph}}\text{P}^{\text{iPr}})]$ (**2f**) measured in CD_2Cl_2 . The signals of the CO ligands are enlarged.

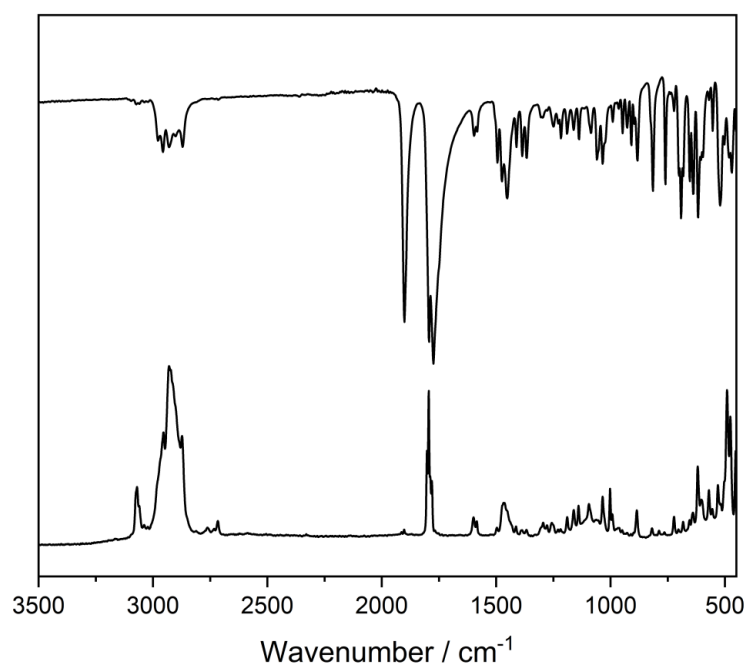


Figure S48: Solid state IR and Raman spectra of $[\text{Mo}(\text{CO})_3(\text{PN}^{\text{Ph}}\text{P}^{\text{iPr}})]$ (**2f**).

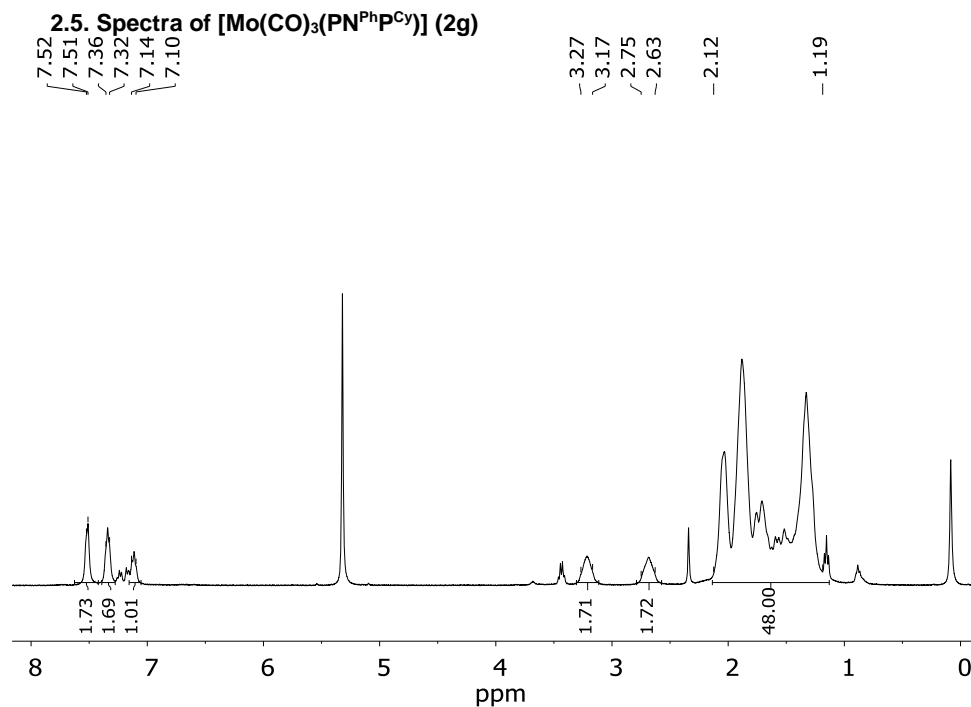


Figure S49: ^1H NMR of $[\text{Mo}(\text{CO})_3(\text{PN}^{\text{Ph}}\text{P}^{\text{Cy}})]$ (2g) measured in CD_2Cl_2 .

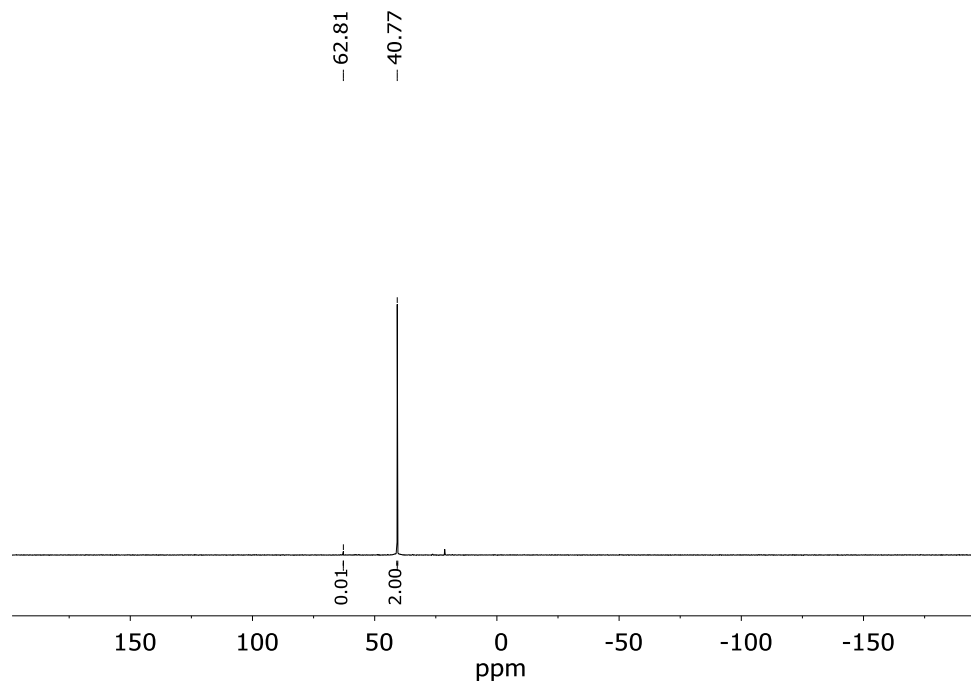


Figure S50: ^{31}P NMR of $[\text{Mo}(\text{CO})_3(\text{PN}^{\text{Ph}}\text{P}^{\text{Cy}})]$ (2g) measured in CD_2Cl_2 .

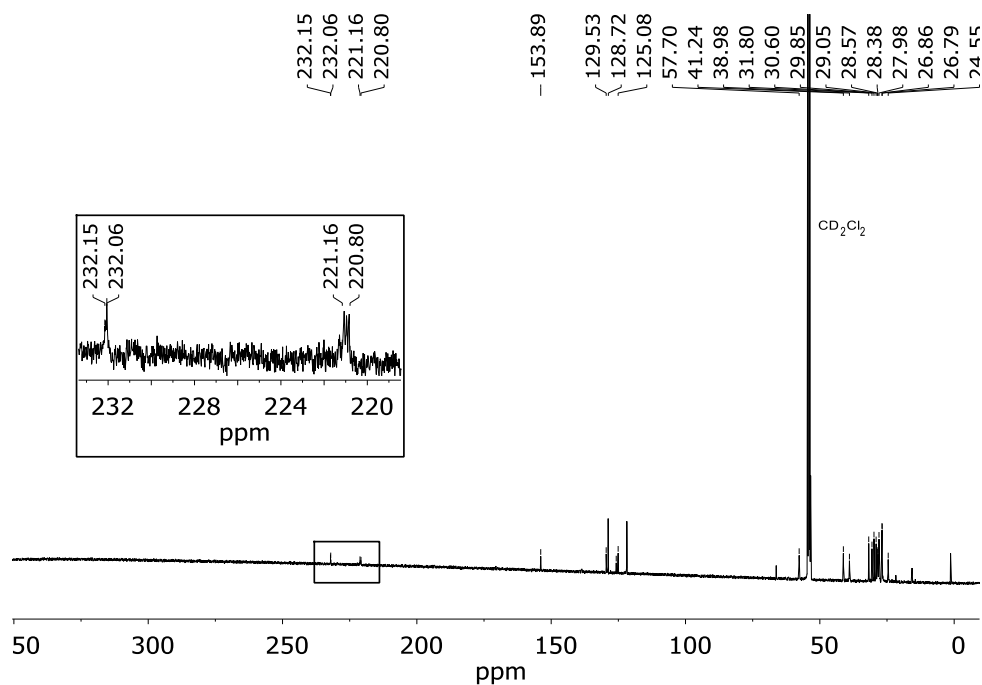


Figure S51: ^{13}C NMR of $[\text{Mo}(\text{CO})_3(\text{PN}^{\text{Ph}}\text{PCy})]$ (**2g**) measured in CD_2Cl_2 . The signals of the CO ligands are enlarged.

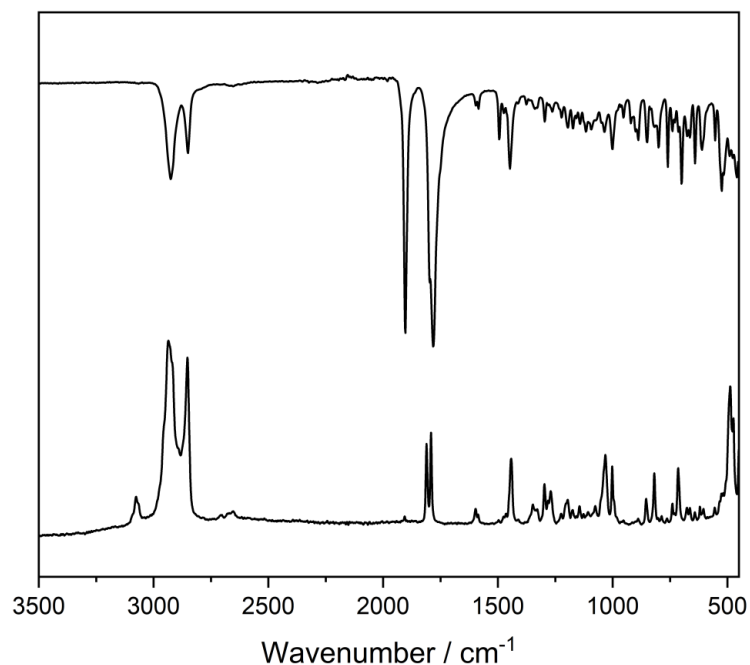


Figure S52: Solid state IR and Raman spectra of $[\text{Mo}(\text{CO})_3(\text{PN}^{\text{Ph}}\text{PCy})]$ (**2g**).

2.6. ABX Spin Systems of the Complexes

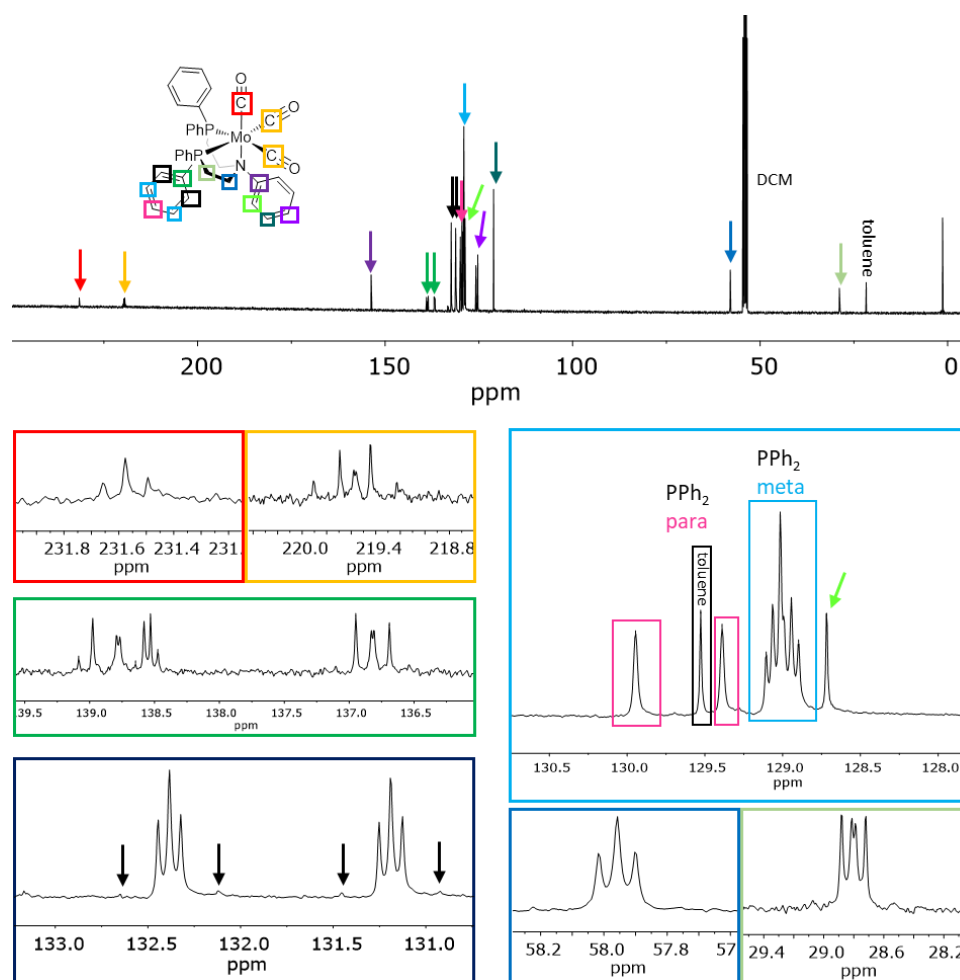


Figure S53: Complete assignment of the ABX and false AA'X patterns of the [Mo(CO)₃(PN^{Ph}P^{Ph})] complex (2a).

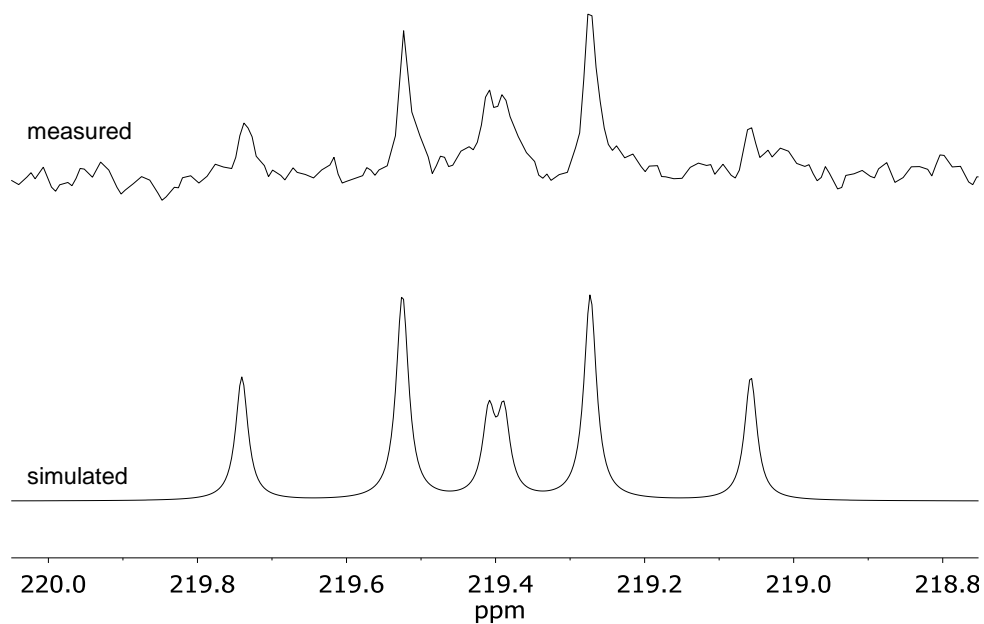


Figure S54: Measured and simulated ABX pattern of the equatorial CO ligands of the $[\text{Mo}(\text{CO})_3(\text{PN}^{\text{Ph}}\text{P}^{\text{Ph}})]$ complex (**2a**).

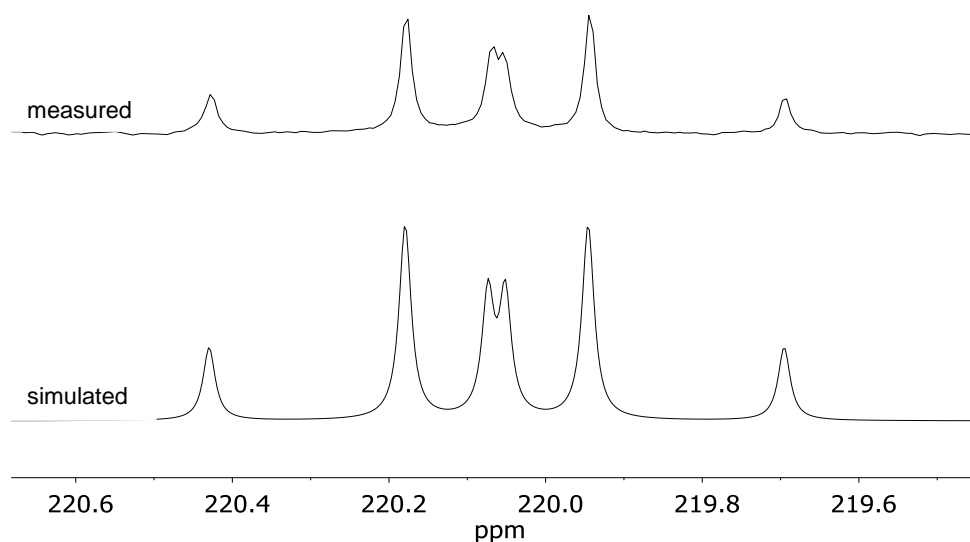


Figure S55: Measured and simulated ABX pattern of the equatorial CO ligands of the $[\text{Mo}(\text{CO})_3(\text{PN}^{\text{Ph}}\text{P}^{\text{Et}})]$ complex (**2c**).

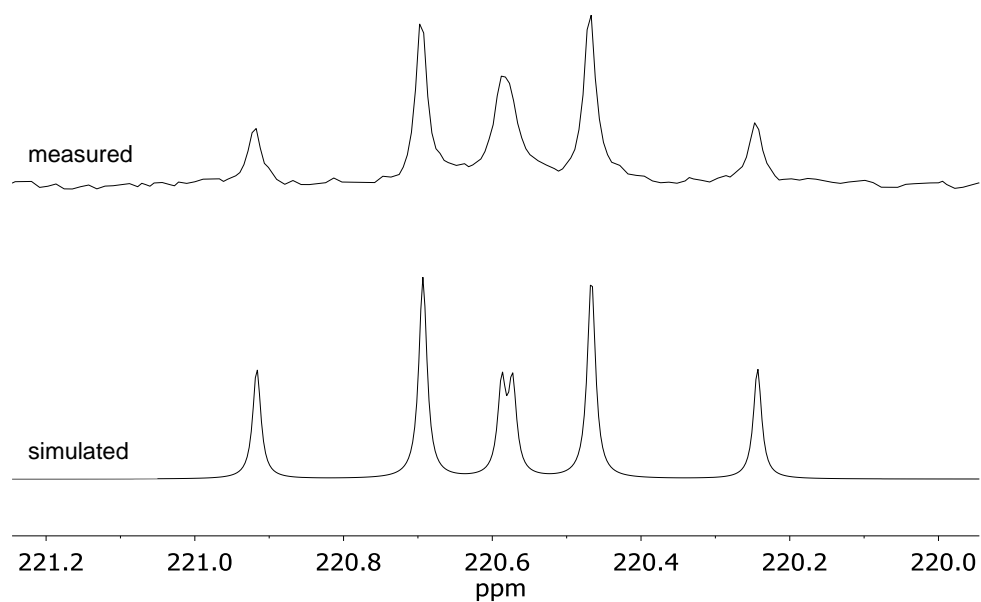


Figure S56: Measured and simulated ABX pattern of the equatorial CO ligands of the $[\text{Mo}(\text{CO})_3(\text{PN}^{\text{Ph}}\text{PCyp})]$ complex (**2e**).

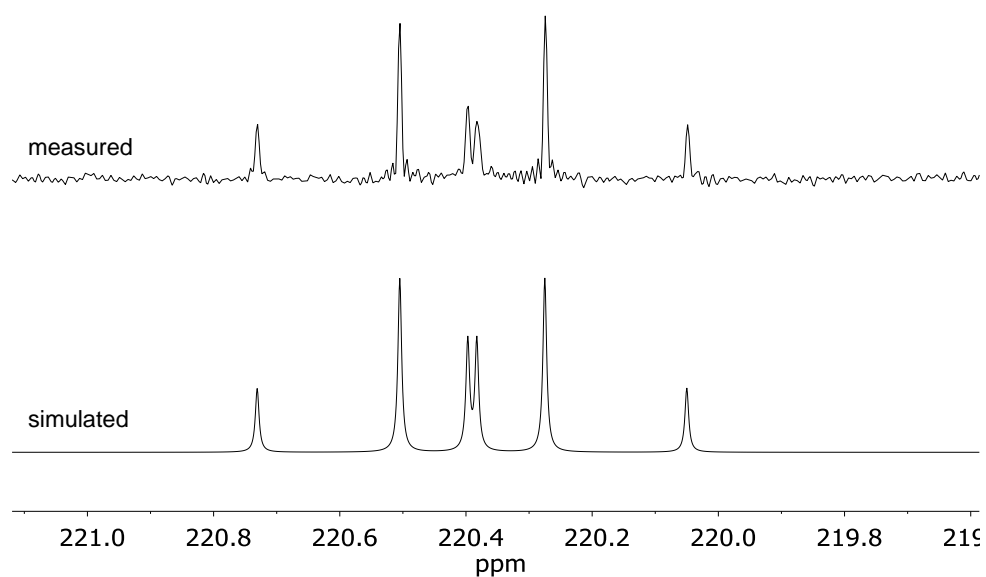


Figure S57: Measured and simulated ABX pattern of the equatorial CO ligands of the $[\text{Mo}(\text{CO})_3(\text{PN}^{\text{Ph}}\text{P}^{\text{iPr}})]$ complex (**2g**).

2.7. fac-mer-ratios of the complexes**Table S1:** Ratio (%) of facial and meridional isomers of the complexes as determined from ^{31}P NMR spectra.

Complex	facial	meridional
$[\text{Mo}(\text{CO})_3(\text{PN}^{\text{Ph}}\text{P}^{\text{Ph}})]$ (2a)	99.6	0.4
$[\text{Mo}(\text{CO})_3(\text{PN}^{\text{Ph}}\text{P}^{\text{Et}})]$ (2c)	99.9	0.1
$[\text{Mo}(\text{CO})_3(\text{PN}^{\text{Ph}}\text{P}^{\text{Cyp}})]$ (2e)	99.2	0.1
$[\text{Mo}(\text{CO})_3(\text{PN}^{\text{Ph}}\text{P}^{\text{Cy}})]$ (2f)	99.2	0.8
$[\text{Mo}(\text{CO})_3(\text{PN}^{\text{Ph}}\text{P}^{\text{iPr}})]$ (2g)	99.8	0.2

3. Calculations

All following calculations were performed on PBE0^[1]/def2-TZVPP^[2] level with Grimmes dispersion correction,^[3] Becke-Johnson damping (D3BJ),^[4] density fitting approximation (RIJCOSX),^[5] and with solvation correction (CPCM),^[6] if values in solution are shown.

3.1. Optimized Structures of the Complexes

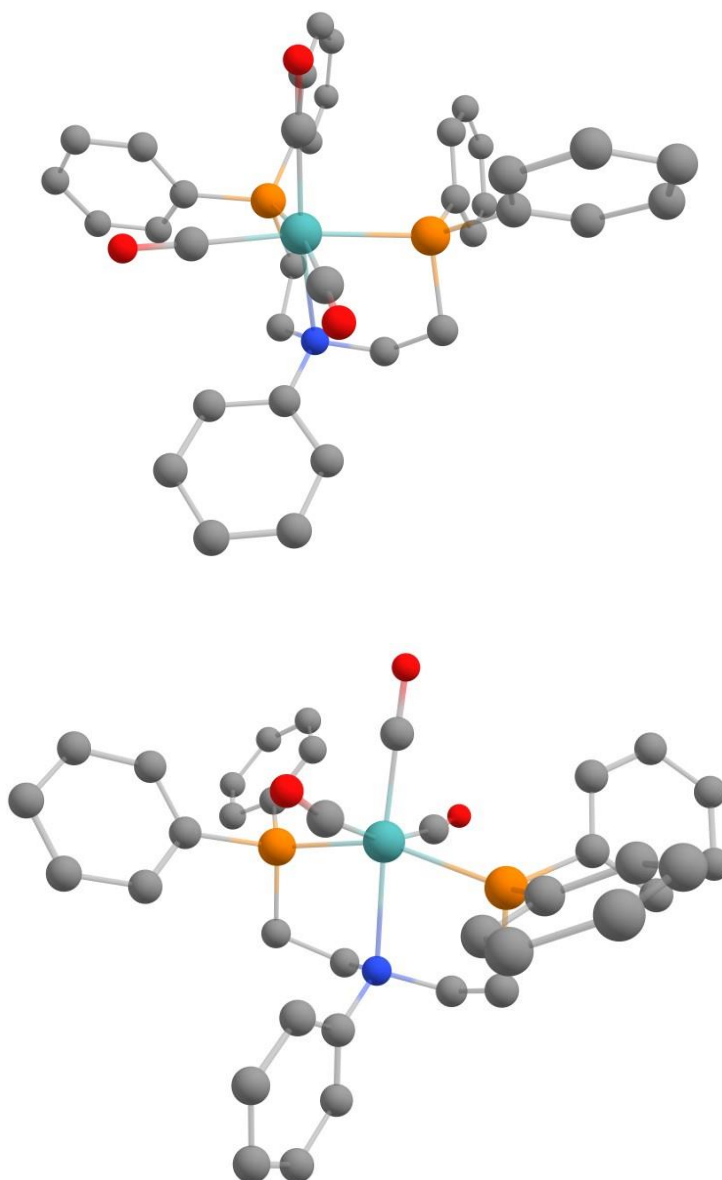


Figure S58: Optimized structures of facial (top) and meridional (bottom) $[\text{Mo}(\text{CO})_3(\text{PN}^{\text{Ph}}\text{P}^{\text{Ph}})]$ (**2a**). H atoms are omitted for clarity.

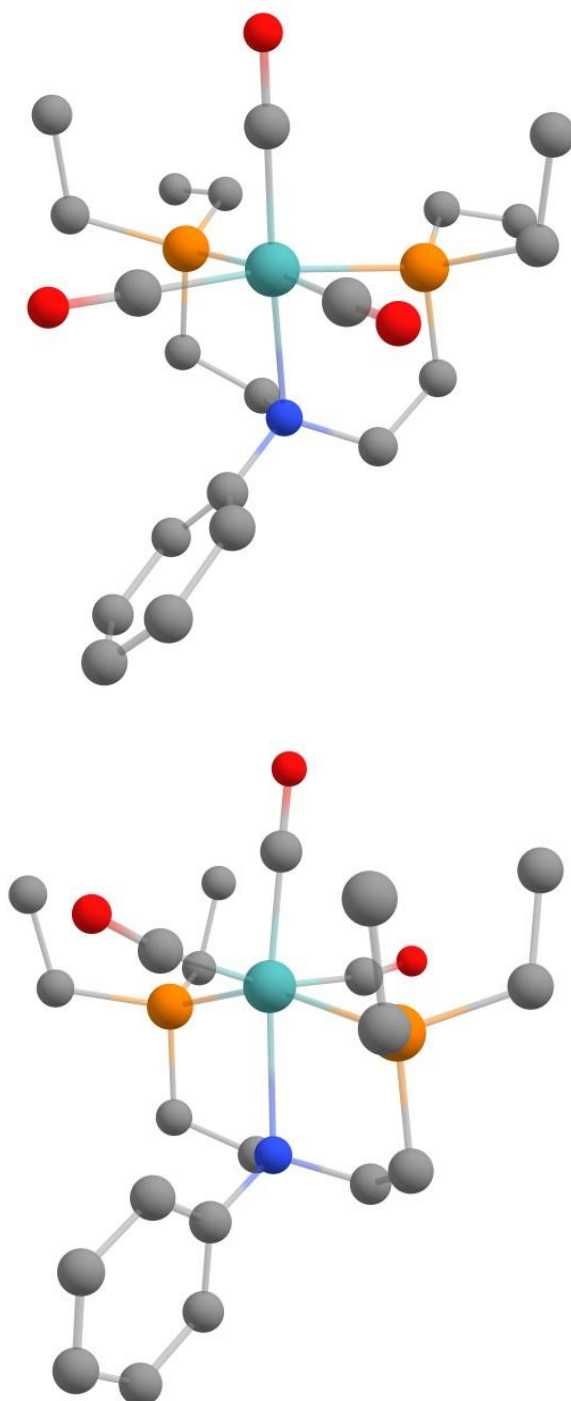


Figure S59: Optimized structures of facial (top) and meridional (bottom) [Mo(CO)₃(PN^{Ph}P^{Et})] (**2c**). H atoms are omitted for clarity.

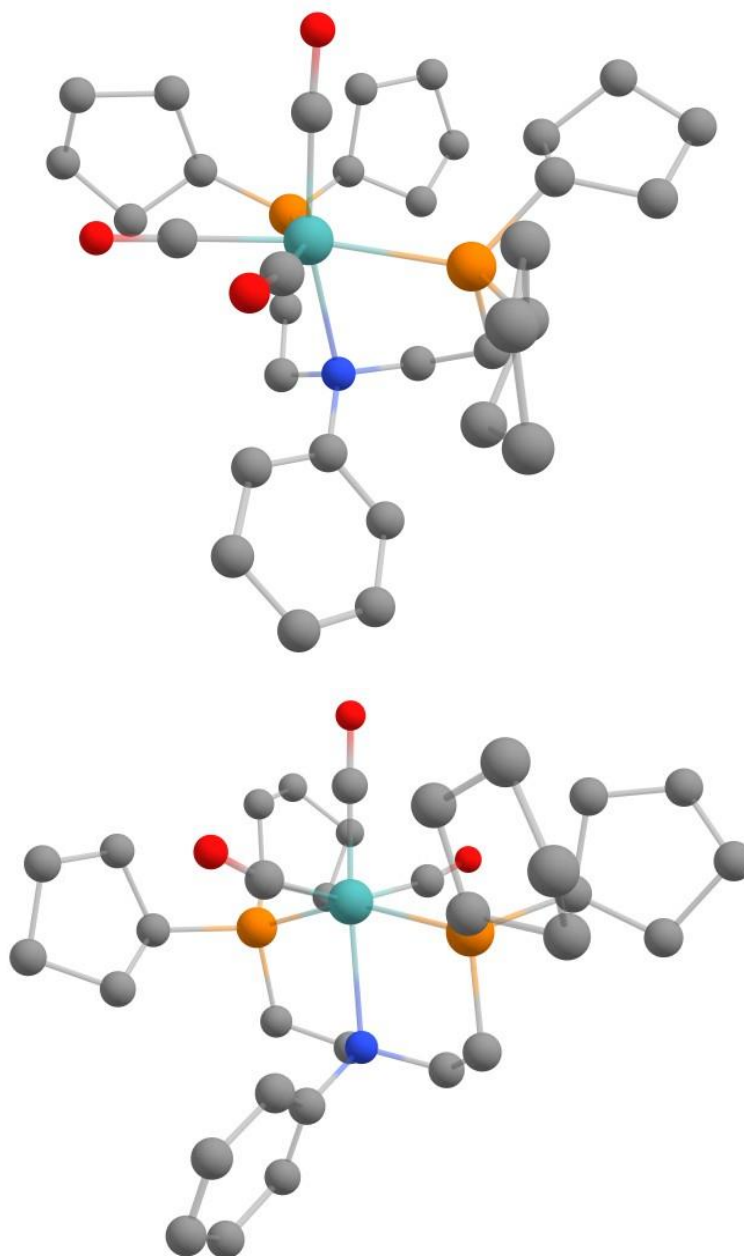


Figure S60: Optimized structures of facial (top) and meridional (bottom) [Mo(CO)₃(PN^{Ph}P^{Cyp})] (**2e**). H atoms are omitted for clarity.

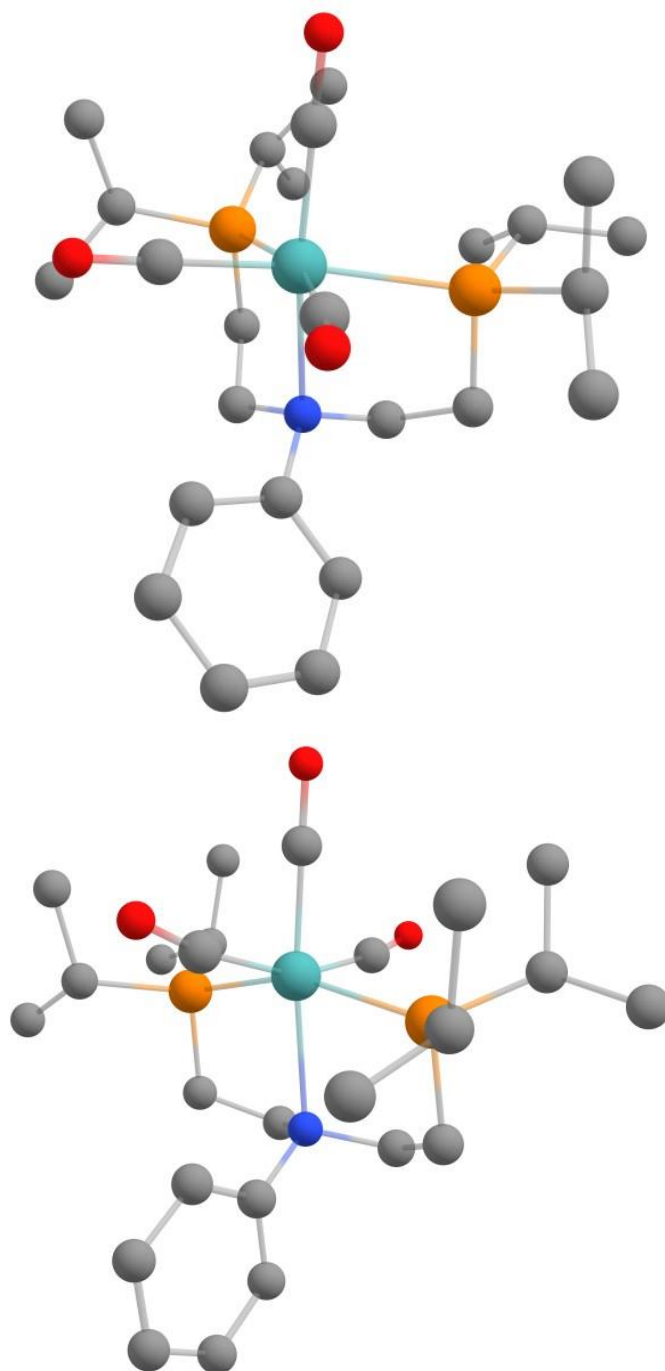


Figure S61: Optimized structures of facial (top) and meridional (bottom) [Mo(CO)₃(PN^{Ph}P^{iPr})] (**2f**). H atoms are omitted for clarity.

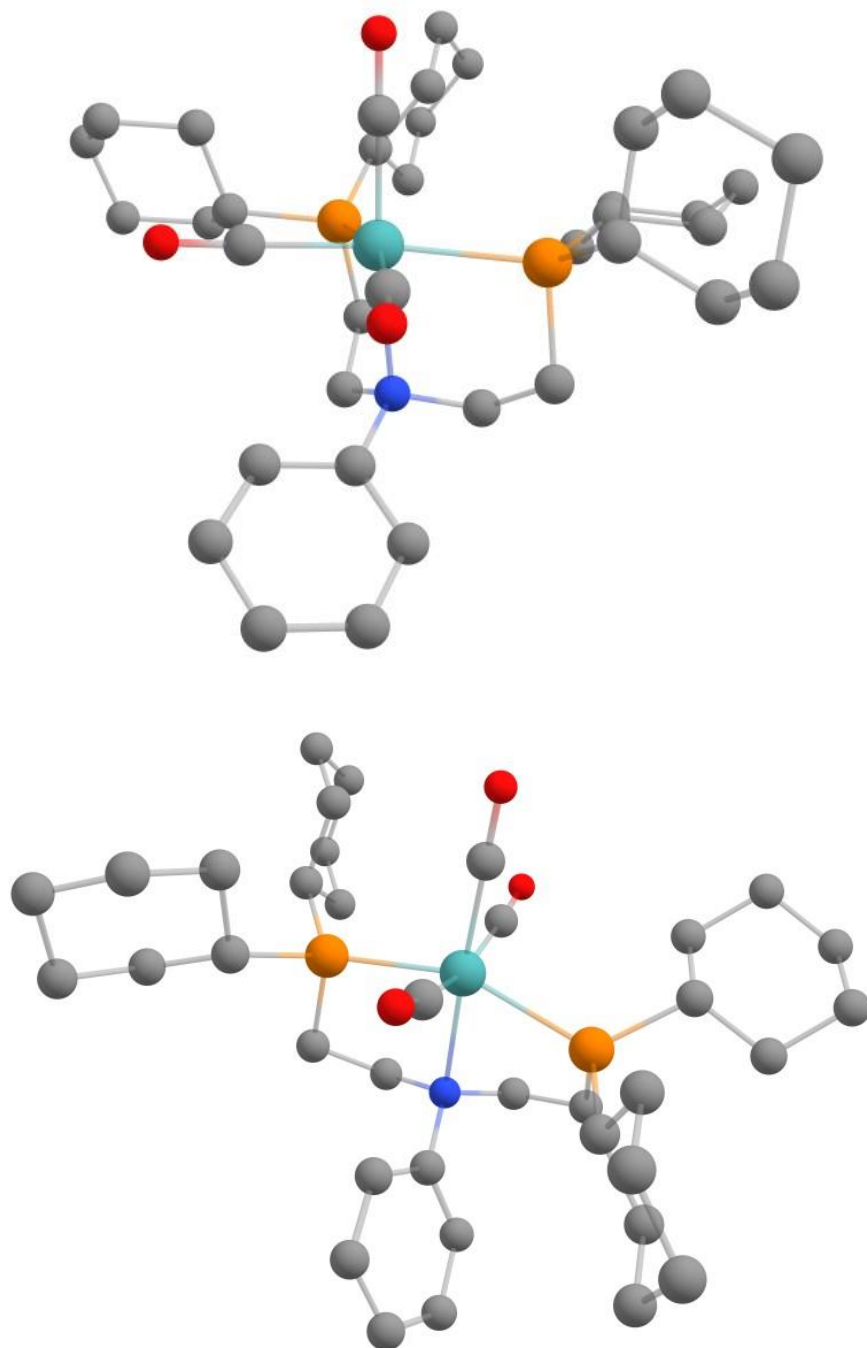


Figure S62: Optimized structures of facial (top) and meridional (bottom) [Mo(CO)₃(PN^{Ph}P^{Cy})] (2g). H atoms are omitted for clarity.

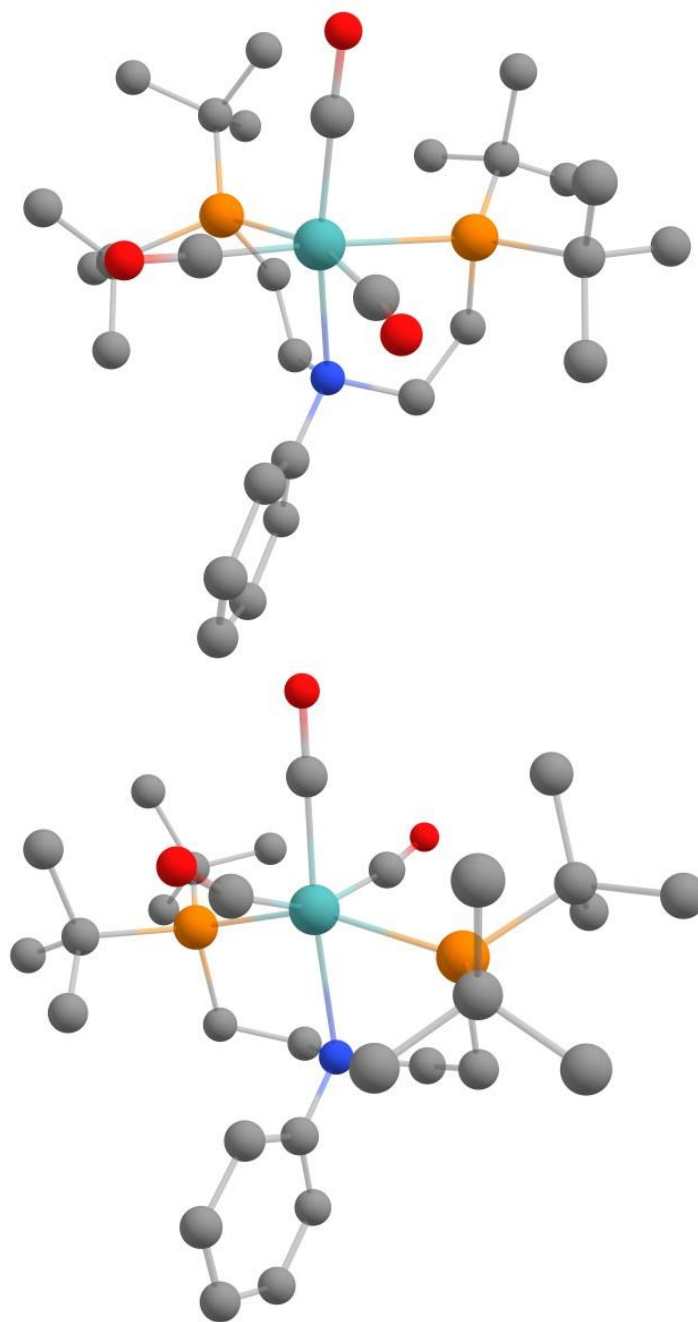


Figure S63: Optimized structures of facial (top) and meridional (bottom) [Mo(CO)₃(PN^{Ph}P^{tBu})] (2h). H atoms are omitted for clarity.

3.2. Metal-ligand bond lengths of the calculated facial and meridional $[\text{Mo}(\text{CO})_3(\text{PN}^{\text{Ph}}\text{P}^{\text{R}})]$ complexes (R = Ph, Et, ⁱPr, Cy, ^tBu).

Table S2: Calculated metal-ligand bond lengths [Å] of *fac*- $[\text{Mo}(\text{CO})_3(\text{PN}^{\text{Ph}}\text{P}^{\text{R}})]$ complexes.

Complexes	Mo-N	Mo-P ₁	facial geometry			Mo-C ₂
			Mo-P ₂	Mo-C _{ax}	Mo-C ₁	
$[\text{Mo}(\text{CO})_3(\text{PN}^{\text{Ph}}\text{P}^{\text{Ph}})]$	2.51679	2.46766	2.46203	1.92362	1.97220	1.97115
$[\text{Mo}(\text{CO})_3(\text{PN}^{\text{Ph}}\text{P}^{\text{Et}})]$	2.47939	2.46676	2.47175	1.93056	1.97026	1.96195
$[\text{Mo}(\text{CO})_3(\text{PN}^{\text{Ph}}\text{P}^{\text{iPr}})]$	2.50413	2.5127	2.51788	1.92641	1.9501	1.95966
$[\text{Mo}(\text{CO})_3(\text{PN}^{\text{Ph}}\text{P}^{\text{Cy}})]$	2.48319	2.50420	2.51880	1.92799	1.95038	1.95851
$[\text{Mo}(\text{CO})_3(\text{PN}^{\text{Ph}}\text{P}^{\text{tBu}})]$	2.6233	2.57207	2.61424	1.91583	1.94421	1.94357

Table S3: Calculated metal-ligand bond lengths [Å] of *mer*- $[\text{Mo}(\text{CO})_3(\text{PN}^{\text{Ph}}\text{P}^{\text{R}})]$ complexes.

Complexes	Mo-N	Mo-P ₁	meridional geometry			Mo-C ₂
			Mo-P ₂	Mo-C _{ax}	Mo-C ₁	
$[\text{Mo}(\text{CO})_3(\text{PN}^{\text{Ph}}\text{P}^{\text{Ph}})]$	2.48178	2.42192	2.41209	1.92562	2.01583	1.99903
$[\text{Mo}(\text{CO})_3(\text{PN}^{\text{Ph}}\text{P}^{\text{Et}})]$	2.49136	2.41263	2.41210	1.92528	2.00727	1.99528
$[\text{Mo}(\text{CO})_3(\text{PN}^{\text{Ph}}\text{P}^{\text{iPr}})]$	2.48644	2.42995	2.43096	1.92158	2.00453	1.99303
$[\text{Mo}(\text{CO})_3(\text{PN}^{\text{Ph}}\text{P}^{\text{Cy}})]$	2.46430	2.43989	2.42000	1.92894	1.99728	1.99897
$[\text{Mo}(\text{CO})_3(\text{PN}^{\text{Ph}}\text{P}^{\text{tBu}})]$	2.49885	2.50332	2.49402	1.91854	1.99670	1.98558

3.3. Energy calculations for *fac*- and *mer*-[Mo(CO)₃(PN^RP^R)] complexes**Table S4:** Calculated Gibbs free energies of [Mo(CO)₃(PN^{Ph}P^R)] (R = Ph, Et, Cyp, ⁱPr, Cy, ^tBu) in the gas phase and solution (DCM, $\epsilon = 8.93$).

Complex	G_{gas} [kcal/mol]	ΔG_{solv} [kcal/mol]	G_{solv} [kcal/mol]
<i>facial</i>			
[Mo(CO) ₃ (PN ^{Ph} P ^{Ph})]	-1543200.24	-31.05532127	-1543231.296
[Mo(CO) ₃ (PN ^{Ph} P ^{Et})]	-1160969.975	-19.85477584	-1160989.83
[Mo(CO) ₃ (PN ^{Ph} P ^{Cyp})]	-1453575.927	-24.22986778	-1453600.157
[Mo(CO) ₃ (PN ^{Ph} P ^{ⁱPr})]	-1259487.163	-20.57049984	-1259507.733
[Mo(CO) ₃ (PN ^{Ph} P ^{Cy})]	-1552121.922	-27.29679252	-1552149.219
[Mo(CO) ₃ (PN ^{Ph} P ^{^tBu})]	-1357988.486	-21.41915313	-1358009.905
<i>meridional</i>			
[Mo(CO) ₃ (PN ^{Ph} P ^{Ph})]	-1543197.817	-30.10114635	-1543227.919
[Mo(CO) ₃ (PN ^{Ph} P ^{Et})]	-1160970.206	-17.97303801	-1160988.179
[Mo(CO) ₃ (PN ^{Ph} P ^{Cyp})]	-1453581.476	-23.40582641	-1453604.882
[Mo(CO) ₃ (PN ^{Ph} P ^{ⁱPr})]	-1259496.428	-18.99073408	-1259515.419
[Mo(CO) ₃ (PN ^{Ph} P ^{Cy})]	-1552125.816	-25.38548414	-1552151.202
[Mo(CO) ₃ (PN ^{Ph} P ^{^tBu})]	-1358003.72	-19.21321983	-1358022.933

Table S5: Calculated Gibbs free energies of $[\text{Mo}(\text{CO})_3(\text{PN}^{\text{H}}\text{P}^{\text{R}})]$ (R = Ph, Et, Cyp, ⁱPr, Cy, ^tBu) in the gas phase and solution (DCM, $\epsilon = 8.93$).

Complex	G_{gas} [kcal/mol]	ΔG_{solv} [kcal/mol]	G_{solv} [kcal/mol]
<i>facial</i>			
$[\text{Mo}(\text{CO})_3(\text{PN}^{\text{H}}\text{P}^{\text{Ph}})]$	-1398383.759	-27.32576674	-1398411.085
$[\text{Mo}(\text{CO})_3(\text{PN}^{\text{H}}\text{P}^{\text{Et}})]$	-1016147.537	-16.96869788	-1016164.506
$[\text{Mo}(\text{CO})_3(\text{PN}^{\text{H}}\text{P}^{\text{iPr}})]$	-1114671.64	-17.60969886	-1114689.249
$[\text{Mo}(\text{CO})_3(\text{PN}^{\text{H}}\text{P}^{\text{Cy}})]$	-1407307.438	-24.06628807	-1407331.505
$[\text{Mo}(\text{CO})_3(\text{PN}^{\text{H}}\text{P}^{\text{tBu}})]$	-1213179.254	-19.06922805	-1213198.323
<i>meridional</i>			
$[\text{Mo}(\text{CO})_3(\text{PN}^{\text{H}}\text{P}^{\text{Ph}})]$	-1398379.578	-28.82606656	-1398408.405
$[\text{Mo}(\text{CO})_3(\text{PN}^{\text{H}}\text{P}^{\text{Et}})]$	-1016155.684	-15.808218	-1016171.492
$[\text{Mo}(\text{CO})_3(\text{PN}^{\text{H}}\text{P}^{\text{iPr}})]$	-1114681.412	-16.9093487	-1114698.322
$[\text{Mo}(\text{CO})_3(\text{PN}^{\text{H}}\text{P}^{\text{Cy}})]$	-1407310.917	-23.68817216	-1407334.605
$[\text{Mo}(\text{CO})_3(\text{PN}^{\text{H}}\text{P}^{\text{tBu}})]$	-1213193.618	-18.33416055	-1213211.952

Table S6: Calculated Gibbs free energies of $\text{PN}^{\text{Ph}}\text{P}^{\text{R}}$ ligands (R = Ph, Et, Cyp, ⁱPr, Cy, ^tBu) in the gas phase and solution (DCM, $\epsilon = 8.93$).

Ligand	G_{gas} [kcal/mol]	ΔG_{solv} [kcal/mol]	G_{solv} [kcal/mol]
$\text{PN}^{\text{Ph}}\text{P}^{\text{Ph}}$	-1287095.097	-28.83574663	-1287123.932
$\text{PN}^{\text{Ph}}\text{P}^{\text{Et}}$	-904857.6438	-16.40151038	-904874.0453
$\text{PN}^{\text{Ph}}\text{P}^{\text{Cp}}$	-1197469.31	-22.84596516	-1197492.156
$\text{PN}^{\text{Ph}}\text{P}^{\text{iPr}}$	-1003386.14	-18.29073567	-1003404.43
$\text{PN}^{\text{Ph}}\text{P}^{\text{Cy}}$	-1296011.52	-24.72663781	-1296036.246
$\text{PN}^{\text{Ph}}\text{P}^{\text{tBu}}$	-1101910.385	-18.8994559	-1101929.284

Table S7: Calculated Gibbs free energies of $\text{PN}^{\text{H}}\text{P}^{\text{R}}$ ligands (R = Ph, Et, Cyp, ⁱPr, Cy, ^tBu) in the gas phase and solution (DCM, $\epsilon = 8.93$).

Ligand	G_{gas} [kcal/mol]	ΔG_{solv} [kcal/mol]	G_{solv} [kcal/mol]
$\text{PN}^{\text{H}}\text{P}^{\text{Ph}}$	-1142269.557	-25.68944953	-1142295.246
$\text{PN}^{\text{H}}\text{P}^{\text{Et}}$	-760035.9299	-13.23454541	-760049.1644
$\text{PN}^{\text{H}}\text{P}^{\text{iPr}}$	-858561.8971	-14.78404314	-858576.6812
$\text{PN}^{\text{H}}\text{P}^{\text{Cy}}$	-1151194.779	-22.45315368	-1151217.233
$\text{PN}^{\text{H}}\text{P}^{\text{tBu}}$	-957085.4904	-15.49833628	-957100.9887

3.4. Relative free energies

Table S8: Calculated relative Gibbs energies for *fac*- and *mer*- $[\text{Mo}(\text{CO})_3(\text{PN}^{\text{H}}\text{P}^{\text{R}})]$ complexes (R = Et, Ph, Cyp, ⁱPr, Cy, ^tBu) in solution (DCM, $\epsilon = 8.93$), visualized in Figure 6. The values are scaled to $[\text{Mo}(\text{CO})_3(\text{PN}^{\text{H}}\text{P}^{\text{Et}})]$ (1), which has the lowest energy.

<i>fac isomer</i>	ΔG_{solv} [kcal/mol]	<i>mer isomer</i>	ΔG_{solv} [kcal/mol]
$[\text{Mo}(\text{CO})_3(\text{PN}^{\text{H}}\text{P}^{\text{Et}})]$ (1)	0	$[\text{Mo}(\text{CO})_3(\text{PN}^{\text{H}}\text{P}^{\text{Et}})]$ (1)	1.650553182
$[\text{Mo}(\text{CO})_3(\text{PN}^{\text{H}}\text{P}^{\text{Ph}})]$ (2)	8.421110196	$[\text{Mo}(\text{CO})_3(\text{PN}^{\text{H}}\text{P}^{\text{Ph}})]$ (2)	11.79810557
$[\text{Mo}(\text{CO})_3(\text{PN}^{\text{H}}\text{P}^{\text{Cyp}})]$ (3)	7.783844423	$[\text{Mo}(\text{CO})_3(\text{PN}^{\text{H}}\text{P}^{\text{Cyp}})]$ (3)	3.058926964
$[\text{Mo}(\text{CO})_3(\text{PN}^{\text{H}}\text{P}^{\text{iPr}})]$ (4)	12.48140657	$[\text{Mo}(\text{CO})_3(\text{PN}^{\text{H}}\text{P}^{\text{iPr}})]$ (4)	4.79556343
$[\text{Mo}(\text{CO})_3(\text{PN}^{\text{H}}\text{P}^{\text{Cy}})]$ (5)	2.811709851	$[\text{Mo}(\text{CO})_3(\text{PN}^{\text{H}}\text{P}^{\text{Cy}})]$ (5)	0.82877226
$[\text{Mo}(\text{CO})_3(\text{PN}^{\text{H}}\text{P}^{\text{tBu}})]$ (6)	35.16368118	$[\text{Mo}(\text{CO})_3(\text{PN}^{\text{H}}\text{P}^{\text{tBu}})]$ (6)	22.13559238

Table S9: Relative Gibbs energies for *fac*- and *mer*-[Mo(CO)₃(PN^HP^R)] complexes (R = Et, Ph, Cyp, ⁱPr, Cy, ^tBu) in solution (DCM, ε = 8.93), visualized in Figure S60. The values are scaled to *mer*-[Mo(CO)₃(PN^HP^{Et})] (1), which has the lowest energy.

<i>fac isomer</i>	ΔG_{solv} [kcal/mol]	<i>mer isomer</i>	ΔG_{solv} [kcal/mol]
[Mo(CO) ₃ (PN ^H P ^{Et})] (1)	6.986096639	[Mo(CO) ₃ (PN ^H P ^{Et})] (1)	0
[Mo(CO) ₃ (PN ^H P ^{Ph})] (2)	6.488786575	[Mo(CO) ₃ (PN ^H P ^{Ph})] (2)	9.169350991
[Mo(CO) ₃ (PN ^H P ^{ⁱPr})] (3)	9.759243651	[Mo(CO) ₃ (PN ^H P ^{ⁱPr})] (3)	0.687018967
[Mo(CO) ₃ (PN ^H P ^{Cy})] (4)	8.055601669	[Mo(CO) ₃ (PN ^H P ^{Cy})] (4)	4.954884871
[Mo(CO) ₃ (PN ^H P ^{^tBu})] (5)	24.99275655	[Mo(CO) ₃ (PN ^H P ^{^tBu})] (5)	11.3645251

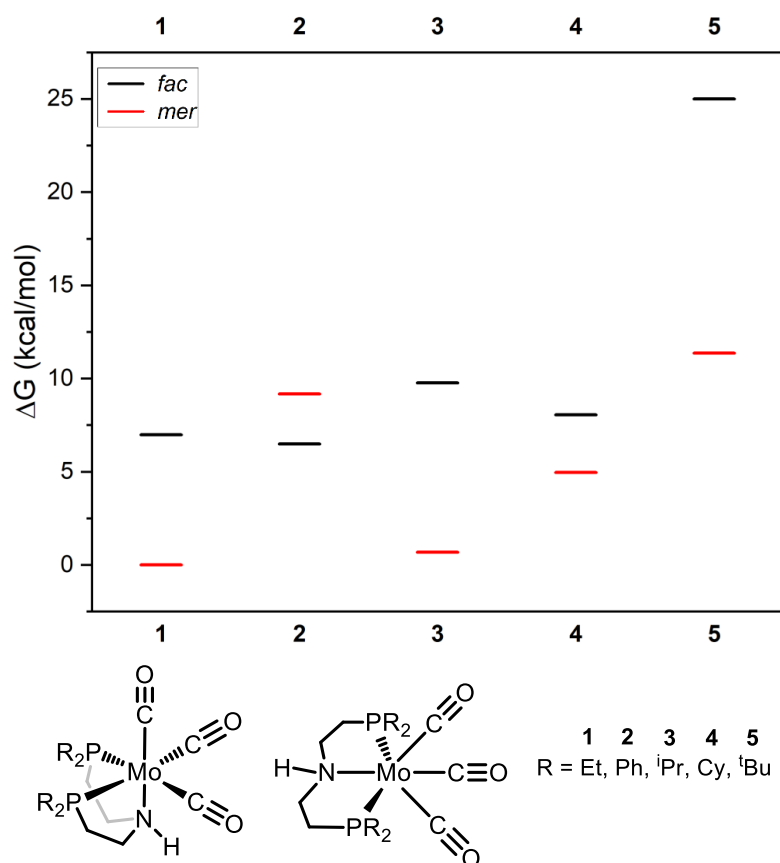


Figure S64: Calculated relative Gibbs energies of the facial and meridional [Mo(CO)₃(PN^HP^R)] complexes in solution (DCM, ε = 8.93) with different phosphine groups (R = Et (2c), Ph (2a), Cyp (2e), ⁱPr (2f), Cy (2g), ^tBu (2h)), relative to the most stable complex *mer*-2c. The complex bearing dicyclopentyl phosphine was not calculated because no comparable system is reported in literature.

3.5. Energy calculations of the relative Gibbs energies for the *fac-mer*-transformations

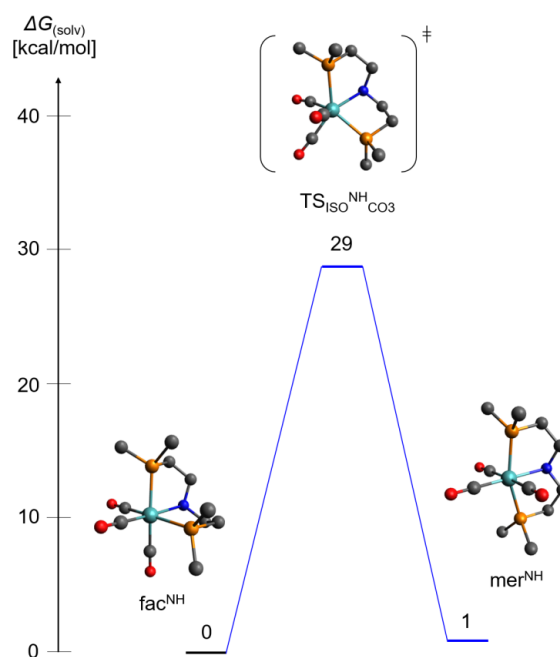


Figure S65: Calculated relative Gibbs energies in solution of the isomeric transformation of *fac*- and *mer*-[Mo(CO)₃(PN^HP^{Me})] model complexes via transition state TS_{ISO}^{NH}_{CO3} including calculated structures with omitted H atoms for clarity.

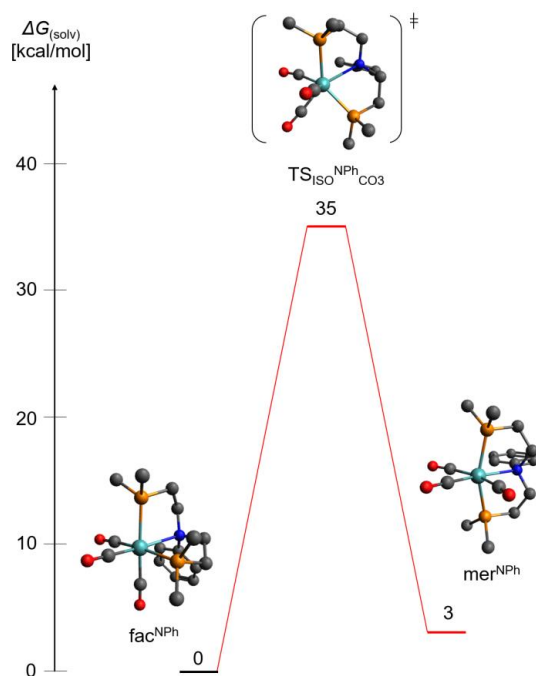


Figure S66: Calculated relative Gibbs energies in solution of the isomeric transformation of *fac*- and *mer*-[Mo(CO)₃(PN^{Ph}P^{Me})] model complexes via transition state TS_{ISO}^{NPh}_{CO3} including calculated structures with omitted H atoms for clarity.

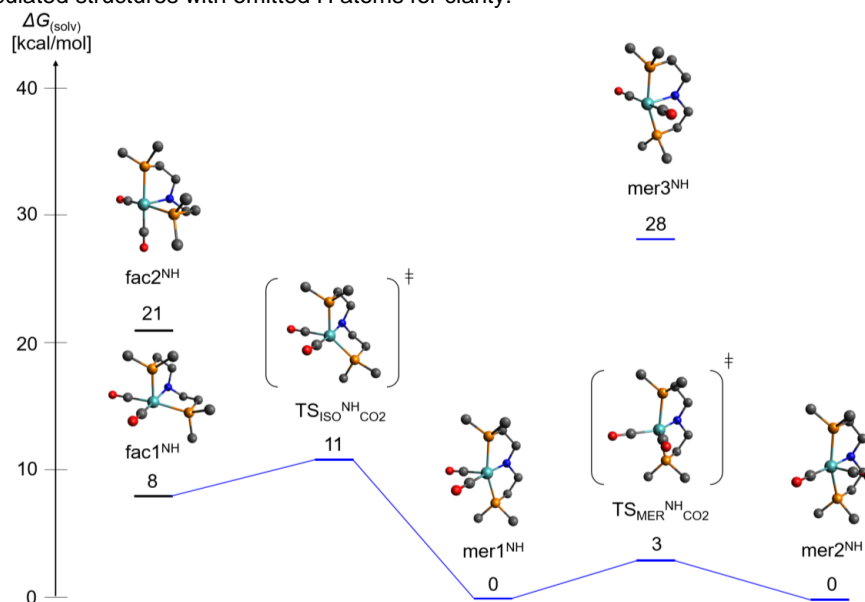


Figure S67: Calculated relative Gibbs energies in solution of the isomers of pentacoordinated model complex [Mo(CO)₂(PN^HP^{Me})], including the isomeric transformation via transition state TS_{ISO}^{NH}_{CO2} and the conversion of the two possible meridional isomers via TS_{MER}^{NH}_{CO2} and calculated structures with omitted H atoms for clarity.

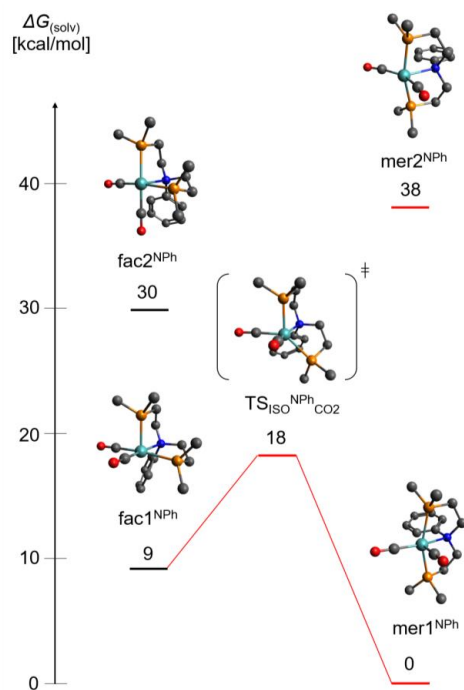


Figure S68: Theoretical relative Gibbs energies in solution of the different isomers of pentacoordinated model complex $[\text{Mo}(\text{CO})_2(\text{PN}^{\text{Ph}}\text{P}^{\text{Me}})]$, including isomeric transformation via transition state ($\text{TS}_{\text{ISO}}^{\text{NPh}_{\text{CO}_2}}$) calculated structures with omitted H atoms for clarity.

Table S10: Calculated thermodynamic data of the different isomers of $[\text{Mo}(\text{CO})_3(\text{PN}^{\text{R}}\text{P}^{\text{Me}})]$ and $[\text{Mo}(\text{CO})_2(\text{PN}^{\text{R}}\text{P}^{\text{Me}})]$ complexes including transition states of the isomerization reactions in solution ($\epsilon = 8.93$, DCM).

Complex [Mo] = $[\text{Mo}(\text{CO})_n(\text{PN}^{\text{R}}\text{P}^{\text{Me}})]$	Gibbs free energy G_{solv} [kcal/mol]	Total Enthalpy H [kcal/mol]	Entropy S [kcal/mol]
n = 3; R = H			
fac-[Mo] (fac ^{NH})	-917655,153	-917608,918	-46,235
mer-[Mo] (mer ^{NH})	-917653,736	-917607,412	-46,324
TS _{ISO} ^H _{CO3}	-917626,020	-917580,634	-45,386
n = 3; R = Ph			
fac-[Mo] (fac ^{NPh})	-1062472,482	-1062420,488	-51,994
mer-[Mo] (mer ^{NPh})	-1062469,760	-1062417,303	-52,457
TS _{ISO} ^{Ph} _{CO3}	-1062436,971	-1062387,021	-49,950
n = 2; R = H			
fac-[Mo] (fac1 ^{NH})	-846549,789	-846506,229	-43,560
fac-[Mo] (fac2 ^{NH})	-846536,643	-846493,315	-43,329
TS _{ISO} ^H _{CO2}	-846546,561	-846503,636	-42,926
mer-[Mo] (mer1 ^{NH})	-846557,820	-846514,045	-43,775
mer-[Mo] (mer2 ^{NH})	-846557,772	-846514,262	-43,510
mer-[Mo] (mer3 ^{NH})	-846529,811	-846486,239	-43,572
TS _{MER} ^H _{CO2}	-846554,912	-846511,956	-42,955
n = 2; R = Ph			
fac-[Mo] (fac1 ^{NPh})	-991372,107	-991323,559	-48,548
fac-[Mo] (fac2 ^{NPh})	-991350,594	-991303,036	-47,558
mer-[Mo] (mer1 ^{NPh})	-991381,733	-991332,674	-49,059
mer-[Mo] (mer2 ^{NPh})	-991343,014	-991294,725	-48,288
TS _{ISO} ^{Ph} _{CO2}	-991363,947	-991316,686	-47,261

4. Crystal structure determination of $[\text{Mo}(\text{CO})_3(\text{PN}^{\text{Ph}}\text{P}^{\text{Et}})]$ (**2c**)**Table S11.** Selected crystal data and details of the single crystal structure refinements for compound **2c**.

compound	2c
formula	$\text{C}_{21}\text{H}_{33}\text{MoNO}_3\text{P}_2$
MW / g mol^{-1}	505.36
crystal system	Monoclinic
space group	$C2/c$
$a / \text{\AA}$	33.1642(2)
$b / \text{\AA}$	7.44970(3)
$c / \text{\AA}$	19.1693(1)
$\alpha / ^\circ$	90
$\beta / ^\circ$	99.524(1)
$\gamma / ^\circ$	90
$V / \text{\AA}^3$	4670.75(4)
T / K	100.0(1)
Z	8
$D_{\text{calc}} / \text{g cm}^{-3}$	1.437
μ / mm^{-1}	6.055
Crystal size / mm^3	0.07×0.07×0.07
$\theta_{\text{max}} / \text{deg}$	74.487
measured refl.	40366
R_{int}	0.0152
unique refl.	4772
refl. $F_0 > 4\sigma(F_0)$	4769
parameter	257
$R_1 [F_0 > 4\sigma(F_0)]$	0.0159
wR_2 [all data]	0.0403
GOF	1.072
$\Delta\rho_{\text{max/min}} / \text{e \AA}^{-3}$	0.342/ -0.408

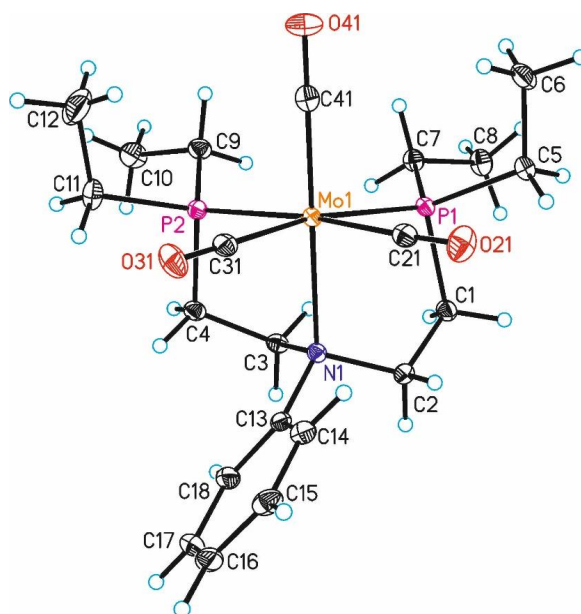


Figure S69: ORTEP plot of compound **2c** with labelling and displacement ellipsoids drawn at the 50% probability level.

Table S12. Selected bond lengths [Å] and angles [°] for compound **2c**.

Mo1	N1	2.4417(11)		Mo1	C21	1.9781(14)	
Mo1	P1	2.5136(3)		Mo1	C31	1.9729(14)	
Mo1	P2	2.5075(3)		Mo1	C41	1.9378(14)	
N1	Mo1	P1	76.85(3)	C31	Mo1	P2	87.22(4)
N1	Mo1	P2	79.09(3)	C31	Mo1	C21	87.97(5)
P2	Mo1	P1	99.130(11)	C41	Mo1	N1	173.50(5)
C21	Mo1	N1	97.36(5)	C41	Mo1	P1	99.13(4)
C21	Mo1	P1	85.07(4)	C41	Mo1	P2	96.69(4)
C21	Mo1	P2	173.64(4)	C41	Mo1	C21	87.29(5)
C31	Mo1	N1	96.77(4)	C41	Mo1	C31	87.90(5)
C31	Mo1	P1	169.85(4)				

5. References

- [1] J. P. Perdew, K. Burke, M. Ernzerhof, *Phys. Rev. Lett.* **1996**, 3865-3686.
- [2] a) F. Weigend, *Phys. Chem. Chem. Phys.* **2006**, 8, 1057; b) A. Hellweg, C. Hättig, S. Höfener, W. Klopper, *Theor. Chem. Acc.* **2007**, 117, 587.
- [3] S. Grimme, J. Antony, S. Ehrlich, H. Krieg, *J. Chem. Phys.* **2010**, 132, 154104.
- [4] S. Grimme, S. Ehrlich, L. Goerigk, *J. Comput. Chem.* **2011**, 32, 1456.
- [5] a) K. Eichkorn, O. Treutler, H. Öhm, M. Häser, Ahlrichs R., *Chem. Phys. Lett.* **1995**, 283; b) K. Eichkorn, O. Treutler, F. Weigend, *Theor. Chem. Acc.*, 1997, 119; c) F. Neese, *J. Comput. Chem.* **2003**, 24, 1740; d) F. Neese, F. Wennmohs, A. Hansen, U. Becker, *J. Chem. Phys.* **2009**, 356, 98.
- [6] V. Barone, M. Cossi, *J. Phys. Chem. A* **1998**, 102, 1995.

Declaration

Hereby I, Sven Froitzheim, declare that this thesis consists only of my own work, except for the advice of my supervisor Prof. Dr. Felix Tuczek and in accordance with the guidelines of good scientific practice of the german research foundation. Furthermore i declare that this dissertation has not been submitted, in whole or in parts, for publication or has been used previously for the application for a degree. Finally i declare that none of my academic degrees have been revoked.

Hiermit erkläre ich, Sven Froitzheim, an Eides statt, dass ich die vorliegende Dissertation, abgesehen von der Beratung durch meinen Doktorvater, allein angefertigt habe und diese nach den Richtlinien guter wissenschaftlicher Praxis der deutschen Forschungsgemeinschaft entstanden ist. Darüberhinaus erkläre ich, dass der Inhalt dieser Arbeit weder ganz, noch in Teilen zuvor veröffentlicht oder zur Veröffentlichung eingereicht wurde. Auch wurde der Inhalt dieser Dissertation nicht im Rahmen eines Prüfungsverfahrens an anderer Stelle eingereicht. Abschließend erkläre ich, dass mir bisher kein akademischer Grad entzogen wurde.

Ort, Datum Sven Froitzheim

List of Figures

2.1	Energy diagram of the conversion from N_2 and H_2 to NH_3 . The blue reaction pathway describes the reaction on the catalysts surface, the red path the direct reaction in the gaseous phase. Adapted from. ^[36,37]	4
2.2	Simple illustration of the nitrogen cycle. The three main stages of the nitrogen cycle are the Fixation, Nitrification, and Denitrification. Adapted from ^[13] . .	6
2.3	Ribbon diagram of the Nitrogenase enzyme complex. Located within the MoFe-protein (light blue & purple) are two units of the FeMoco and the P-cluster. On both ends of the MoFe protein binds the dinitrogenase reductase also called Fe-protein (gold & silver). The active components within the Fe-protein are the F-cluster as well as 2 MgATP. This image was created using PDB entry 1N2C and ChimeraX. ^[71–73]	8
2.4	Structure of the active site of the Nitrogenase - the iron-molybdenum cofactor (A), the P-cluster with surrounding aminoacids (B) and the F-Cluster (C) of the dinitrogenase reductase. Iron is shown in orange, sulfur in yellow, carbon in gray, nitrogen in blue, oxygen in red and the molybdenum in light blue. This image was created using PDB entries 1N2C, 3U7Q and ChimeraX. ^[71–73,80]	9
2.5	Illustration of the THORNELEY-LOWE-model describing the catalytic cycle of the biological nitrogen fixation. Each step of the cycle is represented by an E with an index reflecting the number of electrons transferred. PDB entries 1N2C ^[71] and 3U7Q ^[80] were used for creating the MoFe-, Fe-protein and ferredoxine (PDB 1FRI) images in the iron cycle. Adapted from EINSLE and REES. ^[89] . .	11
2.6	Schematic representation of the alternating and distal mechanism of nitrogenase. ^[107,113]	12
2.7	Left: Illustration of molecular orbital scheme starting from a single nitrogen atom, to the dinitrogen molecule and finally to the bonding situation in a terminal molybdenum complex. Right: Illustration of the interacting orbitals in their respective orientation of the Mo- N_2 fragment. ^[126–130]	14
2.8	Coordination modes of dinitrogen molecule to transition metal centers. ^[123] . .	15
2.9	Illustration of the CHATT cycle, in which dinitrogen is converted to ammonia by a sequence of protonating and reducing steps. ^[21,154,155]	16
2.10	Illustration of the SCHROCK cycle, in which dinitrogen is converted to ammonia by a strictly alternating sequence of protonating and reducing steps. The blue intermediates have been isolated. ^[158–162]	18
2.11	The pincer based system by SCHROCK <i>et al.</i> ^[165]	19

2.12	Iron dinitrogen complexes bearing the variations of the ligand for synthetic nitrogen fixation developed by PETERS <i>et al.</i> ^[166,167]	20
2.13	Illustration of the PCET mediated electrochemical N ₂ -to-NH ₃ reduction by PETERS <i>et al.</i> , exemplified with a tungsten bisdinitrogen complex. Edited after. ^[173]	21
2.14	Selection of complexes used for synthetic nitrogen fixation by NISHIBAYASHI <i>et al.</i> ^[186,190–192]	23
2.15	Examples of different nitrogen complexes synthesized by the TUCZEK group for synthetic nitrogen fixation. ^[214,215,218–223]	26
2.16	The pentaPod concept arose from combination of the tridentate PPP and tripodal PPP ligands. ^[222,227]	27
2.17	[MoCl ₃ (PN ³ P)] complex synthesized by STUCKE capable of ammonia generation (3.12 equiv.) upon addition of [Cp ₂ [*] Cr] and [CoH][OTf]. This is the first system of the TUCZEK group which exhibited catalytic activity. ^[229]	28
3.1	Inert gas cell designed for electrochemical analytics and use in electrocatalytical experiments	43
3.2	The cyclic voltammograms of the [W(N ₂)(P ₂ ^{Me} PP ₂ ^{Ph})] complex (c = 0.06 mmol/L) measured with the cells build for the electrochemical investigations (thf, 0.1 mol/L TBAPF ₆). Display is the overview voltammogram (left) and a measurement of the redox events of the complex (right). Two redox systems are associated with the complex. The first reversible redox system can be assigned to the oxidation/reduction of W ⁰ ⇌ W ^I and the second, quasi-reversible system to the W ^I ⇌ W ^{II}	44
3.3	Setup for investigations towards electrocatalytic activity of the complex using a mercury pool electrode.	45
4.1	Illustration of σ-donation from a PR ₃ ligand to a metal center (left) and the π-backdonation from the d-orbital of the metal to free π [*] -orbitals of the ligand (right). Edited based on ORPEN ^[235] and CRABTREE. ^[236]	47
5.1	Illustration of different methods of deposition of complexes on a surface: direct deposition (top left), self-assembled monolayers (top right) and the platform approach (bottom). It is worth noting that the uniform orientation of the complexes does not represent an experimental case.	66
5.2	Illustration of the molybdenum tricarbonyl complex bearing a modified PN ³ P pincer ligand on an Au(111) surface. The complex is attached to an octyl-TATA platform which is used to vertically deposit the headgroup on the surface. ^[261]	67

5.3	Illustration of the molybdenum tricarbonyl complex bearing a modified tripodal P ₃ ligand on a Au(111) surface. The complex is attached to a TATA-platform which is used to vertically deposit the system on the surface. ^[262]	68
5.4	Illustration of the approaches for depositing a Mo(0) tricarbonyl complex bearing tridentate PNP ligand on gold surface targeted in this project.	69
5.5	³¹ P{ ¹ H} NMR spectrum of ligand 4 . The successful substitution of the terminal chlorides by diphenyl phosphine can be seen from the product signal at -21.1 ppm.	72
5.6	Comparison of the infrared spectra of the [Mo(CO) ₃ (PN ^{Ph} P ^{Ph})] complex (top, red) to the attempted coordination of the surface modified PNP ligand 4 (bottom, black).	73
5.7	³¹ P{ ¹ H} NMR spectrum of the attempted coordination of the surface modified PN ^{Ph} P ^{Ph} ligand 4 using [Mo(CO) ₃ (cht)].	75
5.8	XPS spectra of the first attempt to deposit the dummy molecule 5 in a monolayer on a gold surface without prior reductive conversion of the thiocyanate to a thiol. The deposition was attempted directly starting from the thiocyanate upon cyanide release. The spectra show the presence of multiple species on the surface especially in the sulfur 2p-spectrum (bottom right). The other element spectra (carbon 1s, top left; chlorine 2p, top right; nitrogen 1s, bottom left) show that the substance used was pure.	78
5.9	Top: Aromatic region of the ¹³ C{ ¹ H} NMR spectrum of the inverse attempt shows the successful introduction of the SCN group in the 4-position of the aniline group in every variant of the ligand. Middle: structures of the three ligands obtained in the reaction. Bottom: ³¹ P{ ¹ H} NMR spectrum of the inverse attempt revealed the formation of three main products. The integrals show the percentage quantities of the products.	81
5.10	Comparison of the aromatic region of the ¹³ C{ ¹ H} NMR spectra of the PN ^{Ph} P ^{Ph} ligand (top) and the borane protected PN ^{Ph} P ^{Ph} after the introduction of the thiocyanate group (bottom). The introduction of the SCN group leads to a shift of the two meta carbons (blue arrow) and the <i>para</i> -carbon (red arrow) of the aniline ring.	84
5.11	Comparison of the ³¹ P{ ¹ H} NMR spectra of the PN ^{Ph} P ^{Ph} ligand (9 , top), the borane protected PN ^{Ph} P ^{Ph} ligand (10 , middle) and the borane protected PN ^{Ph} P ^{Ph} after the introduction of the thiocyanate group (11 , bottom). The borane groups successfully withstood the reaction conditions during the introduction of the SCN group.	85
5.12	³¹ P{ ¹ H} NMR spectrum of the attempted removal of the borane groups on SCN modified PN ^{Ph} P ^{Ph} ligand (11). Besides the formation of the product and the halogenated phosphines from the prior step mainly phosphine oxides were formed.	86

5.13 Comparison of the $^{31}\text{P}\{^1\text{H}\}$ NMR spectrum of the prPPHP ligand (top) and the modified ligand 13 (bottom). The enlarged regions show several byproducts and oxidized species. The large signal at -17.0 ppm can be assigned to the PPh_2 groups and the signal at -26.1 ppm to the central phosphine after the substitution of the proton by the aromatic residue.	88
---	----

List of Tables

7.1	Frequencies and references of the measured nuclei.	97
-----	--	----